

Remarks: The model is visually stretched several times on an axis at Y



ПОЛИТЕХ
Санкт-Петербургский
политехнический университет
Петра Великого

Инженерно-строительный институт
Центр дополнительных профессиональных программ
195251, г. Санкт-Петербург, Политехническая ул., 29,
тел/факс: 552-94-60, www.stroikursi.spbstu.ru,
stroikursi@mail.ru

**Приглашает специалистов организаций, вступающих в СРО,
на курсы повышения квалификации (72 часа)**

Код	Наименование программы	Виды работ*
Курсы по строительству		
БС-01-04	«Безопасность и качество выполнения общестроительных работ»	п.1,2, 3, 5, 6, 7, 9, 10, 11, 12, 13, 14
БС-01	«Безопасность и качество выполнения геодезических, подготовительных и земляных работ, устройства оснований и фундаментов»	1,2,3,5
БС-02	«Безопасность и качество возведения бетонных и железобетонных конструкций»	6,7
БС-03	«Безопасность и качество возведения металлических, каменных и деревянных конструкций»	9,10,11
БС-04	«Безопасность и качество выполнения фасадных работ, устройства кровель, защиты строительных конструкций, трубопроводов и оборудования»	12,13,14
БС-05	«Безопасность и качество устройства инженерных сетей и систем»	15,16,17,18,19
БС-06	«Безопасность и качество устройства электрических сетей и линий связи»	20,21
БС-08	«Безопасность и качество выполнения монтажных и пусконаладочных работ»	23,24
БС-12	«Безопасность и качество устройства мостов, эстакад и путепроводов»	29
БС-13	«Безопасность и качество выполнения гидротехнических, водолазных работ»	30
БС-14	«Безопасность и качество устройства промышленных печей и дымовых труб»	31
БС-15	«Осуществление строительного контроля»	32
БС-16	«Организация строительства, реконструкции и капитального ремонта. Выполнение функций технического заказчика и генерального подрядчика»	33
Курсы по проектированию		
БП-01	«Разработка схемы планировочной организации земельного участка, архитектурных решений, мероприятий по обеспечению доступа маломобильных групп населения»	1,2,11
БП-02	«Разработка конструктивных и объемно-планировочных решений зданий и сооружений»	3
БП-03	«Проектирование внутренних сетей инженерно-технического обеспечения»	4
БП-04	«Проектирование наружных сетей инженерно-технического обеспечения»	5
БП-05	«Разработка технологических решений при проектировании зданий и сооружений»	6
БП-06	«Разработка специальных разделов проектной документации»	7
БП-07	«Разработка проектов организации строительства»	8
БП-08	«Проектные решения по охране окружающей среды»	9
БП-09	«Проектные решения по обеспечению пожарной безопасности»	10
БП-10	«Обследование строительных конструкций и грунтов основания зданий и сооружений»	12
БП-11	«Организация проектных работ. Выполнение функций генерального проектировщика»	13
Э-01	«Проведение энергетических обследований с целью повышения энергетической эффективности и энергосбережения»	
Курсы по инженерным изысканиям		
И-01	«Инженерно-геодезические изыскания в строительстве»	1
И-02	«Инженерно-геологические изыскания в строительстве»	2,5
И-03	«Инженерно-гидрометеорологические изыскания в строительстве»	3
И-04	«Инженерно-экологические изыскания в строительстве»	4
И-05	«Организация работ по инженерным изысканиям»	7

*(согласно приказам Минрегионразвития РФ N 624 от 30 декабря 2009 г.)

**По окончании курса слушателю выдается удостоверение о краткосрочном повышении
квалификации установленного образца (72 ак. часа)**

Для регистрации на курс необходимо выслать заявку на участие, и копию диплома об образовании по телефону/факсу: 8(812) 552-94-60, 535-79-92, , e-mail: stroikursi@mail.ru.

<http://www.engstroy.spbstu.ru> – полнотекстовая версия журнала в сети Интернет.
Бесплатный доступ, обновление с каждым новым выпуском

Инженерно-строительный журнал

НАУЧНОЕ ИЗДАНИЕ

ISSN 2071-4726, 2071-0305

Свидетельство о государственной регистрации: ПИ №ФС77-38070, выдано Роскомнадзором

Специализированный научный журнал. Выходит с 09.2008.

Включен в Перечень ведущих периодических изданий ВАК РФ

Периодичность: 8 раз в год

Учредитель и издатель:

Санкт-Петербургский политехнический университет Петра Великого

Адрес редакции:

195251, СПб, ул. Политехническая, д. 29, Гидрокорпус-2, ауд. 227А

Главный редактор:

Екатерина Александровна Линник

Научный редактор:

Николай Иванович Ватин

Технический редактор:

Ксения Дмитриевна Борщева

Редакционная коллегия:

д.т.н., проф. В.В. Бабков;
д.т.н., проф. М.И. Бальзаников;
к.т.н., проф. А.И. Боровков;
д.т.н., проф. Н.И. Ватин;
PhD, проф. М. Вельжкович;
д.т.н., проф. А.Д. Гиргидов;
д.т.н., проф. Э.К. Завадскас;
д.ф.-м.н., проф. М.Н. Кирсанов;
D.Sc., проф. М. Кнежевич;
д.т.н., проф. В.В. Лалин;
д.т.н., проф. Б.Е. Мельников;
д.т.н., проф. Ф. Неправишта;
д.т.н., проф. Р.Б. Орлович;
Dr. Sc. Ing., professor
Л. Пакрастиньш;
Dr.-Ing. Habil., professor
Х. Пастернак;
д.т.н., проф. А.В. Перельмутер;
к.т.н. А.Н. Пономарев;
д.т.н., доцент В.В. Сергеев;
д.ф.-м.н., проф. М.Х. Стрелец;
д.т.н., проф. О.В. Тараканов;
д.т.н., проф. В.И. Травуш

Дата выхода: 30.03.2018

Содержание

Сольский С.В., Орлова Н.Л., Величко А.С. Самозалечивания трещин в глиноцементобетонной диафрагме грунтовой плотины	3
Гиясов Б.И., Леденев В.И., Матвеева И.В. Метод расчета шума при зеркально-рассеянном отражении звука	13
Тюкалов Ю.Я. Конечно элементные модели в напряжениях для задач плоской теории упругости	23
Гравит М.В., Недрышкин О.В., Огидан О.Т. Трансформируемые противопожарные преграды в сооружениях и строениях	38
Петриченко М.Р., Немова Д.В., Котов Е.В., Тарасова Д.С., Сергеев В.В. Вентилируемые фасады, интегрированные с инженерными системами здания для холодного климата	47
Кабанов В.Н. Организационно-технологическая надежность строительного процесса	59
Туснина О.А. Конечно-элементное моделирование и расчёт подкраново-подстропильной фермы	68
Травуш В.И., Конин Д.В., Крылов А.С. Прочность железобетонных балок из высокопрочных бетонов и фибробетонов	90
Мирсаидов М.М., Султанов Т.З., Абдикаримов Р.А., Ишматов А.Н., Юлдошев Б.Ш., Тошматов Э.С., Жураев Д.П. Прочностные параметры грунтовых плотин при различных динамических воздействиях	101
Барашкова П.С., Молодкина Л.М. Промывка и регенерация трековых мембран при очистке природной воды	112
Закревская Л.В., Гавриленко А.А., Авдеев С.Н., Гандельсман И.А., Киреев А.В. Легкий бетон на основе кремнистых композиций природного происхождения	121
Петриченко М.Р., Котов Е.В., Немова Д.В., Тарасова Д.С., Сергеев В.В. Численное моделирование вентилируемых фасадов в экстремальных климатических условиях	130
Терлеев В.В., Никоноров А.О., Гиневский Р.С., Лазарев В.А., Того И., Топаж А.Г., Моисеев К.Г., Павлова В.А., Лайшев К.А., Архипов М.В., Мельничук А.Ю., Дунаева Е.А., Миршель В. Гистерезис водоудерживающей способности почвы	141

© ФГАОУ ВО СПбПУ, 2017

На обложке: иллюстрации авторов к статьям номера

Контакты:

Тел. +7(812)535-52-47 E-mail: mce@spbstu.ru
Web: <http://www.engstroy.spbstu.ru>

<http://www.engstroy.spbstu.ru> – full-text open-access version in Internet. It is updated immediately with each new issue.

Magazine of Civil Engineering

SCHOLAR JOURNAL

ISSN 2071-4726

Peer-reviewed scientific journal

Start date: 2008/09

8 issues per year

Publisher:

Peter the Great St. Petersburg
Polytechnic University

Indexing:

Scopus, Russian Science Citation
Index (WoS), Compendex, DOAJ,
EBSCO, Google Academia, Index
Copernicus, ProQuest, Ulrich's Serials
Analysis System

Corresponding address:

227a Hydro Building, 29
Polytechnicheskaya st., Saint-
Petersburg, 195251, Russia

Editor-in-chief:

Ekaterina A. Linnik

Science editor:

Nikolay I. Vatin

Technical editor:

Ksenia D. Borshcheva

Editorial board:

V.V. Babkov, D.Sc., professor
M.I. Balzannikov, D.Sc., professor
A.I. Borovkov, PhD, professor
M. Veljkovic, PhD, professor
E.K. Zavadskas, D.Sc., professor
M.N. Kirsanov, D.Sc., professor
M. Knezevic, D.Sc., professor
V.V. Lalin, D.Sc., professor
B.E. Melnikov, D.Sc., professor
F. Nepravishita, D.Sc., professor
R.B. Orlovich, D.Sc., professor
L. Pakrastinsh, Dr.Sc.Ing., professor
H. Pasternak, Dr.-Ing.habil.,
professor
A.V. Perelmuter, D.Sc., professor
A.N. Ponomarev, PhD, professor
V.V. Sergeev, D.Sc., associate
professor
M.Kh. Strelets, D.Sc., professor
O.V. Tarakanov, D.Sc., professor
V.I. Travush, D.Sc., professor

Contents

Solsky S.V., Orlova N. L., Velichko A.S. Crack self-healing in clay-cement concrete diaphragm of embankment dam	3
Giyasov G.B., Ledenyov L.V., Matveeva M.I. Method for noise calculation under specular and diffuse reflection of sound	13
Tyukalov Yu.Ya. Finite element models in stresses for plane elasticity problems	23
Gravit M.V., Nedryshkin O.V., Ogidan O.T. Transformable fire barriers in buildings and structures	38
Petrichenko M.R., Nemova D.V., Kotov E.V., Tarasova D.S., Sergeev V.V. Ventilated facade integrated with the HVAC system for cold climate	47
Kabanov V.N. Organizational and technological reliability of the construction process	59
Tusnina O.A. Finite element analysis of crane secondary truss	68
Travush V.I., Konin D.V., Krylov A.S. Strength of reinforced concrete beams of high-performance concrete and fiber reinforced concrete	90
Mirsaidov M.M., Sultanov T.Z., Abdikarimov R.A., Ishmatov A.N., Yuldoshev B.Sh., Toshmatov E.S., Jurayev D.P. Strength parameters of earth dams under various dynamic effects	101
Barashkova P.S., Molodkina L.M. Track-etched membranes back-flushing and regeneration during the natural water purification	112
Zakrevskaya L.V., Gavrilenko A.A., Avdeev S.N., Gandelsman I.A., Kireev A.V. Lightweight concrete based on siliceous compositions of natural origin	121
Petritchenko M.R., Kotov E.V., Nemova D.V., Tarasova D.S., Sergeev V.V. Numerical simulation of ventilated facades under extreme climate conditions	130
Terleev V.V., Nikonorov A.O., Ginevsky R.S., Lazarev V.A., Togo I., Topaj A.G., Moiseev K.G., Pavlova V.A., Layshev K.A., Arkhipov M.V., Melnichuk A.Yu., Dunaieva I.A., Mirschel W. Hysteresis of the soil water-retention capacity: estimating the scanning branches	141

© Peter the Great St. Petersburg Polytechnic University. All rights reserved.

On the cover: authors' illustrations

+7(812) 535-52-47

E-mail: mce@spbstu.ru

Web: <http://www.engstroy.spbstu.ru/eng/index.html>

doi: 10.18720/MCE.77.1

Crack self-healing in clay-cement concrete diaphragm of embankment dam

Самозалечивания трещин в глиноцементобетонной диафрагме грунтовой плотины

S.V. Sol'skiy,
N.L. Orlova,
A.S. Velichko,
"B.E. Vedeneev VNIIG", JSC, Saint Petersburg,
Russia

*Д-р техн. наук, главный научный
сотрудник С.В. Сольский,
научный сотрудник Н.Л. Орлова,
инженер А.С. Величко,
АО "ВНИИГ им. Б.Е. Веденеева",
г. Санкт-Петербург, Россия*

Key words: embankment dam; cement-clay concrete diaphragm; numerical simulation of filtration; self-healing crack; filtration strength; colmatage; healing layer; transient zones; suffosive strength

Ключевые слова: грунтовая плотина; глиноцементобетонная диафрагма; численное моделирование фильтрации; самозалечивание трещин; фильтрационная прочность; кольматаж; залечивающий слой; переходные зоны; суффозионная прочность

Abstract. The article presents the results of the analysis of seepage flow character in an embankment dams with impervious diaphragm made of clay-cement concrete, using the Gotsatlinskaya HPP as an example. The process of slits colmatage was considered in the clay-cement-concrete diaphragm (CCCD), that be caused in the zone of tensile forces or by seismic actions. Mathematical models build in two-dimensional and three-dimensional formulation to study the characteristics of flow in subvertical and subhorizontal cracks. By numerical simulation was received qualitative assessment of the dynamics of gradients of pressure for a non-defective impervious element, for an open crack in impervious element, for a washed-out crack in impervious element. The methods developed for design-experimental substantiation of the parameters of the transition zone (from riding and with the lower side of impervious element), parameters of transition zones for design that provide the process of cracks self-healing in the clay cement-concrete diaphragm. The granulometric composition shall, the capacity and number of layers of the reverse filter provided for the seepage strength of the system: upstream toe – upstream transitional layer – self-healing layer – CCCD – downstream transitional layer – downstream toe, selected according to the method.

Аннотация. В статье представлены результаты анализа характера фильтрационного потока в грунтовых плотинах с противofильтрационной диафрагмой, выполненной из глиноцементобетона, на примере плотины Гоцатлинской ГЭС. Рассмотрен процесс кольматирования щелевидных повреждений глиноцементобетонной диафрагмы (ГЦБД), возникновение которых возможно в зоне растягивающих усилий или вследствие сейсмических воздействий. Разработаны математические модели в двухмерной и в трехмерной постановке для исследования характеристик фильтрационного потока в субвертикальных и субгоризонтальных трещинах. Путем численного моделирования получена качественная оценка динамики значений градиентов напора для случаев: полностью исправного противofильтрационного элемента (ПФЭ), ПФЭ со сквозной трещиной, ПФЭ с замытой трещиной. Разработана методика расчетно-экспериментального обоснования параметров переходных зон (с верховой и с низовой стороны от ПФЭ), обеспечивающих самозалечивание трещин в ГЦБД. Подобранные согласно методике гранулометрический состав грунтов, мощность и количество слоев обратного фильтра, позволяют обеспечить фильтрационную прочность системы: верховая призма – верховой переходный слой – залечивающий слой – ГЦБД – низовой переходный слой – низовая призма.

1. Introduction

The method of diaphragm wall is used to create impervious element in hydroengineering construction. Clay-cement-concrete (CCC) is the material for impervious element, which is performed by the method of diaphragm wall. Clay-cement-concrete is most often used, which under certain conditions in zones of tensile forces is prone to cracking. The design of the embankment dams (ED) can include elements that ensure the colmatage of the cracks formed in the clay-cement-concrete diaphragm (CCCD), that is, their self-healing. Self-healing of possible cracks in the CCCD is ensured by piling the transition zones from the sandy soil in the drilling zone of the bore-cutting wells. The reliability of the dam depends from the proper selection of the composition of the transition zones as a whole. Transition zones are designed to protect the dam from filtration deformations, mechanical suffusion and contact erosion, as well as to self-heal cracks in the event of their formation and to ensure reliable coupling of CCCD to the ground of resistant prisms of dams. A clear algorithm is not available for designing the structures of transitional zones of embankment dams with CCCD, so the development of the algorithm is relevant.

The purpose of this study is to develop an algorithm for the selection of transition zones of embankment dams with impervious element, made of clay-cement-concrete bearing drilling piles. To achieve this goal, it is necessary to solve the following tasks:

- To determine the character, qualitative and quantitative parameters of the filtration flow in the transition zones of both an undisturbed and disturbed impervious device.
- To determine the sequence of the calculation and experimental justification.

The process of ED local seepage strength recovery by a designated subsoil layer due to the so-called crack "healing" has been inadequately treated in the special-purpose literature [1-5]. According to the current standards of the Russian Federation [6] it is required to arrange special layers ensuring the colmatage of emerging cracks. However, previously published research results and standards provisions cover healing of curtain grouting (CG) made of clayey materials, the behavior of which differs significantly from that of clay-cement-concrete (CCC) in case of crack formation. Crack walls in clayey materials swell and close over time, while cracks in the CCC are not distorted. Crack walls in clayey materials with opening of over 1 mm are vulnerable with velocity of groundwater 1–3 cm/s [1]. The CCC scouring resistance depends on its formulation [7–11]. According to the results of the conducted laboratory research [12], walls of cracks in the CCC are normally resistant to scouring at the velocity of groundwater about 200 cm/s. As a result of scouring, clay particles may be entrained downstream from the cracks in clayey materials, thus causing colmatage of the transitional layers material from the downstream side. Formation of cracks in clay cores lying at a depth of 30-50 m from the embankment crest is virtually impossible, as this area is subject to high compressive stresses exceeding the cohesive soils adhesion [1]. While the location of cracks in the CCCD depends on the stress-strain state of the structure and working conditions [13–19], cracks may form at the depths exceeding those specified for clayey impervious elements. The said factors demonstrate different behavior of cracks in clayey materials and in the clay-cement-concrete, while demonstrating impossibility of direct application of all research data and current requirements for clayey impervious elements structures, as well as to impervious elements made of clay-cement-concrete. The clay-cement-concrete diaphragms made using the bored-secant piles technique have a number of apparent advantages over other techniques, such as: high processibility, high level of industrialization of mixtures composition, supply and placing, high construction rate. However, they also have certain disadvantages caused both by its construction process and by the particular nature of its collaboration with the ED construction [20, 21]. The stress-strain state of the ED with CCCD may contribute to development of cracks in tension areas [13, 19] coinciding with the areas of the ED and CCCD combined deflection and longitudinal (downstream) displacements against abutments. Requirements to compensating measures are specified with consideration of the complex, multifactorial and time transgressive nature of crack formation process in the CCCD. A transition zone shall be arranged between the CCCD and the ED downstream toes to ensure seepage strength of the ED in case of potential crack formation in the CCCD. The upstream side of this transition zone shall have a special layer of soil adjacent to the CCCD which ensures the filling of cracks. It is the so-called "healing" layer.

In [5, 21, 22], the authors performed a numerical and laboratory-experimental simulation of the processes of self-healing of cracks in CCCD. The analysis of stress-stain state was carried out to clarify the most dangerous zones of development of cracks of the CCCD, by using numerical modeling [13]. Within the framework of this work, filtration modeling in two-dimensional and three-dimensional formulations has been performed to solve the tasks, and an analysis has been made of the characteristics of filtration flows for embankment dams up to 60 m in height with clay-cement-concrete diaphragms. New qualitative regularities are established of changes in the effective pressure gradients in

various CCCD zones with a through and with a washed crack (for example, the embankment dam of the Gotsatlinskaya HPP).

A technique is proposed for calculating and experimental substantiation of the characteristics and parameters of the transition layers providing self-healing of cracks in the CCCD, on the basis of the analysis of the obtained results, which includes the following blocks:

- Analysis of stress-strain state - to location, opening of potential crack in CCCD;
- Filtration modeling - to expected pressure gradients in transition zones and contact areas;
- Laboratory-experimental modeling - to confirm washing, clarify the nature of the wash, depending on the granulometric composition of the soil of the healing layer and the operating gradients;
- Selection of the optimal "soil mixture" and verification of its filtering-suffosive characteristics, the possibility of penetration into the crack, the possibility of penetration into the downstream transitional layer;
- Clarification of the necessary volume of the healing material.

Thus, the objectives of the research have been fulfilled.

2. Methods

The crack healing process proceeds as follows: in case of formation and opening of cracks in the CCCD, the escape (towards the crack cavity) head gradients J , exceeding the critical head gradient values for this layer, of soil, appear at the contact with the healing layer. At the contact with the CCCD, due to temporary loss of its seepage strength, the healing layer soil material is entrained by the seepage flow into cracks formed in the CCC. Thus, the cracks are filled with the material of the self-healing layer, and the integrity of impervious elements is recovered.

The data on nature and structure of the ED with CCCD total seepage flow shall provide a more vivid representation of the self-healing procedure. The data were obtained during simulation of the steady-state seepage process for the channel damsite of Gotsatlinskaya HPP using Plax Flow (2D modeling) software unit (Fig. 1) and Feflow6.2 (3D modeling) software package [22] (Fig. 2).

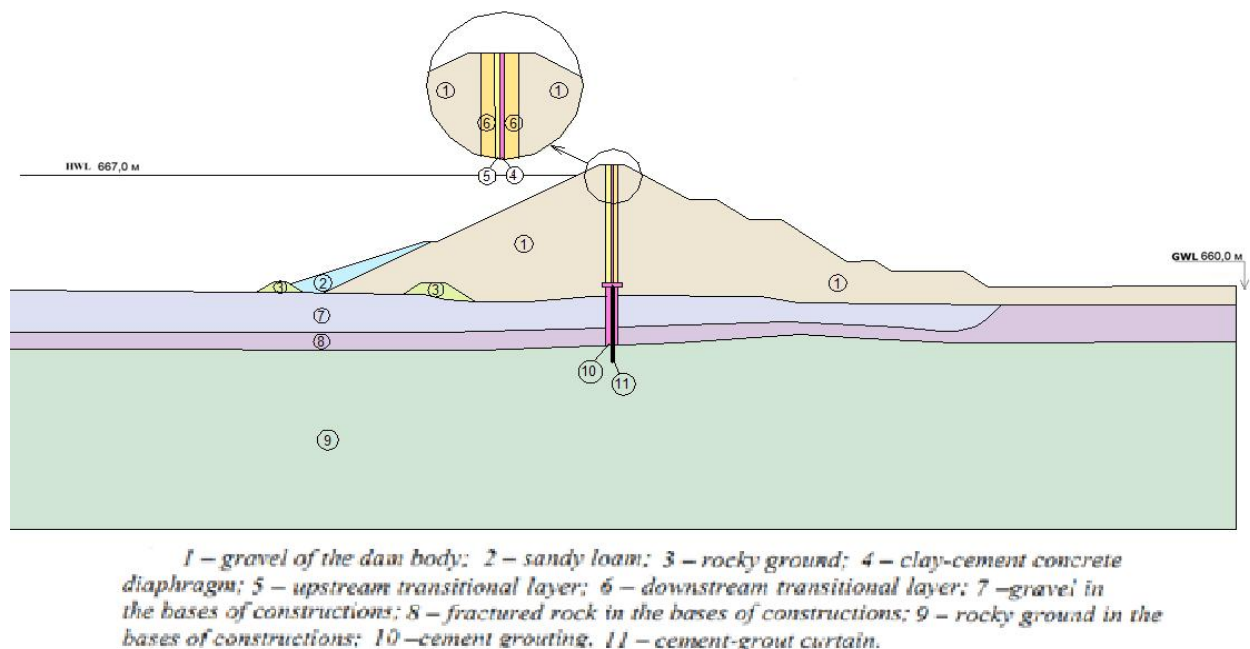


Figure 1. Seepage model for the embankment dam of Gotsatlinskaya HPP for the option with impervious elements from the CCCD

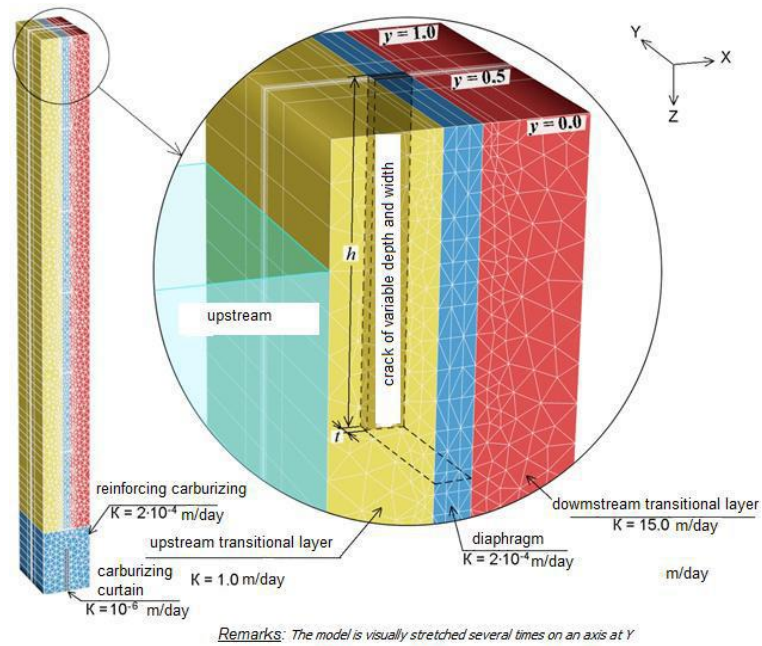


Figure 2. Three-dimensional model of a vertical crack in CCCD

3. Results and Discussion

The results of numerical modeling of filtration for the embankment dam with a clay-cement-concrete diaphragm, for example the embankment dam of the Gotsatlinskaya HPP, obtained by the authors earlier [22], are presented in Figures 3–5:

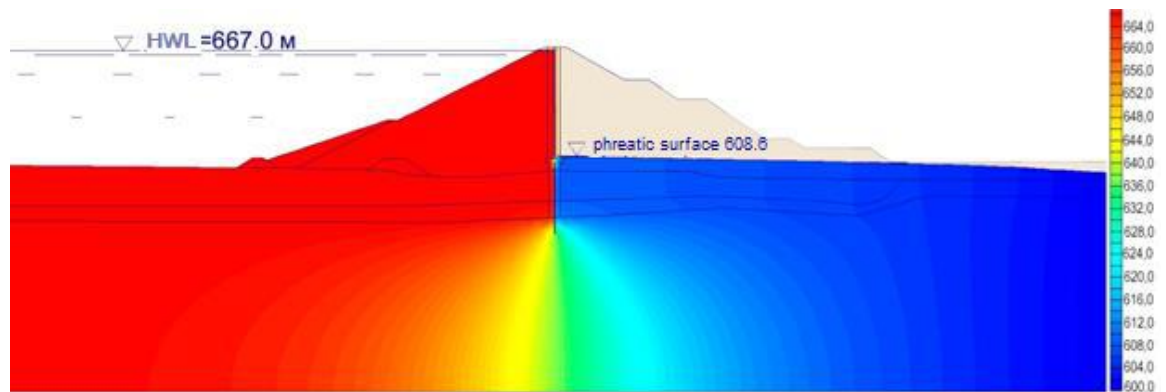


Figure 3. Phreatic surfaces and lines of total head in the body and the foundation of an embankment dam with impervious element from CCC with a working condition of the diaphragm

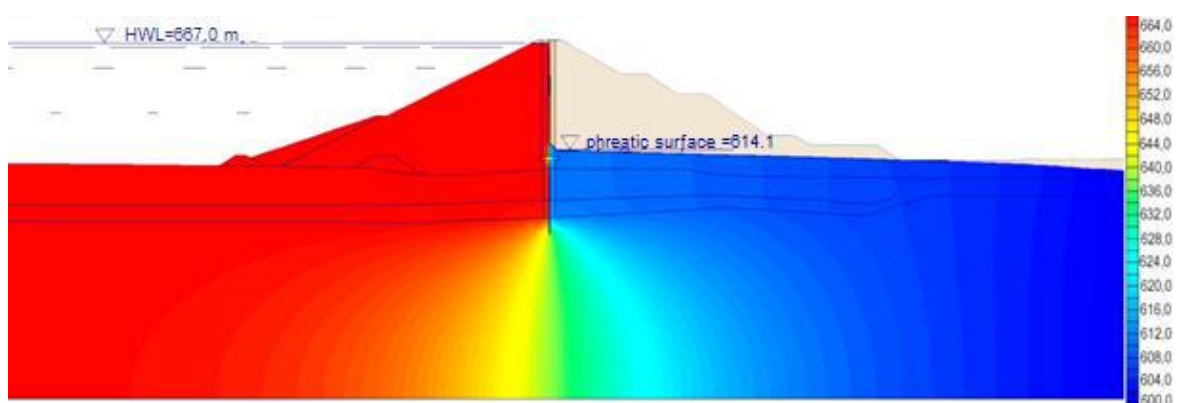


Figure 4. Phreatic surfaces and lines of total head in the body and foundation of an embankment dam with impervious element from CCC in the broken state of the diaphragm with a "healed" crack, opening 0.3 m

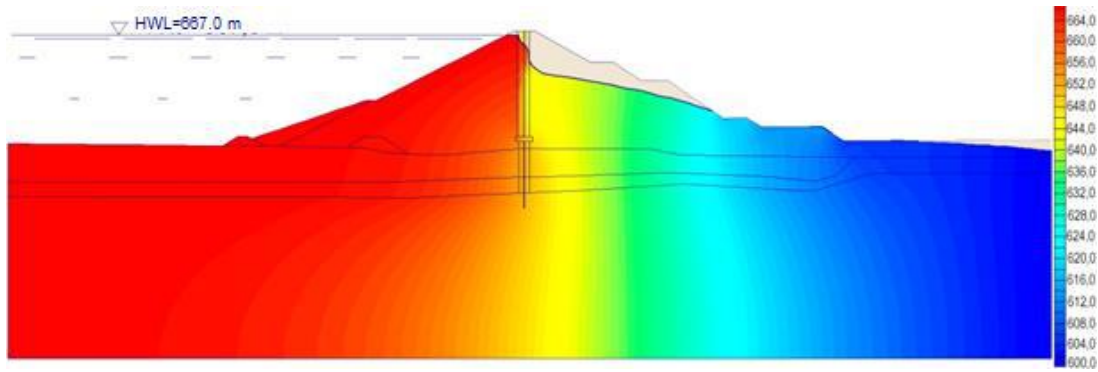


Figure 5. Phreatic surfaces and lines of total head in the body and foundation of an embankment dam with impervious element from CCC with complete diaphragm degradation

Results of the modeling follows for a clean vertical crack the maximum pressure gradients at the input $J_{max} = 1850$ and at the output $J_{max} = 117$ are predicted with its minimum opening $\delta = 5.0$ mm, the gradients decrease with increasing crack opening; curves $J(\delta)$ in Figure 6 are trends of the form:

$$J = a \cdot \delta^b, -0.7 < b < -0.6$$

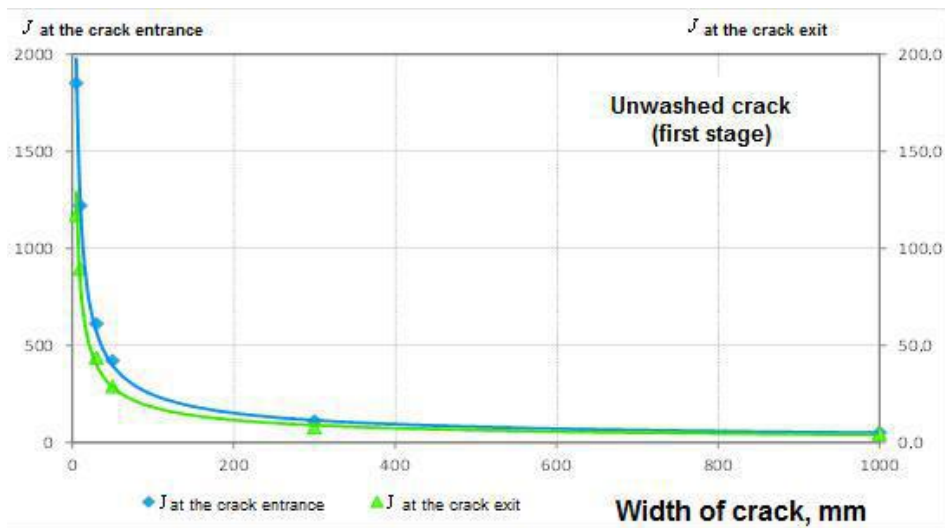


Figure 6. Dependence of pressure gradients on width an unwashed horizontal crack

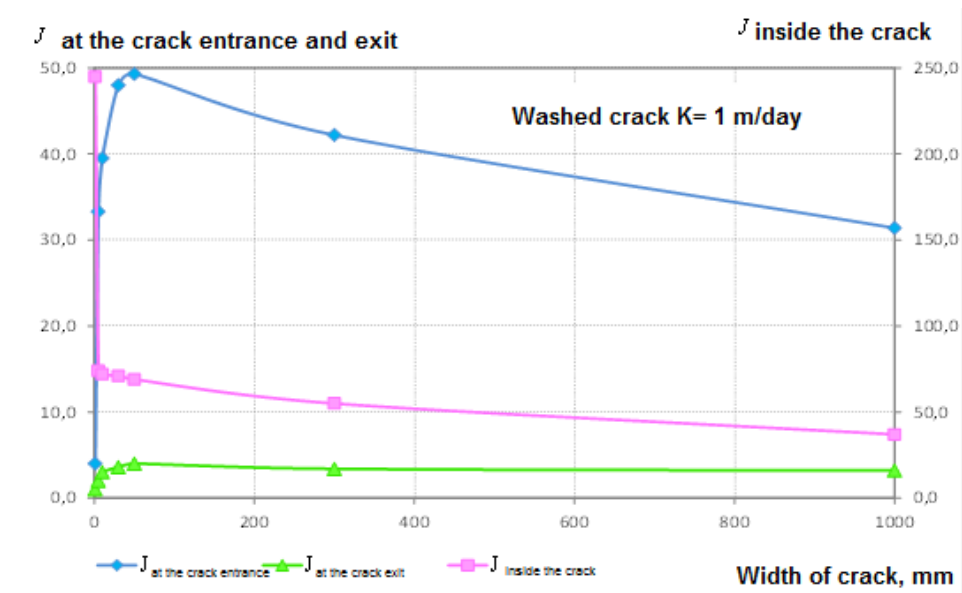


Figure 7. Dependence of pressure gradients on width washed horizontal crack

After self-healing of the horizontal crack (Fig. 7), gradients increase at the inlet and outlet with increasing its opening from 1 to 50 mm, reaching, at $\delta_0 = 50$ mm, the maximum values of $J_{\max} = 49.0$ and 4.0, respectively. With further expansion of the crack ($\delta > 50$ mm), the gradients decrease; within the same crack, the maximum calculated gradient $J_{\max} = 245.0$ is fixed at its minimum calculated width $\delta = 1$.

Simulation results for the specified design of the ED with CCCD of Gotsatlinskaya HPP has allowed to establish common patterns of the seepage flow structure at the crack entrance, inside the crack and at the crack exit. At the crack entrance high head gradient values were recorded; inside the crack the head gradient values reduce significantly; at the crack exit the head gradient values are also considerable. Moreover, a wide difference has been observed between the head gradient values (by decades) for cracks that have and have not been washed out. This pattern has also been observed during laboratory-based experiments on physical models [5, 21]. Virtually all head losses occur at the CCCD (for the ED type with a core of dam).

In case of crack formation in the CCCD (with due account, differing coefficient of permeability of downstream toes and transition zone material), substantial head losses in the crack area occur largely in the transition zone material, being aggravated at the initial stage of crack opening by discontinuities within the seepage area.

Thus, at the initial stage of crack formation in the CCCD, all ED head applies to the upstream transitional layer while generating pressure gradients with the values conforming to the head distribution diagram, with the head losses in the transitional layer and at the crack entrance. If the seepage flow integrity is maintained, head losses occur in the crack itself, at the crack exit and in the downstream transition zone material (Fig. 8, Line 2).

At this stage, which shall be designated as Stage 1, or Dynamic Stage, it may also be assumed that after crack formation in the CCCD the downstream transitional layer is also affected by the head, after losses in the transitional layer and in the CCCD crack. The head generates pressure gradients with the values conforming to the head distribution diagram, and the exit gradient values at the contact with the downstream toe depending on the width of the downstream transitional layer.

If the head gradients exceeding relevant critical values appear in the "self-healing layer - crack" contact area, the healing layer material loses its seepage strength under the weight of seepage flow, and fills the crack cavity. At this moment, due to the emerging seepage resistance in a washed out crack, the entrance pressure gradients reduce, in some instances until complete stop of the colmatage process. Thus, a new seepage area with new head gradient distribution is formed (Fig. 8, Line 3).

If we continue the analysis of seepage flow structure in the ED with CCCD, while the seepage area integrity is recovered according to the self-healing procedure, we shall obtain a new head distribution diagram for the ED. By indicating this status with a healed crack as Stage 2 or Static Stage, it is noted that virtually the entire head applies to the embankment dam section consisting of the upstream transition zone material, crack filling material and downstream transition zone material.

In the design of the transition zone, consideration shall be given to these two stages different in the following:

the first "dynamic" stage defines the possibility of seepage strength loss by the transition zone healing layer, and filling of the opening crack with its material, while maintaining the healing layer residual integrity on the upstream side and the seepage strength of the "downstream transitional layer - downstream toe material" contact under the increased head gradients;

the second "static" stage defines seepage strength of the ED section in the area of well-formed crack filling material protected by the downstream transition zone material on the downstream side.

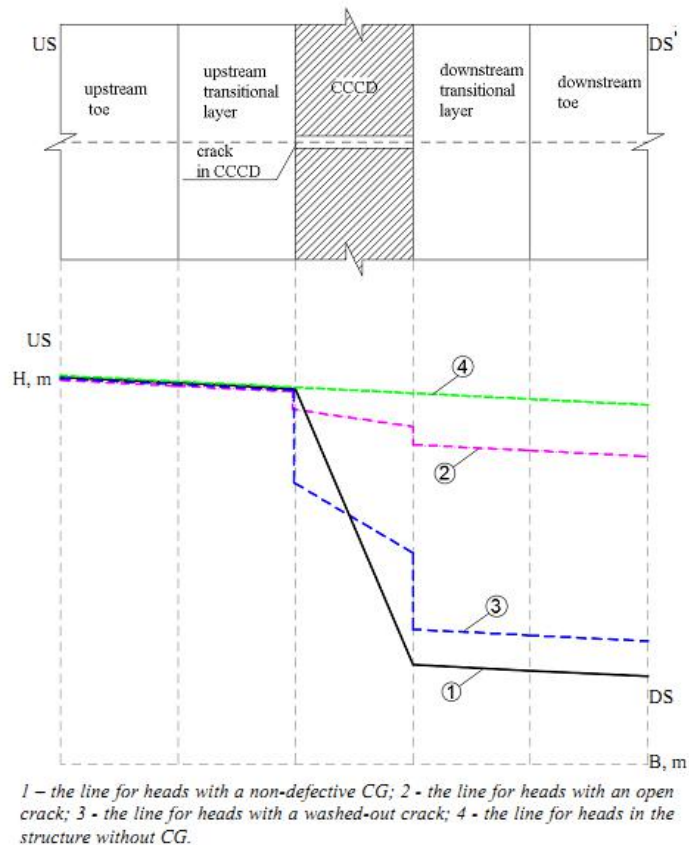


Figure 8. Head Patterns in the ED with CCCD

The general principles for design of transition zones in the ED with CCCD comply with the requirements to the transition zones and reverse filters of the embankment dam with impervious elements made of clayey materials, and are set out in [6, 23–27]. With due account for the nature of CCCD crack formation, and of the current head gradients at various sections of cracks and of the ED design in general, a number of special requirements to the design of the ED with CCCD and the CCCD “protection system”, which includes the healing layer and transition zones, may be formulated:

The healing layer material shall penetrate freely into the crack from the initial stage of its formation, i.e. penetrate into the finest cracks (1 mm and more), as it is these cracks that have the highest incoming head pressure gradients.

On the downstream side, the healing layer material filling the crack shall be sealed in the crack by a layer of reverse filter, i.e. the downstream transition zone material granulometric composition shall be selected so that the healing layer particles do not penetrate into the embankment dam downstream toe.

The healing layer thickness shall ensure filling up of the volume of formed cracks in the CCCD and prevent entrainment of the upstream transition zone material towards the crack to avoid crack clogging with coarse grain “coves”. The minimum healing layer thickness depends on its mechanized placing ability during the ED construction operations in the reverse filter area.

Reshaping of reverse filter layers on the upstream side shall not cause void formation and excessive deposits in the ridge area of the embankment dam.

According to the analysis of unique features of the “ED – CCCD” system operation: its stress-strain state, seepage flow structures at various stages of its life cycle, stated requirements to the healing material, a procedure for calculated justification of the design ensuring self-healing of cracks in CCCD was developed (Fig. 9).

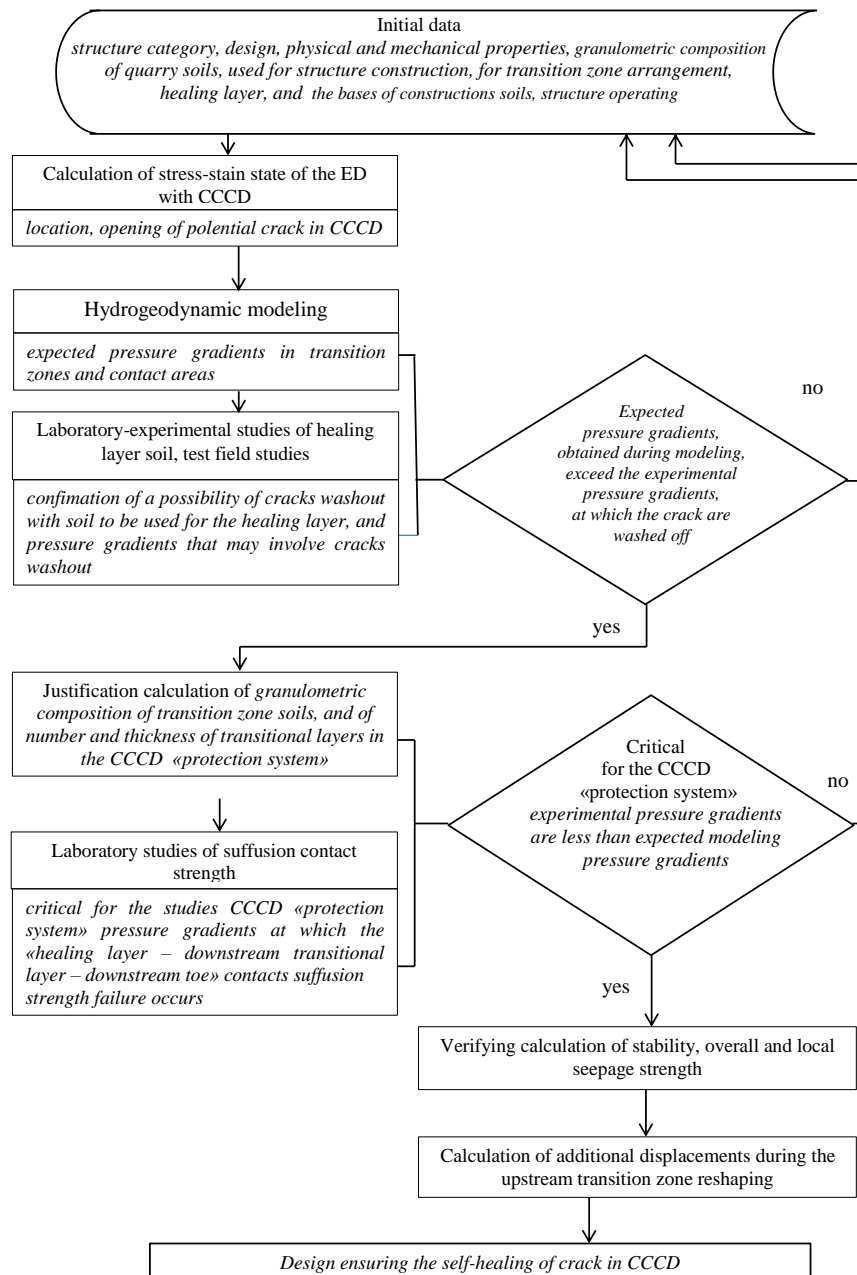


Figure 9. Block diagram of calculated justification of the design ensuring self-healing of cracks in the CCCD

4. Conclusions

The results was based of the simulation filtering in two-dimensional and three-dimensional analysis of fluid flow characteristics for embankment dams up to a height of 60 m with clay-cement-concrete diaphragms. Found that colmatage cracks in CCCD, the occurrence of which is possible in areas of tension or due to seismic effects, is almost complete (90 %) restoration of membrane properties of the diaphragm material specially selected to self-healing layer.

The proposed method of design-experimental substantiation of characteristics and parameters of transition layers. The method is a sequence of operations, determining methods of numerical simulation of pressure gradients in the transitional layers, and crack, rated selection of particle size distribution and the determination of the power transition layers of experimental verification of seepage-suffusion characteristics of selected materials and evaluate their bridging ability.

Presents the results of investigations contribute to the implementation in practice of hydrotechnical construction of new effective technologies of construction of the impervious elements from clay-cement-concrete in embankment dams.

References

1. Zhilenkov V.N. *Vodoupornyye svoystva gruntov yader i ekranov vysokikh plotin* [Waterproof properties of core and diaphragm soils of high dams]. Leningrad: Energia, 1968. (rus)
2. Ivanov N.N., Pravednyy G.Kh. The technique of laboratory experiments on the self-healing of cracks in clay kernels and screens of soil dams [Methods of laboratory experiments for self-healing of cracks in clayey cores and diaphragms of embankment dams]. *Proceedings of Conferences and Meetings on Hydraulic Engineering / B.E. Vedeneev VNIIG, JSC.* 1983. Pp. 136–139. (rus)
3. Solsky S.V., Lopatina M.G., Dombaska A. Laboratory Studies of Seepage Strength of Incoherent Rocks Thin Interlayers [Laboratornyye issledovaniya fil'tratsionnoy prochnosti tonkikh prosloyev nesvyaznykh gruntov]. *Izvestia of B.E. Vedeneev VNIIG, JSC.* 2015. Vol. 275. Pp. 59–68. (rus)
4. Nikbakhtan B., Osanloo M. Effect of grout pressure and grout flow on soil physical and mechanical properties in jet grouting operations. *International Journal of Rock Mechanics and Mining Sciences.* 2009. Vol. 46. No. 3. Pp. 498–505.
5. Solsky S., Beiendir E., Lopatina M. Filtration and suffusion studies of clay and cement concrete for antifiltration diaphragm of a subsurface dam. *Zapory-bezpieczenstwo i kierunki rozwoju. Instytut Meteorologii i Gospodarki Wodnej. Panstwowy Instytut Badawczy. Warszawa,* 2013. Pp. 17–25.
6. *Russian Set of Rules SP 39.13330.2012 Code of Practice: Rock Fill Dams. Updated Edition of SNiP 2.06.05-84**
7. Solsky S.V., Legina Ye.Ye., Orischuk R.N., Vasilieva Z.G., Velichko A.S. Analysis of the Impact of CCC components on its characteristics. *Vestnik MGSU.* 2016. No. 10. Pp. 80–93. (rus)
8. Joshi K. et al. Laboratory and in situ tests for long-term hydraulic conductivity of a cement-bentonite cutoff wall. *Journal of Geotechnical and Geoenvironmental Engineering.* 2009. Vol. 136. No. 4. Pp. 562–572.
9. Hong C.S., Shackelford C.D., Malusis M.A. Consolidation and hydraulic conductivity of zeolite-amended soil-bentonite backfills. *Journal of Geotechnical and Geoenvironmental Engineering.* 2011. Vol. 138. No. 1. Pp. 15–25.
10. Mahboubi A., Ajorloo A. Experimental study of the mechanical behavior of plastic concrete in triaxial compression. *Cement and Concrete Research.* 2005. Vol. 35. No. 2. Pp. 412–419.
11. Hinchberger S., Weck J., Newson T. Mechanical and hydraulic characterization of plastic concrete for seepage cut-off walls. *Canadian Geotechnical Journal.* 2010. Vol. 47. No. 4. Pp. 461–471.
12. Solsky S.V., Lopatina M.G., Legina Ye.Ye., Orischuk R.N., Orlova N.L. Results of laboratory studies of clay-cement concrete seepage characteristics [Rezultaty laboratornykh issledovaniy fil'tratsionnykh kharakteristik glinotsementobetonov]. *Hydrotechnical Construction.* 2016. No. 8. Pp. 36–40. (rus)
13. Prokopovich V.S., Velichko A.S., Orischuk R.N. Analysis of stress-strain state of embankment dam with CCCD [Napryazhenno-deformirovannoye sostoyaniye zemlyanoy plotiny s glinotsementobetonnoy diafragmoy na primere zemlyanoy plotiny Gotsatlinskoy GES]. *Izvestia of B.E. Vedeneev VNIIG, JSC.* 2016. Vol. 282. Pp. 87–98. (rus)
14. Sainov M.P. Analysis of the performance of a stone dam with a combination of anti-filtration elements - a reinforced concrete screen and a clay cement concrete wall. *Magazine of Civil Engineering.* 2016. No.4. Pp. 3–9.
15. Sainov M.P., Anisimov O.V. Stress-strain state of seepage-control wall constructed for repairs of earth rock-fill dam.

Литература

1. Жиленков В.Н. Водоупорные свойства грунтов ядер и экранов высоких плотин. Энергия, 1968. 113 с.
2. Иванов Н.Н., Праведный Г.Х. Методика лабораторных опытов по самозалечиваемости трещин в глинистых ядрах и экранах грунтовых плотин. ВНИИГ им. Б.Е. Веденеева, 1983. С. 136–139.
3. Сольский С.В., Лопатина М.Г., Домбска А. Лабораторные исследования фильтрационной прочности тонких прослоев несвязных грунтов // Известия ВНИИГ им. Б.Е. Веденеева. 2015. Т. 275. С. 59–68.
4. Nikbakhtan B., Osanloo M. Effect of grout pressure and grout flow on soil physical and mechanical properties in jet grouting operations // *International Journal of Rock Mechanics and Mining Sciences.* 2009. Vol. 46. No. 3. Pp. 498–505.
5. Solsky S., Beiendir E., Lopatina M. Filtration and suffusion studies of clay and cement concrete for antifiltration diaphragm of a subsurface dam // *Zapory-bezpieczenstwo i kierunki rozwoju // Instytut Meteorologii i Gospodarki Wodnej. Panstwowy Instytut Badawczy. Warszawa,* 2013. Pp. 17–25.
6. СП 39.13330.2012 Плотины из грунтовых материалов. Актуализированная редакция СНиП 2.06.05-84*
7. Сольский С.В., Легина Е.Е., Орищук Р.Н., Васильева З.Г., Величко А.С. Анализ влияния компонентов глиноцементобетона на его характеристики // Вестник МГСУ. 2016. Т. 10. С. 80–93.
8. Joshi K. et al. Laboratory and in situ tests for long-term hydraulic conductivity of a cement-bentonite cutoff wall // *Journal of Geotechnical and Geoenvironmental engineering.* 2009. Vol. 136. No. 4. Pp. 562–572.
9. Hong C.S., Shackelford C.D., Malusis M.A. Consolidation and hydraulic conductivity of zeolite-amended soil-bentonite backfills // *Journal of Geotechnical and Geoenvironmental Engineering.* 2011. Vol. 138. No. 1. Pp. 15–25.
10. Mahboubi A., Ajorloo A. Experimental study of the mechanical behavior of plastic concrete in triaxial compression // *Cement and concrete research.* 2005. Vol. 35. No. 2. Pp. 412–419.
11. Hinchberger S., Weck J., Newson T. Mechanical and hydraulic characterization of plastic concrete for seepage cut-off walls // *Canadian Geotechnical Journal.* 2010. Vol. 47. No. 4. Pp. 461–471.
12. Сольский С.В., Лопатина М.Г., Легина Е.Е., Орищук Р.Н., Орлова Н.Л. Результаты лабораторных исследований фильтрационных характеристик глиноцементобетона // Гидротехническое строительство. 2016. № 8. С. 36–40.
13. Прокопович В.С., Величко А.С., Орищук Р.Н. Напряженно-деформированное состояние земляной плотины с глиноцементобетонной диафрагмой на примере земляной плотины Готатлинской ГЭС // Известия ВНИИГ им. Б.Е. Веденеева. 2016. Т. 282. С. 87–98.
14. Саинов М.П. Анализ работоспособности каменной плотины с комбинацией противофильтрационных элементов – железобетонного экрана и глиноцементобетонной стены // Инженерно-строительный журнал. 2016. № 4(64). С. 3–9.
15. Саинов М.П., Анисимов О.В. Напряженно-деформированное состояние противофильтрационной стены, выполненной для ремонта каменно-земляной плотины // Инженерно-строительный журнал. 2016. № 8(68). С. 3–17.
16. Саинов М.П., Котов Ф.В. Напряженно-деформированное состояние и работоспособность высокой грунтовой плотины с инъекционной завесой //

- Magazine of Civil Engineering*. 2016. No. 8. Pp. 3–17.
16. Sainov M.P., Kotov F.V. Stress-strain state and performance of a high rockfill dam with a grout curtain. *Magazine of Civil Engineering*. 2017. No. 1. Pp. 44–55.
 17. Xiong H. et al. Stress deformation analysis of plastic concrete cut-off wall for the first stage cofferdam of Shawan hydropower station. *Journal of Hydroelectric Engineering*. 2010. Vol. 2. P. 035.
 18. Zheng S., Yaolong C., Shouyi L. Stress-deformation Analysis of Plastic Concrete Diaphragm Wall in Dam Foundation Earth-rockfill Dam [J]. *Water Power*. 2008. Vol. 2. P. 014.
 19. Rasskazov L.N., Radzinsky A.V., Sainov M.P. Dams with clay-cement concrete diaphragm stress-strain state and strength [Plotiny s glinotsementobetonnoy diafragmoy: napryazhenno-deformirovannoye sostoyaniye i prochnost']. *Hydrotechnical Construction*. 2014. No. 9. Pp. 37–44. (rus)
 20. Radchenko V.G., Lopatina M.G., Nikolaychuk Ye.V., Radchenko S.V. Experience of soil-cement mixture water-repellent barrier construction [Opyt vozvedeniya protivofiltratsionnykh ustroystv iz gruntosementnykh smesey]. *Hydrotechnical Construction*. 2012. No. 6. Pp. 46–54. (rus)
 21. Solsky S.V., Orischnik R.N., Lopatina M.G., Orlova N.L. Study of crack self-healing in clay-cement concrete diaphragms (using the example of Gotsatlinskaya HPP) [Issledovaniye samozalechivaniya treshchin v glinotsementobetonnykh diafragmakh (na primere zemlyanoy plotiny Gotsatlinskoy GES)]. *Izvestia of VNIIG*. 2017. Vol. 283. Pp. 19–29. (rus)
 22. Solsky S.V., Lopatina M.G., Orischnik R.N., Frolova L.A., Savelieva Yu.Yu. Analysis of seepage flow structure in clay-cement concrete diaphragm of Gotsatlinskaya HPP [Analiz struktury filtratsionnogo potoka v glinotsementobetonnoy diafragme plotiny Gotsatlinskoy GES]. *Hydrotechnical Construction*. 2017. No. 7. Pp. 14–21. (rus)
 23. Huang J., Han J. 3D coupled mechanical and hydraulic modeling of a geosynthetic-reinforced deep mixed column-supported embankment. *Geotextiles and Geomembranes*. 2009. Vol. 27. No. 4. Pp. 272–280.
 24. Luo Z.J., Zhang Y.Y., Wu Y.X. Finite element numerical simulation of three-dimensional seepage control for deep foundation pit dewatering. *Journal of Hydrodynamics*. 2008. Vol. 20. No. 5. Pp. 596–602.
 25. *Recommendations on Design of Reverse Filters for Hydraulic Engineering Structures*. St. Petersburg: VNIIG, 1991. Pp. 56–90.
 26. Nikbakhtan B., Osanloo M. Effect of grout pressure and grout flow on soil physical and mechanical properties in jet grouting operations. *International Journal of Rock Mechanics and Mining Sciences*. 2009. Vol. 46. No. 3. Pp. 498–505.
 27. *Recommendations on Design of Transition Zones of Embankment -and-Rock-Fill Dams*. Leningrad, VNIIG, 1989. Pp. 35–87.
 - Инженерно-строительный журнал. 2017. № 1(69). С. 44–55.
 17. Xiong H. et al. Stress deformation analysis of plastic concrete cut-off wall for the first stage cofferdam of Shawan hydropower station // *Journal of Hydroelectric engineering*. 2010. Vol. 2. P. 035.
 18. Zheng S., Yaolong C., Shouyi L. Stress-deformation Analysis of Plastic Concrete Diaphragm Wall in Dam Foundation Earth-rockfill Dam [J] // *Water Power*. 2008. Vol. 2. P. 014.
 19. Рассказов Л.Н., Радзинский А.В., Саинов М.П. Плотины с глиноцементобетонной диафрагмой: напряженно-деформированное состояние и прочность // *Гидротехническое строительство*. 2014. № 9. С. 37–44.
 20. Радченко В.Г., Лопатина М.Г., Николайчук Е.В., Радченко С.В. Опыт возведения противofiltrационных устройств из грунтоцементных смесей // *Гидротехническое строительство*. 2012. № 6. С. 46–54.
 21. Сольский С.В., Орищук Р.Н., Лопатина М.Г., Орлова Н.Л. Исследование самозалечивания трещин в глиноцементобетонных диафрагмах (на примере земляной плотины Гоцатлинской ГЭС) // *Известия ВНИИГ им. Б.Е. Веденеева*. 2017. Т. 283. С. 19–29.
 22. Сольский С.В., Лопатина М.Г., Орищук Р.Н., Фролова Л.А., Савельева Ю.Ю. Анализ структуры фильтрационного потока в глиноцементобетонной диафрагме плотины Гоцатлинской ГЭС // *Гидротехническое строительство*. 2017. № 7. С. 14–21.
 23. Huang J., Han J. 3D coupled mechanical and hydraulic modeling of a geosynthetic-reinforced deep mixed column-supported embankment // *Geotextiles and Geomembranes*. 2009. Vol. 27. № 4. Pp. 272–280.
 24. Luo Z.J., Zhang Y.Y., Wu Y.X. Finite element numerical simulation of three-dimensional seepage control for deep foundation pit dewatering // *Journal of Hydrodynamics*. 2008. Vol. 20. № 5. Pp. 596–602.
 25. Рекомендации по проектированию обратных фильтров гидротехнических сооружений. ВНИИГ, Санкт-Петербург, 1991. С. 56–90.
 26. Nikbakhtan B., Osanloo M. Effect of grout pressure and grout flow on soil physical and mechanical properties in jet grouting operations // *International Journal of Rock Mechanics and Mining Sciences*. 2009. Vol. 46. № 3. Pp. 498–505.
 27. Рекомендации по проектированию переходных зон Каменно-земляных плотин. ВНИИГ, Санкт-Петербург, 1989. С. 35–87.

Stanislav Solsky,
+7(921)964-36-05; solsky@yandex.ru

Natalia Orlova,
+7(911)256-00-39; ornata.76@mail.ru

Aleksey Velichko,
+7(981)124-64-63; aleksej.velichko.26@mail.ru

Станислав Викторович Сольский,
+7(921)964-36-05; эл. почта: solsky@yandex.ru

Наталья Леонидовна Орлова,
+7(911)256-00-39; эл. почта: ornata.76@mail.ru

Алексей Сергеевич Величко,
+7(981)124-64-63;
эл. почта: aleksej.velichko.26@mail.ru

© Solsky S.V., Orlova N. L., Velichko A.S., 2018

doi: 10.18720/MCE.77.2

Method for noise calculation under specular and diffuse reflection of sound

Метод расчета шума при зеркально-рассеянном отражении звука

B.I. Giyasov,
Moscow State University of Civil Engineering
National Research University (MGSU), Moscow,
Russia

V.I. Ledenyov ,
I.V. Matveeva ,
Tambov State Technical University, Tambov,
Russia

Канд. техн. наук, заведующий кафедрой
Б.И. Гиясов,

Национальный исследовательский
Московский государственный
строительный университет (МГСУ),
г. Москва, Россия

д-р техн. наук, профессор В.И. Леденев,
канд. техн. наук, доцент И.В. Матвеева,
Тамбовский государственный технический
университет, г. Тамбов, Россия

Key words: production buildings; noise; noise protection measures; noise calculation method; sound reflection from barriers

Ключевые слова: производственные здания; шум; шумозащитные мероприятия; метод расчета шума; отражение звука от ограждений

Abstract. Selection and designing of noise protection aids in industrial buildings require numerous calculations of energy characteristics typical for noise fields of their facilities. The efficiency of designed soundproof measures is relying on their accuracy. The degree of accuracy is defined by recording completeness in the method of measurement of factors, which affect the processes of noise fields in buildings. One of these factors is the type of sound reflection from barriers. The analysis of reflected sound energy distribution revealed that sound reflection in industrial buildings follows mirror-scattered pattern. It forms two reflected fields, mirror-like and diffusely scattered, where reflected sound energy originates and propagates on different principles. The paper offers a combined method for calculation of energy characteristics of such fields; specular reflected energy is calculated by ray tracing, and diffusely scattered one is calculated by a numerical energy method. The paper describes the basic principles for making the combined design model and offers scattering factors of reflexible sound energy that are necessary for the implementation of design model and were obtained from experiments and calculations. The accuracy of the combined method was assessed by a comparative analysis, and experimental and calculation data in production facilities of various proportions. Disagreement between calculations and experiments did not exceed 2 dB. The method fits for solving problems of construction acoustic aids of noise reduction in industrial buildings. Unlike the existing methods, in the proposed method the real process of gradual transition from emerging mirror-reflected energy to diffusely dispersed energy is modeled. At the same time, the method takes into consideration certain acoustic characteristics of each section of enclosure such as sound attenuation coefficient and reflection coefficient. In the suggested form the method allows making calculations of noise in the buildings with any complex space-planning parameters.

Аннотация. При выборе и проектировании средств шумозащиты в производственных зданиях выполняются многократные расчеты энергетических характеристик шумовых полей помещений. От их точности зависит эффективность проектируемых шумозащитных мер. Степень точности определяется полнотой учета в методе расчета факторов, влияющих на процессы формирования шумовых полей в помещениях. Одним из них является характер отражения звука от ограждений. В результате анализа распределения отраженной звуковой энергии установлено, что в производственных помещениях отражение звука имеет зеркально-рассеянный характер. В этом случае в них образуются два отраженных поля – зеркальное и диффузно рассеянное, имеющие разные принципы возникновения и распространения отраженной звуковой энергии. Для расчета энергетических характеристик таких полей в статье предложен комбинированный метод расчета, в котором зеркально отражаемая энергия рассчитывается методом прослеживания лучей, а диффузно рассеянная – численным энергетическим методом. Изложены все основные

Гиясов Б.И., Леденев В.И., Матвеева И.В. Метод расчета шума при зеркально-рассеянном отражении звука // Инженерно-строительный журнал. 2018. № 1(77). С. 13–22.

принципы построения комбинированной расчетной модели и приведены необходимые для реализации расчетной модели коэффициенты рассеяния отражаемой звуковой энергии, полученные в работе экспериментально-расчетным путем. Точность предложенного комбинированного метода оценена путем сравнительного анализа экспериментальных и расчетных данных в производственных помещениях различных пропорций. В отличие от существующих методов в предложенном методе моделируется реальный процесс постепенного перехода возникающей зеркально отраженной энергии в диффузно рассеянную. При этом метод учитывает конкретные акустические характеристики каждого участка ограждений, а именно его коэффициент звукопоглощения и коэффициент отраженной звуковой энергии. В предложенной форме метод позволяет производить расчеты шума в помещениях с любыми сложными объемно-планировочными параметрами.

1. Introduction

Acoustic and economic efficiencies of selecting and designing noise protection aids in industrial buildings depend on the accuracy of calculation methods for noise characteristics that are used for the assessment of noise energy distribution before and after probable use of noise protection aids in industrial buildings. Reliability of noise energy distribution calculation method rests on the extent of the factors that influence the formation of noise fields in the facilities [1]. The most important factor is the type of sound reflection from barriers: it influences the accuracy of the calculation method. Calculation results agree with experimental data when the type of sound reflection adopted for the method fits actual conditions of its reflection from the. On the contrary, results are unsatisfactory when actual reflection disagrees with the one adopted for design model [1].

Sound reflection from barriers depends on complicated dimensional dependencies that rely on the surface shape, material structure, angle of sound incidence and other parameters. This makes exact description of type of the sound reflection from barriers a problem difficult to solve [2]. The existing method of calculations uses two ideal models of sound reflection – mirror-like and diffuse ones.

Mirror reflection is considered to observe the equality between incidence and reflection angles of sound rays from barriers. It is encountered when sound reflects from surfaces of size much greater than the length of waves that fall on them, whose irregularities are much smaller than the lengths [2, 3]. Now, mirror sound reflection from barriers can be found in design models based on geometric theory of facilities acoustics [4, 5]. Such models calculate noise via the method of apparent sources with its main provisions established in the first half of the 20th century [6], and the ray tracing method, M. Schreder offered initially for research of halls acoustics [7], and later adapted it to other problems, including noise calculation in industrial facilities [8].

The practice of noise calculations for industrial buildings most often uses design models and appropriate methods of implementation based on vision of diffuse type of sound reflection from barriers. Diffuse reflection implies total dissipation of reflected energy in accordance with the directional pattern that cosine dependence approximates by Lambert law. In terms of design models based on distribution of reflected sound energy, two design models appear definable. The first one employs classical theory of diffused sound field, that obeys the conditions of energy distributing uniformly throughout the volume of the facility and isotropic arrival of reflected sound rays to any point of the facility [9, 10]. This model is a base for developing statistic methods for solving practical problems of noise control in buildings with proportional facilities, e.g. in residential buildings [11, 12]. The second one rests on the notion that diffused sound reflection creates quasi-diffused sound fields in the facilities; they, unlike ideal diffused fields do not obey the feature of uniform energy distribution in the volume, but do keep the feature of isotropic angular directivity of sound rays that arrive to any point of the volume [13]. Such fields are formed in industrial facilities of large volume. As directed flows of reflected sound energy exist in quasi-diffused fields, the methods developed for noise calculations are based on statistical energy approach to estimation of reflected sound fields [14]. These methods are used in solving the practical problems at manufacturing companies, buildings and facilities of various purpose [15, 16].

Similar energetic approach to estimation of reflected sound energy distribution in facilities is also used in foreign practice [17–23]. In [17–23], a mathematical model for the distribution of sound energy in rooms with diffuse reflection of sound from walls is used. It is based on the idea that particles diffuse in a medium containing spherical scattering objects, and the assumption that the density gradient of the reflected sound energy and the density of its flux in the reflected sound field have a stable connection. The studies confirmed the possibility of using this model to solve various practical problems.

We analyzed the influence the type of sound reflection from barriers has on the accuracy of calculation methods. Comparing the calculations obtained by methods that employ mirror and diffused

models of reflection with the data of experiments held in production facilities of various proportions and various sound absorbing characteristics showed that the actual nature of sound reflection carries traits of both mirror-like and diffused models of reflection. It was found that, as compared to the experimental data, the calculated levels of sound pressure in the mirror model were higher in the area furthest from the source, while in the diffused model, they were lower.

From the results of this comparative analysis, we found the necessity of a new method of calculation that would employ a mixed mirror-diffused model of sound reflection, when one part of energy is reflected under the mirror model, while the other one is scattered diffusely under the Lambert's law.

As a result, a reflected sound field of the facility forms two components for the reflected energy density, mirror-like and diffused, that obey different laws of formation. Mirror component depends on reflections of mirror-like part of rays, while the diffused one depends on the part of energy that converts into diffused energy while reflection of rays. The mirror component is defined by reflections of mirror-like elements of the rays, and diffusive element is defined by energy which transits at reflections of mirror rays from enclosures to dispersed energy. Thus, the calculation of energy characteristics of such a field needs the method for separate finding of mirror-like and diffused components. The process should consider for continuous transition of some mirror energy to diffused energy. Finally, the calculated levels of sound pressure are to be found from superposition principle from the sum of densities of direct sound energy, mirror and diffused components of reflected energy density:

$$L_i = 10 \lg \left[(\varepsilon_i^{dir} + \varepsilon_i^{mir} + \varepsilon_i^{dif}) c / I_0 \right], \quad (1)$$

where ε_i^{dir} , ε_i^{mir} , ε_i^{dif} are densities of direct sound energy, mirror-like and diffused components of reflected sound energy in i -th designed point of the facility volume; I_0 means intensiveness of sound at the threshold of hearing; c means velocity of sound in the air.

According to the above, the article aims to develop a noise calculation method, which takes into consideration a mirror-dispersed type of sound reflection from enclosure. During its development the following tasks were accomplished: the accounting model for forming of the reflected sound field was proposed; this model also takes into consideration the constant transition of mirror-reflected energy to diffusely scattered energy; the definition of the coefficient of dispersion of energy reflected from enclosure for typical groups of industrial buildings was done by experimental calculations, the experimental assessment of the combined method by comparing the results of experiments and calculations in production buildings of various geometrical proportions was made.

A practical use of the combined method is supported with the computer program that can estimate noise mode in facilities and acoustic efficiency of noise reduction aids designed.

2. Methods

In the combined method offered, densities of direct sound and mirror-like component are calculated with a ray tracing method. The method has been selected because it finds direct and reflected energies as well as the part of the energy that converts into diffused energy during reflections of mirror rays. A diffused component of reflected energy is calculated with numerical statistical energy method, developed earlier for estimation of diffusely reflected energy distribution in a quasi-diffused sound field [13, 14].

The backbone of the combined calculation method consists in the following.

A sound source, in accordance with its directional pattern, irradiates the amount of rays found probabilistically, each of them carrying a part of sound energy of the source. Each ray is tracked up to a calculated point with account to its contacts with barrier surfaces. During reflection from surface, the part of energy remained after ray energy absorption reflects under mirror law, while other follows diffused Lambert's law. The energy reflected under the mirror law is tracked until the next act of reflection, when, after reflection, mirror energy converts into diffused one. Each ray is tracked until it completely loses its energy due to absorption at surfaces, attenuation in the air and conversion of some mirror energy into diffused one. Thus, all rays that come from the source are tracked, with summarized direct and mirror reflected energies of all rays that pass the calculated point. Energy distribution of diffusely scattered rays is estimated with numerical statistical energy method. What follows are the main principles of plotting the combined calculation method.

As numerical method is employed for the calculation of diffused component of reflected energy, at first all the volume of facility is broken down elementary volumes, where the nature of diffusely reflected energy density's change can be accepted as linear [13].

Then, densities of direct sound energy ε_i^{dir} and of mirror reflected energy ε_i^{mir} , that arrive to each i -th elementary volume, can be obtained from the formulas

$$\varepsilon_i^{dir} = \sum_{k=1}^K W_{ki}^{dir} / cS_{red}, \quad (2)$$

$$\varepsilon_i^{mir} = \sum_{k=1}^K W_{ki}^{mir} / cS_{red}, \quad (3)$$

where W_{ki}^{dir} is an energy of direct sound each k -th ray transmits per a unit of time into i -th elementary volume

$$W_{ki}^{dir} = \frac{W}{N} \exp(-m_a R_{ki}), \quad (4)$$

W_{ki}^{mir} is a sound energy brought per a unit of time by each k -th mirror reflected ray that enters the i -th volume

$$W_{ki}^{mir} = \frac{W}{N} \exp(-m_a R_{ki}) \prod_{p=1}^P [(1-\alpha_p)(1-\beta_p)]^{D_p}, \quad (5)$$

W is sound power of the source, W ; N is a number of rays going out of the source; m_a is space coefficient of sound attenuation in the air, m^{-1} ; R_{ki} is a distance k -th ray passes from between the sound source and the i -th elementary volume, m ; α_p is a coefficient of sound absorption of p -th barrier surface, to where the tracked ray fell; P is a total amount of reflection acts of k -th ray from all surfaces it encounters during propagation to distance R_{ki} up to i -th elementary volume; D_p is number of incident acts of k -th ray to p -th surface during its propagation to distance R_{ki} ; β_p is a part of mirror diffusely scattered energy of k -th ray after its reflection from p -th surface of barrier; k is a number of rays that pass through the elementary volume; S_{red} is a reduced sectional area of elementary volume. In case, when all the volume of the facility is broken down elementary volume shaped as cubes or parallelepiped, square S_{red} is taken as a square of cross section of the sphere equal in volume to elementary cube or parallelepiped.

Density of diffusely reflected energy ε_i^{dif} in the combined method is calculated with the numerical energy method that implements a mathematical model presenting distribution of density energy in quasi-diffused sound field as an equation of second order partial derivatives

$$\eta \nabla^2 \varepsilon^{dif} - c m_a \varepsilon^{dif} = 0 \quad (6)$$

with boundary conditions

$$\bar{q}|_{dS} = \beta(1-\alpha)I|_{dS} - \frac{c \cdot \alpha}{2(2-\alpha)} \varepsilon^{dif} \Big|_{dS}. \quad (7)$$

In expressions (6) and (7), $\eta = 0.5cl_{cp}$ a coupling coefficient for flow density and density gradient of diffusely reflected energy in quasi-diffused sound field [13]; l_{cp} is a length of mean free run of diffusely reflected sound rays; α , β are coefficients of sound absorption and scattering of mirror energy at the considered element of dS surface; I is intensiveness of direct and reflected mirror sound energy with regard to incident angle of sound rays that fall on element dS .

The first member in the right part of boundary conditions (7) define entering of diffusely scattered energy into the volume of facility from the surface of element dS when mirror rays fall on it. The second member define intensiveness of absorption of diffusely scattered energy that falls on element dS .

In the case of a numerical decision of equation (6) with boundary conditions (7) each elementary volume $V_{i,j,d}$ (see Figure 1) receives an equation for balance of diffusely reflected sound energy per unit of time. Total distribution of density of diffusely reflected energy is obtained by doing the system of algebraic equations.

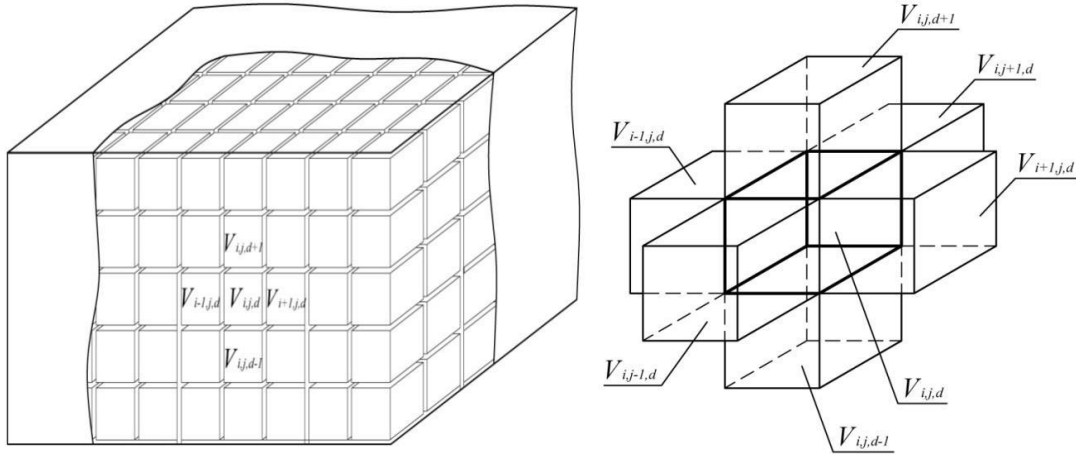


Figure 1. Patterns of facility breaking into elementary volumes

Balance of reflected energy for each i,j,d -th elementary volume with regard to absorption of sound in the air is generally written as

$$\sum_{n=1}^N q_n S_n + \sum_{m=1}^{6-N} W_m^{dif} - \sum_{m=1}^{6-N} q_{(\alpha)m} S_m - cm_a \varepsilon_{i,j,d}^{dif} V_{i,j,d} = 0. \quad (8)$$

Here, q_n is densities of diffused energy flows between i,j,d -th volume and adjacent contacting volumes through surfaces S_n , that connect them, W/m^2 ; W_m^{dif} is a diffuse component of sound energy that enters i,j,d -th volume after reflection of rays from m -th surface of this volume of square S_m , being barrier surface of facility, W ; $q_{(\alpha)m}$ is a density of diffuse energy flow that is absorbed at m -th surface of i,j,d -th volume, being a barrier surface for the facility of square S_m , W/m^2 ; N is a number of elementary volumes that contact with i,j,d -th volume; $6-N$ man a number of facets of i,j,d -th volume, being barrier surface of the facility; $V_{i,j,d}$ is a volume of an elementary parallelepiped, m^3 ; $\varepsilon_{i,j,d}^{dif}$ is a density of diffusely reflected energy in i,j,d -th volume, J/m^3 .

For the inner volume not contacting with barriers and equipment, the balance of reflected energy is written as

$$\sum_{n=1}^6 q_n S_n - cm_a \varepsilon_{i,j,d}^{dif} V_{i,j,d} = 0. \quad (9)$$

Final members of equations (8) and (9) show losses of energy in i,j,d -th volume because of its absorption in the air.

Densities of energy flows q_n are defined as

$$q_n = -\eta (\varepsilon_{i,j,d}^{dif} - \varepsilon_n^{dif}) / h_n. \quad (10)$$

where index $n \in \{i-1, j, d; i+1, j, d; i, j-1, d; i, j+1, d; i, j, d-1; i, j, d+1\}$; h_n means a distance between centers of i,j,d -th volume and contacting volumes in direction characterized by index n .

Density of flows $q_{(\alpha)m}$ is obtained from the formula

$$q_{(\alpha)m} = \frac{\alpha_m \cdot c \varepsilon_{i,j,d}^{dif}}{2(2 - \alpha_m)}, \quad (11)$$

where α_m means coefficient of sound absorption of m -th surface i,j,d -th volume.

Value W_m^{dif} is a sum of energies of rays that converted to reflected diffused component when rays reflect from m -th surface i,j,d -th volume, that make a part of facility barrier surface. In accordance with formulas (4) and (5) and given the ray incidence angle on the surface, W_m^{dif} is calculated by the formula

$$W_m^{dif} = \beta_m (1 - \alpha_m) \left[\sum_{k=1}^K \frac{W}{N} \exp(-m_a R_{ki,j,d}) \cos \theta_{mi,j,d} + \sum_{k=1}^K \frac{W}{N} \exp(-m_a R_{ki,j,d}) \cos \theta_{mi,j,d} \prod_{p=1}^P [(1 - \alpha_p)(1 - \beta_p)]^{D_p} \right], \quad (12)$$

where K is a number of direct rays or mirror reflected rays, that fell on m -th surface i,j,d -th volume, being a barrier surface; β_m is a portion of diffusely scattered energy of k -th ray after its reflection from m -th barrier surface i,j,d -th volume; $\theta_{mi,j,d}$ is an incident angle of k -th ray that falls on m -th surface in i,j,d -th volume.

A complicated problem in use of combined method of calculation consists in finding the scattering coefficient of reflected sound energy β . We based on experimental research and appropriate calculations to set coefficients β for typical groups of facilities in production buildings (see Table 1). Similar research is now being held for other groups of industrial and civil buildings not included in Table 1.

Table 1. Recommended values of scattering coefficients β

No.	Characteristics of the facility	Examples of facilities	Scattering coefficient
1	Empty facilities and facilities of simple shape with flat containing surfaces	Air ducts, channels, crosses, tunnels	0.1
2	Empty facilities with forms of facility slightly distorted from flat surfaces	Corridors, empty facilities without equipment	0.2
3	Facilities of simple form with flat ceiling and equipment installed	Production facilities in multistoreyed buildings	0.3-0.4
4	Facilities with complicated ceiling and equipment installed	Production facilities in onestoreyed buildings	0.5-0.8
5	Facilities of complicated form with many equipment, including large-size pieces, and scattering elements at the ceiling	Production facilities in onestoreyed buildings	0.9-1.0

3. Results and Discussion

To estimate the accuracy of the combined method offered, we did a comprehensive comparative analysis of experimental and calculated data in industrial facilities of various proportions.

The experimental research was held in proportional facilities that, in accordance with [5] have not more than 5 ratio between the largest and the smallest size, in long facilities where ratio between length D , height H and width G make $D/H > 5$, $G/H < 4$, and in flat facilities with $D/H > 5$, $G/H \geq 4$ size ratio. All facilities were of regular rectangular shape. During experiment, long facilities contained no equipment. Proportional and flat facilities had several pieces of equipment.

The hardware support of experiments included sources of sound energy, a set of noise metering instruments and metering equipment for reverberation time. The experiment employed noise source IOSh-1A produced by Etalon plant, and omnidirectional sound source (dodecahedron) OED-P-012-600. Sound power of source IOSh-1A in frequency range 63-8000 Hz was not less than 80 dB, dodecahedron power was 90 dB and more. Directivity index of sources was not more than ± 5 dB. Some measurements were made with the equipment by Bruel & Kjaer, while other measurements were made with the equipment by Kompania OKTAVA+ OOO that affords recording and analysis of time and energy characteristics of noise in the facilities. The measurement methods of sound pressure levels agreed with GOST 12.1.050-86. The number and layout of measurement points in facilities fit the requirements of reflected energy distribution analysis in terms of sound reflection type and facilities proportions influence on it.

The calculations were made by the specially designed computer program that can apply combined method for calculations with any values of β in the range between $\beta=0$ (fully mirror reflection) and $\beta=1.0$ (fully diffused scattering).

The analysis proved that in proportional facilities noise may be calculated with methods that employ both mirror and diffused reflection of sound from barriers. Results of calculations with statistic and geometry methods agree with experimental data. The example is shown in Figure 2. It is seen that experimental and calculated data in the zone furthest from the noise source differ not more than ± 1.5 dB. Potential analysis of geometry method for rays tracking and numerical statistical energy method proves

Giyasov G.B., Ledenyov L.V., Matveeva M.I. Method for noise calculation under specular and diffuse reflection of sound. *Magazine of Civil Engineering*. 2018. No. 1. Pp. 13–22. doi: 10.18720/MCE.77.2.

that in proportional facilities of complicated forms or when numerous repetitive calculations are required, numerical method is more attractive in terms of efficiency, as it offers faster performance (see Figure 2) for the same accuracy.

Figure 3 shows the results of calculations and an experiment held in long facilities of corridor type. It can be seen that for mirror model of reflection ($\beta=0$) calculations are much higher, and for diffused model ($\beta=1$) they are much lower. The results closest to the experiment were obtained for mirror-diffused reflection, when $\beta=0.2$, that fits well with the data of Table 1.

Calculated characteristics and experimental levels of sound pressure obtained in typical flat facility without equipment are shown in Figure 4. It is seen that like in case of long facilities, the mirror model of reflection increases calculated levels, while diffused model reduces them. As before, the calculation with mirror-diffused reflection with $\beta=0.2$ brings the most satisfactory results.

Generally, the results of the comparative analysis demonstrate that evaluation of the noise mode required the calculation methods that are based on the mirror-diffused reflection of sound from barriers and, in particular, the combined method of calculation presented in this paper.

The suggested method is substantially different from the previously developed accounting models based on formal combinations of geometrical and statistical methods: they offered using the imaginary source method, which takes into account the remaining part of reflected energy [13]. Such approach was also suggested in foreign practice [24, 25]. In this case, to define the first reflection the method of ray tracing is used instead of the imaginary source method. The said methods formally consider the separation of mirror- and diffusely reflected energy and, accordingly, their accuracy is defined by the accuracy of this separation. Unlike them, in the suggested combined method the constant process of transition of the mirror energy to energy dispersed at certain parts of enclosure while taking into account their position regarding the noise source and acoustic characteristics of the surface is shown. Numerical realization of the combined accounting model allows conducting calculations for buildings of any complexity.

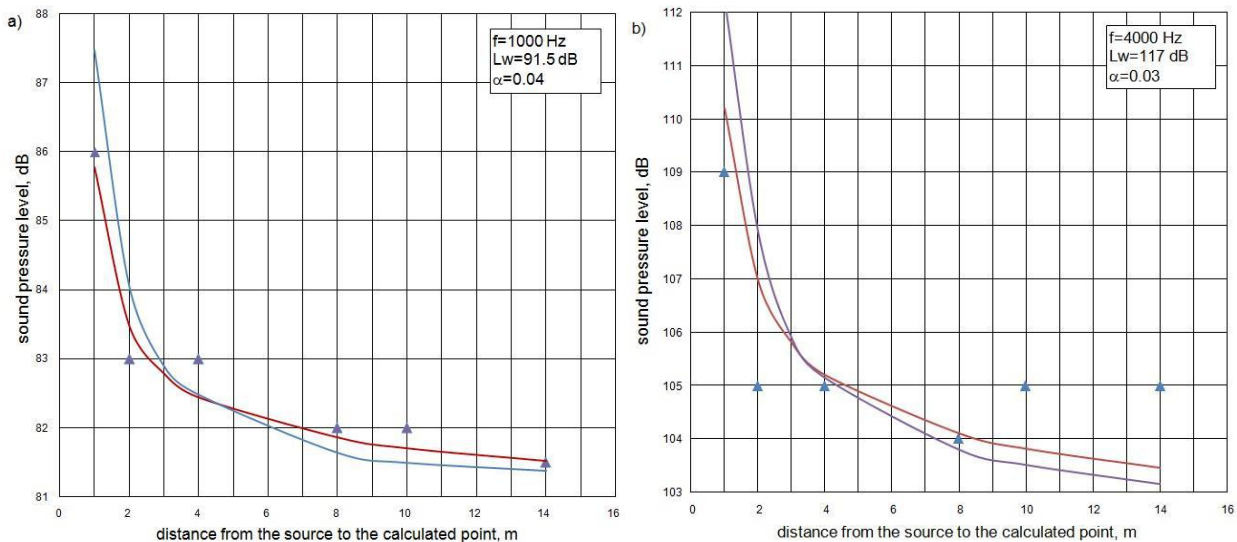


Figure 2. Experimental and calculated levels of sound pressure in proportional 18×15×4.5 m facility: ▲ – experimental data; — (red) – calculation with $\beta=1$ (fully scattered reflection); — (blue) – calculation with $\beta=0$ (fully mirror reflection)

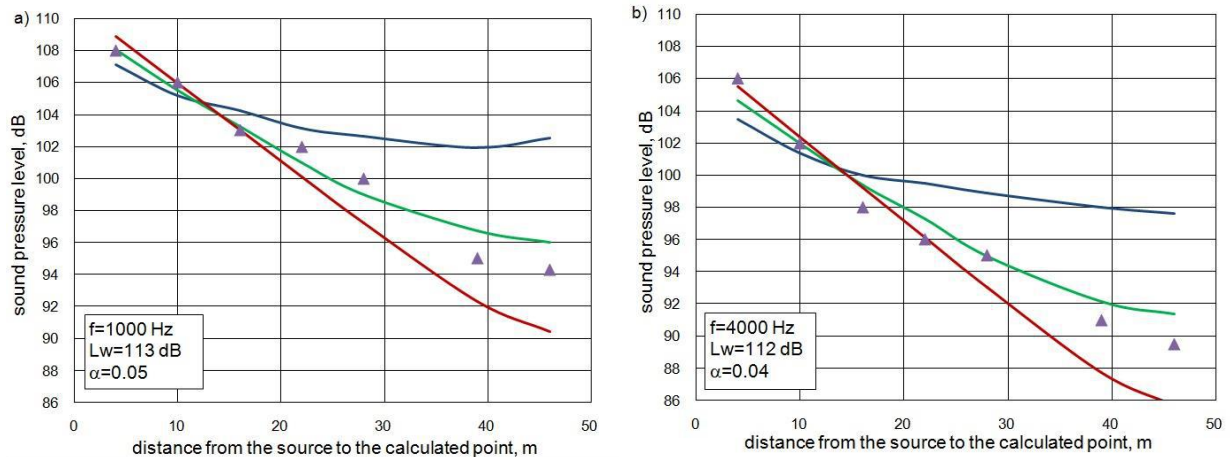


Figure 3. Experimental and calculated levels of sound pressure in long 49.6×2.5×3.5 m facility:
 ▲ – experimental data; — (red) – calculation with $\beta=1$ (fully scattered reflection);
 — (blue) – calculation with $\beta=0$ (fully mirror reflection);
 — (green) – calculation with $\beta=0.2$ (mirror-diffused model of reflection)

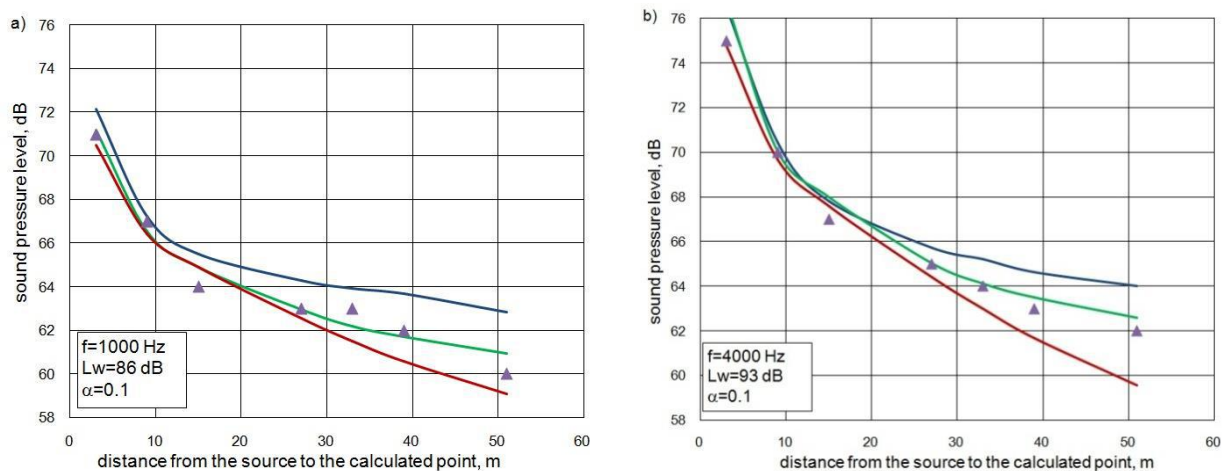


Figure 4. Experimental and calculated levels of sound pressure in flat 72×36×6 m facility:
 ▲ – experimental data; — (red) – calculation with $\beta=1$ (fully scattered reflection);
 — (blue) – calculation with $\beta=0$ (fully mirror reflection);
 — (green) – calculation with $\beta=0.2$ (mirror-diffused model of reflection)

4. Conclusions

The research done and the results obtained lead to the following conclusions:

1. The accuracy in the calculating levels of sound pressure in facilities depend on the extent the calculation method accounts for the actual type of sound reflection from barriers. In industrial facilities, the sound reflection from barriers has distinctive mirror-diffused type.

2. Calculation of noise in industrial facilities with mirror-diffused type of sound reflection requires the use of the developed combined method of calculations based on the ray tracing method for estimation of mirror energy distribution, and the numerical statistical energy method for estimation of diffused-scattered energy.

3. The accuracy of the combined calculation method depends largely on the reliability of finding the scattering coefficient β . Its value depends on the structure of the enclosure surfaces, on the presence in the premises of the sound-scattering equipment, the shape and proportions of the rooms. This paper gives values of scattering coefficients β for the most typical groups of production facilities. An additional research of values β for other groups of facilities not mentioned in the Table 1 is required.

4. The method offered and the software for its implementation can estimate noise mode in production facilities for any scattering coefficient β in the range between $\beta=0$ (fully mirror scattering) and $\beta=1$ (fully diffused scattering). Error for calculation of the most difficult cases is not more than ± 2.0 dB that

Giyasov G.B., Ledenyov L.V., Matveeva M.I. Method for noise calculation under specular and diffuse reflection of sound. *Magazine of Civil Engineering*. 2018. No. 1. Pp. 13–22. doi: 10.18720/MCE.77.2.

fits the required accuracy of practical calculations for estimation of noise mode and development of construction-acoustic aids of noise reduction in production buildings.

References

1. Antonov A.I., Batsunova A.V., Shubin I.L. Usloviya, opredelyayushchie protsessy formirovaniya shumovogo rezhima v zamknutykh ob'emakh, i ikh uchet pri otsenke raspredeleniya zvukovoy energii v pomeshcheniyakh [Conditions that determine the processes of formation of the noise regime in closed volumes, and their accounting for the evaluation of the distribution of sound energy in the premises]. *Privolzhsky Scientific Journal*. 2015. No. 3(35). Pp. 89–96. (rus)
2. Skuchik E. *Osnovy akustiki* [Basics of acoustics]. Moscow: Foreign Literature Publishing House, 1959. Vol.2. 565 p. (rus)
3. Leyzer I.G. O primenimosti metodov geometricheskoy akustiki dlya rascheta otrazheniy zvuka ot ploskikh poverkhnostey [On the applicability of geometric acoustics methods for calculating sound reflections from planar surfaces]. *Acoustic journal*. 1966. Vol. XII. No. 2. Pp. 206–212. (rus)
4. Antonov A.I. Matematicheskoe modelirovanie protsessov rasprostraneniya zvukovoy energii v zdaniyakh [Mathematical modeling of sound energy propagation in buildings]. *Problems of Contemporary Science and Practice. Vernadsky University*. 2014. No. 3(53). Pp. 17–23. (rus)
5. *Snizhenie shuma v zdaniyakh i zhilykh rayonakh* [Noise reduction in buildings and residential areas]. Ed. G.L. Osipova, E.Ya. Yudina. Moscow: Stroyizdat, 1987. 558 p. (rus)
6. Rozenberg L.D. Metod rascheta zvukovykh poley, obrazovannykh raspredelennymi sistemami izluchateley, rabotayushchikh v zakrytykh pomeshcheniyakh [Method for calculating the sound fields formed by distributed systems of emitters operating in enclosed spaces]. *Journal of Technical Physics*. 1942. Vol. 12. P.220. (rus)
7. Schroeder M.R. Progress in architectural acoustics and artificial reverberation. Concert hall acoustics and number theory. *Journal of the Audio Engineering Society*. 1984. Vol. 32. No. 4 Pp. 194–203.
8. Ondet A.M., Barbry J.L. Modeling of sound propagation in fitted workshops using ray tracing. *Journal of the Acoustical Society of America*. 1989. Vol. 85. No. 2. Pp. 787–796.
9. Furduev V.V. *Elektroakustika* [Electroacoustics]. Moscow: Gostekhteorizdat, 1948. 515 p. (rus)
10. Kuttruff H. *Room acoustics*. London: Applied Science, 1973. 298 p.
11. Antonov A.I., Zhogoleva O.A., Ledenev V.I., Shubin I.L. Metod rascheta shuma v kvartirakh s yacheykovymi sistemami planirovki [The method of calculating noise in apartments with cellular planning systems]. *Zhilishchnoe Stroitel'stvo* [Housing construction]. 2013. No. 7. Pp. 33–35. (rus)
12. Zhogoleva O.A., Giyasov B.I., Matveeva I.V., Fedorova O.O. Statistical method of apartment noise level calculation and its experimental validation. *Vestnik MGSU*. 2017. Vol. 12. No. 4(103). Pp. 381–389. (rus)
13. Ledenev V.I. *Statisticheskie energeticheskie metody rascheta shumovykh poley pri proektirovanii proizvodstvennykh zdaniy* [Statistical energy methods for calculating noise fields in the design of industrial buildings]. Tambov, 2000. 156 p. (rus)
14. Ledenev V.I., Antonov A.I., Zhdanov A.E. Statisticheskie energeticheskie metody rascheta otrazhennykh shumovykh poley pomeshcheniy [Statistical energy methods for calculating the reflected noise fields of rooms]. *Transactions of the TSTU*. 2003. Vol. 9. No. 4. Pp. 713–717. (rus)

Литература

1. Антонов А.И., Бацунова А.В., Шубин И.Л. Условия, определяющие процессы формирования шумового режима в замкнутых объемах, и их учет при оценке распределения звуковой энергии в помещениях // Приволжский научный журнал. 2015. № 3(35). С. 89–96.
2. Скучик Е. Основы акустики М.: Издательство иностранной литературы, 1959. Т.2. 565 с.
3. Лейзер И.Г. О применимости методов геометрической акустики для расчета отражений звука от плоских поверхностей // Акустический журнал. 1966. Т. XII. № 2. С. 206–212.
4. Антонов А.И. Математическое моделирование процессов распространения звуковой энергии в зданиях // Вопросы современной науки и практики. Университет им. В.И. Вернадского. 2014. № 3(53). С. 17–23.
5. Снижение шума в зданиях и жилых районах / Под ред. Г.Л. Осипова, Е.Я. Юдина. М.: Стройиздат, 1987. 558 с.
6. Розенберг Л.Д. Метод расчета звуковых полей, образованных распределенными системами излучателей, работающих в закрытых помещениях // ЖТФ. 1942. Т. 12. С. 220.
7. Schroeder M.R. Progress in architectural acoustics and artificial reverberation. Concert hall acoustics and number theory // Journ. Audio Eng. Soc. 1984. Vol. 32. № 4. Pp. 194–203.
8. Ondet A.M., Barbry J.L. Modeling of sound propagation in fitted workshops using ray tracing // Journal of the Acoustical Society of America. 1989. Vol. 85. № 2. Pp. 787–796.
9. Фурдуев В.В. Электроакустика. М.: Гостехтеориздат, 1948. 515 с.
10. Kuttruff H. Room acoustics. London: Applied Science, 1973. 298 p.
11. Антонов А.И., Жоголева О.А., Леденев В.И., Шубин И.Л. Метод расчета шума в квартирах с ячейковыми системами планировки // Жилищное строительство. 2013. № 7. С. 33–35.
12. Жоголева О.А., Гиясов Б.И., Матвеева И.В., Федорова О.О. Статистический метод расчета шума, возникающего в квартирах от внутриквартирных источников звука и его экспериментальная проверка // Вестник МГСУ. 2017. Т. 12. № 4(103). С. 381–389.
13. Леденев В.И. Статистические энергетические методы расчета шумовых полей при проектировании производственных зданий. Тамбов, 2000. 156 с.
14. Леденев В.И., Антонов А.И., Жданов А.Е. Статистические энергетические методы расчета отраженных шумовых полей помещений // Вестник Тамбовского государственного технического университета. 2003. Т. 9. № 4. С. 713–717.
15. Гусев В.П., Леденев В.И., Матвеева И.В. Метод оценки распространения шума в крупно-габаритных газоздушных трактах энергетических объектов // Academia. Архитектура и строительство. 2009. № 5. С. 104–107.
16. Соломатин Е.О., Антонов А.И., Леденев В.И., Гусев В.П. Метод оценки шумового режима в производственных помещениях энергетических объектов // Academia. Архитектура и строительство. 2009. № 5. С. 250–252.
17. Visentin C., Valeau V., Prodi N., Picaut J. A numerical investigation of the sound intensity field in rooms by using diffusion theory and particle tracing // Proceedings of the 20th International Congress on Acoustics, ICA-2010.

Гиясов Б.И., Леденев В.И., Матвеева И.В. Метод расчета шума при зеркально-рассеянном отражении звука // Инженерно-строительный журнал. 2018. № 1(77). С. 13–22.

15. Gusev V.P., Ledenev V.I., Matveeva I.V. Metod otsenki rasprostraneniya shuma v krupnogaba-ritnykh gazovozdushnykh traktakh energeticheskikh ob'ektov [The method for estimating the propagation of noise in large-sized gas-air paths of power facilities]. *Academia. Arkhitektura i stroitel'stvo*. 2009. No. 5. Pp. 104–107. (rus)
16. Solomatin E.O., Antonov A.I., Ledenev V.I., Gusev V.P. Metod otsenki shumovogo rezhima v proizvodstvennykh pomeshcheniyakh energeticheskikh ob'ektov [The method of estimating the noise regime in production rooms of power facilities]. *Academia. Arkhitektura i stroitel'stvo*. 2009. No. 5. Pp. 250–252. (rus)
17. Visentin C., Valeau V., Prodi N., Picaut J. A numerical investigation of the sound intensity field in rooms by using diffusion theory and particle tracing. *Proceedings of the 20th International Congress on Acoustics, ICA-2010*. Sydney, Australia, 2010. Pp. 23–27.
18. Billon A., Picaut J., Valeau V., Sakout A. Acoustic Predictions in Industrial Spaces Using a Diffusion Model. *Hindawi Publishing Corporation Advances in Acoustics and Vibration*. Vol. 2012.
19. Visentin C., Prodi N., Valeau V., Picaut J. A numerical and experimental validation of the room acoustics diffusion theory inside long rooms // 21st International Congress on Acoustics. Canada. 2013.
20. Visentin C., Prodi N., Valeau V., Picaut J. A numerical investigation of the Fick's law of diffusion in room acoustics // *The Journal of the Acoustical Society of America*. 2012.
21. Foy C., Picaut J., Valeau V. Modeling the reverberant sound field by a diffusion process: analytical approach to the scattering // *Proceedings of Internoise – 2015*. San Francisco. 2015.
22. Foy C., Picaut J., Valeau V. Introduction de la diffusivity des parois au sein du modèle de diffusion acoustique // *CFA / VISHNO – 2016*. 2016.
23. Foy C., Valeau V., Picaut J., Prax C., Sakout A. Spatial variations of the mean free path in long rooms: Integration within the room-acoustic diffusion model // *Proceedings of the 22 International Congress on Acoustics – 2016*. Buenos Aires, 2016.
24. Hodgson M. Measurements of the influence of fittings and roof pitch on the sound field in panel-roof factories / M.Hodgson // *Applied Acoust* - 1983. No. 4. Pp. 369–391.
25. Santon F., Daumas A. Prevision des niveaux de bruit dans les ateliers textiles. *Rev. d'acoustique*. 1983. No. 65. Pp. 109–112.
- Sydney, Australia, 2010. Pp. 23–27.
18. Billon A., Picaut J., Valeau V., Sakout A. Acoustic Predictions in Industrial Spaces Using a Diffusion Model // *Hindawi Publishing Corporation Advances in Acoustics and Vibration*. Vol. 2012.
19. Visentin C., Prodi N., Valeau V., Picaut J. A numerical and experimental validation of the room acoustics diffusion theory inside long rooms // 21st International Congress on Acoustics. Canada. 2013.
20. Visentin C., Prodi N., Valeau V., Picaut J. A numerical investigation of the Fick's law of diffusion in room acoustics // *The Journal of the Acoustical Society of America*. 2012.
21. Foy C., Picaut J., Valeau V. Modeling the reverberant sound field by a diffusion process: analytical approach to the scattering // *Proceedings of Internoise – 2015*. San Francisco. 2015.
22. Foy C., Picaut J., Valeau V. Introduction de la diffusivity des parois au sein du modèle de diffusion acoustique // *CFA / VISHNO – 2016*. 2016.
23. Foy C., Valeau V., Picaut J., Prax C., Sakout A. Spatial variations of the mean free path in long rooms: Integration within the room-acoustic diffusion model // *Proceedings of the 22 International Congress on Acoustics – 2016*. Buenos Aires, 2016.
24. Hodgson M. Measurements of the influence of fittings and roof pitch on the sound field in panel-roof factories / M.Hodgson // *Applied Acoust* - 1983. No. 4. Pp. 369–391.
25. Santon F., Daumas A. Prevision des niveaux de bruit dans les ateliers textiles. *Rev. d'acoustique*. 1983. No. 65. Pp. 109–112.

Botir Giyasov,
+7(919)964-89-81; dandyр@mail.ru

Vladimir Ledenyov,
+7(475)263-09-20; gsiad@mail.tambov.ru

Irina Matveeva,
+7(475)263-09-20; gsiad1@mail.tambov.ru

Ботир Иминжонович Гиясов,
+7(919)964-89-81; эл. почта: dandyр@mail.ru

Владимир Иванович Леденев,
+7(475)263-09-20;
эл. почта: gsiad@mail.tambov.ru

Ирина Владимировна Матвеева,
+7(475)263-09-20;
эл. почта: gsiad1@mail.tambov.ru

© Giyasov G.B., Ledenyov L.V., Matveeva M.I., 2018

doi: 10.18720/MCE.77.3

Finite element models in stresses for plane elasticity problems

Конечно элементные модели в напряжениях для задач плоской теории упругости

*Yu.Ya. Tyukalov,
Vyatka State University, Kirov, Russia*

*Д-р техн. наук, профессор Ю.Я. Тюкалов,
Вятский государственный университет,
г. Киров, Россия*

Key words: finite elements; stress approximation; functional of additional energy; Lagrange multipliers

Ключевые слова: конечные элементы; аппроксимация напряжений; функционал дополнительной энергии; множители Лагранжа

Abstract. The solution of the plane problems of elasticity theory on the basis of stress approximation is considered. To construct the solution, the additional energy functional is used. With the help of the principle of possible displacements, algebraic equations of equilibrium of the nodes of the grid of finite elements are constructed. Equilibrium equations are included in the functional of additional energy by means of Lagrange multipliers. The necessary relations for rectangular and triangular finite elements are obtained. Variants with constant and piecewise-constant approximations of stresses in the region of the finite element are considered. The ribbon width of system of the solving linear equations is estimated. Calculations have been made for the bended beam and for stretched plate with the hole, for the different grids of finite element. It is made comparison of the solutions obtained in stresses with the solutions obtained by finite element method in displacements and with exact solutions. It is shown, that for plane problems in the theory of elasticity, solutions based on stress approximations make it possible to obtain convergence of displacements to exact values from above. For coarse grids, solutions based on piecewise constant stresses much more accurate results, but require large computational costs, since the width of the ribbon of non-zero elements of the resolving system of linear algebraic equations is approximately twice as large as in the other considered variants. Finite elements models in stresses allow constructing solutions, which are alternative to solutions obtained by finite element method in displacements.

Аннотация. Рассмотрено решение плоских задач теории упругости на основе аппроксимации напряжений. Для построения решения используется функционал дополнительной энергии. При помощи принципа возможных перемещений составляются алгебраические уравнения равновесия узлов сетки конечных элементов. Уравнения равновесия включаются в функционал дополнительной энергии при помощи множителей Лагранжа. Получены необходимые соотношения для прямоугольных и треугольных конечных элементов. Рассмотрены варианты с постоянными и кусочно-постоянными аппроксимациями напряжений по области конечного элемента. Даны оценки ширины ленты системы линейных разрешающих уравнений. Выполнены расчеты на изгиб консольной балки и на растяжение пластины с отверстием при различных сетках конечных элементов. Выполнено сравнение полученных решений с решениями по методу конечных элементов в перемещениях и точными решениями. Показано, что для плоских задач теории упругости решения на основе аппроксимации напряжений позволяют получить сходимость перемещений к точным значениям сверху. При грубых сетках решения на основе кусочно-постоянных напряжений дает существенно более точные результаты, но требуют больших вычислительных затрат, так как ширина ленты ненулевых элементов разрешающей системы линейных алгебраических уравнений примерно в два раза больше, по сравнению с другими рассмотренными вариантами. Модели конечных элементов в напряжениях позволяют строить решения, альтернативные решениям, полученным методом конечных элементов в перемещениях.

1. Introduction

Many fundamental works have been devoted to the development of the theoretical foundations of the finite element method in displacements [1–4]. They present the basic variational principles based on which finite element solutions can be constructed. The principles of minimum potential energy and additional energy are considered. Hybrid and mixed approaches are also considered. In these studies, it is noted that solutions based on the principle of minimum potential energy give the lower limit of the solution, and based on the principle of additional energy can give an upper bound. Applying different approximations for displacements in the finite element region, we thereby reduce the number of degrees of freedom of the system under consideration, which leads to an increase in its rigidity. Therefore, the values of displacements determined by the finite element method in displacements. will always be less than the exact values. In addition, as a rule, the approximations used for displacements do not ensure the continuity of deformations, and therefore stresses, along the boundaries of finite elements. This leads to the appearance of gaps of stress fields along the boundaries of finite elements and, correspondingly, additional difficulties and inaccuracies in solving physically nonlinear problems. Special algorithms for calculating stresses are required [5]. In [3], methods based on the stress fields approximations are also considered.

Based on the finite element method, various algorithms for solving geometrically and physically nonlinear problems of rods, plates, shells, and bulk problems of the theory of elasticity are developed [6–11]. The finite element method in displacements is also successfully used for solving problems with allowance for geometric nonlinearity, problems with taking account of the shear deformations and for calculation the thin-walled constructions [12–14]. The finite element method also conveniently solves the problems of stability and the dynamics of structures [10, 15].

The mixed variants of the finite element method are considered in [17–22]. In mixed versions, approximations of both displacements and stresses (forces) are used. Therefore, the solution obtained by the mixed finite element method, when crushing the grid, can approach an exact solution both from below and from above and does not give either the lower or upper boundaries of the displacements. In [23], hybrid finite element models are considered, in which the equilibrium equations inside the elements are satisfied on average, and the resolving equations are reduced to the form, which allowing to apply the standard techniques used in the rigidity method. The paper [24] is devoted to the application of a mixed approach to the solution of plane problems in the theory of elasticity, in which piecewise constant approximations are used for displacements. Works [25, 26] are devoted to a semi-analytical method for solving the problems of building mechanics. The proposed method has a high solution accuracy, but has a limited application area.

In [27–32], solutions are constructed by the finite element method, which based on the approximation of stresses (forces). In [27], a combination of the principles of possible displacements and possible stressed states is used to obtain the solution. In [29–32], the solution is based on the use of the principle of minimum of the additional energy and the principle of possible displacements. This approach allows us to find solutions that are alternative solutions obtained by the finite element method in displacements, and can provide a lower bound of displacements.

The finite element method in displacements gives an approximate, one-sided solution of the problem under consideration. Therefore, despite the great successes in the use of the finite element method in displacements, the search for and development of additional, alternative solutions is topical.

The purpose of this paper is to develop the method for calculating planar rod systems based on various approximations of stresses over the region of the finite element.

2. Methods

The solutions of the plane problems of the theory of elasticity in stresses can be obtained using the functional of additional energy [3]:

$$\Pi^c = U^* + V^* = \frac{1}{2} \int \{\sigma\}^T [E]^{-1} \{\sigma\} d\Omega - \int \{T\}^T \{\bar{\Delta}\} dS \rightarrow \min, \quad (1)$$

U^* – additional energy of the strains, V^* – potential of boundary forces corresponding to the specified displacements [1]; $\{\bar{\Delta}\}$ – vector given displacements of nodes; $\{T\}$ – vector boundary forces; S –

boundary surface, on which the displacement nodes are given; Ω – subject area; $\{\sigma\} = \begin{Bmatrix} \sigma_x \\ \sigma_y \\ \tau_{xy} \end{Bmatrix}$ – stresses vector; $[E]$ – material stiffness matrix.

The functions approximating the stress fields in (1) must satisfy the differential equations of equilibrium. Since, in the general case, it is practically impossible to find such functions, the following approach is proposed in [29–32]. The construction is dividing into rectangular or triangular finite elements. The stress fields in the region of the finite element can be approximated by linear, constant, or piecewise constant functions (Fig. 1). Linear approximating functions (Fig. 1a) ensure continuity of stresses fields over the entire subject area. Constant functions (Fig. 1b) are discontinuous along the boundaries of finite elements, but they satisfy differential equations of equilibrium in the absence of distributed loads. Piecewise-constant functions (Fig. 1c) also satisfy differential equations of equilibrium, are continuous along boundaries but have discontinuities inside finite elements.

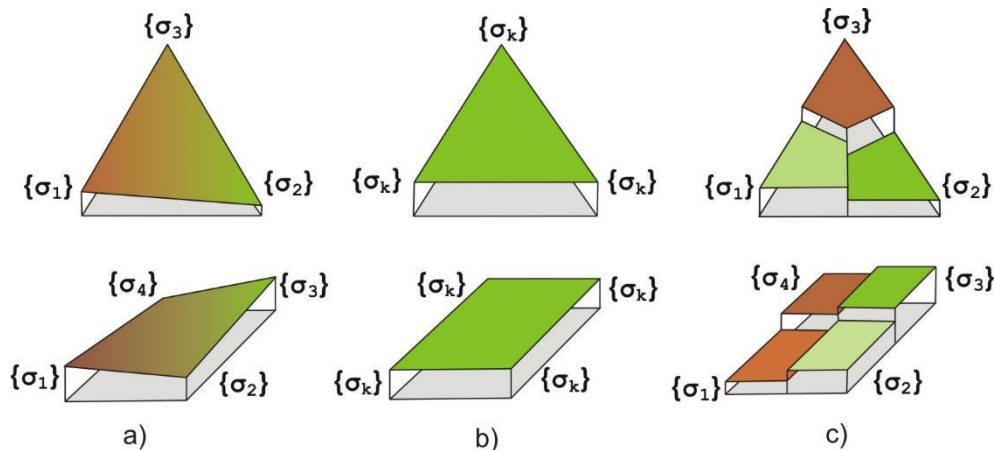


Figure 1. Variants of the approximation of stresses over the region of the finite element: a) the stresses vary linearly; b) the stresses are constant; c) the stresses are piecewise constant.

For simplicity, we assume that there are no given node displacements. Then, using any variant of the approximating functions for the stresses (Fig. 1), the expression for the functional (1) can be written in the following matrix form:

$$\Pi^c = \frac{1}{2} \{\sigma\}^T [D] \{\sigma\} \rightarrow \min, \quad (2)$$

$\{\sigma\}$ is the vector of unknown stresses for the whole system; $[D]$ is the matrix of flexibility for the whole system. Then, using the principle of possible displacements, for all non-fixed directions of nodes along the coordinate axes, we compose algebraic equations of equilibrium of forces:

$$\begin{aligned} \{C_{i,x}\}^T \{\sigma_i\} + \bar{P}_{i,x} &= 0, & i \in E_x, \\ \{C_{i,y}\}^T \{\sigma_i\} + \bar{P}_{i,y} &= 0, & i \in E_y. \end{aligned} \quad (3)$$

$\{\sigma_i\}$ – vector of unknown stresses of finite elements, connected to node i ; E_x, E_y – sets of nodes that have non-fixed displacements along the X, Y axes, respectively; $\bar{P}_{i,x}, \bar{P}_{i,y}$ – generalized forces, corresponding to the potential of external loads, for possible unit displacements of node i along the axes X, Y ; $\{C_{i,x}\}, \{C_{i,y}\}$ – vectors containing coefficients for unknown nodal stresses in the equations of equilibrium of the node i along the axes X, Y .

Thus, we have obtained the problem of minimizing the quadratic function of several variables (2) in the presence of constraints in the form of the system of linear algebraic equations (3). The unknown parameters are either nodal stresses (Figs. 1a, 1c) or stresses in the finite element (Fig. 1b). The solution of this problem was considered in [31, 32] using the penalty function method (4):

$$\Pi^c = \frac{1}{2} \{\sigma\}^T [D] \{\sigma\} + \sum_{j=x,y} \sum_{i \in E_j} \alpha \left(\{C_{i,j}\}^T \{\sigma_i\} + \bar{P}_{i,j} \right)^2 \rightarrow \min. \quad (4)$$

α – penalty parameter. Equating the derivatives, along the unknown stresses, to zero, we obtain the system of linear algebraic equations. The matrix of coefficients of this system of equations will have a ribbon structure of non-zero elements for any variant of stresses approximations.

In this paper, to solve we use the method of Lagrange multipliers:

$$\Pi^c = \frac{1}{2}\{\sigma\}^T[D]\{\sigma\} + \sum_{j=x,y} \sum_{i \in \mathcal{E}_j} u_{i,j} \left(\{C_{i,j}\}^T \{\sigma_i\} + \bar{P}_{i,j} \right) \rightarrow \min, \quad (5)$$

$u_{i,j}$ – displacement of node i in direction j . In this solution, it is appeared additional unknowns in the form of node displacements. But we must emphasize that the approximation of the displacement fields in the region of the finite element is not used in (5).

Expression (5) can be represented in a more convenient form for constructing the solution:

$$\Pi^c = \frac{1}{2}\{\sigma\}^T[D]\{\sigma\} + \{u\}^T(\{F\} - [L]\{\sigma\}) \rightarrow \min, \quad (6)$$

$\{u\}$ – global vector of unknown nodal displacements; $\{F\}$ – vector, whose elements are equal to the work of external forces on the corresponding unit displacements of the nodes; $[L]$ – “equilibrium” matrix, whose rows are formed from the corresponding vectors $\{C_{i,j}\}$. If we equate the derivatives Π^c along the vector $\{\sigma\}$ to zero, we obtain the equations of compatibility of the deformations in the stresses:

$$[D]\{\sigma\} - [L]^T\{u\} = 0. \quad (7)$$

The derivatives Π^c along the vector $\{u\}$ represent the system of equations of the equilibrium of nodes

$$\{F\} - [L]\{\sigma\} = 0. \quad (8)$$

Combining (7) and (8), we obtain the following system of linear algebraic equations:

$$\begin{bmatrix} [D] & -[L]^T \\ -[L] & [0] \end{bmatrix} \begin{Bmatrix} \{\sigma\} \\ \{u\} \end{Bmatrix} = \begin{Bmatrix} 0 \\ -\{F\} \end{Bmatrix}. \quad (9)$$

Expressing the vector $\{\sigma\}$ from the first matrix equation and substituting it into the second, we obtain

$$[K] = [L][D]^{-1}[L]^T, \quad (10)$$

$$[K]\{u\} = \{F\}, \quad (11)$$

$$\{\sigma\} = [D]^{-1}[L]^T\{u\}. \quad (12)$$

Thus, solving the system of algebraic equations (11), we obtain the values of the node displacements $\{u\}$, and then the stress vector $\{\sigma\}$ from (12).

Next, we obtain the necessary expressions for the elements of the matrices $[D]$, $[L]$ and the vector $\{F\}$, entering in (6), when rectangular and triangular finite elements are used to discredit the subject area (Fig. 2).

If linear functions are used to approximate stresses (Fig. 1a), then the matrix $[K]$ will be filled and the solution of the system of linear algebraic equations (11) requires large computational costs. Therefore, below, two variants of approximating the stresses in the region of the finite element will be considered – constant and piecewise-constant functions. In these cases, the matrix $[K]$ will have a ribbon structure of non-zero elements.

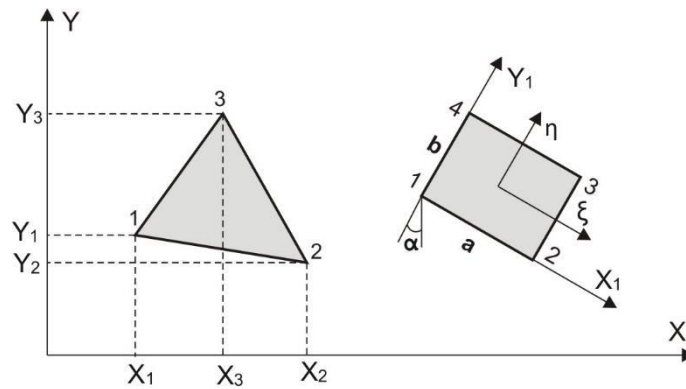


Figure 2. Triangular and rectangular finite elements

2.1. Variant 1. The stresses are constant in the region of the finite element

In the case of constant stresses in the region of the finite element, the vector of unknowns for the k -th finite element in the local coordinate system $\{\bar{\sigma}^k\}$ will have three elements:

$$\{\bar{\sigma}^k\} = \begin{Bmatrix} \bar{\sigma}_x^k \\ \bar{\sigma}_y^k \\ \bar{\tau}_{xy}^k \end{Bmatrix}. \tag{13}$$

The symbols with the top dash denoted the parameters related to the local coordinate system, associated with the finite element. The superscript k is the serial number of the finite element. The vectors of stresses in the global $\{\sigma^k\}$ and local $\{\bar{\sigma}^k\}$ coordinate systems are connected by the matrix of direction cosines:

$$[S_\sigma^k] = \begin{bmatrix} \sin^2\alpha & \cos^2\alpha & 2\sin\alpha \cdot \cos\alpha \\ \cos^2\alpha & \sin^2\alpha & -2\sin\alpha \cdot \cos\alpha \\ -\sin\alpha \cdot \cos\alpha & \sin\alpha \cdot \cos\alpha & -\sin^2\alpha - \cos^2\alpha \end{bmatrix}, \quad \{\bar{\sigma}^k\} = [S_\sigma^k]\{\sigma^k\}. \tag{14}$$

α – angle between the vertical axes of the global and local coordinate systems (Fig. 2).

The additional strain energy for a finite element of thickness t_k from an isotropic material is determined by the area integral:

$$\Pi_k^c = U_k^* = \frac{1}{2} \int t^k \{\sigma\}^T [E]^{-1} \{\sigma\} dA, \tag{15}$$

where:

$$\{\sigma\} = \begin{Bmatrix} \sigma_x \\ \sigma_y \\ \tau_{xy} \end{Bmatrix}, \quad [E]^{-1} = \frac{1}{E} \begin{bmatrix} 1 & -\mu & 0 \\ -\mu & 1 & 0 \\ 0 & 0 & 2(1 + \mu) \end{bmatrix}. \tag{16}$$

Substituting $\{\sigma^k\}$ in {14} instead of $\{\sigma\}$, we obtain an expression for the additional deformation energy in the global coordinate system

$$U_k^* = \frac{1}{2} A^k t^k \{\sigma^k\}^T [E]^{-1} \{\sigma^k\}, \tag{17}$$

where: A^k – area of the k -th finite element. The local matrix of a finite element flexibility has following form:

$$[D^k] = A^k t^k [E]^{-1}. \tag{18}$$

Summing the additional deformation energies of all n finite elements, we obtain the following expression for the flexibility matrix $[D]$ for the whole system:

$$[D] = \begin{bmatrix} [D^1] & \dots & 0 \\ \vdots & \ddots & \vdots \\ 0 & \dots & [D^n] \end{bmatrix}. \quad (19)$$

The matrix $[D]$ will have block-diagonal structure and is therefore easily reversible. This is important, since the inverse matrix $[D]^{-1}$ is subsequently will used to obtain the matrix $[K]$ (10).

$$[D]^{-1} = \begin{bmatrix} [D^1]^{-1} & \dots & 0 \\ \vdots & \ddots & \vdots \\ 0 & \dots & [D^n]^{-1} \end{bmatrix}. \quad (20)$$

For rectangular finite element, we introduce the local coordinate system $\xi\eta$, connected with its center (Fig. 2), and basic functions, which are expressed in normalized local coordinates in the following form:

$$N_i(x, y) = \frac{(1 + \xi_i\xi)(1 + \eta_i\eta)}{4}, \quad \xi = \frac{2x}{a_k}, \quad \eta = \frac{2y}{b_k}, \quad i = 1, 2, 3, 4. \quad (21)$$

The index i denotes the local order number of node of the finite element; x, y – the coordinates along the axes X_1 and Y_1 , respectively; ξ_i, η_i – local normalized coordinates of node i , taking values 1 or -1. The nodes of finite element are numbered counterclockwise, beginning with the lower-left node.

As possible displacements of each node, consider the displacements $\delta\bar{u}_i$ and $\delta\bar{v}_i$ along the axes of the local coordinate system X_1 and Y_1 . Possible displacements in the region of rectangular finite element are expressed by means of the linear approximation functions in the following form:

$$\delta\bar{u}(x, y) = N_i(x, y)\delta\bar{u}_i, \quad \delta\bar{v}(x, y) = N_i(x, y)\delta\bar{v}_i. \quad (22)$$

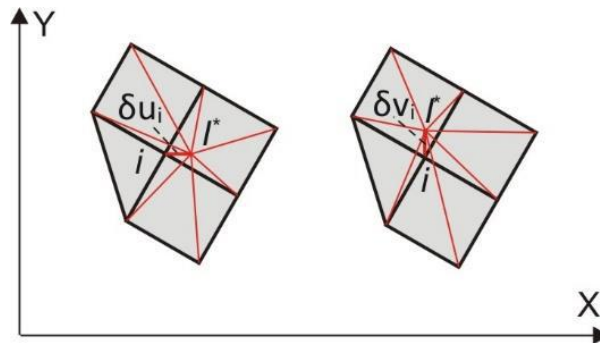


Figure 3. Possible displacements of node i in the global coordinate system

Since the possible displacements $\delta\bar{u}_i$ and $\delta\bar{v}_i$ can be any, we take them equal to unity and in subsequent transformations we omit them. Then, the deformations arising in the element k at the possible displacement $\delta\bar{u}_i = 1$, directed along the X_1 axis will be as follows:

$$\delta\varepsilon_x = \frac{\partial(\delta\bar{u})}{\partial x} = \frac{\xi_i(1 + \eta\eta_i)}{2a_k}, \quad \delta\gamma_{xy} = \frac{\partial(\delta\bar{u})}{\partial y} = \frac{\eta_i(1 + \xi\xi_i)}{2b_k}. \quad (23)$$

The possible energy of deformations of the rectangular finite element with number k , arising at the possible displacement $\delta\bar{u}_i = 1$

$$\delta\bar{U}_{i,x}^k = \int_0^{b_k} \int_0^{a_k} t^k (\sigma_x \delta\varepsilon_x + \tau_{xy} \delta\gamma_{xy}) dx dy = \frac{t^k b_k}{2} \xi_i \bar{\sigma}_x^k + \frac{t^k a_k}{2} \eta_i \bar{\tau}_{xy}^k. \quad (24)$$

We write expression (24) in vector form:

$$\delta\bar{U}_{i,x}^k = \{C_{i,x}^k\}^T \{\bar{\sigma}^k\}, \quad \{C_{i,x}^k\} = \begin{Bmatrix} \frac{t^k b_k}{2} \xi_i \\ 0 \\ \frac{t^k a_k}{2} \eta_i \end{Bmatrix}. \quad (25)$$

Similarly, for the possible displacement $\delta \bar{v}_i = 1$

$$\delta \bar{U}_{i,y}^k = \{C_{i,y}^k\}^T \{\bar{\sigma}^k\}, \quad \{C_{i,y}^k\} = \begin{Bmatrix} 0 \\ \frac{t^k a_k}{2} \eta_i \\ \frac{t^k b_k}{2} \xi_i \end{Bmatrix}. \quad (26)$$

The energy of deformations of all rectangular finite elements adjoined to the node under consideration is determined in the form of sums

$$\delta \bar{U}_{i,x} = \sum_k \{C_{i,x}^k\}^T \{\bar{\sigma}^k\}, \quad \delta \bar{U}_{i,y} = \sum_k \{C_{i,y}^k\}^T \{\bar{\sigma}^k\}. \quad (27)$$

The potential of external concentrated and uniformly distributed loads for possible displacements of node i along the global coordinate axes is determined by (28).

$$\delta V_{i,j} = P_{i,j} + \frac{1}{4} \sum_k q_j^k a_k b_k = R_{i,j}, \quad j = x, y. \quad (28)$$

$P_{i,j}$ – forces, which concentrated in the node; q_j^k – load, which evenly distributed over the element. The generalized forces $R_{i,j}$ taken with the minus sign, are placed in the vector $\{F\}$ (see (6)).

Using the expressions (25) and (26), we introduce the following matrix notations:

$$\{\delta \bar{U}^k\} = \begin{Bmatrix} \delta \bar{U}_{1,x}^k \\ \delta \bar{U}_{1,y}^k \\ \delta \bar{U}_{2,x}^k \\ \delta \bar{U}_{2,y}^k \\ \delta \bar{U}_{3,x}^k \\ \delta \bar{U}_{3,y}^k \\ \delta \bar{U}_{4,x}^k \\ \delta \bar{U}_{4,y}^k \end{Bmatrix}, \quad [\bar{L}^k] = \frac{t^k}{2} \begin{bmatrix} -b_k & 0 & -a_k \\ 0 & -a_k & -b_k \\ b_k & 0 & -a_k \\ 0 & -a_k & b_k \\ b_k & 0 & a_k \\ 0 & a_k & b_k \\ -b_k & 0 & a_k \\ 0 & a_k & -b_k \end{bmatrix}. \quad (29)$$

Expressions for the energy of deformation for possible displacements of nodes of a finite element will be written in the matrix form:

$$\{\delta \bar{U}^k\} = [\bar{L}^k] \{\bar{\sigma}^k\} = [\bar{L}^k] [S_{\sigma}^k] \{\sigma^k\}. \quad (30)$$

To obtain the equilibrium equations for a node, it is necessary to consider the possible displacements $\delta u_i, \delta v_i$ along the global coordinate axes X and Y (Fig. 3). Displacements along global and local axes are connected by the matrix of direction cosines

$$[l] = \begin{bmatrix} \sin \alpha & -\cos \alpha \\ \cos \alpha & \sin \alpha \end{bmatrix}, \quad \begin{Bmatrix} \delta u_i \\ \delta v_i \end{Bmatrix} = [l] \begin{Bmatrix} \delta \bar{u}_i \\ \delta \bar{v}_i \end{Bmatrix}. \quad (31)$$

Using (31), we obtain the expressions for the strain energy for possible displacements of the nodes along the axes of the global coordinate system:

$$\{\delta U^k\} = [L^k] \{\sigma^k\}, \quad [L^k] = [S_{uv}^k] [\bar{L}^k] [S_{\sigma}^k], \quad [S_{uv}^k] = \begin{bmatrix} [l] & 0 & 0 & 0 \\ 0 & [l] & 0 & 0 \\ 0 & 0 & [l] & 0 \\ 0 & 0 & 0 & [l] \end{bmatrix}. \quad (32)$$

The matrix $[L^k]$, conditionally, can be called the local matrix of equilibrium of the finite element. From matrices $[L^k]$ for finite elements, in accordance with the numbering of the nodes and elements, the global equilibrium matrix $[L]$ is formed for the whole system.

To derive the relations for the triangular finite element, we use triangular coordinates [3], which allow us to obtain the matrix $[L^k]$ directly in the global coordinate system. The triangular coordinate for the finite element T_i^k is determined by the formula

$$T_i^k = \frac{1}{2A^k} (a_i^k + b_i^k x + c_i^k y), \quad i = 1, 2, 3. \quad (33)$$

where:

$$a_i^k = x_{i+1}y_{i+2} - x_{i+2}y_{i+1}, \quad b_i^k = y_{i+1} - y_{i+2}, \quad c_i^k = x_{i+2} - x_{i+1}.$$

A^k – the area of the triangular finite element k ; x_i, y_i – coordinates of node i .

We can express possible displacements in the region of the triangular finite element by means of triangular coordinates in the following form:

$$\delta u(x, y) = T_i^k \delta u_i, \quad \delta v(x, y) = T_i^k \delta v_i. \quad (34)$$

$\delta u_i, \delta v_i$ – the possible displacements of the node i along the global coordinate axes. We take $\delta u_i = 1, \delta v_i = 1$. Then, the deformations arising in the element at the possible displacement of the node along the global X axis, will be as follows:

$$\delta \varepsilon_x = \frac{\partial(\delta u)}{\partial x} = \frac{b_i^k}{2A^k}, \quad \delta \gamma_{xy} = \frac{\partial(\delta u)}{\partial y} = \frac{c_i^k}{2A^k}. \quad (35)$$

Then

$$\delta U_{i,x}^k = \iint t^k (\sigma_x^k \delta \varepsilon_x + \tau_{xy}^k \delta \gamma_{xy}) dA = \frac{t^k b_i^k}{2} \sigma_x^k + \frac{t^k c_i^k}{2} \tau_{xy}^k. \quad (36)$$

Similarly, for the possible displacement along the Y axis, we get:

$$\delta \varepsilon_y = \frac{\partial(\delta v)}{\partial y} = \frac{c_i^k}{2A_k}, \quad \delta \gamma_{xy} = \frac{\partial(\delta v)}{\partial x} = \frac{b_i^k}{2A_k}, \quad (37)$$

$$\delta U_{i,y}^k = \iint t^k (\sigma_y^k \delta \varepsilon_y + \tau_{xy}^k \delta \gamma_{xy}) dA = \frac{t^k c_i^k}{2} \sigma_y^k + \frac{t^k b_i^k}{2} \tau_{xy}^k. \quad (38)$$

Using the expressions (36) and (38), we obtain the following matrix of equilibrium $[L^k]$ of the triangular finite element in the global coordinate system:

$$[L^k] = \frac{t^k}{2} \begin{bmatrix} b_1^k & 0 & c_1^k \\ 0 & c_1^k & b_1^k \\ b_2^k & 0 & c_2^k \\ 0 & c_2^k & b_2^k \\ b_3^k & 0 & c_3^k \\ 0 & c_3^k & b_3^k \end{bmatrix}. \quad (39)$$

The potential of external concentrated and uniformly distributed loads for possible displacements of node i is determined by (40).

$$\delta V_{i,j} = P_{i,j} + \frac{1}{3} \sum_k q_j^k A^k = R_{i,j}, \quad j = x, y. \quad (40)$$

The global equilibrium matrix $[L]$ for the whole system will have ribbon structure of non-zero elements. Numbering of unknown stresses are assigned in accordance with the numbering of the finite elements. Therefore, the width of the ribbon of non-zero elements of the matrix $[L]$ will be determined by the maximum difference of order numbers of the finite elements adjoined to node. The structure of the matrix $[L]$ must be considered when storing its elements, as well as when calculating the matrix $[K]$ (10).

We note, that as a result, the width of the ribbon of non-zero elements of the matrix $[K]$ equal with the width of the ribbon of the system of equations of the finite element method in displacements.

2.2. Variant 2. The stresses are piecewise-constant in the region of the finite element

In this case, nodal stresses are taken as unknowns. The stresses fields in the region of the finite element are discontinuous and piecewise-constant (Fig. 1c). We introduce the notation: $\{\bar{\sigma}_i\} = \begin{pmatrix} \bar{\sigma}_{i,x} \\ \bar{\sigma}_{i,y} \\ \bar{\tau}_{i,xy} \end{pmatrix}$

– stresses in node i in the local coordinate system; $\{\sigma_i\} = \begin{pmatrix} \sigma_{i,y} \\ \sigma_{i,x} \\ \tau_{i,xy} \end{pmatrix}$ – stresses in node i in the global coordinate system. The expression for the additional strains energy in the global coordinate system can be written in the form of a simple sum:

$$U^* = \frac{1}{2} \sum_{i=1}^m t_i A_i \{\sigma_i\}^T [E]^{-1} \{\sigma_i\}, \tag{41}$$

$$A_i = \sum_{s=1}^{n_R} \frac{1}{4} A^s + \sum_{s=1}^{n_T} \frac{1}{3} A^s. \tag{42}$$

m – the total number of nodes; t_i – the thickness of the plate at node i , n_R – the number of rectangular elements adjoined to node i ; n_T – number of triangular elements adjoined to node i ; A^s – the area of S – the finite element.

We introduce the notation for the flexibility matrix of "neighborhoods" of the node i :

$$[D_i] = t_i A_i [E]^{-1}. \tag{43}$$

The global flexibility matrix for the entire system $[D]$ consists of matrices of flexibility $[D_i]$ for all nodes of the system and has the following block-diagonal form:

$$[D] = \begin{bmatrix} [D_1] & \dots & 0 \\ \vdots & \ddots & \vdots \\ 0 & \dots & [D_m] \end{bmatrix}. \tag{44}$$

Consider a possible displacement of the node $\delta \bar{u}_i = 1$ along the local axis X_1 of the rectangular finite element. The possible energy of deformations of the rectangular finite element with number k

$$\delta \bar{U}_{i,x}^k = \int_0^{b_k} \int_0^{a_k} t^k (\sigma_x \delta \varepsilon_x + \tau_{xy} \delta \gamma_{xy}) dx dy = \sum_{j=1}^4 \frac{b_k t^k}{8} \xi_i \left(1 + \frac{\eta_i \eta_j}{2}\right) \bar{\sigma}_{x,j} + \sum_{j=1}^4 \frac{a_k t^k}{8} \eta_i \left(1 + \frac{\xi_i \xi_j}{2}\right) \bar{\tau}_{xy,j}. \tag{45}$$

Similarly, for the possible displacement $\delta \bar{v}_i = 1$

$$\delta \bar{U}_{i,y}^k = \int_0^{b_k} \int_0^{a_k} t^k (\sigma_y \delta \varepsilon_y + \tau_{xy} \delta \gamma_{xy}) dx dy = \sum_{j=1}^4 \frac{a_k t^k}{8} \eta_i \left(1 + \frac{\xi_i \xi_j}{2}\right) \bar{\sigma}_{y,j} + \sum_{j=1}^4 \frac{b_k t^k}{8} \xi_i \left(1 + \frac{\eta_i \eta_j}{2}\right) \bar{\tau}_{xy,j}. \tag{46}$$

In expressions (45) and (46), j is the local order number of node in the finite element. Using (45) and (46), we write the expression for the matrix of equilibrium for the rectangular finite element $[\bar{L}^k]$.

$$[\bar{L}^k] = \frac{t^k}{16} \begin{bmatrix} -3b_k & 0 & -3a_k & -3b_k & 0 & -a_k & -b_k & 0 & -a_k & -b_k & 0 & -3a_k \\ 0 & -3a_k & -3b_k & 0 & -a_k & -3b_k & 0 & -a_k & -b_k & 0 & -3a_k & -b_k \\ 3b_k & 0 & -a_k & 3b_k & 0 & -3a_k & b_k & 0 & -3a_k & b_k & 0 & -a_k \\ 0 & -a_k & 3b_k & 0 & -3a_k & 3b_k & 0 & -3a_k & b_k & 0 & -a_k & b_k \\ b_k & 0 & a_k & b_k & 0 & 3a_k & 3b_k & 0 & 3a_k & 3b_k & 0 & a_k \\ 0 & a_k & b_k & 0 & 3a_k & b_k & 0 & 3a_k & 3b_k & 0 & a_k & 3b_k \\ -b_k & 0 & 3a_k & -b_k & 0 & a_k & -3b_k & 0 & a_k & -3b_k & 0 & 3a_k \\ 0 & 3a_k & -b_k & 0 & a_k & -b_k & 0 & a_k & -3b_k & 0 & 3a_k & -3b_k \end{bmatrix} \tag{47}$$

We write expressions for the strain energy, at possible unit displacements of the nodes of the finite element k in the local coordinate system in a matrix form analogous to (30):

$$\{\delta \bar{U}^k\} = [\bar{L}^k] \{\bar{\sigma}^k\} = [\bar{L}^k] [C_\sigma^k] \{\sigma^k\}. \quad (48)$$

$[C_\sigma^k]$ – the matrix of transformation of the unknown stress vector for the finite element from the local to the global coordinate system. This matrix consists of the matrices $[S_\sigma^k]$ (14) and has the following form:

$$[C_\sigma^k] = \begin{bmatrix} [S_\sigma^k] & 0 & 0 & 0 \\ 0 & [S_\sigma^k] & 0 & 0 \\ 0 & 0 & [S_\sigma^k] & 0 \\ 0 & 0 & 0 & [S_\sigma^k] \end{bmatrix}. \quad (49)$$

Going to possible displacements in the global coordinate system, we obtain the matrix of equilibrium for the finite element

$$[L^k] = [S_{uv}^k] [\bar{L}^k] [C_\sigma^k]. \quad (50)$$

From the matrices $[L^k]$, for all finite elements, a global matrix of equilibrium of the whole system $[L]$ is formed.

For a triangular finite element, expressions like expressions (45) and (46), but in the global coordinate system, will have the following form:

$$\delta U_{i,x}^k = \frac{t^k b_i^k}{6} \sum_{j=1}^3 \sigma_{x,j} + \frac{t^k c_i^k}{6} \sum_{j=1}^3 \tau_{xy,j}, \quad (51)$$

$$\delta U_{i,y}^k = \frac{t^k c_i^k}{6} \sum_{j=1}^3 \sigma_{y,j} + \frac{t^k b_i^k}{6} \sum_{j=1}^3 \tau_{xy,j}, \quad (52)$$

In a triangular element, the stresses are constant in each third of the area adjoined to the node, and equal to the stresses in the given node. Since the possible deformations, in accordance with expressions (35) and (37), are constant values throughout the entire element, the strain energy is equal to the sum of multiplies the stresses, deformations and the area of one third of the element. Using (51) and (52), we obtain the following matrix of equilibrium $[L^k]$ of the finite element in the global coordinate system:

$$[L^k] = \frac{t^k}{6} \begin{bmatrix} b_1^k & 0 & c_1^k & b_1^k & 0 & c_1^k & b_1^k & 0 & c_1^k \\ 0 & c_1^k & b_1^k & 0 & c_1^k & b_1^k & 0 & c_1^k & b_1^k \\ b_2^k & 0 & c_2^k & b_2^k & 0 & c_2^k & b_2^k & 0 & c_2^k \\ 0 & c_2^k & b_2^k & 0 & c_2^k & b_2^k & 0 & c_2^k & b_2^k \\ b_3^k & 0 & c_3^k & b_3^k & 0 & c_3^k & b_3^k & 0 & c_3^k \\ 0 & c_3^k & b_3^k & 0 & c_3^k & b_3^k & 0 & c_3^k & b_3^k \end{bmatrix}. \quad (53)$$

Expressions of the potential of external concentrated and uniformly distributed loads for possible displacements of the node (28) and (40) do not depend on the type of stress approximation.

The global equilibrium matrix $[L]$ will also have a ribbon structure of non-zero elements. When determining the width of the ribbon of non-zero elements, the minimum and maximum node numbers of all finite elements adjacent to the node under consideration are determined for each node. The maximum difference of these numbers, multiplied by three, will determine the width of the tape of nonzero elements of the matrix $[L]$. Note, that the width of the ribbon of non-zero elements of the matrix $[K]$ is approximately twice the width of the ribbon of the system of equations of the finite element method in displacements.

3. Results and Discussion

By program developed in Mathcad 14.0, calculations of the cantilever beam for the action of a uniformly distributed vertical load were performed (Fig. 4b). The thickness of the beam – 1m., the modulus of elasticity – $E = 10000 \text{ kN/m}^2$, the coefficient of transverse deformations – 0.25. The results of calculations of the cantilever beam are presented in Figures 4–7 and in Tables 1–2. In Figures,

solutions based on piecewise constant approximations of stresses are denoted by digit 1; solutions based on constant stresses - denoted by digit 2; solutions based on FEM in displacements – denoted by digit 3.

The results of calculations for five variants of finite element grids show that solutions based on stress approximation allow obtaining convergence of displacements to the exact values from above and are more flexibility as compared to solutions obtained by FEM in the LIRA-SAPR displacements (Fig. 4a).

The stresses in the clamp of the beam with the use of piecewise constant stresses approximations are always greater than the stresses obtained using both constant stresses and with the use of FEM in displacements (Table 2). This is since for piecewise constant stresses approximations we use, as unknowns, the stresses at the nodes of the finite element grid, which allows us to obtain stress values directly in external fibers and better model the edge effect. The difference in the stress values (for the smallest grid), in comparison with the FEM in the displacements, is 15.6 %, 35.6 % and 26.4 %, respectively, for the stresses σ_x , σ_y and τ_{xy} .

When using constant stresses in the region of the finite element, the stress σ_x is also always greater than the stresses obtained by the FEM in displacements. For the coarsest grid, the values differ by 9.3 %, and for the smallest by 1.5 %. The stresses σ_y and τ_{xy} are smaller in the case of using constant stresses. The stresses σ_y differ by 39 % for the coarsest grid and by 29 % for the shallowest grid. The stresses τ_{xy} differ by 5 % and 15 %, respectively.

Note that the stress σ_x in this case is much greater than the stresses σ_y and τ_{xy} . In addition, due to the edge effect, when we crash the grid, all the stresses increase, and it is not possible to compare the values obtained with precise values. When the solution of the problem is constructed in a physically nonlinear formulation, then solutions based on the approximation of stresses, giving large stresses for the same grids, should provide a greater reserve of strength in comparison with the FEM decisions in displacements.

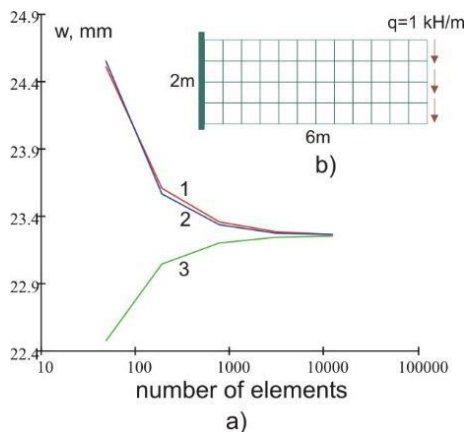


Figure 4. Cantilever beam: a) vertical movements; b) finite element grid 12x4

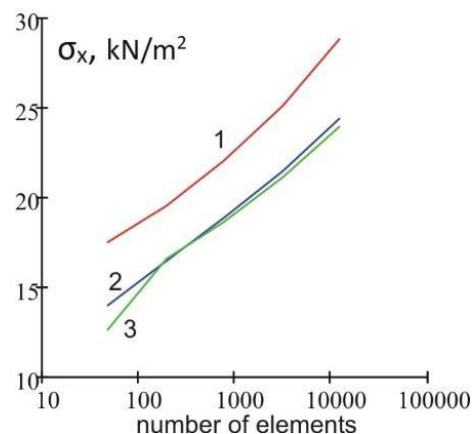


Figure 5. The stress σ_x in the upper fiber in the clamp

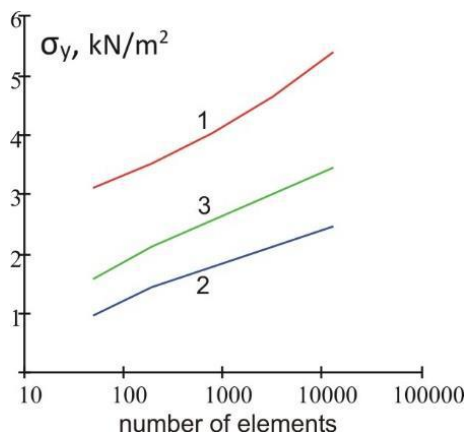


Figure 6. Stresses σ_y in the upper fiber in the clamp

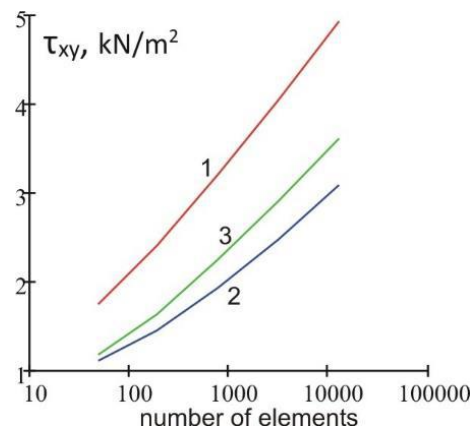


Figure 7. Stresses τ_{xy} in the upper fiber in the clamp

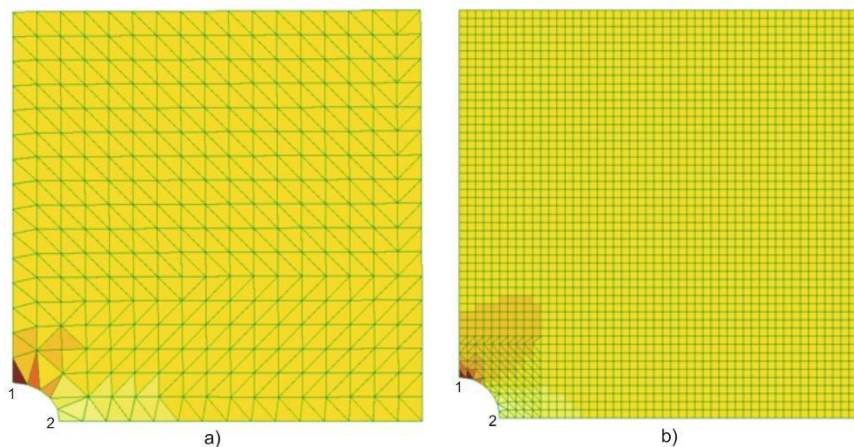
Table 1. Vertical displacements of the console

N	Grid	Piecewise constant stresses		Constant stresses		FEM in displacements LIRA-SAPR	
		Ribbon width	w, mm	Ribbon width	w, mm	Ribbon width	w, mm
1	12x4	26	24.5166	14	24.5578	14	22.4760
2	24x8	42	23.6121	22	23.5639	22	23.0436
3	48x16	74	23.3552	38	23.3325	38	23.1990
4	96x32	138	23.2845	70	23.2762	70	23.2410
5	192x64	266	23.2653	134	23.2624	134	23.2531

Table 2. Stresses in the upper fiber of the section in the clamp

N	Grid	Piecewise constant stresses			Constant stresses			FEM in displacements LIRA-SAPR		
		σ_x , kN/m^2	σ_y , kN/m^2	τ_{xy} , kN/m^2	σ_x , kN/m^2	σ_y , kN/m^2	τ_{xy} , kN/m^2	σ_x , kN/m^2	σ_y , kN/m^2	τ_{xy} , kN/m^2
1	12x4	17.556	3.118	1.745	13.957	0.954	1.113	12.652	1.571	1.172
2	24x8	19.548	3.521	2.402	16.527	1.433	1.447	16.005	2.120	1.631
3	48x16	22.063	4.031	3.215	18.911	1.783	1.931	18.584	2.565	2.239
4	96x32	25.160	4.645	4.055	21.447	2.102	2.486	21.123	2.994	2.912
5	192x64	28.909	5.375	4.927	24.399	2.439	3.081	24.020	3.460	3.623

Also, calculations were made for the stretched square plate with the hole. In Figure 8 the finite-element grids are shown for the one-fourth of the plate. The size of the side of plate is $10m$., the diameter of hole is $1m$., the thickness is $1m$., the modulus of elasticity is $E = 10000 kN/m^2$, the coefficient of transverse deformations is 0.25 . The stretching load is $q = 10 kN/m^2$. For this problem, the exact values of the stresses at points 1 and 2 are known (Fig. 8). At the point 1 $\sigma_x = 30 kN/m^2$, at the point 2 $\sigma_y = -10 kN/m^2$ [3]. Table 2 shows the stress values obtained at points 1 and 2. In the variant in Fig. 8a only triangular finite elements are used and the number of grid nodes is 322, in the variant in Fig. 8b both rectangular and triangular elements are used, and the number of nodes is 2579.

**Figure 8. One quarter of the square plate with the hole.**

Variants of finite element grid and stress distribution σ_x , obtained by FEM in displacements

Table 2. Stresses in the square plate with the hole

Scheme	Point 1 – σ_x , kN/m^2			Point 2 – σ_y , kN/m^2		
	Piecewise constant stresses	Constant stresses	FEM in displacements, LIRA-SAPR	Piecewise constant stresses	Constant stresses	FEM in displacements, LIRA-SAPR
a)	27.697	25.853	25.853	-8.003	-5.244	-5.244
b)	29.871	29.865	29.845	-9.290	-9.577	-9.559

The results obtained show that for the coarser grid (scheme a), a solution based on piecewise constant stresses give substantially more accurate results. The solution differs from the exact one by 7.7 % at point 1 and by 20 % at point 2. For variants with constant stresses and for FEM in displacements, the differs from the exact solution for point 1 is 13.8 % and 47.6 % for point 2. For the triangular finite element, the FEM in displacements also simulates constant stresses, so the solutions for the scheme in Figure 8a, which obtained by the FEM in displacements, and obtained on the basis of constant stresses, coincided.

For the fine grid (Fig. 8b), the solutions obtained by all methods are very close. In this case, solutions based on the approximation of stresses, are also closer to an exact solution.

4. Conclusions

1. For plane problems of the theory of elasticity, solutions based on the approximation of stresses make it possible to obtain convergence of displacements to the exact values from above.

2. For coarse grids, solutions based on piecewise constant stresses much more accurate results, but require large computational costs, since the width of the ribbon of non-zero elements of the resolving system of linear algebraic equations is approximately twice as large as in the other considered variants.

3. Solutions based on the approximation of stresses make it possible, with the same grids, to obtain more accurate stress values in comparison with the FEM solutions in displacements. By difference of solutions, by the method based on the approximation of stresses and FEM in displacements for identical grids, one can estimate the accuracy of the approximate solutions obtained.

4. Finite elements models in stresses allow constructing solutions, which are alternative to solutions obtained by finite element method in displacements.

References

- Zenkevich O. *Metod konechnykh elementov v tekhnike* [The finite element method in technique]. Moscow: Mir, 1975. 541 p.(rus)
- Zenkevich O., Morgan K. *Konechnyye elementy i approksimatsiya* [Finite Elements and Approximation]. Moscow: Mir, 1986. 318 p.(rus)
- Gallager R. *Metod konechnykh elementov. Osnovy* [Finite element method. Basics]. Moscow: Mir, 1984. 428 p.(rus)
- Rozin L.A. *Metod konechnykh elementov v primeneni k uprugim sistemam* [Finite element method in application to elastic systems]. Moscow: Stroyizdat, 1977. 129 p.(rus)
- Stein E., Ahmad R. An equilibrium method for stress calculation using finite element displacement models. *Comput. Meth. Appl. Mech. And Eng.* 1977. Vol. 10. No. 2. Pp. 175–198.
- Nguen-Xuan H. A polygonal finite element method for plate analysis. *Computers & Structures.* 2017. Vol. 188. Pp. 45–62.
- Di Paola M., Fileccia Scimemi G. Finite element method on fractional visco-elastic frames. *Computers & Structures.* 2016. Vol. 164. Pp. 15–22.
- Lyashko A.D., Tayupov Sh.I., Timerbayev M.R. Skhemy metoda konechnykh elementov vysokogo poriyadka tochnosti dlya sistemy ellipticheskikh uravneniy s vyrozhdayushchimisya koeffitsiyentami na interval [Schemes of the method of finite elements of high order of accuracy for a system of elliptic equations with degenerate

Литература

- Зенкевич О. *Метод конечных элементов в технике.* М.: Мир, 1975. 541 с.
- Зенкевич О., Морган К. *Конечные элементы и аппроксимация.* М.: Мир, 1986. 318 с.
- Галлагер Р. *Метод конечных элементов. Основы.* М.: Мир, 1984. 428 с.
- Розин Л. А. *Метод конечных элементов в применении к упругим системам.* М.: Стройиздат, 1977. 129 с.
- Stein E., Ahmad R. An equilibrium method for stress calculation using finite element displacement models // *Comput. Meth. Appl. Mech. And Eng.* 1977. Vol. 10. No. 2. Pp. 175–198.
- Nguen-Xuan H. A polygonal finite element method for plate analysis // *Computers & Structures.* 2017. Vol. 188. Pp. 45–62.
- Di Paola M., Fileccia Scimemi G. Finite element method on fractional visco-elastic frames // *Computers & Structures.* 2016. Vol. 164. Pp. 15–22.
- Ляшко А.Д., Таюпов Ш.И., Тимербаев М.Р. Схемы метода конечных элементов высокого порядка точности для системы эллиптических уравнений с вырождающимися коэффициентами на интервале // *Известия высших учебных заведений. Математика.* 2009. № 7. С. 22–34.
- Лалин В.В., Рыбаков В.А., Морозов С.А.. Исследование конечных элементов для расчета тонкостенных стержневых систем // *Инженерно-строительный*

- coefficients on the interval]. *Izvestiya vysshikh uchebnykh zavedeniy. Matematika*. 2009. No. 7. Pp. 22–34. (rus)
9. Lalin V.V., Rybakov V.A., Morozov S.A.. Issledovaniye konechnykh elementov dlya rascheta tonkostennykh sterzhnevnykh sistem [Finite element analysis for the calculation of thin-walled rod systems]. *Magazine of Civil Engineering*. 2012. Vol. 27. No. 1. Pp. 53–73. (rus)
 10. Lalin V.V., Rozin L.A., Kushova D.A. Variatsionnaya postanovka ploskoy zadachi geometricheski nelineynogo deformirovaniya i ustoychivosti uprugikh sterzhney [Variational formulation of the plane problem of geometrically nonlinear deformation and stability of elastic rods]. *Magazine of Civil Engineering*. 2013. No. 1(36). Pp. 87–96. (rus)
 11. Lalin V.V., Zdanchuk Ye.V., Kushova D.A., Rozin L.A. Variatsionnyye postanovki nelineynykh zadach s nezavisimymi vrashchatelnymi stepenyami svobody [Variational formulations of nonlinear problems with independent rotational degrees of freedom]. *Magazine of Civil Engineering*. 2015. No. 4(56). Pp. 54–65. (rus)
 12. Lalin V.V., Belyayev M.O. Izgib geometricheski nelineynogo konsolnogo sterzhnya. Resheniye po teoriyam Kirkhgofa i Kossera – Timoshenko [Bending of a geometrically nonlinear cantilever rod. Decision by the theories of Kirchhoff and Kosser - Tymoshenko]. *Magazine of Civil Engineering*. 2015. No. 1(53). Pp. 39–55. (rus)
 13. Lalin V., Rybakov V., Alexander S. The finite elements for design of frame of thin-walled beams. *Applied Mechanics and Materials*. 2014. Vol. 578–579. Pp. 858–863.
 14. Dyakov S.F., Lalin V.V. Postroyeniye i analiz konechnogo elementa tonkostennogo sterzhnya s uchetom deformatsiy sdviga dlya resheniya zadach dinamiki [Construction and analysis of a finite element of a thin-walled rod with allowance for shear deformations for solving problems of dynamics]. *Internet-zhurnal Naukovedeniye*. 2013. No. 5(18). Pp. 93. (rus)
 15. Perelmutter A.V., Slivker V.I. Ustoychivost ravnovesiya konstruksiy i rodstvennyye problem [Stability of structural equilibrium and related problems]. Vol. 1. Moscow: SKAD SOFT, 2010. 704 p.
 16. Gordeyeva A.O., Vatin N.I. Raschetnaya konechno-elementnaya model kholodnognutogo perforirovannogo tonkostennogo sterzhnya v programmno-vychislitelnom komplekse SCAD Office [Estimated finite element model of a cold-bended perforated thin-walled rod in the software complex SCAD Office]. *Magazine of Civil Engineering*. 2011. No. 3(21). Pp. 36–46. (rus)
 17. Mu L., Wang J., Ye X. A hybridized formulation for the weak Galerkin mixed finite element method. *Journal of Computational and Applied Mathematics*. 2016. Vol. 307. Pp. 335–345.
 18. Ignatyev A.V., Yefremova N.S. Raschet kosougolnoy plastiny po metodu konechnykh elementov v forme klassicheskogo smeshannogo metoda [Calculation of an skew plate by the finite element method in the form of a classical mixed method]. *Stroitel'naya mekhanika i konstruksii*. 2016. Vol. 1. No. 12. Pp. 39–44. (rus)
 19. Ignatyev A.V., Ignatyev V.A., Bochkov M.I. Primeneniye metoda konechnykh elementov v forme klassicheskogo smeshannogo metoda k raschetu sistem s odnostoronnimi svyaziyami [The application of the finite element method in the form of a classical mixed method to the calculation of systems with unilateral constraints]. *Stroitel'naya mekhanika i raschet sooruzheniy*. 2017. No. 2(271). Pp. 52–61. (rus)
 20. Verbitskiy V.V., Verbitskiy A.V. Smeshanny metod konechnykh elementov v zadache o pologoy obolochke s funktsiyey napryazheniy [A mixed finite element method in the problem of a shallow shell with a stress function]. *Izvestiya vysshikh uchebnykh zavedeniy. Matematika*. 2009. No. 5. Pp. 13–23. (rus)
 21. Kulikov G.M., Plotnikova S.V. A hybrid-mixed four-node журнал. 2012. № 1(27). С. 53–73.
 21. Лалин В.В., Розин Л.А., Кушова Д.А. Вариационная постановка плоской задачи геометрически нелинейного деформирования и устойчивости упругих стержней // Инженерно-строительный журнал. 2013. № 1(36). С. 87–96.
 21. Лалин В.В., Зданчук Е.В., Кушова Д.А., Розин Л.А. Вариационные постановки нелинейных задач с независимыми вращательными степенями свободы // Инженерно-строительный журнал. 2015. № 4(56). С. 54–65.
 21. Лалин В.В., Беляев М.О. Изгиб геометрически нелинейного консольного стержня. Решение по теориям Кирхгофа и Коссера – Тимошенко // Инженерно-строительный журнал. 2015. № 1(53). С. 39–55.
 21. Lalin V., Rybakov V., Alexander S. The finite elements for design of frame of thin-walled beams // *Applied Mechanics and Materials*. 2014. Vol. 578–579. Pp. 858–863.
 21. Дьяков С.Ф., Лалин В.В. Построение и анализ конечного элемента тонкостенного стержня с учетом деформаций сдвига для решения задач динамики // Интернет-журнал Науковедение. 2013. № 5(18). С. 93.
 21. Перельмутер А.В., Сливкер В.И. Устойчивость равновесия конструкций и родственные проблемы. Т. 1. М.: СКАД СОФТ, 2010. 704 с.
 21. Гордеева А.О., Ватин Н.И. Расчетная конечно-элементная модель холодногогнутого перфорированного тонкостенного стержня в программно-вычислительном комплексе SCAD Office // Инженерно-строительный журнал. 2011. № 3(21). С. 36–46.
 21. Mu L., Wang J., Ye X. A hybridized formulation for the weak Galerkin mixed finite element method // *Journal of Computational and Applied Mathematics*. 2016. Vol. 307. Pp. 335–345.
 21. Игнатьев А.В., Ефремова Н.С. Расчёт косоугольной пластины по методу конечных элементов в форме классического смешанного метода // *Строительная механика и конструкции*. 2016. Т. 1. № 12. С. 39–44.
 21. Игнатьев А.В., Игнатьев В.А., Бочков М.И. Применение метода конечных элементов в форме классического смешанного метода к расчету систем с односторонними связями // *Строительная механика и расчет сооружений*. 2017. № 2(271). С. 52–61.
 21. Вербицкий В.В., Вербицкий А.В. Смешанный метод конечных элементов в задаче о полой оболочке с функцией напряжений // *Известия высших учебных заведений. Математика*. 2009. № 5. С. 13–23.
 21. Kulikov G.M., Plotnikova S.V. A hybrid-mixed four-node quadrilateral plate element based on sampling surfaces method for 3D stress analysis // *International journal for numerical methods in engineering*. 2016. Vol. 108. No. 1. Pp. 26–54.
 21. Stupishin L.U., Nikitin K.E. Mixed finite element for geometrically nonlinear orthotropic shallow shells of revolution // *Advanced Materials Research*. 2014. Vol. 919. Pp. 1299–1302.
 21. Wolf J.P. Alternate hybrid stress finite element models // *International Journal for Numerical Methods in Engineering*. 1975. Vol. 9. № 3. Pp. 601–615.
 21. Qiu W., Demkowicz L. Mixed hp-finite element method for linear elasticity with weakly imposed symmetry: stability analysis // *SIAM J. Numer. Anal.* 2011. Vol. 49. № 2. Pp. 619–641.
 21. Elakkad A., Bennani M.A., Mekkaoui J., Elkhalfi A. A mixed finite element method for elasticity problem // *International Journal of Advanced Computer Science and Applications*. 2013. Vol. 4. No. 2. Pp. 161–166.
 21. Akimov P.A., Negrozov O.A. Semianalytical structural analysis based on combined application of finite element method and discrete-continual finite element method part 1:

- quadrilateral plate element based on sampling surfaces method for 3D stress analysis. *International journal for numerical methods in engineering*. 2016. Vol. 108. No. 1. Pp. 26–54.
22. Stupishin L.U., Nikitin K.E. Mixed finite element for geometrically nonlinear orthotropic shallow shells of revolution. *Advanced Materials Research*. 2014. Vol. 919. Pp. 1299–1302.
 23. Wolf J.P. Alternate hybrid stress finite element models. *International Journal for Numerical Methods in Engineering*. 1975. Vol. 9. No. 3. Pp. 601–615.
 24. Qiu W., Demkowicz L. Mixed hp-finite element method for linear elasticity with weakly imposed symmetry: stability analysis. *SIAM J. Numer. Anal.* 2011. Vol. 49. No. 2. Pp. 619–641.
 25. Elakkad A., Bennani M.A., Mekkaoui J., Elkhalfi A. A mixed finite element method for elasticity problem. *International Journal of Advanced Computer Science and Applications*. 2013. Vol. 4. No. 2. Pp. 161–166.
 26. Akimov P.A., Negrozov O.A.. Semianalytical structural analysis based on combined application of finite element method and discrete-continual finite element method part 1: two-dimensional theory of elasticity. *Procedia Engineering*. 2016. Vol. 153. Pp. 8–15.
 27. Akimov P.A., Negrozov O.A.. Semianalytical structural analysis based on combined application of finite element method and discrete-continual finite element method part 2: three-dimensional theory of elasticity. *Procedia Engineering*. 2016. Vol. 153. Pp. 16–23.
 28. Gienke E. A simple “mixed” method for plate and shell problems. *Nuclear Engineering and Design*. 1974. Vol. 29. No. 1. Pp. 141–155.
 29. Kuo Y.-L. Stress-based finite element analysis of sliding beams // *Appl. Math. Inf. Sci.* 2015. Vol. 9. No. 2. Pp. 609–616.
 30. Тюкалов Ю.Я. Определение частот свободных колебаний методом конечных элементов в напряжениях // *Инженерно-строительный журнал*. 2016. № 7(67). С. 39–54
 31. Тюкалов Ю.Я. Функционал дополнительной энергии для анализа устойчивости пространственных стержневых систем // *Инженерно-строительный журнал*. 2017. № 2(70). С. 18–32.
 32. Тюкалов Ю.Я. Расчет оболочек произвольной формы методом конечных элементов в напряжениях // *Строительная механика и расчет сооружений*. 2006. № 1. С. 65–74.
 33. Тюкалов Ю.Я. Решение плоской задачи теории упругости методом конечных элементов в напряжениях // *Строительная механика и расчет сооружений*. 2006. № 2. С. 34–38.

Yury Tyukalov,
+7(912)821-89-77; yutvgu@mail.ru

Юрий Яковлевич Тюкалов,
+7(912)821-89-77; эл. почта: yutvgu@mail.ru

© Tyukalov Yu.Ya., 2018

doi: 10.18720/MCE.77.4

Transformable fire barriers in buildings and structures

Трансформируемые противопожарные преграды в сооружениях и строениях

**M.V. Gravit,
O.V. Nedryshkin,
O.T. Ogidan,**

*Peter the Great St. Petersburg Polytechnic
University, St. Petersburg, Russia*

**Канд. техн. наук, заместитель
заведующего кафедры по НИРС
М.В. Гравит,**

**аспирант О.В. Недрышкин,
студент О.Т. Огидан,
Санкт-Петербургский политехнический
университет Петра Великого,
г. Санкт-Петербург, Россия**

Key words: fire curtains; fire barriers; fire resistance; fireproof doors; Intumescent fire retardant coating; IFRC

Ключевые слова: противопожарные шторы; противопожарные барьеры; противопожарные двери; вспучивающееся огнезащитное покрытие

Abstract. Fire curtains are used in case of fire to create a temporary barrier in open technological openings, openings of buildings and structures. The paper presents the results of tests for fire resistance of samples of fire curtains. The ability of intumescent formulations to effectively prevent the spread of heat has been studied. The article presents the results of testing various compositions of Intumescent fire retardant coating (IFRC) with the addition of latex for fire curtains based on silica fiber. The temperature of samples from the non-heated side did not exceed 260 °C (the temperature in the furnace of the test facility did not exceed 1200 °C). The temperature of the sample with the addition of TiO₂ at the end of the test did not rise above 196 °C. The results obtained in the work are compared with similar tests of other researchers for the period 2012–2017 fire curtains based on silica fiber.

Аннотация. Трансформируемые противопожарные преграды (противопожарные шторы) используется в случае пожара для создания временного барьера в открытых технологических проемах, проемах зданий и сооружений. В работе представлены результаты испытаний на огнестойкость образцов противопожарных штор. Изучена способность вспучивающихся составов эффективно предотвращать распространение тепла. В статье представлены результаты испытаний различных композиций интумесцентного вспучивающегося состава с добавлением латекса для противопожарных штор на основе кремнеземного волокна. Температура образцов с не обогреваемой стороны не превышала 260 °C (температура в печи испытательной установке не превышала 1200 °C). Температура образца с добавлением TiO₂ по окончании испытания не поднялась выше 196 °C. Результаты, полученные в работе, сравниваются с аналогичными испытаниями других исследователей за период 2012–2017 противопожарных штор на основе кремнеземного волокна.

1. Introduction

As practice shows, the most effective way of simultaneous provision of safe evacuation of people in case of fire and preservation of material values is the measures established by Federal Law No. 123-FZ [1] to limit the spread of fire, within the framework for which provision is made for the installation of fire barriers - building structures with a standard fire resistance limit.

Fire protection is aimed at finding the most effective, economically feasible and technically sound methods and means of preventing fires and their elimination with minimal damage with the most rational use of forces and technical means of extinguishing [2–7]. Automatic fire curtains are designed to divide sections of premises and structures into fire compartments for the purpose of localizing a fire, as well as filling openings in fire barriers. If a fire occurs, due to a signal from a fire alarm sensor or a signal from a fire station, the blind automatically falls and locates the fire. In [8] the statistics of fires in the cultural and entertainment facilities, and describes the various options for action in case of fire. One of the most

important is a method to increase the evacuation of people from buildings. It involves the use of indoor fire barriers.

In the proposed article [9], the basic advantages of using fire-prevention curtains, as well as prospects for their development. After this are the main technical characteristics of fire barriers.

The authors of [10–12] bring the characteristics of modern fire-prevention structures used to improve the fire safety of buildings and structures. Also described are the design features of fire protection gates, doors, windows, curtains.

The authors [13] developed a mathematical model that describes the physical processes occurring in the fire curtain in the fire and determine its fire. The effectiveness of fire curtains investigated by the authors in [14–19]. With CUrisk model, the authors in [20] analyzed the development of the fire, the model is able to provide data about the failure of fire curtains and calculate the possible options for the spread of hazards fire. In his articles [21–23], the authors consider the materials of which can be made passive fire protection, as well as describe the testing methods of fire barriers in fire conditions.

Such curtains are made of fireproof sheet, which consists of glass fibers. In the initial position, the firewall is wound on a shaft of steel. The shaft is housed in a galvanized case made of steel sheet. Mounted on a wall, ceiling, suspended ceilings. The curtain fabric at the lower end has a special cutting bar. It allows you to keep the canvas unfolded. Bottom edges do not bend, do not let smoke pass. In the collapsed state, the tire is hidden among the recesses of the hull structure, so it is not visible.

Fireproof curtains are often designed as part of engineering and technical measures when developing special technical conditions.

Traditional fire protection solutions with curtains:

- separation of spaces into fire compartments;
- overlapping of window, door, elevator and other openings;
- fencing atriums, escalators, stairs;
- as a fire curtain for the separation of the auditorium and the stage space;
- the formation of pockets for collecting smoke in the under-ceiling space;
- protection against fire from nearby and adjacent buildings;
- protection of openings in fire walls, incl. when the conveyors are installed in them;
- protection of places of increased fire danger;
- as an alternative to glass fire barriers, fireproof windows and fireproof gates.

Fire-prevention curtains are used in production and logistics complexes, in parking lots and at gas stations, at railway stations, in film-concert complexes, museums, in hotel, trade and multifunctional complexes.

The purpose of this work is the development of a flame retardant polymer composition for the treatment of the silica core of a fire curtain, which will increase the fire resistance of the structure.

2. Methods

Testing of experimental samples of fire curtains with intumescent composition was carried out to determine the limiting states of the samples presented on the basis of the test method of the national standard of Russia 53307-2009 Fire doors and gates. Test methods for fire resistance [24] with certain assumptions. The furnace temperature, according to ISO 834-1: 1999, Fire-resistance tests – Part 1: General requirements [25], must be monitored and controlled in such a way that it corresponds to the ratio 1.

$$T = 345 \log_{10}(8t + 1) + 20 \quad (1)$$

where

T – is the average furnace temperature, degrees Celsius;

t – is the time, un minutes.

3. Results and Discussion

Tests have been carried out on the development of an intumescent type fire retardant composition that can become the backbone of a fire retardant curtain when applied to a silica fiber. Under fire conditions, the fireproof composition significantly expands in volume with the formation of a heat-insulating foam-coke layer. The expansion process takes place with a significant endothermic effect, and the resulting heat-insulating layer has a thermal conductivity close in value to the thermal conductivity of the air. According to a number of authors [26], the heat transfer towards the protected surface is reduced by up to 100 times due to the foam box. Before application of the intumescent compound to the sample of the fire curtain, it was mixed with a latex solution to obtain a 4: 1 ratio to achieve elasticity.

Intumescent compositions have been manufactured and tested, the formulations of which are given in Table 1.

Table 1. Shows the comparative information about the Intumescent composition

№	Name	Content, %			
		Sample № 1	Sample № 2	Sample № 3	Sample № 4
1	Graphite IR	-	12	-	-
2	Vermiculite	-	8	-	-
3	Pentaerythritol	10	8	-	-
4	Melamine	10	8	-	-
5	Titanium dioxide	5	5	12	15
6	Ammonium polyphosphate	25	21	10	12
7	Dispersant	0.02	0.02	0.02	0.03
8	Defoamer	0.02	0.02	0.02	0.05
9	Biocide	0.02	0.02	0.02	0.03
10	Thickener	0.03	-	0.03	0.04
11	Aluminum hydroxide	-	-	21	18
12	Vinyl Dispersion	30	30	32	30
13	Plasticizer	4	5	5	3
14	Coalescent	1	-	1	1
15	Microtalk	4	2	5	6

Previously, samples of fire retardants were applied to pieces of 10 to 10 cm foil for testing for flexibility, swelling and ignition. The composition was applied evenly over the entire area of the foil until a thickness of 1 mm was reached. The results are shown in Table 2.

Table 2. Study of intumescent formulations for flexibility, flammability and intumescence

№	Name	Sample № 1	Sample № 2	Sample № 3	Sample № 4
1	Cracked	Yes	No	No	No
2	Flammable	No	No	No	No
3	Height of foam coke	No	3mm	5 mm	5mm

These compositions were applied to a silica cloth, a dry film thickness of 1 mm was achieved. After this, the intumescent properties of the web were tested. For fire tests, the composition was applied to silica cloth 10 × 10 cm on both sides with one layer. The test results were taken as the mean temperature over the area from the unheated side of the samples.

Tools, equipment for testing.

- micrometer;
- gas burner with sample chamber;
- Stopwatch;

- pyrometer ADA TemPro 550;
- ruler.

A visual inspection of each sample for uniformity and homogeneity of the application of the flame retardant coating was carried out. The color of each sample is fixed.

The tests were performed alternately for each sample.

The sample was fixed around the perimeter of the fire chamber. The length of the burner flame was preset within 40–60 mm. When the burner was switched on, the stopwatch was turned on at the same time. The flame temperature of the butane burner is up to 1200 °C. The test flame retention time is 60 min. During the experiment, visual observation of the sample was carried out and recorded:

- intensity of smoke evolution;
- the presence of dripping;
- burning of the sample;
- temperature on the unheated side of the sample.

At the end of the experiment, the area of flame damage was measured.

Sample No.1 before fire test, exposure to flame in the test installation, formed foam with unheated side and state of the silica/glass fiber from the heated side (about 1200 °C) after the tests are presents on Figures 1–4.

Based on the test results, the temperature curves are plotted (Fig. 5). At the entrance of the test, the intensity of the smoke was low / moderate. Combustion of samples 1–2 was not observed throughout the entire experiment.



Figure 1. Sample No.1 before fire test



Figure 2. Exposure to flame in the test installation



Figure 3. Formed foam with unheated side



Figure 4. The state of the silica/glass fiber from the heated side (about 1200 °C) after the tests

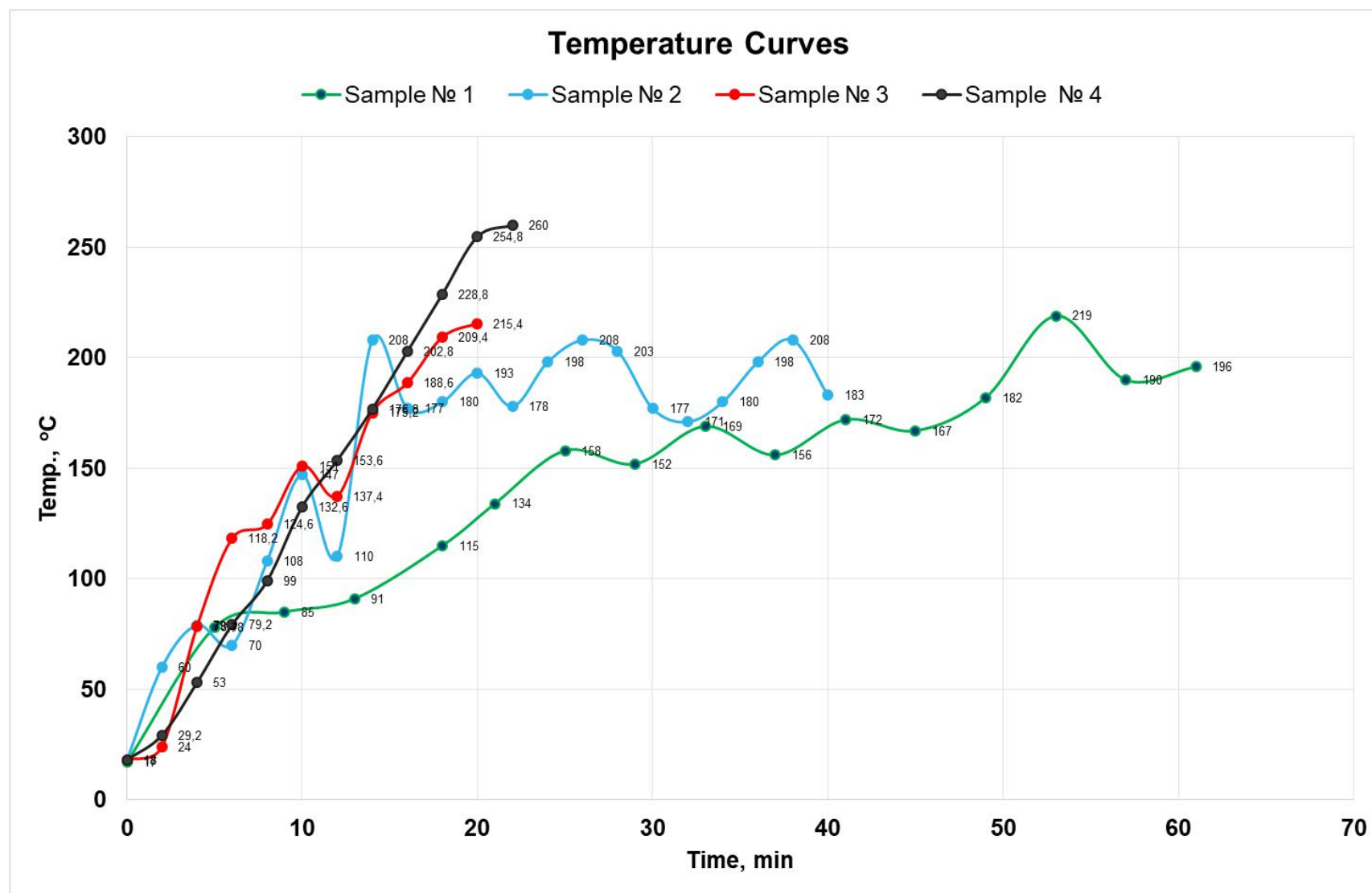


Figure 5. Temperatures curves

Sample No. 1, fire curtain with Intumescent composition (Pentaerythritol, melamine, titanium dioxide, ammonium polyphosphate, dispersant, defoamer, biocide, thickener, vinyl dispersion, plasticizer, coalescent, microtalk): During the tests, there was no sign of loss of integrity (E), as well as loss of thermal insulation (I). The maximum temperature of 219 °C was recorded at the 53 minute test. The temperature from the unheated side of the sample averaged 196 °C on the average in the 60th minute of the test. Sample No. 2 fire curtain with Intumescent composition (graphite IR, pentaerythritol, melamine, titanium dioxide, ammonium polyphosphate, dispersant, defoamer, biocide, vinyl dispersion, plasticizer, coalescent, microtalk): At the 40th minute of the test, there were signs of loss of integrity (E) and signs of loss of thermal insulation (I) did not come. The maximum temperature of 208 °C was recorded on the 26th and 38th minute of the test. The temperature from the unheated side of the sample averaged 183 °C on the average in the 40 minute test. Sample No. 3, fire curtain with Intumescent composition (Vermiculite, graphite IR, pentaerythritol, melamine, titanium dioxide, ammonium polyphosphate, dispersant, defoamer, biocide, thickener, vinyl dispersion, plasticizer, microtalk, aluminum hydroxide): On the 20th minute of the test, there were signs of loss of integrity (E) and signs of loss of thermal insulation (I) did not come. The maximum temperature of 215.4 °C was recorded on the 20th minute of the test. Sample No. 4 fire curtain with Intumescent composition (Vermiculite, graphite IR, pentaerythritol, melamine, ammonium polyphosphate, dispersant, defoamer, biocide, thickener, vinyl dispersion, plasticizer, microtalk, aluminum hydroxide): During the 23 minute test, there were signs of loss of integrity (E) and signs of loss of thermal insulation (I) did not come. The maximum temperature of 260 °C was recorded on the 23 minute test.

In [27–28] the author investigates the characteristics of intumescent composition, the qualitative difference of which is the addition of fiberglass to the composition. One of the presented intumescent compositions provided thermal insulation protection of the steel sample to 197 °C.

This paper [29] described the thermal efficiency of alumina and kaolin clay filler based on Intumescent fire retardant coating. Results showed that by using small quantity of fillers; physically good char structure with uniform expansion was achieved as illustrated by furnace test and it was stable for 2h. Under conditions of heat exposure of 500 °C, the samples of the compositions provided thermal insulation in the range from 100 to 200 °C.

The work [30–31] describes the tests of the intumescent composition in the temperature range 950–1100 °C. Published results are comparable with those obtained in the present work. The temperature of the samples with the intumescent residue presented did not rise above 150 °C. With the exception of the applicability of the formulation to the transformable fire-resistant structures such as fire curtains.

This paper [33–35] discuss the synergistic effects of titanium dioxide (TiO₂) and zinc borate on thermal stability and water resistance of intumescent fire retardant coatings. As in Ref. [35], we used in our Sample No. 1 5 % TiO₂. The composition in [35] protects the surface during testing and the sample temperature does not rise above 150 °C. The comparison results paper [27, 29, 30, 35] are shown in Figure 6.

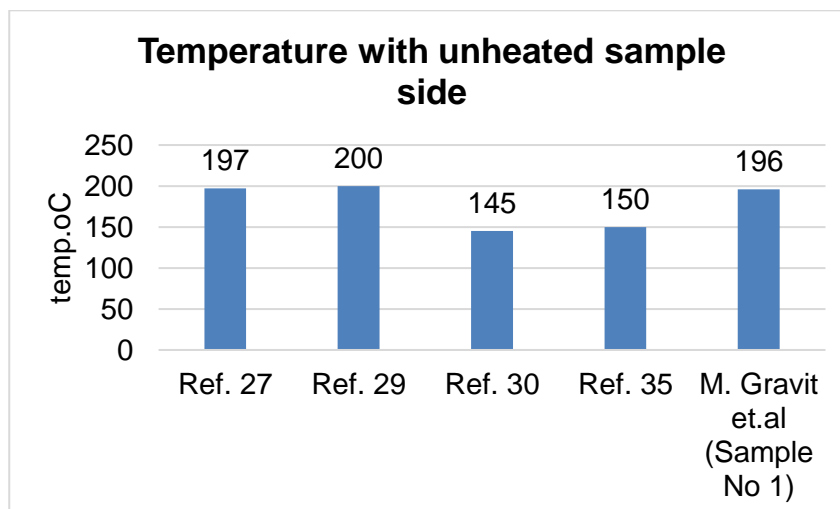


Figure 6. Comparison results of maximum temperature

The results obtained in present work are comparable with similar studies also in the presented work the composition contains latex for maintaining the elasticity, which influenced the nature of intumescence and fireproof properties.

4. Conclusions

The obtained results testify to the effectiveness of applied composition No. 1 (Pentaerythritol, melamine, titanium dioxide, ammonium polyphosphate, dispersant, defoamer, biocide, thickener, vinyl dispersion, plasticizer, coalescent, microtalk). This will be used in the design of a full-scale experiment where the temperature field on the unheated side of the fire curtain of 9 m² will be investigated. Previously, tests were conducted to study the thermosetting of silica tissue. When field tests of silica cloth without special treatment and without coating by intumescent composition, the shrinkage corresponds to the declared range of the manufacturer [36].

References

1. The Federal law of 22 July 2008 № 123-FZ «Technical regulations on fire safety requirements». *Rossiyskaya gazeta*. 2008. No. 163.
2. Korolchenko A.Yu., Getalo D.P. Protivopozharnyye shtory (obzor) [Fire curtains (overview)]. *Fire and Explosion Safety*. 2015. No. 24. Pp. 55–66. (rus)
3. Zaykin S.V., Strakhov V.L. Transformiruyushchiesya ognезashchitnyye zashchitnyye konstruksii povyshennoy ognestoykosti [Transforming fire retardant designs with increased fire resistance]. *Vestnik MGSU*. 2009. No. 4. Pp. 107–112. (rus)
4. Barakovskiy S.A., Ivanov V.A. Razrabotka ustroystv dlya oslableniya teplovogo izlucheniya pri protivopozharnoy zashchite ob'yektov neftegazovogo kompleksa [Development of devices for the attenuation of thermal radiation in the fire protection of oil and gas facilities]. *Izvestiya vysshikh uchebnykh zavedeniy. Neft i gaz*. 2011. No. 1. Pp. 61–66. (rus)
5. Zharov S. Osobennosti i problemy avtomaticheskoy protivopozharnoy zashchity skladov s vysotnym stellazhnykh khraneniym [Features and problems of automatic fire protection of warehouses with high-bay storage]. *Algoritm bezopasnosti*. 2006. No. 5. Pp. 6–9. (rus)
6. Almiyeva L.P., Ashirova A.D. Metody zashchity atriumov [Methods of protecting atriums]. *Sovremennyye tekhnologii obespecheniya grazhdanskoj oborony i likvidatsii posledstviy chrezvychaynykh situatsiy*. 2015. No. 1(6). Pp. 53–56.
7. Krivkov Yu.V., Ladygina I.R., Pivovarov V.V. Protivopozharnyye i protivodymnyye shtory i ekrany [Fire and smoke protection screens and screens]. Moscow: «NITs» Stroitelstvo », 2012. 84p. (rus)
8. Sultanova S.F. Pozharnaya opasnost i sistemy protivopozharnoy zashchity kulturno-zrelishchnykh uchrezhdeniy [Fire danger and fire protection systems of cultural and entertainment establishments]. *Sovremennyye tekhnologii obespecheniya grazhdanskoj oborony i likvidatsii posledstviy chrezvychaynykh situatsiy*. 2014. No.1(5). Pp. 166–169. (rus)
9. Sergunina T. V. Ogne- i dymozashchitnyye pregrady [Fire and smoke protective barriers]. *Pozharnaya bezopasnost v stroitelstve*. 2010. No. 1. Pp. 42–45. (rus)
10. Krutova Ye.V., Sevostyanova K.V. Arkhitekturno-stroitelnyye resheniya po pozharnoy bezopasnosti [Architectural and Building Solutions for Fire Safety]. *Materials of the Interuniversity Scientific and Technical Conference*. No.1. SPb.:SPBGPU, 2006. P. 136. (rus)
11. Jimenez M. et. al. Characterization of the performance of an intumescent fire protective coating. *Surface & Coating Technology*. 2006. Vol. 201. Pp. 979–987.
12. Lyapin A.V. Sovremennyye ogne- i dymozashchitnyye pregrady [Modern fire and smoke protective barriers]. *Fire and Explosion Safety*. 2008. No. 17. Pp. 49–56. (rus)

Литература

1. Федеральный закон от 22.07.2008 № 123-ФЗ «Технический регламент о требованиях пожарной безопасности» // Российская газета. 2008. № 163.
2. Корольченко А.Ю., Гетало Д.П. Противопожарные шторы (обзор) // Пожаровзрывобезопасность 2015. № 24. С. 55–66.
3. Зайкин С.В., Страхов В.Л. Трансформирующиеся огнезащитные защитные конструкции повышенной огнестойкости // Вестник МГСУ. 2009. № 4. С. 107–112.
4. Бараковский С.А., Иванов В.А. Разработка устройств для ослабления теплового излучения при противопожарной защите объектов нефтегазового комплекса // Известия высших учебных заведений. Нефть и газ. 2011. № 1. С. 61–66.
5. Жаров С. Особенности и проблемы автоматической противопожарной защиты складов с высотным стеллажным хранением // Алгоритм безопасности. 2006. № 5. С. 6–9.
6. Алмиева Л.П., Аширова А.Д. Методы защиты атриумов // Современные технологии обеспечения гражданской обороны и ликвидации последствий чрезвычайных ситуаций. 2015. № 1(6). С. 53–56.
7. Кривков Ю.В., Ладыгина И.Р., Пивоваров В.В. Противопожарные и противодымные шторы и экраны. М.: «НИЦ» Строительство », 2012. 84 с.
8. Султанова С.Ф., Пожарная опасность и системы противопожарной защиты культурно-зрелищных учреждений // Современные технологии обеспечения гражданской обороны и ликвидации последствий чрезвычайных ситуаций. 2014. № 1(5). С. 166–169.
9. Сергунина Т.В. Огне- и дымозащитные преграды // Пожарная безопасность в строительстве. 2010. № 1. С. 42–45.
10. Крутова Е.В., Севостьянова К.В. Архитектурно-Строительные решения по пожарной безопасности // Материалы Межвузовской научно-технической конференции. № 1. СПб.: Изд-во СПбГПУ, 2006. С. 136.
11. Jimenez M. et. al. Characterization of the performance of an intumescent fire protective coating // Surface & Coating Technology. 2006. Vol. 201. Pp. 979–987.
12. Ляпин А.В. Современные огне- и дымозащитные преграды // Пожаровзрывобезопасность. 2008. № 17. С. 49–56.
13. Страхов В.Л., Зайкин С.В. Расчет оптимальных параметров огнестойкого экрана противопожарных штор и укрытий // Транспорт на альтернативном топливе. 2010. № 3. С. 20–24.
14. Ройтман В.М. Инженерные решения по оценке огнестойкости проектируемых и реконструируемых зданий. М.: Ассоциация «Пожарная безопасность и наука», 2001. 385 с.
15. Гравит М.В., Еремина Т.Ю., Дмитриева Ю.Н. Конструктивные средства огнезащиты. Анализ

Гравит М.В., Недрышкин О.В., Огидан О.Т. Трансформируемые противопожарные преграды в сооружениях и строениях // Инженерно-строительный журнал. 2018. № 1(77). С. 38–46.

13. Strakhov V.L., Zaikin S.V. Raschet optimalnykh parametrov ognestoykogo ekrana protivopozharnykh shtor i ukrytiy [Calculation of the optimal parameters of the fire-resistant screen of fire curtains and shelters]. *Transport na alternativnom toplive*. 2010. No. 3. Pp. 20–24. (rus)
14. Roitman V.M. *Inzhenernyye resheniya po ocenke ognestoykosti proektiruemykh i rekonstruirovannykh zdaniy* [Engineering solutions for assessing the fire resistance of designed and reconstructed buildings]. Moscow: Associatsiya «Pozharnaya bezopasnost' i nauka», 2001. 385 p. (rus)
15. Gravit M.V., Yeremina T.Yu., Dmitriyeva Yu.N. Konstruktivnyye sredstva ognезashchity. Analiz yevropeyskikh normativnykh dokumentov [Constructive means of fire protection. Analysis of European regulations]. *Fire and Explosion Safety*. 2012. No. 9. Pp. 31–36. (rus)
16. Korsun V., Vatin N., Franchi A., Korsun A., Crespi P., Mashtaler S. The strength and strain of high-strength concrete elements with confinement and steel fiber reinforcement including the conditions of the effect of elevated temperatures. *Procedia Engineering*. 2015. Vol. 117. Pp. 970–979.
17. Гравит М. В., Хасанов И. Р., Еремина Т. Ю., Макеев А. А. Использование принципа расширенного применения результатов испытаний строительных конструкций и материалов в европейской системе нормирования пожарной безопасности // Архитектура и строительство России. 2013. № 3. С. 24–28.
18. Гравит М.В. Распространение результатов испытаний на огнестойкость светопрозрачных ограждающих не несущих конструкций // Пожаровзрывобезопасность. 2016. № 11. С. 42–45.
19. Turco M., Lhotsky P., Hadjisophocleous G. Investigation into the use of a water curtain over openings to prevent fire spread // MATEC Web of Conferences. 2016. № 46. Pp. 1–11.
20. Li X., Sun X., Wong C.F., Hadjisophocleous G. Effects of fire barriers on building fire risk – a case study using CURisk // *Procedia Engineering*. 2016. № 135. Pp. 445–454.
21. Mróz K., Hager I., Korniejenko K. Material solutions for passive fire protection of buildings and structures and their performances testing // *Procedia Engineering*. 2016. № 151. Pp. 284–291.
22. Kandola B.K., Akonda M.H., Horrocks A.R. Fibre-reinforced glass/silicate composites: effect of fibrous reinforcement on intumescence behaviour of silicate matrices as a fire barrier application // *Materials and Design*. 2015. № 86. Pp. 80–88.
23. Kozlowski R., Malgorzata M., Bozena M. Comfortable, flexible upholstery fire barriers on base of bast, wool and thermostable fibres // *Polymer Degradation and Stability*. 2011. № 96. Pp. 396–398.
24. ГОСТ Р 53307-2009 Конструкции строительные. Противопожарные двери и ворота. Метод испытаний на огнестойкость
25. ISO 834-1:1999 Fire-resistance tests - Elements of building construction – Part 1: General requirements. System requirements:
26. Shkulin S. et al. Intumescent coatings and processes taking place in them // *Chemical fibers*. 2004. Pp. 33–38.
27. Ahmad F., Ullah S., Hamizol M.S. To study the effect of aluminium trihydrate and fumed silica on Intumescent fire retardant coating // *J. Appl. Sci.* 2012. Vol. 12. Pp. 2631–2635.
28. Amira N. et.al. Effects of hybrid fibre reinforcement on fire resistance performance and char morphology of intumescent coating // MATEC Web of Conferences. 2016. Vol. 38. 03001.
29. Aziza H. et.al. Effect of kaolin clay and alumina on thermal performance and char morphology of intumescent fire retardant coating // MATEC Web of Conferences. 2014. Vol. 13. 04013.
30. Ullah S. et al. Development and testing of intumescent fire retardant coating on various structural geometries // *Applied Mechanics and Materials*. 2016. Vol. 699. Pp. 360–365.
31. Ullah S. et al. Effects of ammonium polyphosphate and boric acid on the thermal degradation of an intumescent fire retardant coating // *Progress in Organic Coatings*. 2017. Vol. 109. Pp. 70–82.
32. Puri R.G., Khanna A.S. Effect of cenospheres on the char formation and fire protective performance of water-based intumescent coatings on structural steel // *Progress in Organic Coatings*. 2016. Vol. 92. Pp. 8–15.
33. Aziz H. et al. Effect of titanium oxide on fire performance of европейских нормативных документов // Пожаровзрывобезопасность. 2012. № 9. С. 31–36.

28. Amira N. et.al. Effects of hybrid fibre reinforcement on fire resistance performance and char morphology of intumescent coating. *MATEC Web of Conferences*. 2016. Vol. 38. 03001.
29. Aziza H. et.al. Effect of kaolin clay and alumina on thermal performance and char morphology of intumescent fire retardant coating. *MATEC Web of Conferences*. 2014. Vol. 13. 04013.
30. Ullah S. et al. Development and testing of intumescent fire retardant coating on various structural geometries. *Applied Mechanics and Materials*. 2016. Vol. 699. Pp. 360–365.
31. Ullah S. et al. Effects of ammonium polyphosphate and boric acid on the thermal degradation of an intumescent fire retardant coating. *Progress in Organic Coatings*. 2017. Vol. 109. Pp. 70–82.
32. Puri R.G., Khanna A.S. Effect of cenospheres on the char formation and fire protective performance of water-based intumescent coatings on structural steel. *Progress in Organic Coatings*. 2016. Vol. 92. Pp. 8–15.
33. Aziz H. et al. Effect of titanium oxide on fire performance of intumescent fire retardant coating. *Advanced Materials Research*. 2014. Vol. 935. Pp. 224–228.
34. Apaydin K., Laachachi A., Ball V., Jimenez M., Bourbigot S., Ruch D. Layer-by-layer deposition of a TiO₂-filled intumescent coating and its effect on the flame retardancy of polyamide and polyester fabrics. *Colloids and Surfaces A: Physicochemical and Engineering Aspects*. 2015. Vol. 469. Pp. 1–10.
35. Amir N., Ahmad F. et.al. Synergistic effects of titanium dioxide and zinc borate on thermal degradation and water resistance of epoxy based intumescent fire retardant coatings. *Key Engineering Materials*. 2017. Vol. 740. Pp. 41–47.
36. Nedryshkin O., Gravit M., Lyapin A., Voronin V. Overview of fire curtains in constructions. *MATEC Web of Conferences IPICSE-2016*. 2016. № 86. 04052.

Marina Gravit,
+7(921)912-64-07; marina.gravit@mail.ru

Oleg Nedryshkin,
+7(999)205-58-52; nedryshkin@gmail.com

Olamipe Ogidan,
+7(911)096-77-45; ogidano@gmail.com

Марина Викторовна Гравит,
+7(921)912-64-07;
эл. почта: marina.gravit@mail.ru

Олег Вячеславович Недрышкин,
+7(999)205-58-52;
эл. почта: nedryshkin@gmail.com

Оламипе Тимоти Огидан,
+7(911)096-77-45;
эл. почта: ogidano@gmail.com

© Gravit M.V., Nedryshkin O.V., Ogidan O.T., 2018

doi: 10.18720/MCE.77.5

Ventilated facade integrated with the HVAC system for cold climate

Вентилируемые фасады, интегрированные с инженерными системами здания для холодного климата

M.R. Petrichenko,

D.V. Nemova,

E.V. Kotov,

D.S. Tarasova,

V.V. Sergeev,

*Peter the Great St. Petersburg Polytechnic
University, St. Petersburg, Russia*

Д-р техн. наук, заведующий кафедрой

М.Р. Петриченко,

канд. техн. наук, доцент, директор центра

Д.В. Немова,

аспирант Е.В. Котов,

ассистент Д.С. Тарасова,

д-р техн. наук, профессор,

член-корреспондент РАН, проректор по

научной работе В.В. Сергеев,

Санкт-Петербургский политехнический

университет Петра Великого,

г. Санкт-Петербург, Россия

Key words: convective heat transfer; energy performance; building energy performance; energy efficiency; integrated systems; energy conservation; civil engineering; structural engineering; building and construction

Ключевые слова: термогравитационная конвекция; замкнутый термогравитационный контур; гидравлика воздушных потоков; энергоэффективность зданий и сооружений; тепломассоперенос; ресурсосбережение; конструктивное энергосбережение

Abstract. The application of convective heat transfer for air mass displacement in ventilation systems without the mechanical draft (integration of Double Skin Facade with HVAC Systems of the building) has a real practical perspective for Building energy performance. The purpose of this article is development of the theory of heat and mass transfer in capillary-porous media, air flows and building structures. The engineering purpose is a concept development of a closed ventilating circuit with convective heat flow to reduce the pressure on the environment, improve the comfort of the building and reduce operating costs. The subject of this research is a closed ventilating circuit with convective heat flow in constructive energy system (ventilated facade integrated with the HVAC system). It was the mathematical modeling of convective heat flow in ventilated facades. Based on the results obtained the concept of a closed ventilating circuit with convective heat flow is developed. The proposed system uses Convective heat transfer in a ventilated facade for the ejection and injection facilities, heat recovery in the buffer zone of the façade. It allows reducing ecological pressure on the environment and the application of energy resources.

Аннотация. Использование термогравитационной конвекции для перемещения воздушных масс в системах вентиляции без применения механического побуждения при условии интеграции вентиляционной системы с фасадными конструкциями здания имеет реальные практические перспективы. Целью данной статьи является развитие теории тепломассопереноса в гетерогенных средах, в том числе в капиллярно-пористых средах, воздушных потоках и строительных конструкциях. Технической целью статьи является создание концепции замкнутого вентиляционного контура (система вентиляции и кондиционирования, интегрированная с фасадными конструкциями) с термогравитационным течением, предназначенного для снижения экологического давления на окружающую среду, повышения комфортности здания и снижения эксплуатационных затрат. Объектом исследования является замкнутый термогравитационный контур в системе конструктивного энергосбережения (фасадные конструкции, интегрированные с системами вентиляции и кондиционирования). Разработана математическая модель замкнутого вентиляционного контура с термогравитационным течением, не требующая механического оборудования для организации движения воздуха. Предлагаемая система использует термогравитационную конвекцию в вентилируемом фасаде для эжекции и инъекции в

Петриченко М.Р., Немова Д.В., Котов Е.В., Тарасова Д.С., Сергеев В.В. Вентилируемые фасады, интегрированные с инженерными системами здания для холодного климата // Инженерно-строительный журнал. 2017. № 1(77). С. 47–58.

помещениях, рекуперацию теплоты в буферной зоне фасада, что позволяет снизить экологическое давление на окружающую среду, сократить использование невозобновляемых энергетических ресурсов.

1. Introduction

Control of indoor climate systems, ventilation, heating and air conditioning systems usually implies a high energy and economic costs. For heat exchange between the flows of supply and exhaust air are typically used air-to-air heat exchangers. Heat exchangers produce a transfer of tangible (visible) energy due to temperature difference on the surfaces. However, after a long period, the temperature difference between the air flows in the air intake is usually reduced and as a consequence some of the energy becomes insignificant. Another typical energy-saving solution is the introduction of ventilated facades using external or internal air, for reduction of thermal loads [1–5].

The design principles of envelope structures with the use of modern technology “active energy efficiency” and the recovery heat flow are investigated in the works [6–11]. The paper presents data on the transmission of heat recovery and special organization of the admission conditions of a flow of external air and its subsequent passage through the building envelope. The scientific groups provide theoretical and experimental data on the study of integration of ventilated facade systems with ventilation systems [12–14].

The combination of these technologies allows for the recovery of thermal energy and represents the implementation of the building envelope, mechanical ventilated exhaust the internal air outlet of the ventilated façade must have a temperature lower than the outdoor temperature in summer or in winter [15-16].

In the article [17-18] a numerical study of the efficiency of integrated energy-saving system consisting of a mechanically ventilated opaque façade and air-to-air heat exchanger. The transfer of energy from an external flow of air to the inside, leaving an air gap.

Exhaust air in the ventilated facade is subjected to a process of evaporative cooling at the beginning and throughout the height of the building.

In [19] numerical modeling for light frame building structures having different values of the resistance of heat transfer for different external conditions and for various internal heat loads. The energy efficiency of the proposed system is compared with efficiency of conventional systems: the traditional wall with an air gap and a recovery system of air, where the air is transferred from the supply system to exhaust the air and out of the building.

Currently, the typical functioning of the systems of ventilation and conditioning of modern buildings directly associated with high energy consumption for moving large volumes of air masses and maintain the required parameters of the microclimate (humidity, temperature, carbon dioxide concentration). They are designed, usually with the use of inefficient mechanical equipment and require additional allocation of usable space and volume to accommodate and service and the relevant regulatory measures for their maintenance. To operate such a relatively inefficient system consumes considerable additional non-renewables, accompanied by additional environmental pressure on the environment [20–24].

One of the promising directions in the construction is high-rise buildings. One of the many tasks due to the altitude is the specificity of the design and installation of ventilated façade system.

The metal thin-walled structure of the hinged facade works separately from the main wall. In this regard, with the incorrect method of calculating the facade structure, there is a risk of deformation of the structure and its further collapse [25–29].

The systems of ventilation and conditioning with rare exceptions do not provide for integration with façade and limited use of the capabilities of thermo-gravitational convection.

It is obvious that there is a real practical prospects for the use of thermo-gravitational convection for movement of air masses in ventilation systems without the use of mechanical impulses when integrated ventilation system with front designs of the building. Maintenance of such a system would not require energy resources, reducing ecological pressure on the environment, increases the comfort of the building and dramatically reduce maintenance costs.

The purpose of this article is development of the theory of heat and mass transfer in capillary-porous media, air flows and building structures. The engineering purpose is a concept development of a closed ventilating circuit with convective heat flow to reduce the pressure on the environment, improve the comfort of the building and reduce operating costs.

Petrichenko M.R., Nemova D.V., Kotov E.V., Tarasova D.S., Sergeev V.V. Ventilated facade integrated with the HVAC system for cold climate. *Magazine of Civil Engineering*. 2018. No. 1. Pp. 47–58. doi: 10.18720/MCE.77.5.

The subject of this research is a closed ventilating circuit with convective heat flow in constructive energy system (ventilated facade integrated with the HVAC system).

2. Methods

2.1. The development of hydraulic methods for solving problems of heat-gravitational convective flows

The main applied mathematical apparatus is numerical modeling of flows and fields of conservative impurity (temperature and moisture concentration) in licensed packages of programs using difference and variational-difference methods for solving parabolic and elliptic systems of equations (motion, momentum transfer, energy, impurity, heat propagation), allowing to obtain so-called "strong" solutions in the topology of uniform grid convergence. For validation of the numerical methods, it is planned to conduct full-scale physical experiments.

Processing and verification of experimental data is carried out using standard packages of mathematical statistics. Since technical solutions in the field of energy-efficient construction are mainly focused on normative materials produced empirically, the unity of the methods used to solve the problems of building Thermophysics can be seen in the theory of heat and mass transfer of solid and elastic capillary-porous bodies forming heterophase systems.

Currently, all known approaches to solving problems for such systems have insufficient connection with the basic provisions of the physics of surface phenomena. Therefore, it is planned to develop a physical model of non-stationary processes of interconnected heat and mass transfer taking into account the intensity of mass transfer between phases, thermocapillary flows, conditions of mechanical and dynamic equilibrium on curved surfaces of the phases. It is also assumed to propose and justify the rheological model of heterophase systems, characterized by the possibility of application in a wide range of unstable temperature and humidity conditions.

Next, we formulate the system of differential equations and boundary conditions for the nonstationary heat and mass transfer with account of capillary forces in the capillary-porous media taking into account the thermodynamics and physics of surface phenomena, with one voice describes the filtering process in case of incomplete saturation with the aim of optimizing the process of heat transfer and management.

The theory of heat-gravitational convective flows should not be considered by hydrodynamic theory of heat-gravitational convection with its set of methods and solutions including the theory of jet boundary layers [30–33].

Below the basic position of the hydraulic theory of heat-gravitational convective flows are listed in a dogmatic form. In part it demonstrates the possibilities of this theory and it is adapted for simple solutions of specific ventilation's problem.

The hydraulic calculation methods of heat-gravitational convective flows are based on the following assumptions:

1). The Boussinesq approximation: the pressure distribution in the heat-gravitational convective flows is hydrostatic:

$$\frac{dp}{\rho} + g dz = 0,$$

where z – is a vertical coordinate [3]

The momentum equation at the vertical plane has the form:

$$u_z \frac{\partial u_z}{\partial z} + u_y \frac{\partial u_z}{\partial y} = g\theta + \frac{\partial \tau}{\partial y},$$

where τ – is the friction force, $u_{z,y}$ – components of the velocity vector u , y – is a coordinate directed across the flow, $\theta = \frac{T - T_c}{T_h - T_c} \in (0,1)$, $T_c < T_h$;

2). It is considered that heat-gravitational convective flows – is a barotropic flow, $p = p(\rho)$. More precisely the condition of barotropicity is replaced by the condition of polytropes: $p = p_0 \left(\frac{\rho}{\rho_0} \right)^n$, with the

polytropic exponent n . In the case of thermal equilibrium (stationary gas), $n=k$, k – for a perfect diatomic gas (air) $k=7/5$. In the case of barotropic motion with the supply of heat from the hot wall: $n < k$. Then if $1 < n < k$, it is the cooling air in the flow's direction. If $n < 1$, the air is continuously heated in the direction of heat-gravitational convective flows.

3). The polytropic exponent n is uniquely determined by the intensity of heat exchange between the air and the hot wall. If $S_i=0 \rightarrow n=k$; $S_i=\infty$, $n=1$. Then, for example, when $1 < n < k$ at a convenient approximation $n = k - (k-1) \text{th} St$, $St = \text{arth} \frac{k-n}{k-1} = \ln \sqrt{\frac{2k-n-1}{n-1}}$, $1 < n < 2k-1$, where $St := \frac{\alpha}{\rho C_p v}$ -

the Stanton's number, α - the coefficient of heat transfer from hot wall to the stream, v – the average velocity in heat-gravitational convective flows;

4). The momentum equation contains 3 density distribution sought for (pressure and 2 components of velocity). A system of equations is compiled: the momentum equation is contained by the energy equation and the displacement continuity equation. The density associated with the barotropic pressure connection (barotropicity condition). In the hydraulic version of heat-gravitational convective flows the density distribution are replaced by the distributions: velocity by average velocity, temperature by average flow temperature.

5). The corresponding equality are formulated for the integral distribution:

$$v = \varphi \sqrt{2gL(1 - T_c / T_h)},$$

$$\frac{dT}{d\bar{x}} + StT = StT_h,$$

$$\dot{m} := \rho v h = \text{const},$$

where h – channel width, L – its length, φ – velocity coefficient, $\varphi = \frac{1}{\sqrt{1+\zeta}}$, ζ – pressure loss factor [3].

The first relation is a consequence of energy integral (Bernoulli) for the heat-gravitational convective flows, and the second relation is a consequence of the first start to flow in a heated channel (the condition of entropy balance) and finally, the third relation is the displacement continuity condition.

The dependence is fair for average velocity [4]:

$$v = \varphi \frac{gL}{\sqrt{RT_c}} \sqrt{\frac{1}{n} - \frac{1}{k}},$$

R – the individual gas constant. For air, approximately, $R=287 \text{ m}^2/(\text{s}^2\text{K})$.

$$\text{Then: } v = \varphi \frac{gL}{\sqrt{RT_c}} \sqrt{\frac{k-1}{k}} \approx \frac{\varphi}{2} \frac{gL}{\sqrt{RT_c}}.$$

The last expression in dimensionless form is possible to write in "similarity criterion":

$$v / \sqrt{gL} = \frac{\varphi}{2} \sqrt{\frac{gL}{RT_c}}. \text{ Indeed, } v / \sqrt{gL} := Fr - \text{ the Froude number for heat-gravitational convective}$$

flows, $\sqrt{gL/RT_c} = Ba$ - number Barstow, measuring the ratio of the Lagrangian velocity \sqrt{gL} to the velocity of sound in cold air, $\sqrt{RT_c}$. Then:

$$Fr/Ba = \varphi \sqrt{\frac{k-1}{k}} = \varphi/2$$

$$\text{or } Fr = \varphi \sqrt{2(1 - T_c/T_h)}$$

The use of variables similarity is convenient for simulations of real building structures in laboratory settings (Fig.1)



Figure 1. Physical model

6). For a real air flow in heat-gravitational convective flows the assessment is evaluated $\frac{v^2}{2} \ll \frac{p}{\rho}$.

Therefore the integral of the kinetic energy can be neglected velocity head [3];

7). For example, if the vertical ventilation manifold with constant cross section A is equal to the releases section A_e and coefficient loss factor ζ. Let, further, an icon 1 shows the flow parameters in the reservoir before release, icon 2 – after the release and the icon e in the news. Given: velocity v₁, pressure p₁, square section of the vent of the collector editions, A, A_e. Find the velocity and velocity distribution along the length of the manifold [5]. The equation of balance of kinetic energy with the use limitations of paragraph 6 is:

$$p_1 A v_1 = p_2 A v_2 + p_e A_e v_e + \zeta A_e \rho \frac{v_e^2}{2}$$

$$p_2 = p_1 - \frac{\rho}{2} (v_1^2 - v_2^2) = p_1 - \frac{\rho}{2} (v_1^2 - (v_1 - n v_e)^2), n := A_e / A < 1$$

We assume p_e=0. Then the sequence of velocities in the sections between the editions forms a geometric progression:

- after the first issue: $v_2 = v_1 \frac{\zeta - n}{\zeta + n}$;

- after any k-1 issue: $v_k = v_1 \left(\frac{\zeta - n}{\zeta + n} \right)^k$;

- velocity in k issue:

$$v_{e,k} = n^{-1}(v_{k-1} - v_k) = n^{-1}v_1 z^{k-1}(1-z), k = 2(1)\omega, z := \frac{\zeta - n}{\zeta + n} < 1$$

ω – the number of issues:

- pressure on any part of the header $p_k = p_{k-1} - \rho/2(v_{k-1}^2 - v_k^2)$.

Then it turns out that to align the costs of air releases and average velocity along the length of the collector it is necessary to design issues so that the least z different from 1, i.e. to either $\zeta \gg 1$, or $n \ll 1$, either simultaneously fulfill both inequalities. Real air editions of the condition $n < 0,1$ guarantees the homogeneity of the flow releases;

8). Dissipation power flow in the collector of the ventilation shaft is determined by the standard according to the formula:

$$P_w := \frac{1}{2} \rho A \sum_{k=2}^{\omega} v_{k-1} (v_{k-1}^2 - v_k^2) = \frac{1}{2} \rho A v_1^3 \sum_{k=2}^{\omega} z^{2(k-1)} (1-z) = \frac{1}{2} \rho A v_1^3 (1 - z^{2\omega}).$$

If the number of issues $\omega \gg 1$, then $P_w \leq 1/2 \rho A v_1^3$. Power dissipation by releases is

$$P_w^{(e)} = \frac{1}{2n} \rho A_e v_1^3 \zeta (1 - z^{\omega}) \leq \frac{1}{2n} \rho A_e v_1^3.$$

For example, if $A=1 \text{ m}^2$, $v=20 \text{ m/s}$, air density is standard, $\rho = 1.19 \text{ kg/m}^3$, the dissipation heat in the collector capacity will be the quantity of the order 4 kW. The same power dissipated on releases. The total value of dissipation heat power is about 8kW. Taking into account the efficiency of the ventilation installation, the electric power consumption will be approximately 10 kW. Supplied with a ventilation manifold in space consumption will be about 70000 m^3/h . It is easy to recalculate the vent manifold to any other air flow;

9). Hydraulic theory of heat-gravitational convective flows intersects with accurate hydro-mechanical theory in the model boundary layer. The fact is that, in vertical channels when the Rayleigh numbers

$$Ra := \sigma \frac{gL^3}{\nu^2} \frac{T_h - T_c}{T_h} \leq 10^9, \text{ heat-gravitational convective flows are laminar. The near-wall}$$

boundary layer lift force has a thickness $\delta = \sqrt[4]{\frac{\nu^2 x}{g}}$, σ – Prandtl number, a maximum of a few millimeters

and never fills the entire vertical width of the ventilated channel, contrary to the assertions of some authors [7].

In these circumstances the description of the flow is reduced to limit the problem of Case [6] for the dimensionless stream function $f := \psi / \sqrt{\nu dz}$, $f \in (0, a)$ and the dimensionless temperature difference

$\theta := \frac{T - T_c}{T_h - T_c} \in (0, 1)$. It is considered that $f=f(\zeta)$, $\theta=\theta(\zeta)$, $\zeta:=y/\delta$, $0 < \zeta < \infty$. We denote the derivative touches

the required distributions f and θ variable ζ . Then $f' = df/d\zeta$ proportional to the local longitudinal velocity in the boundary layer, $f'' = d^2f/d\zeta^2$ proportional to the friction, $\theta' = d\theta/d\zeta$ proportional to the heat flow across the heat-gravitational flow from the hot wall. The ultimate objective of Case can be formulated as follows:

$$f''' + 3ff'' - 2f'^2 + \theta = 0,$$

$$\theta'' + 3\sigma f\theta' = 0,$$

$$f(0) = f'(0) = \theta(0) - 1 = \theta(\infty) = f'(\infty) = 0.$$

Main results:

- velocity distribution $f'(\zeta) = \zeta \exp(-3\sigma a \zeta)$ and the maximum velocity are near the hot wall. The velocity profile is the same as in grazing torch (wall jet);

- temperature distribution $\theta = \exp(-3a\sigma\zeta)$;

- the distribution of friction decreases in ζ from a maximum value at the hot wall, $\zeta=0$, to zero outside the boundary layer, $\zeta=\infty$: $f''(\zeta) = \exp(-3a\sigma\zeta) - 3a\sigma\zeta \exp(-3a\sigma\zeta)$;

- the heat flux distribution is monotone-decreasing quantity of ζ : $\theta'(\zeta) = 3a\sigma \exp(-3a\sigma\zeta)$.

Having a local velocity profiles and temperature difference, it is easy to spend an averaging across the width of the channel and the flow rate and find the hydraulic distribution (average velocity and average flow temperature).

2.2. Optimization of the heat and mass transfer in systems of constructive energy saving

To minimize heat losses through the external envelope the research of flow and heat transfer in capillary-porous medium in building structures.

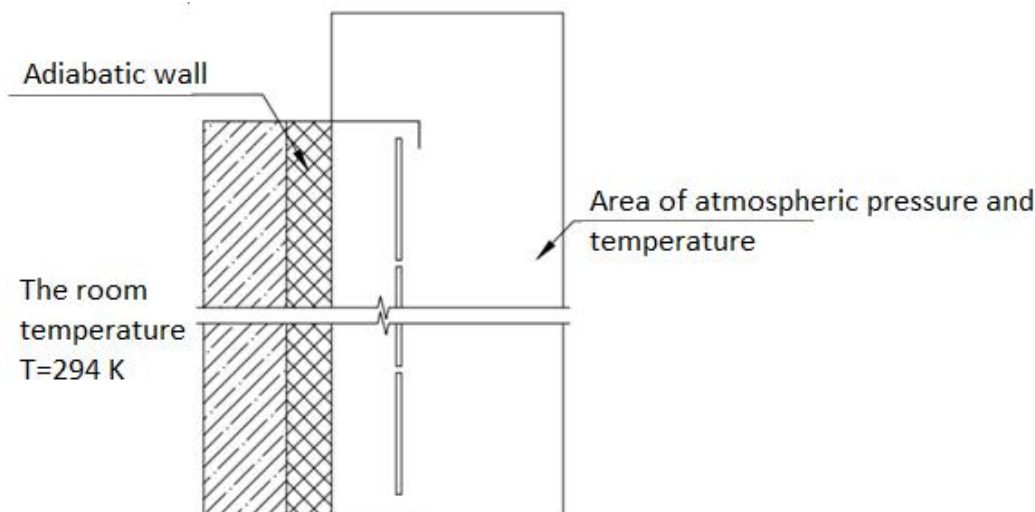
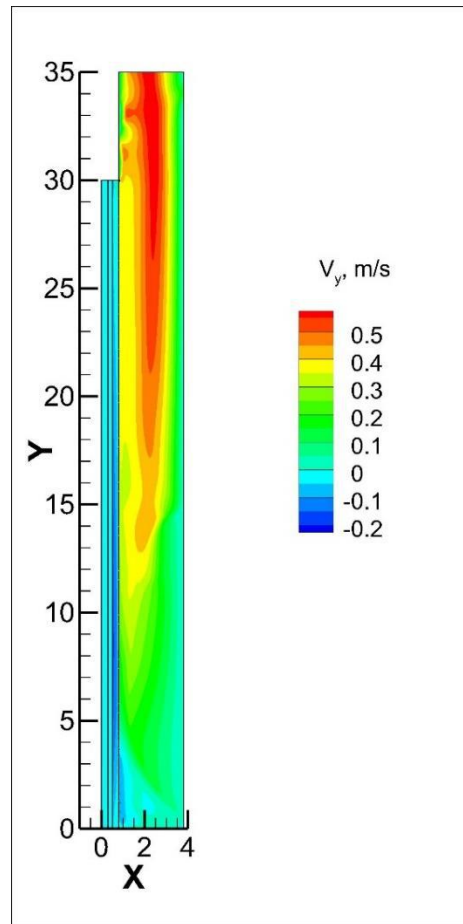
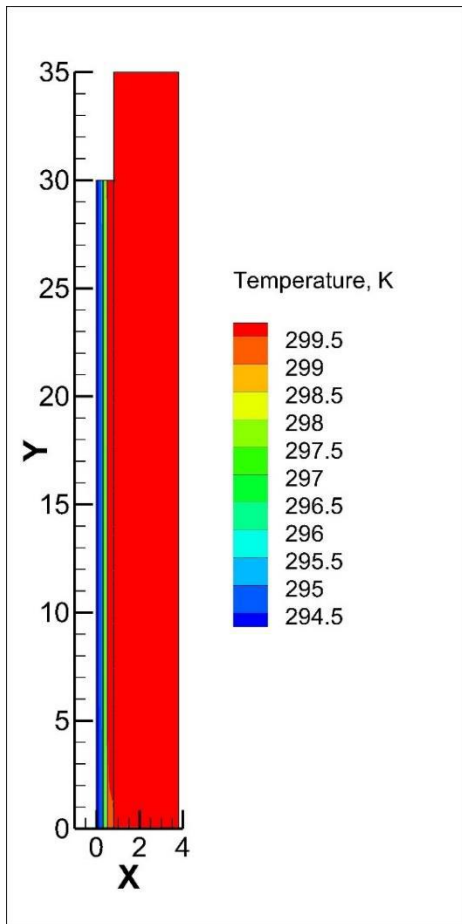


Figure 2 The estimated model of the external envelope

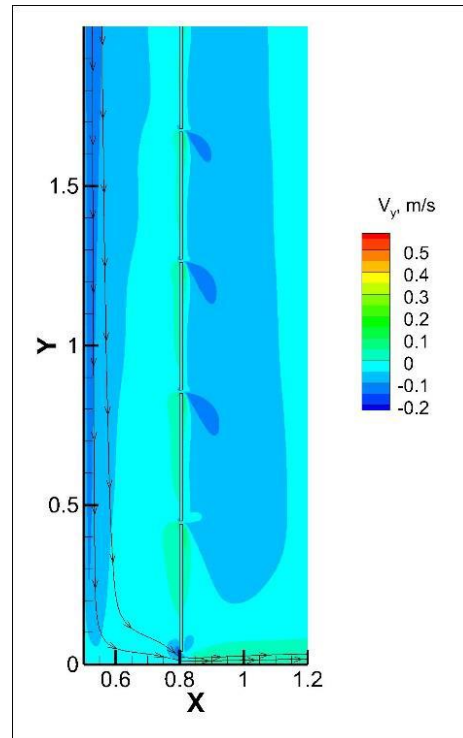
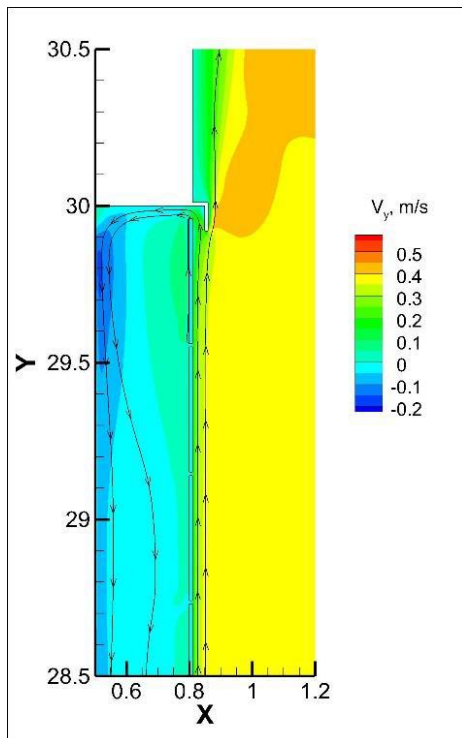
To calculate the following temperatures is used:

- 235.4 K the regions with large difference in temperature throughout the year;
- 289.8 K – the temperature outside equals the temperature of the outer surface of the insulation;
- 300 K – high ambient temperature.

Below there are results of calculations for different climatic zones for buildings with a height 30m



Figures 3–4. Isotherms, isolines of velocity ($d=300\text{mm}$ $L=30\text{m}$. $T=300\text{K}$)



Figures 5–6. Velocity vectors ($d=300\text{mm}$ $L=30\text{m}$. $T=300\text{K}$) in the upper and lower parts.

3. Results and Discussion

In recent years the systems of ventilated facades are widely spread in different regions with different climatic conditions. This is due to the fact that modern ventilated facades possess such qualities as energy efficiency, reducing the influence of solar insolation on the microclimate inside the building, protection from noise impacts and a wide range of design solutions. Considering all these qualities of ventilated facades, the solution of the organization of heating and ventilation to the building to increase its efficiency is proposed.

Principles of design of envelope structures with the use of modern technology of “active energy efficiency” and the recovery heat flux are investigated [6–11]. The paper presents data on the transmission of heat recovery and special organization of the conditions of admission of a flow of external air and its subsequent passage through the building envelope. The scientific groups provide theoretical and experimental data on the study of integration of ventilated facade systems with ventilation systems [12–14]. In this paper the minor energy consumptions with respect to a basic configuration consisting of a traditional closed cavity wall and recovery equipment wherein energy is transferred from the outdoor air to the exhaust air extracted from within the building, are also calculated by introducing a cooling performance index and discussed in full details. A dimensional empirical correlation that expresses such cooling performance index as a function of the several independent variables considered is also proposed [15].

The thermo-circuit is shown at figure 7. In basis of thermo-circuit is the natural convection and the recovery of the energy expended for air heating in the facade. The principle of operation of the circuit as follows: air enters from the atmosphere through the rusty to the channel between the facade and insulation. Due to the temperatures difference on the thermal insulation and facade air is heated in the channel and begins naturally rising to the top. Next the heated air is collected around the perimeter of the roof and is supplied to filtration-pumping station. But before it get into it, the oxygen level of taking air mass are monitored (if the oxygen level is low, the filtration-pump system is able to collect air from the environment). Filtration-pumping system consists of three main elements: the numeral 1 is a high performance air pump high pressure; 2 – filter system (cyclone separator); 3 – heating device. After filtration and pumping the air gets into the ventilation shaft to the rooms to provide the necessary climate conditions. It is possible to adjust the resistance at the outlet of the ventilation ducts leading from the mine to the premises. To adjust the operation of the filtration and pumping system the sensors pressure is installed in the ventilation shaft, which you can adjust the mass flow in the circuit. Supply air to the rooms is carried out through the ducts in the floor. Due to the natural convection the heated air rises to the ceiling, then it gets into the output part of the ventilation system which leads the air back to the ventilated façade.

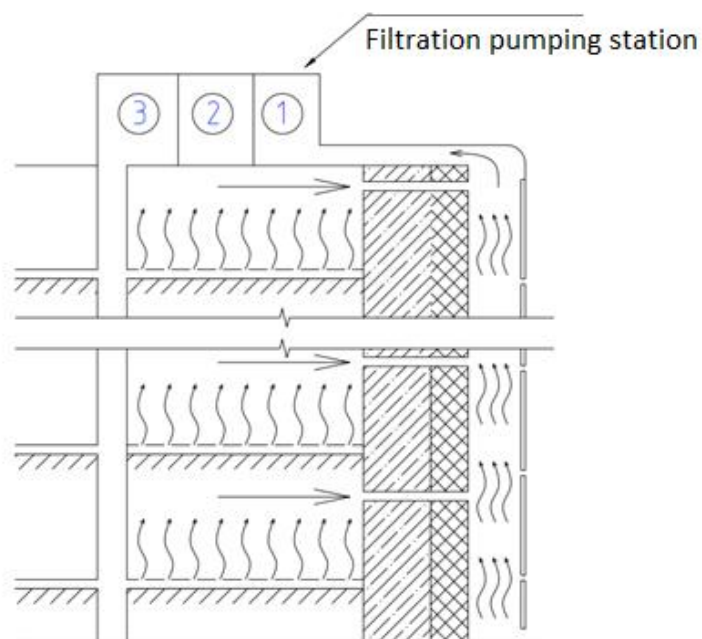


Figure 7. The closed ventilating circuit with convective heat flow

4. Conclusions

It is developed hydraulic methods of calculation of heat-gravitational flows, complicated heat and mass transfer, allowing proposing specific design solutions and reasonable methods of determining parameters and dimensions of the elements of the circuit. It is established that paving a local velocity profiles and temperature difference, it is easy to spend an averaging across the width of the channel and the flow rate and find the hydraulic distribution (average velocity and average flow temperature).

The concept of closed ventilating circuit with convective heat flow is developed (HVAC integrated with ventilated system facade) based on heat-gravitational convection, does not require mechanical equipment to air displacement. The proposed system uses thermo-gravitational convection in a ventilated facade for the ejection and injection facilities, recovery of heat in the buffer zone of the facade. The air flows in the facade through the holes on the outer face of the facade and perceive the warmth of the inner face of the facades and air flow induced from the premises. The buffer zone acts as a heat exchanger and is used as a heat-shielding layer of the building. In this system the air as incompressible fluid, the fluid obeying the laws of hydraulics. The velocity distribution $f'(\zeta) = \zeta \exp(-3\sigma\alpha\zeta)$ and the maximum velocity are near the hot wall. The velocity profile is the same as in grazing torch (wall jet); the distribution of friction decreases in ζ from a maximum value at the hot wall, $\zeta=0$, to zero outside the boundary layer, the heat flux distribution is monotone-decreasing quantity by ζ .

It is offered the optimization of flows and heat transfer in systems of constructive energy saving: vertical constructions and ventilation systems to minimize the cost of power to move the coolant (air). (analytical calculations, the numerical experiments in specialized software systems, preparing a physical model).

Reference

- Mingotia N., Chenvidyakarn T., Woods A.W. Woods. Combined impacts of climate and wall insulation on the energy benefit of an extra layer of glazing in the façade. *Energy and Buildings*. 2013. No. 58. Pp. 237–249
- Balocco C. A simple model to study ventilated facades energy performance. *Energy and Buildings*. 2002. No. 34(5). Pp. 469–475.
- Petrichenko M.R., Petrochenko M.V., Yavtushenko Ye.B. A hydraulically optimum ventilated gap. *Magazine of Civil Engineering*. 2013. No. 2(37). Pp. 112–113. (rus)
- Petrichenko M.R., Petrochenko M.V. Hydraulics of natural convection flows in building walling with air gap. *Magazine of Civil Engineering*. 2011. No. 8(26). Pp. 51–56. (rus)
- Nemova D.V. Integrated characteristics of thermogravitational convection in the air layer of ventilated facades. *Magazine of Civil Engineering*. 2013. No. 2(37). Pp. 25–34. (rus)
- Yavtushenko Y.B., Petrochenko M.V. The diffuser design of ventilated facades. *Magazine of Civil Engineering*. 2013. No. 8(43). Pp. 38–45. (rus)
- Guillén I., Gómez-Lozano V., Fran J.M., López-Jiménez P.A. Thermal behavior analysis of different multilayer façade: Numerical model versus experimental prototype. *Energy and Buildings*. 2014. No. 79. Pp. 184–190.
- Aparicio-Fernández C., Vivancos J.-L., Ferrer-Gisbert P., Royo-Pastor R. Energy performance of a ventilated façade by simulation with experimental validation. *Applied Thermal Engineering*. 2014. No. 66(1-2). Pp. 563–570.
- Iribar-Solaberrieta E., Escudero-Revilla C., Odriozola-Maritorea M., Campos-Celador A., García-Gáfaró C. Energy performance of the opaque ventilated façade. *Energy Procedia*. 2015. No. 78. Pp. 55–60.
- Peci López F., Ruiz de Adana Santiago M. Sensitivity study of an opaque ventilated façade in the winter season in different climate zones in Spain. *Renewable Energy*. 2015. No. 75. Pp. 524–533.
- Ancrossed D Signelković A.S., Mujan I., Dakić S. Experimental validation of a Energy Plus model: Application of a multi-storey naturally ventilated double skin façade. *Energy and Buildings*. 2016. No. 118. Pp. 27–36.

Литература

- Mingotia N., Chenvidyakarn T., Woods A.W. Combined impacts of climate and wall insulation on the energy benefit of an extra layer of glazing in the façade // *Energy and Buildings*. 2013. № 58. Pp. 237–249
- Balocco C. A simple model to study ventilated facades energy performance // *Energy and Buildings*. 2002. № 34(5). Pp. 469–475.
- Петриченко М.Р., Петроченко М.В., Явтушенко Е.Б. Гидравлически оптимальная вентилируемая щель // *Инженерно-строительный журнал*. 2013. № 2(37). С. 35–39.
- Петриченко М.Р., Петроченко М.В. Гидравлика свободноконвективных течений в ограждающих конструкциях с воздушным зазором // *Инженерно-строительный журнал*. 2011. № 8(26). С. 51–56.
- Немова Д.В. Интегральные характеристики термогравитационной конвекции в воздушной прослойке навесных вентилируемых фасадов // *Инженерно-строительный журнал*. 2013. № 2(37). С. 25–34.
- Явтушенко Е.Б., Петроченко М.В. Диффузорная конструкция навесного вентилируемого фасада // *Инженерно-строительный журнал*. 2013. № 8(43). С. 38–45
- Guillén I., Gómez-Lozano V., Fran J.M., López-Jiménez P.A. Thermal behavior analysis of different multilayer façade: Numerical model versus experimental prototype // *Energy and Buildings*. 2014. № 79. Pp. 184–190.
- Aparicio-Fernández C., Vivancos J.-L., Ferrer-Gisbert P., Royo-Pastor R. Energy performance of a ventilated façade by simulation with experimental validation // *Applied Thermal Engineering*. 2014. № 66(1-2). Pp. 563–570.
- Iribar-Solaberrieta E., Escudero-Revilla C., Odriozola-Maritorea M., Campos-Celador A., García-Gáfaró C. Energy performance of the opaque ventilated façade // *Energy Procedia*. 2015. № 78. Pp. 55–60.
- Peci López F., Ruiz de Adana Santiago M. Sensitivity study of an opaque ventilated façade in the winter season in different climate zones in Spain // *Renewable Energy*. 2015. № 75. Pp. 524–533.
- Ancrossed D Signelković A.S., Mujan I., Dakić S. Experimental validation of a Energy Plus model: Application

Petrichenko M.R., Nemova D.V., Kotov E.V., Tarasova D.S., Sergeev V.V. Ventilated facade integrated with the HVAC system for cold climate. *Magazine of Civil Engineering*. 2018. No. 1. Pp. 47–58. doi: 10.18720/MCE.77.5.

12. Diarce G., Campos-Celador A., Martin K., Urresti A., García-Romero A., Sala J.M. A comparative study of the CFD modeling of a ventilated active façade including phase change materials. *Applied Energy*. 2014. No. 126. Pp. 307–317.
13. de Gracia A., Navarro L., Castell A., Cabeza L.F. Energetic performance of a VDSF with CPM under different weather conditions. *Materials Science and Technology Conference and Exhibition*. 2014. No. 3. Pp. 1659–1666.
14. de Gracia A., Castell A., Fernández C., Cabeza L.F. A simple model to predict the thermal performance of a ventilated facade with phase change materials. *Energy and Buildings*. 2015. No. 93. Pp. 137–142.
15. de Gracia A., Navarro L., Castell A., Cabeza L.F. Energy performance of a ventilated double skin facade with PCM under different climates. *Energy and Buildings*. 2015. No. 91. Pp. 37–42.
16. Cianfrini C., Corcione M., Habib E., Quintino A. Energy performance of a lightweight opaque ventilated facade integrated with the HVAC system using saturated exhaust indoor air. *Energy and Buildings*. 2012. No. 20. Pp. 26–34.
17. Mohammed Saleh Z., Alibaba H.Z. Integration of double skin facade with HVAC systems: the state of the art on building energy efficiency *International Journal of Recent Research in Civil and Mechanical Engineering*. 2016. No. 2. Pp. 37–50.
18. Manca O., Nardini S. Thermal design of uniformly heated inclined channels in natural convection with and without radiative effects. *Heat Transfer Engineering*. 2001. Vol. 22. No. 2. Pp. 13–28.
19. Auletta A., Manca O. Heat and fluid flow resulting from the chimney effect in a symmetrically heated vertical channel with adiabatic extensions. *International Journal of Thermal Sciences*. 2002. Vol. 41. Pp. 1101–1111.
20. Colla L., Fedele L., Manca O., Marinelli L., Nardini S. Experimental and numerical investigation on forced convection in circular tubes with nanofluids. *Heat Transfer Engineering*. 2016. Vol. 37. Pp. 1201–1210. DOI: 10.1080/01457632.2015.1112617.
21. Manca O., Ricci D., Nardini S., Di Lorenzo G. Thermal and fluid dynamic behaviors of confined laminar impinging slot jets with nanofluids. *International Communications in Heat and Mass Transfer*. 2016. Vol. 70. Pp. 15–26. DOI: 10.1016/j.icheatmasstransfer.2015.11.010;
22. Corral R., Crespo J. A hybrid unstructured/spectral method for the resolution of Navier-Stokes equations. *Proceedings of the ASME Turbo Expo*. 2009.
23. Corral R., Crespo J. A harmonic balance method in graphics processing units for vibrating blades. *11th European Conference on Turbomachinery Fluid Dynamics and Thermodynamics, ETC 2015*.
24. Minea A.A. Uncertainties in modeling thermal conductivity of laminar forced convection heat transfer with water alumina nanofluids. *International Journal of Heat and Mass Transfer*. 2014. No. 68. Pp. 78–84.
25. Korniyenko S. Complex analysis of energy efficiency in operated high-rise residential building: Case stud. *E35 Web of Conferences*. 2018. No. 32. 02005.
26. Korniyenko S. Advanced hygrothermal performance of building component at reconstruction of S. Radonezhskiy Temple in Volgograd. *MATEC Web of Conferences*. 2016. No. 53. 01003.
27. Korniyenko S. The experimental analysis and calculative assessment of building energy efficiency. *Applied Mechanics and Materials*. 2014. No. 618. Pp. 509–513.
28. Gorshkov A., Murgul V. Calculation of heat energy consumption by a typical historical building with a courtyard. *Advances in Intelligent Systems and Computing*. 2018. No. 69. Pp. 577–591. DOI: 10.1007/978-3-319-70987-1_61
- of a multi-storey naturally ventilated double skin façade // *Energy and Buildings*. 2016. № 118. Pp. 27–36.
12. Diarce G., Campos-Celador A., Martin K., Urresti A., García-Romero A., Sala J.M. A comparative study of the CFD modeling of a ventilated active façade including phase change materials // *Applied Energy*. 2014. № 126. Pp. 307–317.
13. de Gracia A., Navarro L., Castell A., Cabeza L.F. Energetic performance of a VDSF with CPM under different weather conditions // *Materials Science and Technology Conference and Exhibition*. 2014. № 3. Pp. 1659–1666.
14. de Gracia A., Castell A., Fernández C., Cabeza L.F. A simple model to predict the thermal performance of a ventilated facade with phase change materials // *Energy and Buildings*. 2015. № 93. Pp. 137–142.
15. de Gracia A., Navarro L., Castell A., Cabeza L.F. Energy performance of a ventilated double skin facade with PCM under different climates // *Energy and Buildings*. 2015. № 91. Pp. 37–42.
16. Cianfrini C., Corcione M., Habib E., Quintino A. Energy performance of a lightweight opaque ventilated facade integrated with the HVAC system using saturated exhaust indoor air // *Energy and Buildings*. 2012. № 20. Pp. 26–34.
17. Mohammed Saleh Z., Alibaba H.Z. Integration of double skin facade with HVAC systems: the state of the art on building energy efficiency // *International Journal of Recent Research in Civil and Mechanical Engineering*. 2016. № 2. Pp. 37–50.
18. Manca O., Nardini S. Thermal design of uniformly heated inclined channels in natural convection with and without radiative effects // *Heat Transfer Engineering*. 2001. Vol. 22. № 2. Pp. 13–28.
19. Auletta A., Manca O. Heat and fluid flow resulting from the chimney effect in a symmetrically heated vertical channel with adiabatic extensions // *International Journal of Thermal Sciences*. 2002. Vol. 41. Pp. 1101–1111.
20. Colla L., Fedele L., Manca O., Marinelli L., Nardini S. Experimental and numerical investigation on forced convection in circular tubes with nanofluids // *Heat Transfer Engineering*. 2016. Vol. 37. Pp. 1201–1210. DOI: 10.1080/01457632.2015.1112617.
21. Manca O., Ricci D., Nardini S., Di Lorenzo G. Thermal and fluid dynamic behaviors of confined laminar impinging slot jets with nanofluids // *International Communications in Heat and Mass Transfer*. 2016. Vol. 70. Pp. 15–26. DOI: 10.1016/j.icheatmasstransfer.2015.11.010;
22. Corral R., Crespo J. A hybrid unstructured/spectral method for the resolution of Navier-Stokes equations // *Proceedings of the ASME Turbo Expo*. 2009.
23. Corral R., Crespo J. A harmonic balance method in graphics processing units for vibrating blades // *11th European Conference on Turbomachinery Fluid Dynamics and Thermodynamics, ETC 2015*.
24. Minea A.A. Uncertainties in modeling thermal conductivity of laminar forced convection heat transfer with water alumina nanofluids // *International Journal of Heat and Mass Transfer*. 2014. № 68. Pp. 78–84.
25. Korniyenko S. Complex analysis of energy efficiency in operated high-rise residential building: Case stud // *E35 Web of Conferences*. 2018. № 32. 02005.
26. Korniyenko S. Advanced hygrothermal performance of building component at reconstruction of S. Radonezhskiy Temple in Volgograd // *MATEC Web of Conferences*. 2016. № 53. 01003.
27. Korniyenko S. The experimental analysis and calculative assessment of building energy efficiency. *Applied Mechanics and Materials*. 2014. № 618. Pp. 509–513.
28. Gorshkov A., Murgul V. Calculation of heat energy consumption by a typical historical building with a courtyard

Петриченко М.Р., Немова Д.В., Котов Е.В., Тарасова Д.С., Сергеев В.В. Вентилируемые фасады, интегрированные с инженерными системами здания для холодного климата // *Инженерно-строительный журнал*. 2017. № 1(77). С. 47–58.

29. Garifullin M., Vatin N., Jokinen T., Heinisuo M. Numerical solution for rotational stiffness of RHS tubular joints. *Advances and Trends in Engineering Sciences and Technologies II - Proceedings of the 2nd International Conference on Engineering Sciences and Technologies*. 2017. Pp. 81–86.
30. Korniyenko S.V., Vatin N.I., Gorshkov A.S. Thermophysical field testing of residential buildings made of autoclaved aerated concrete blocks. *Magazine of Civil Engineering*. 2016. No. 64(4). Pp. 10–25. DOI: 10.5862/MCE.64.2
31. Nazmeeva T.V., Vatin N.I. Numerical investigations of notched C-profile compressed members with initial imperfections. *Magazine of Civil Engineering*. 2016. No. 2(62). Pp. 92–101.
32. Muravyeva L., Vatin N. Elaboration of the Method for Safety Assessment of Subsea Pipeline with Longitudinal Buckling. *Advances in Civil Engineering*. 2016. 7581360
33. Ulybin A., Lanko A., Vatin N., Lysnytska K. Examination of the Basement of Historic Buildings in Investment Activity. *MATEC Web of Conferences*. 2016. No. 73. 01007
- // *Advances in Intelligent Systems and Computing*. 2018. № 69. Pp. 577–591. DOI: 10.1007/978-3-319-70987-1_61
29. Garifullin M., Vatin N., Jokinen T., Heinisuo M. Numerical solution for rotational stiffness of RHS tubular joints // *Advances and Trends in Engineering Sciences and Technologies II - Proceedings of the 2nd International Conference on Engineering Sciences and Technologies*. 2017. Pp. 81–86.
30. Корниенко С.В., Ватин Н.И., Горшков А.С. Натурные теплофизические испытания жилых зданий из газобетонных блоков // *Инженерно-строительный журнал*. 2016. № 4(64). С. 10–25.
31. Назмеева Т.В., Ватин Н.И. Численные исследования сжатых элементов из холодногнутого просечного С-профиля с учетом начальных несовершенств // *Инженерно-строительный журнал*. 2016. № 2(62). С. 92–101.
32. Muravyeva L., Vatin N. Elaboration of the Method for Safety Assessment of Subsea Pipeline with Longitudinal Buckling. *Advances in Civil Engineering*. 2016. 7581360
33. Ulybin A., Lanko A., Vatin N., Lysnytska K. Examination of the Basement of Historic Buildings in Investment Activity. *MATEC Web of Conferences*. 2016. No. 73. 01007

Mikhail Petrichenko,
+7(921)330-04-29; fonpetrich@mail.ru

Darya Nemova,
+7(921)890-02-67; nemova_dv@spbstu.ru

Evgeny Kotov,
+7(921)346-13-12; ekotov.cfd@gmail.com

Darya Tarasova,
+7(931)256-45-94; tarasovads@gmail.com

Vitaly Sergeev,
+7(921)980-54-37; sergeev_vitaly@mail.ru

Михаил Романович Петриченко,
+7(921)330-04-29; эл. почта: fonpetrich@mail.ru

Дарья Викторовна Немова,
+7(921)890-02-67;
эл. почта: nemova_dv@spbstu.ru

Евгений Владимирович Котов,
+7(921)346-13-12;
эл. почта: ekotov.cfd@gmail.com

Дарья Сергеевна Тарасова,
+7(931)256-45-94;
эл. почта: tarasovads@gmail.com

Виталий Владимирович Сергеев,
+7(921)980-54-37;
эл. почта: sergeev_vitaly@mail.ru

© Petrichenko M.R., Nemova D.V., Kotov E.V., Tarasova D.S., Sergeev V.V., 2018

doi: 10.18720/MCE.77.6

Organizational and technological reliability of the construction process

Организационно-технологическая надежность строительного процесса

V.N. Kabanov,
National Research Moscow State Civil
Engineering University, Moscow, Russia

Д-р экон. наук, профессор В.Н. Кабанов,
Национальный исследовательский Московский
государственный строительный
университет, г. Москва, Россия

Key words: organizational and technological reliability of construction; organizational-technological solutions of construction; duration of construction; cost of construction products; organizational and technological design of construction processes

Ключевые слова: организационно-технологическая надежность; строительный процесс; организационно-технологическое решение строительства; продолжительность строительства; стоимость строительной продукции; организационно-технологическое проектирование строительных процессов

Abstract. Construction projects of buildings and structures, as well as plans of construction and installation works are often subjected to fair criticism from the Pro-producers of the work. Such criticism is that the calculated cost value and long lasting-STI CMP does not take into account the specificity of real contractors. To address these criticisms and proposals were developed for the assessment of such intensity values of SMR production, which most realistically take into account the actual conditions of construction and Contracting organization. The application of the classical methods of probability theory simplifies the procedure of collecting background information and in some cases allows you to use the results of the numerical experiment. Computational procedures require special training and is easily amenable to automation (programming). The result of the research represents the author's method of estimating the quantitative strength value of organizational and technological reliability with regard to construction, manual processes, and technological solutions providing leading mechanization, subject to the calculation of the intensity of works as the sum of labor productivity of employed workers.

Аннотация. Проекты возведения зданий и сооружений, а также планы производства строительно-монтажных работ весьма часто подвергаются справедливой критике со стороны производителей работ. Такая критика состоит в том, что расчетные значения стоимости и продолжительности СМР не учитывают специфику реальных подрядных организаций. Для устранения этих критических замечаний разработаны предложения по оценке такого значения интенсивности производства СМР, которое наиболее реально учитывает фактические условия строительства и подрядной организации. Применение классических методов теории вероятностей значительно упрощает процедуры сбора исходной информации, а в некоторых случаях позволяет использовать результаты численного эксперимента. Вычислительные процедуры не требуют специальной подготовки и легко поддаются автоматизации (программированию). Результат выполненных исследований представляет собой авторский способ оценки количественного значения организационно-технологической надежности применительно к строительным процессам, выполняемым вручную, а также к технологическим решениям предусматривающим работу ведущих средств механизации при условии вычисления интенсивности производства работ как суммы производительности труда занятых рабочих.

1. Introduction

The aim of the study was to determine the order of evaluation of organizational and technological reliability of construction processes.

In practice, organizational-technological design, the calculated values of the duration cost and duration of construction are very often at odds with actual unit price of construction products, as well as terms of input of objects in operation. Over the past 50 years did not stop attempts to increase the level of

reliability of the duration and cost of construction, including as a result of practical application of the index of organizational-technological reliability (OTR) the project indicators. For the period developed many approaches to the calculation of quantitative values of OTR. From the point of view of the author, the stump of the reliability obtained in the design of organizational and technological solutions does not always provide the required accuracy.

Object of research are the processes of production of construction works. Subject of research: the ability of organizational and technological processes construction of buildings and structures to make construction products in a specified period (including, without exceeding the set price).

Most of the authors of the publications included in this work, under the organizational and technological reliability (OTR) understand quite exhaustive, which became a classic definition provided by one of the pioneers of engineering in construction A. A. Gusakov [1]. It is important to emphasize that the concept of organizational– technological reliability in the publications is rather widespread. The results of the study while this index in a variety of fields including design, creation of construction products and buildings and structures allow you to combine the application of OTR in three groups: the design of building structures, operation of machines, mechanisms and technological equipment and construction and installation works manually.

Probabilistic structural analysis most often relies on the formal definition of distribution functions of magnitude "reliability". Calculation of quantitative indicators of sustainability, values of strain are considered as the result of changes in external loads and simultaneous variations of the resistance of structures to external influences. The problem of determining the reliability of structures is reduced to calculating the probability of a loss of resistance (the onset of the limit state), which is represented by the graphical intersection of the distribution function of the loads (or forces) and the distribution function of measure describing the resistance to these loads [2].

Assessment of organizational and technological reliability of operation of means of mechanization in construction can be subdivided into two parts. The first part involves determining the probability of failure-free operation of machines and mechanisms, and the second is providing the most comprehensive resource utilization of mechanization in the construction of buildings and structures. If the order of evaluation of reliability of technical systems is governed by the regulations of the current Russian national system of standards GOST R 5190.5-2005, the assessment of the OTR operation of technological systems and kits has a variety of original approaches [3].

To calculate the value of OTR in relation to the execution of construction works in Russia there is no normative document that defines the execution order of the calculations. Probably, the lack of a standard should explain the impressive number of published proprietary methodologies designed to assess the reliability of the processes of construction of buildings and structures, each of which uses, sometimes, unique conceptual apparatus and offers to determine the OTR: "the construction organization [4], elements of the organizational structure of an investment construction project", "housing construction [5–7]". You should pay attention to the practical application of the indicator OTR when planning: defining "matching sequentially executed [8]", using the "binary structure in terms of a probabilistic temporal parameters [9]", "definition of duration of the critical path [10, 11]". Approaches to the assessment of organizational and technological reliability, taken separately is the technological process are cited in published works A.A. Lapidous [12], I.K. Poteryaeva [3], P.P. Oleynik [13], V.R. Molodetskiy [14], P.N. Kurochkin [15].

Among the methods used to calculate quantitative values of OTR found in the published works, include:

- methods of probability theory: determination of the mathematical expectation [8, 9] as the evaluation of reliability (probability) of the results (the accuracy of the prediction table. 1 [3]); the integral of the distribution density function of Laplace [16], Poisson "flow" of failures [17], the function of the beta distribution probability density of a random variable [18], assessment of deviations from specified parameters [19], the "clearance" of a number to adequately sample [20];

- the construction of mathematical models: spatial reliability using K-dimensional cube [4], a simulation model "input – output" [21], ABC-analysis [22], the Kohonen self-organizing maps for clustering of network elements [23], figure Kiviat petal-type [24], "dummy poles" on the histogram [14], the model Black–Scholes [25];

- application of fuzzy set theory [12];

- the use of standard methods [26], Russian State Standard GOST R 27.606-2013, based on the RCM methodology [27, 28];

- expert evaluation [15];
- structural-matrix approach [29];
- PRI-reliability index as the ratio of the actually performed volume to the plan [30, 31].

Summing up the interim, it is necessary to note especially the definition of organizational and technological reliability. To assess the technical reliability (availability or time to failure) are characteristics of operational reliability, among which the most often are: time to failure, probability of failure, the overhaul life of components and aggregates, factors of readiness, technical use. In addition, technical systems, in most cases, belong to this category of systems in which the creation of reserves, providing a given level of reliability, very difficult, but if possible, it is quite expensive. Unlike technical systems, organizational and technological decisions of construction of buildings and armed represent the interaction of people and mechanization. This interaction is stochastic in nature, which is "absolutely not taken into account either by the organizational-technological documentation, nor in the existing normative-reference base (building regulations, etc.) [4]". These methods estimate the probabilistic nature of intensity of construction and installation works, or time-consuming and require special training, or do not provide the required accuracy of calculations.

The aim of the study was to determine the order of evaluation of organizational and technological reliability of construction processes.

Objectives of the study:

- to systematize calculation methods of organizational-technological reliability in the practice, the development of projects of construction of buildings and structures;
- to define the scope of the practical application of the author's approach taking into account the specifics of construction processes.

2. Research methods

In this paper we use classical methods of probability theory, suggesting the most likely outcome observations, and if such measurements are impossible (or difficult) to apply the methods of numerical experiment. The curve of cumulative probability (cumulative curve) is performed using standard methods of probability theory, based on the conditions not more (or less) of a given (technical or normative) values. For sampling the initial values describing the behavior of the process is proposed to carry out field

3. Results and Discussion

Differences of reliability of functioning of technical systems and organizational-technological solutions of the construction pay attention to the features of the sequence of construction and installation works. The degree of involvement of technical systems in the processes of construction of building structures it is easy to identify three groups:

- the first group includes jobs that are mechanized (for example, earth-wide, performed for the most part manipulators: bulldozers, scrapers, excavators);
- the second should include the processes involving the interaction of people and leading machines, it is impossible to perform work in the absence of at least one of the parts (for example, installation of precast concrete structures: interaction of the lifting mechanism and management (team) installers, or concrete mixture, where interact the leading machine – paver and link concrete workers);
- the third fall of work carried out without direct participation of the master, i.e., hand (stonework, installation of partitions of gypsum boards, installation of reinforcement frame, etc.), including the use of hand-held power tool.

The calculation of the reliability of the operation processes assigned to the first group, defined by the uptime manipulators (technical systems) and governed by applicable regulations GOST R 51901.5-2005. The performance of the funds mechanization in this case depends on the skill of the driver (operator) driving the car, as well as rational formations of a set of machines (such as excavator – car-truck). As the experience of the author, it is rarely possible to avoid complex (for example, when working excavator – car-truck most often, the number of the auxiliary machines is chosen considering the conditions of continuous operation of the presenter unit of the excavator).

For organizational and technological solutions related to the second group, we have to solve the problem of determining the rational ratio of the number of workers in the chain necessary to ensure the

smooth operation of the master based on the current state elemental estimate standards for construction work (SEES). As an example we present the calculation for the number of workers in the link to organizational and technological solutions representing the interaction of people and the main machine (crane and concrete pump) that is used when laying concrete mixture in the overlap (Russian state itemized construction estimates GESN 81-02-06-2017.). The results of the calculations are given in table 1.

Table 1. Labor costs and time the leading machines for the construction of slabs in small-panel formworks (concrete mixture), for 10 m² of the ceiling structure (SEES 06-01-103)

No	Table SEES	Costs time the main machine mash.h.	Labour cost, people.	The estimated number of workers in the link, people.
The concrete mixture, tower crane, lifting capacity 8 tons.				
1	06-01-103-1	1.79	20.35	11.37
2	06-01-103-2	1.90	20.35	10.71
3	06-01-103-3	2.02	20.83	10.31
4	06-01-103-4	2.14	21.06	9.84
The concrete mixture, the concrete with the capacity of 65 m ³ / h.				
5	06-01-103-5	0.81	20.01	24.70
6	06-01-103-6	0.93	20.01	21.52
7	06-01-103-7	1.16	20.47	17.65
8	06-01-103-8	1.28	20.71	16.18

Does not require proof procedure for computing the number of workers required for laying of concrete mixes with the target intensity (performance):

$$N_R = \frac{R}{R_M} \quad (1)$$

where N_R is the number of workers in the team (crew), persons (column 5, tab. 1);

- R – the cost of labor established a standard to perform unit work volume, person / h (column 4, table. 1);

- R_M – time costs of the basic technological machines set the standard for of the compliance unit volume of the work, mash. h (column 3, tab. 1).

Different values of the number of workers (column 5, tab. 1) are not integers. In this regard, the engineer-technologist to calculate the duration of works (in this example, bridging), you must set the intensity value of the production for maintenance of organizational-technological solutions of laying of concrete mixes. Obviously, to take the number of workers in a part different from an integer value, contrary to common sense. In this regard, for practical calculations the author uses the expression:

$$W_I = \frac{N_R}{R} - W_M \begin{cases} > 0 \Rightarrow W_I = W_M \\ < 0 \Rightarrow W_I = \frac{N_R}{R} \end{cases} \quad (2)$$

where W_I – the intensity (capacity) of the production work for the given organizational-technological solutions;

- W_M – performance main (host) machine organizational and technological process involving the interaction of people means of mechanization of construction and erection works (performance of the basic machine is associated with downtime of the machine, necessary to perform individual scope of work the proportion: $W_I = \frac{I}{R_M}$).

The study of the expression 2 to calculate the intensity of construction and installation works in the functioning of organizational and technological solutions, which is the interaction between machines and workers, can make a simple conclusion about the existence of reserve production capacity. The reserve is the result of rounding up or down the number of workers in the team (team). The value of the stock of production capacity, the formation of financed project as a result of rounding, is given in table. 2.

Table 2. The estimated intensity value for the organizational-technological solutions of laying of concrete mix in the overlap (SEES 06-01-103) and the amount of internal reserve power

Table SEES	Option 1: working with a lack				Option 2: working with excess			
	Col. working, people., N_R	The intensity of work, m2 in h., W_i	Stock power on the car:		Col. working, people., N_R	The intensity of work, m2 in h., W_i	Power reserve working	
			m2 in h	%			m2 in h	%
1	2	3	4	5	6	7	8	9
The concrete mixture, tower crane, lifting capacity 8 tons.								
06-01-091-1	11	5.41	0.18	3.24	12	5.59	0.31	5.26
06-01-091-2	10	4.91	0.35	6.63	11	5.26	0.14	2.63
06-01-091-3	10	4.80	0.15	3.02	11	4.95	0.33	6.26
06-01-091-4	9	4.27	0.40	8.55	10	4.67	0.08	1.59
The concrete mixture, the concrete with the capacity of 65 m3 / h.								
06-01-091-5	24	11.99	0.35	2.85	25	12.35	0.15	1.19
06-01-091-6	21	10.49	0.26	2.40	22	10.75	0.24	2.20
06-01-091-7	17	8.30	0.32	3.66	18	8.62	0.17	1.96
06-01-091-8	16	7.73	0.09	1.11	17	7.81	0.40	4.83

In the case that the duration of works is calculated in terms of intensity equal to the operating performance the main (host) machine ($W_I = W_M$, variant 2, column 7, table. 2), then the value of organizational-technological reliability largely depends on the probability of uninterrupted operation of machines and tools and is evaluated on the basis of the existing norm of positive documents (GOST). If

the duration calculation done on the total value of productivity of workers ($W_I = \frac{N_R}{R}$, option 1, column 3,

tab. 2), then OTR is determined by the probability of replacement jobs in the prescribed volume element of concrete (for this example). These findings do not take into account the economic impact of the length for alternatives 1 and 2 (table. 2).

Organizational and technological reliability of construction works performed manually, in most cases, eliminates the calculation of the technical reliability of the means of mechanization used as the master process. However, the destabilizing factors make the technology of construction of building structures in stochastic processes. These methods assess the reliability, as a rule, very time consuming, and their practical use requires special training in the field of probability theory and mathematical statistics. According to the author, to simplify the estimation of the probability of execution of works in time is possible under condition of the compliance calculation procedures in relation to the array of values that describes the measure of productivity for a certain period of time.

The accumulation of information about the performance of the work, describing construction processes performed manually may take from several days to several months. For example, when monitoring the productivity per hour for the accumulation of an array of 100 values enough 13 shifts. If the initial information to consider the performance in change, can require up to 4 months. It is important to emphasize that in terms of time performance in shift, you must enter the correction factors that account for the unevenness of the intensity of work for one shift (or example, the performance one hour before a lunch break is often lower afternoon by 25–35 %).

The practical application of the indicator "organizational and technological reliability" involves the solution of tasks that are correctly grouped into two groups. The first group – the task of finding the reliability (validity) of the quantitative values of indicators describing the process of functioning of technological process in construction (typically, the performance or the intensity of production work). The second group includes tasks that are usually called about the inverse, that is, for a given level of reliability (reliability) should be determined quantitative value of the indicator. From the point of view of the author, the greatest value in practice, the construction of objects of civil and industrial use has increased intensity (productivity) of the work. The solution of direct and inverse problem, it is advisable to illustrate on the graph (Fig. 1a, b).

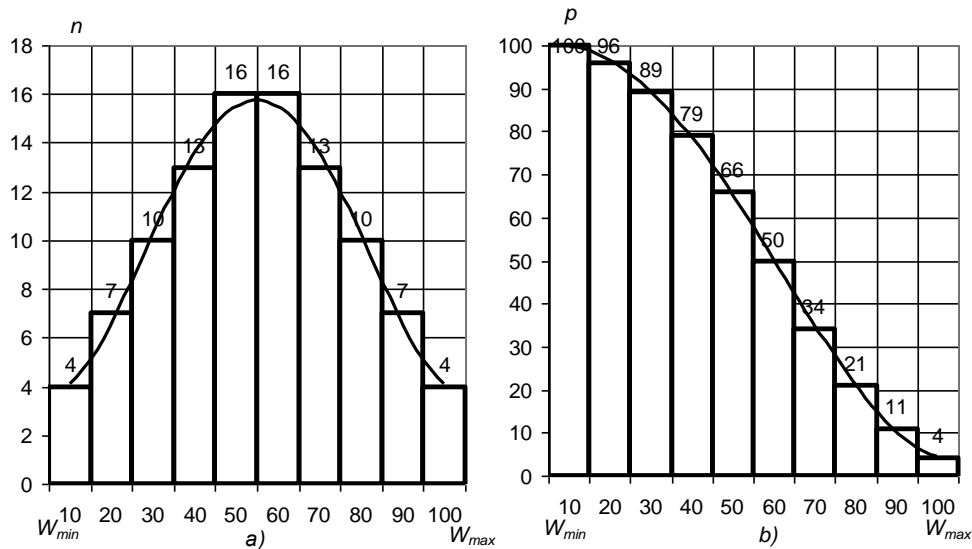


Figure 1. Schedule of functions of random variables WI: a) distribution density; b) the curve of cumulative probabilities

On the chart (Fig. 1 a, b) the x-axis shows the change in the intensity of production work ($W_{lmax} > W_l > W_{lmin}$) in percent. The ordinate of the graph of a probability density function (Fig. 1 a) shows the number of values from the set of values $W_l(N)$ located in the corresponding interval (range of area on 0 to 100%, $W_{lmin} = 0\%$, $W_{lmax} = 100\%$). The ordinate of the curve of cumulative probability (Fig. 1 b)- shows the changing probabilities depending on the magnitude of intensity of production (W_l).

From the position of the classical conception of probability theory, the probability of each of values constituting the set of values $W_l(N)$ equal to $p = 0.01$ (if number of values in a sample $N = 100$). However, when considering the probabilities of each of the intervals of the $W_{lmax} > W_l > W_{lmin}$ obviously, the highest probability interval of 0.4 $W_{lmax} > W_l > 0.6 W_{lmax}$ and equal to $p = 0.16$ (see Fig. 1a).

In practice, when calculating the duration of the construction works of no special interest is the probability value of each element of the sample, and even separately of each interval. Actually, it really is important to determine the probability that the intensity of production work will not be below the estimated (or specified design) values [32]. To achieve this purpose, perfect use of the curve of cumulative probability (Fig. 1b).

The solution of the direct problem involves calculating the probability that the intensity value of the production of works in the course of erection of building structures, will not be less than the set value, for example 0.8 [33] (W_{ln}). With this purpose it is necessary to set the interval in which the estimated intensity value on the x-axis and then determine the corresponding probability value on the y-axis (Fig. 1b). The reverse procedure can be applied when solving the opposite problem: finding the estimated intensity values for a given probability value (OTR). This approach allows us to assess the specific conditions, regardless of the existence of the counterpart [34].

Practical determination of the intensity of production in individual manufacturing process (e.g., concrete mixture) is performed by the author on the basis of the specified level of organizational and technological reliability. The specified level for the most part, is taken equal to $R = 0.8$. The validity of this approach is confirmed by published results of research of Molodetskiy V.R. [14]. The author's approach is that instead of the interval of intensity values when calculating the length of production work, use a discrete value for a given level of probability. It is important to emphasize that this approach allows us to estimate the probability of activity (performance) of the employee and does not require assessment "health of the human operator by means of professional selection, training, health monitoring [35]".

Indeed, in case of representation of the OTR graph of a curve of the accumulated probability, it is necessary and sufficient set of values of the intensity of production work (W_{ln}) to split into two parts. The first contains values less than the calculated value (not satisfying the condition). This separation allows you to find an indicator which divides a set of values, that is, a border. With this purpose it is necessary to sort the values by ascending order (lowest to highest). It is obvious that the likelihood (OTR) $p = 0.8$, boundary value will correspond to the index, which occupies in the sample number $n = 21$ (assuming that the number of values in a sample $N = 100$).

Thus, for a given value of p (for example $p = 0.8$) is necessary and sufficient to take from the ordered sample ($N = 100$) the value of $n = 21$. To retrieve the number of values which is different from 100, it is recommended to use the equation to find the number corresponding to the calculated (design) value of the intensity of production work:

$$n = 100N(1 - p) + 1 \quad (3),$$

where n is the indicator number in the ordered sample values;

- p – the set level of organizational and technological reliability (probability, e.g., $p = 0.8$);
- N – number of values in the array.

4. Conclusions

Thus, when determining the calculated (design) values of the intensity of construction and installation works it is necessary to take into account the peculiarities of the processes of the erection of the discussion of buildings and structures: fully mechanized working together machines and people, as well as performed entirely by hand.

For fully mechanized processes, the assessment of organizational and technological reliability is advantageously carried out by applying the standard (in accordance with Russian State Standard GOST) methods of assessment of technical reliability.

For the processes of construction of building structures manually determining the design value of the intensity of the production of works corresponding to a given level of reliability, should be performed by dividing the set of values obtained as a result of observations into two groups (compliant and non compliant design value). The value of the corresponding edge, it is advisable to determine how the project (or defined for calculating, for example, duration).

The most effective field of application of the described approach of calculation of OTR should include construction processes performed entirely by hand and using leading technology of mechanization, subject to the calculation of the intensity of production work on the total performance.

Reference

1. Gusakov A.A. *Organizatsionno-tekhnologicheskaya nadezhnost stroitel'nogo proizvodstva* [Organizational and technological reliability of construction production]. Moscow: Stroyizdat. 1974. 252 p. (rus)
2. Ivashenko Yu.A., Ferder A.V. Sistema uravneniye dlya opredeleniya funktsii raspredeleniya pri veroyatnostnykh metodakh rascheta [The system equation for determining the distribution function in probabilistic calculation methods]. *Bulletin of the South Ural state University*. 2017. No. 1. Pp. 34–37. (rus)
3. Poteryayev I.K. Metodika rascheta chisla transportnykh sredstv v transportnykh operatsiyakh asfaltobetonnoy smesi [The method of calculating the number of vehicles in the transportation operations asphalt mixture]. *Bulletin of the Kuzbass technical University*. 2016. No. 1. Pp. 83–88. (rus)
4. Ginzburg A.V. Organizatsionno-tekhnologicheskaya nadezhnost stroitelnykh sistem [Organizational-technological reliability of building systems]. *Vestnik MGSU*. 2010. No. 4. Pp. 251–255. (rus)
5. Morozenko A.A., Voronkov I.E. Problemy otsenki povysheniya nadezhnosti elementov organizatsionnoy struktury investitsionno- stroitel'nogo proyekta [Problems of assessment of reliability of elements of the organizational structure investment - construction project]. *Industrial and civil construction*. 2014. No. 12. Pp. 30–32. (rus)
6. Mikhaylova E.V. Osobennosti stroitel'nogo kompleksa Volgogradskoy oblasti [Characteristics of the construction complex of Volgograd region]. *Business. Education. Right. Bulletin of the Volgograd Institute of business*. 2011. No. 4. Pp. 44–47. (rus)
7. Vasilenko Zh.A. Kriterii otsenki nadezhnosti sistemy upravleniya zhillishchnym stroitel'stvom [Evaluation criteria reliability of control system of housing construction]. *Engineering journal of Don*. 2012. No. 3. Pp. 702–705. (rus)

Литература

1. Гусаков А.А. Организационно-технологическая надежность строительного производства. М.: Стройиздат, 1974. 252 с.
2. Ивашенко Ю.А., Фердер А.В. Система уравнение для определения функции распределения при вероятностных методах расчета // Вестник Южно-Уральского государственного университета. 2017. № 1. С. 34–37.
3. Потеряев И.К. Методика расчета числа транспортных средств в транспортных операциях асфальтобетонной смеси // Вестник Кузбасского технического университета. 2016. № 1. С. 83–88.
4. Гинзбург А.В. Организационно-технологическая надежность строительных систем // Вестник МГСУ. 2010. № 4. С. 251–255.
5. Морозенко А.А., Воронков И.Е. Проблемы оценки повышения надежности элементов организационной структуры инвестиционно- строительного проекта // Промышленное и гражданское строительство. 2014. № 12. С. 30–32.
6. Михайлова Е.В. Особенности строительного комплекса Волгоградской области // Бизнес. Образование. Право. Вестник Волгоградского института бизнеса. 2011. № 4. С. 44–47.
7. Василенко Ж.А. Критерии оценки надежности системы управления жилищным строительством // Инженерный вестник Дона. 2012. № 3. С. 702–705.
8. Болотин С.А., Котовская М. А. Адаптация метода критической цепи при поточной организации работ // Недвижимость: экономика, управление. 2014. № 3-4. С. 38–43.
9. Калугин Ю.Б. Графоаналитическая модель и приближенный метод оценки сроков выполнения проекта с вероятностными временными параметрами //

8. Bolotin S.A., Kotovskaya M. A. Adaptatsiya metoda kriticheskoy tsepi pri potочноy organizatsii rabot [The adaptation of the method of critical chain in a production organization of work]. *Real Estate: economy, management*. 2014. No. 3-4. Pp. 38–43. (rus)
9. Kalugin Yu.B. Grafoanaliticheskaya model i priblizhennyi metod otsenki srokov vypolneniya proyekta s veroyatnostnymi vremennymi parametrami [Graphical-analytical model and an approximate method of assessment of the timing of the project with probabilistic time parameters]. *News of higher educational institutions. Construction*. 2015. No. 7. Pp. 26–37. (rus)
10. Goldratt E.M. *Critical Chain*. Great Barrington, MA: North River Press, 1997.
11. Goldratt E.M. *Theory of Constrains*. Croton-on-Hudson, NY: North River Press, 1990.
12. Lapidus A.A., Makarov A.N. Teoriya nechetkikh mnozhestv na etapakh modelirovaniya organizatsii stroitelnykh protsessov vozvedeniya mnogoetazhnykh zdaniy [The theory of fuzzy sets in the modelling stages of the construction processes the construction of high-rise buildings]. *Industrial and civil construction*. 2016. No. 6. Pp. 66–71. (rus)
13. Oleynik P.P. Analiz i razrabotka norm prodolzhitel'nosti stroitelstva zhilykh zdaniy tipovykh seriy [Analysis and development of norms of duration of construction of residential buildings of typical series]. *Mechanization of construction*. 2008. No. 2. Pp. 18–23. (rus)
14. Molodetskiy V.R., Martysh A.A. Veroyatnostnyye parametry vypolneniya otdelnoy stroitelno-montazhnoy raboty [Probabilistic parameters of implementation of different construction works]. *Bulletin of Prydniprovsk state Academy of civil engineering and architectures*. 2013. No. 3. Pp. 8–14. (rus)
15. Kurochka P.N., Molozin S.V., Telykh V.G. Otsenka nadezhnosti elementov organizatsionnoy sistemy [Evaluation of the reliability of the elements of the organizational system]. *Bulletin of Voronezh state technical University*. 2010. No. 7. Pp. 27–30. (rus)
16. Shulzhenko N.A., Pushilina Yu.N., Chubarov D.I. Otsenka organizatsionno-tekhnologicheskoy nadezhnosti pri organizatsii podgotovki territorii pod zastroyku [Evaluation of organizational and technological reliability in the provision of training areas for development]. *Izvestiya of the Tula state University*. 2016. No. 7-2. Pp. 152–157. (rus)
17. Pakhomova E.G., Bredikhina N.V. Veroyatnostnyye zakonomernosti vozniknoveniya otkazov stroitel'nogo potoka [Probabilistic patterns of occurrence of failures of construction flow]. *Izvestiya of southwest state University*. 2016. No. 6. Pp. 35–40. (rus)
18. Velichkin V.Z. Upravleniye i nadezhnost realizatsii stroitelnykh program [Management and implementation of reliability programs construction]. *Engineering construction magazine*. 2014. No. 7. Pp. 74–79. (rus)
19. Kostyuchenko V.V. Upravleniye protsessom povysheniya effektivnosti organizatsionno-tekhnologicheskikh stroitelnykh sistem [Managing the process of improving the efficiency of the organizational and technological construction systems]. *Engineering journal of Don*. 2012. No. 1. Pp. 536–542. (rus)
20. Nedavniy O.I., Kuznetsov S.M., Kandaurova N.M. Obosnovaniye vremeni proizvodstva stroitelnykh rabot [Justification for the production of building work]. *News of higher educational institutions. Construction*. 2013. No. 9. Pp. 107–114. (rus)
21. Gusev B.V., Guseva A.Yu., Litvinovskiy E.M. Ustoychivost i nadezhnost raboty konveyernykh tekhnologicheskikh liniy po proizvodstvu sbornogo zhelezobetona [The stability and reliability of the conveyor technological lines for manufacture of precast reinforced concrete]. *Concrete Technology*. 2015. No. 7-8. Pp. 30–31. (rus)
22. Rakhutin M.G., Pankratenko N.A. Ispolzovaniye AVS – analiza pri issledovanii nadezhnosti tonnelleprohodcheskogo kompleksa dlya prokladki Izvestiya vysshiykh uchebnykh zavedeniy. *Stroitel'stvo*. 2015. № 7. С. 26–37.
23. Goldratt E.M. *Critical Chain*. Great Barrington, MA: North River Press, 1997.
24. Goldratt E.M., *Theory of Constrains*, Croton-on-Hudson, NY: North River Press, 1990.
25. Лapidus A.A., Макаров A.Н. Теория нечетких множеств на этапах моделирования организации строительных процессов возведения многоэтажных зданий // *Промышленное и гражданское строительство*. 2016. № 6. С. 66–71.
26. Олейник П.П. Анализ и разработка норм продолжительности строительства жилых зданий типовых серий // *Механизация строительства*. 2008. № 2. С. 18–23.
27. Молодецкий В.Р., Мартыш А.А. Вероятностные параметры выполнения отдельной строительно-монтажной работы // *Вісник придніпровської державної академії будівництва та архітектури*. 2013. № 3. С. 8–14.
28. Курочка П.Н., Молозин С.В., Тельных В.Г. Оценка надежности элементов организационной системы // *Вестник Воронежского государственного технического университета*. 2010. № 7. С. 27–30.
29. Шульженко Н.А., Пушилина Ю.Н., Чубаров Д.И. Оценка организационно-технологической надежности при организации подготовки территории под застройку // *Известия Тульского государственного университета*. 2016. № 7-2. С. 152–157.
30. Пахомова Е.Г., Бредихина Н.В. Вероятностные закономерности возникновения отказов строительного потока // *Известия Юго-Западного государственного университета*. 2016. № 6. С. 35–40.
31. Величкин В.З. Управление и надежность реализации строительных программ // *Инженерно-строительный журнал*. 2014. № 7. С. 74–79.
32. Костюченко В.В. Управление процессом повышения эффективности организационно-технологических строительных систем // *Инженерный вестник Дона*. 2012. № 1. С. 536–542.
33. Недавний О.И., Кузнецов С.М., Кандаурова Н.М. Обоснование времени производства строительных работ // *Известия высших учебных заведений. Строительство*. 2013. № 9. С. 107–114.
34. Гусев Б.В., Гусева А.Ю., Литвиновский Е.М. Устойчивость и надежность работы конвейерных технологических линий по производству сборного железобетона // *Технологии бетонов*. 2015. № 7-8. С. 30–31
35. Рахутин М.Г., Панкратенко Н.А. Использование АВС – анализа при исследовании надежности тоннелепроходческого комплекса для прокладки эскалаторного тоннеля // *Известия высших учебных заведений. Горный журнал*. 2013. № 1. С. 40–43.
36. Мелькумов В.Н., Кузнецова Г.А., Кобылев А.Н. Использование кластерного анализа для повышения надежности инженерных сетей // *Вестник Воронежского государственного технического университета*. 2012. № 11. С. 141–145.
37. Газарян Р.К., Чулков В.О., Грабовый К.П., Кулаков К.Ю. Оценка уровня организационно-технологической надежности функционирования строительных промышленных предприятий // *Вестник МГСУ*. 2012. № 3. С. 218–222.
38. Кабанов В.Н., Михайлова Е.В. Определение организационно-технологической надежности строительной организации // *Экономика строительства*. 2012. № 4. С. 67–79.
39. Беляков М. Формирование оптимальной программы обслуживания оборудования с использованием RCM-анализа // *Сухие строительные смеси*. 2015. № 5. С. 41–44.

- eskalatornogo tonnelya [The use of ABC – analysis in the study of reliability of equipment for laying an escalator tunnel]. *News of higher educational institutions. Mining journal*. 2013. No. 1. Pp. 40–43. (rus)
23. Melkumov V.N., Kuznetsova G.A., Kobylev A.N. Ispolzovaniye klasterного analiza dlya povysheniya nadezhnosti inzhenernykh setey [The use of cluster analysis to improve the reliability of engineering networks]. *Vestnik Voronezh state technical University*. 2012. No. 11. Pp. 141–145. (rus)
 24. Gazaryan R.K., Chulkov V.O., Grabovyy K.P., Kulakov K.Yu. Otsenka urovnya organizatsionno-tekhnologicheskoy nadezhnosti funktsionirovaniya stroitelnykh promyshlennykh predpriyatiy [Assessment of the level of organizational and technological reliability of construction of industrial enterprises]. *Vestnik MGSU*. 2012. No. 3. Pp. 218–222. (rus)
 25. Kabanov V.N., Mikhaylova E.V. Opredeleniye organizatsionno-tekhnologicheskoy nadezhnosti stroitelnoy organizatsii [The definition of the organizational-technological reliability of construction organizations]. *Economics of construction*. 2012. No. 4. Pp. 67–79. (rus)
 26. Belyakov M. Formirovaniye optimalnoy programmy obsluzhivaniya oborudovaniya s ispolzovaniyem RCM-analiza [The formation of the optimal program of equipment maintenance using RCM analysis]. *Dry mixes*. 2015. No. 5. Pp. 41–44. (rus)
 27. Nowlan F.S., Heap H.F. *Reliability-centered Maintenance*. San Francisco: Dolby Access Press, 1978. 466 p.
 28. Moubrey J. *Reliability-centered Maintenance*. Second Edition. NY: Industrial Press Inc, 1997. 426 p.
 29. Мишланова М.Ю. Развитие структурно-матричного подхода в организационной диагностике // Вестник МГСУ. 2012. № 4. С. 220–225.
 30. Ballard G. *Lean Construction and EPC Performance Improvement*. Alarcón, L. F. (ed), Lean Construction, A.A. Balkema, The Netherlands, 1993. 497 pp.
 31. González V., Alarcón L.F., Maturana S., Bustamante J.A., Mundaca F. Work-in-process buffer management using the rational commitment model in repetitive projects // *Proceedings 16th Annual Conference of International Group for Lean Construction*, Manchester, UK, 2008.
 32. Лapidус А.А. Актуальные проблемы организационно-технологического проектирования // Технология и организация строительного производства. 2013. № 3. С. 1–13.
 33. Połoński M. Rozkład czasu trwania czynności a termin zakończenia przedsięwzięcia z nieuwzględnieniem elementów analizy ryzyka // *Acta Scientiarum Polonorum. Architectura*. 2005. Vol. 4. № 2. Pp. 95–106.
 34. Радкевич А.В., Худенко В.Ф., Глуценко В.М. Анализ существующих проблем организационно-технологической надежности кровельных систем // Наука та прогресс транспорту. 2015. № 2. С. 222–230
 35. Самсонкин В.Н., Каривский Ф.А., Петренко Р.Б., Петин Я.П. Обеспечение надежности «человеческого фактора» на железнодорожном транспорте Украины: как есть и как нужно // Железнодорожный транспорт Украины. 2014. № 4. С. 12–18.

Vadim Kabanov,
+7(905)398-36-63; kabanovvn@yandex.ru

Вадим Николаевич Кабанов,
+7(905)398-36-63;
эл. почта: kabanovvn@yandex.ru

Kabanov V.N., 2018

doi: 10.18720/MCE.77.7

Finite element analysis of crane secondary truss

Конечно-элементное моделирование и расчёт
подкраново-подстропильной фермы

O.A. Tusnina,
National Research Moscow State Civil
Engineering University, Moscow, Russia

Канд. техн. наук, доцент О.А. Туснина,
Национальный исследовательский
Московский государственный строительный
университет, г. Москва, Россия

Key words: crane secondary truss; thin-walled closed profile; restrained torsion; finite element analysis

Ключевые слова: подкраново-подстропильная ферма; тонкостенный замкнутый профиль; стесненное кручение; конечно-элементный расчет

Abstract. Finite element analysis of the crane secondary truss of top-blown oxygen vessel plant with the span of 36m is considered in the paper. Analysis of crane secondary truss is quiet difficult because of necessity of taking into account actual stiffness of its joints and also because of the fact that lower belt of truss made of thin-walled closed profile is experiencing restrained torsion because of eccentricity crane load acting. For these reasons modeling of crane secondary truss with the use of beam finite elements not allows to obtain correct results. That is why the shell finite elements should be used to model crane secondary truss. The required finite element mesh is determined in the paper. Participation of the truss into work of entire building skeleton is analyzed and the design scheme of the framework that allowed to obtain reliable results is selected.

Аннотация. В статье рассмотрен конечно-элементный расчет подкраново-подстропильной фермы (ППФ) конвертерного цеха пролетом 36 м. Расчет подкраново-подстропильной фермы достаточно сложен в связи с необходимостью учета фактической жесткости узлов фермы, а также в связи с тем, что нижний пояс фермы, выполненный из тонкостенного замкнутого профиля из-за эксцентричного приложения нагрузки от крана, кроме изгиба испытывает стесненное кручение. По этим причинам, применение стержневых конечных элементов для расчета ППФ не позволяет получить точные результаты и расчет фермы необходимо выполнять с применением конечных элементов оболочки. В статье определена требуемая сетка разбиения стержней фермы на конечные элементы. Проанализировано включение фермы в пространственную работу всего сооружения и выделена расчетная схема каркаса, в составе которой необходимо выполнять расчет фермы для получения достоверных результатов.

1. Introduction

The crane secondary trusses are applied in industrial buildings. In this case crane secondary truss is not taking load only from crane but it works also like secondary truss and takes load from roof [1]. Such structures are widespread in industrial buildings of metallurgical plants. The spans of crane secondary trusses can be up to 48 m and crane lifting capacity can be 400 tons and more. Crane operation modes on metallurgical plants are 7K, 8K. To execute sufficiently accurate calculation of such responsible structures is complicated because of the next reasons:

- elements of truss are made of large welded I-beams and closed box profiles which have great stiffness as in the plane of truss so from the plane;
- the actual stiffness of joints of the truss should be taken into account [2], besides there are transverse edges and sheets of local reinforcement of profiles in the joints that should be taken into account when analyzing stress strain-state of the truss;
- the large local concentrated crane forces applied with eccentricity to the lower belt of truss made of thin-walled welded box cause its restrained torsion;
- the complexity of the development of the finite element model of the truss made with the use of beam or shell or solid elements;

- the problem of analysis crane secondary truss because of the complexity of the precise determination of the impacts on it taking into account the work of the truss as the part of spatial framework of the building;
- the analysis of large design schemes of the building with the trusses included in the scheme.

The greatest problem is the analysis of lower belt of the truss made of thin-walled box profile which experiences torsion. The stress-strain state of a thin-walled beam when its work in torsion rather complicated, additional normal stresses and deformations occurs in it. [3]. The classical theory of calculation on torsion of thin-walled beams with closed profile was developed by A.A. Umansky [4]. The investigations of stress-strain state of thin-walled closed profile beams and different method of analysis are proposed in the papers [5–10]. In the articles [11, 12] the influence of shear on the behavior of closed profile in torsion is analyzed. The papers [13, 14] are devoted to the problems of buckling of such profiles. Modeling of support contour of the membrane made of thin-walled closed profile that experiences considerable torsion with the use of beam finite elements gives incorrect results, and it is necessary to use shell finite elements for analysis [15].

It is advisable to carry out analysis of crane secondary truss with the use of finite element method implemented in many modern software systems.

The model of crane secondary truss made with the use of beam elements are most simple. Such a model can be easy built in the spatial design scheme of the framework of building. Impacts on the truss on the side of the structures adjacent to it are determined by the calculation of spatial construction. However, the beam model does not fully reflect the features of the design as it does not allow to determine the stress-strain state of the joints taking into account the ribs and reinforcement sheets in them.

The use of beam finite elements for modeling of the truss does not allow obtaining reliable results for a number of reasons:

- big height of the lower belt (up to 3 m) made of thin-walled closed profile, its complexity stress-strain state and its torsion;
- necessity of taking into account of actual stiffness of truss joints which can not be done with the use of beam elements.

In addition, the fatigue cracks and other defects are arise in the elements of truss because of the heavy operation mode of the cranes, their heavy load capacity and dynamic impact of the load [16–21]. And to take into account the actual condition of the structure and the actual location of the defects in estimating truss bearing capacity it is advisable to perform analysis using shell finite elements.

The finite element mesh should be carefully chosen when forming the finite element model of the truss. To select a finite element mesh, a number of test calculations are performed, on the basis of which it is possible to accept the minimum necessary mesh of elements, providing the required accuracy at an acceptable counting time. A finite element model of this kind is difficult to use as part of the spatial scheme of the framework because of the large number of elements in this case and, as a consequence, the large time of the calculation. It seems important to allocate from the spatial finite element model of a fragment including the crane secondary truss and allowing taking into account the influence on the truss behavior of the remaining structures of the building.

The aim of the work is to substantiate the methodology of numerical analysis of a crane secondary truss, taking into account its actual work as a part of the framework of the building. The problem of most accurate account of the constructive features of the truss needs to be solved. The influence on the work of the truss of its joints conjunctions, shape and dimensions of truss rods, presence of the edges and ribs should be taken into account.

To develop recommendations on practical finite-element analysis of crane secondary truss that allow to obtain reliable results without significant complication of the design scheme the following tasks have been accomplished:

- justification of the optimal finite-element mesh of the crane secondary truss made with the use of shell elements;
- an estimation of the impact on stress-strain state of the truss its participation in the work of the entire framework of the building and the allocation of the design scheme of skeleton necessary to obtain reliable results.

2. Methods

The object of study is the crane secondary frame with the span of 36 m (Figure 1) built in the top-blown oxygen vessel plant No. 2 on Novolipetsk Iron and Steel Work (NLMK).

The lattice of the truss is made of welded I-beams 1 m high, the lower belt is a thin-walled beam with closed box profile with the height of 2.88 m. The bars of the outer panels of the upper belt represent lattice braces (the belts of these braces are made of hot-rolled channels 30 and the two-plane lattice are made of the angels L63x5). The bars of the outer panels attached to the column by bolts installed into oval holes to admit free longitudinal displacement of brace. So when the truss is loaded no longitudinal forces arise in these rods.

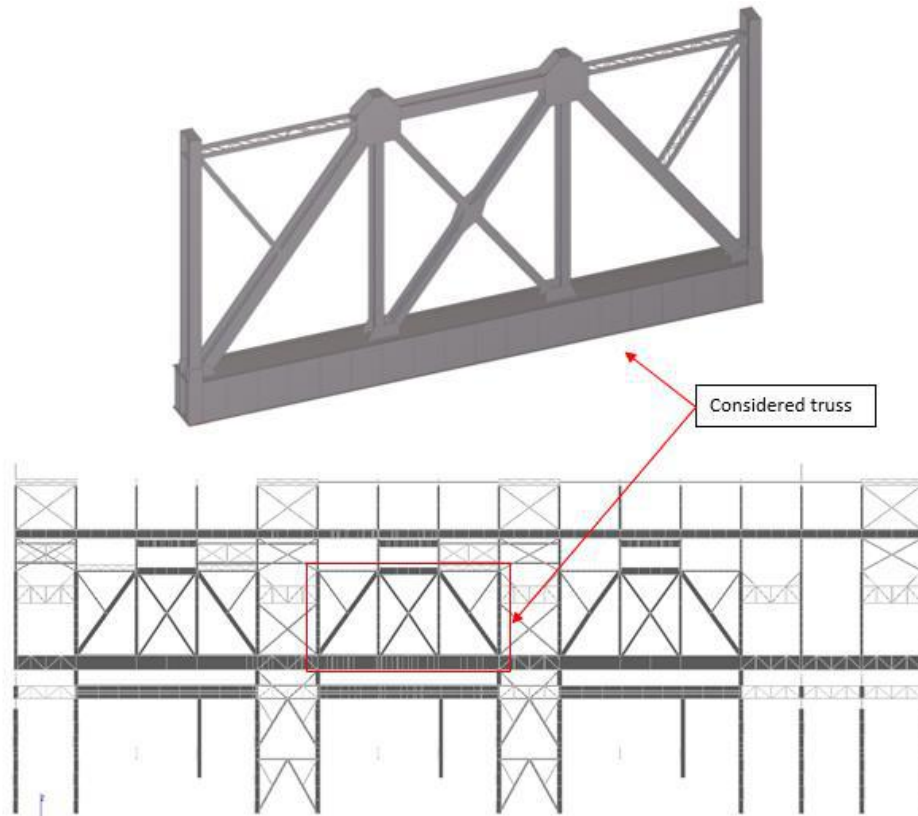


Figure 1. Crane secondary truss with the span of 36 m in in the top-blown oxygen vessel plant No. 2 on Novolipetsk Iron and Steel Work

The main task of this work was to perform a finite element calculation of the truss in order to analyze its stress-strain state. In order to solve this problem competently it was necessary to perform a number of test calculations.

By the reasons mentioned above the crane-secondary truss should be analyzed with the use of shell finite elements.

It is necessary to note that there are beam finite elements with 7 degree of freedom in the node, which corresponds to distortion of the cross-section of the beam. In particular such elements are used in programs Nastran and ANSYS, where it is possible to make an analysis with hinged (free distortion) or rigid (distortion is impossible) boundary condition in the nodes of the beam. But the use of such elements do not allow to take into account construction of the joint included ribs, plates and other elements which prevent free distortion but also can not provide a complete prohibition of distortion. So, the use of shell finite element model allows accounting elastic pliability in the joints and influence of construction solution of the joint on the work of structure, while the use of mentioned beam finite elements is not.

At the first step of the research it was necessary to determine the finite-element mesh of the truss which allow us to obtain correct results.

At first we determined adequate finite element mesh of lower belt of the truss, which is a closed box thin-walled profile with the height of 2.88 m.

The next finite element mesh was assigned: the 15 finite elements along the height of the lower belt made of thin-walled closed profile and 14 finite elements along its width were appointed. The size of the element is not more than 0.2 m. The diaphragms and other stiffeners of the lower belt were modeled.

To estimate the reliability of the results obtained with such a finite element mesh the lower belt of the truss was analyzed separately under the following boundary conditions and loads:

- as a cantilever beam loaded at the end with a concentrated force $Q=1000$ kN (Figure 2);
- as a cantilever beam loaded at the end with a torque $M=3990$ kNm (Figure 3);
- as hinged beam loaded at the points of racks attachment to the belt (at a distance $a=12.5$ m from the edge) by concentrated forces $Q=1000$ kN (Figure 4).

The length of the beam is 36.5 m.

To confirm the reliability of obtained results, the finite element model compiled using shell elements with mentioned mesh were analyzed with the use of two different computing programs – Lira-SAPR 2013 and Femap 11.1.2 using the NX Nastran solver.

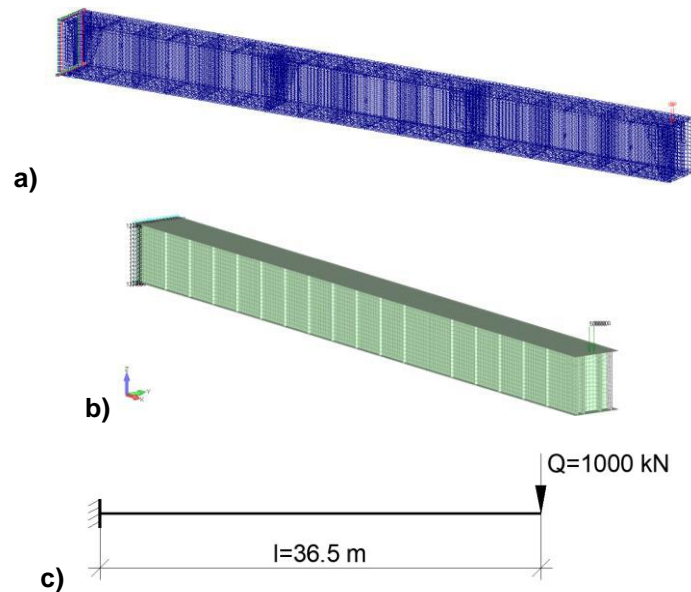


Figure 2. The design scheme of lower bent as cantilever beam loaded by concentrated force at the end (a – Lira-SAPR 2013; b – Femap 11.1.2; c – beam model)

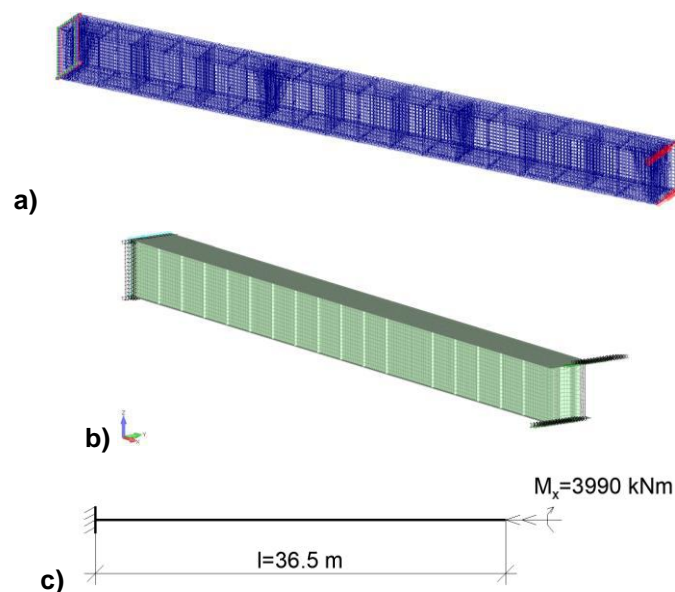


Figure 3. The design scheme of lower bent as cantilever beam loaded by torque at the end (a – Lira-SAPR 2013; b – Femap 11.1.2; c – beam model)

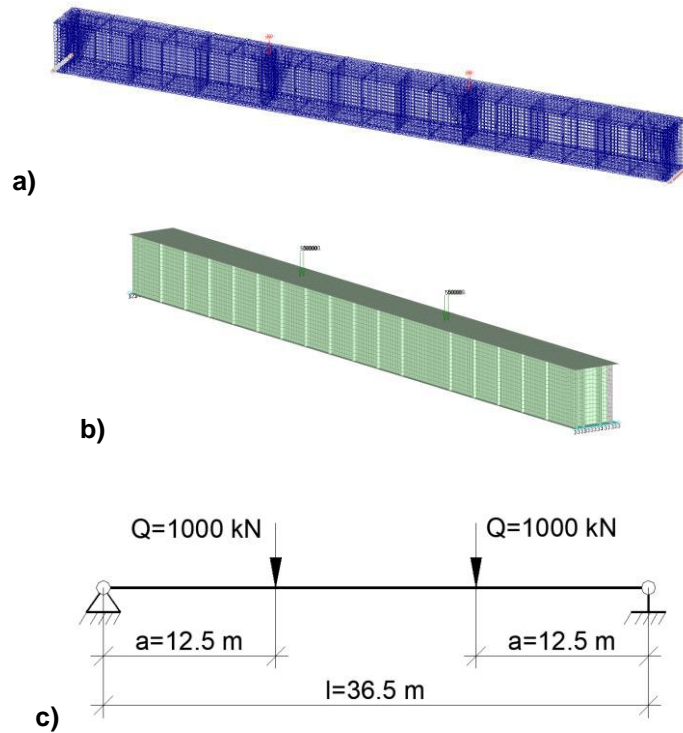


Figure 4. The design scheme of lower bent as hinge beam (a – Lira-SAPR 2013; b – Femap 11.1.2; c – beam model)
 *a=12.5 m is distance taken in accordance with the length of the truss panel

Theoretical equations for displacements and rotational angles are represented below.

For the cantilever beam loaded at the end by concentrated force (Figure 5):

- vertical displacement of the end of the beam is determined by the following equation:

$$f = \frac{Ql^3}{3EI} \quad (1)$$

- rotational angle of the end of the beam:

$$\varphi = \frac{Ql^2}{2EI} \quad (2)$$

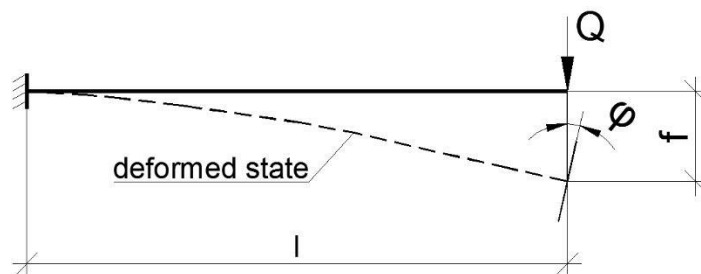


Figure 5. The scheme of deformation of the cantilever beam loaded by concentrated force at the end

For the hinged beam loaded as mentioned above (Figure 6):

- vertical displacement of the middle of the beam span:

$$f = \frac{Ql^3}{24EI} \left(4 \frac{a^3}{l^3} - 3 \frac{a}{l} \right) \quad (3)$$

- rotational angel of the support cross-section of beam:

$$\varphi = \frac{Qa}{2EI}(l-a) \quad (4)$$

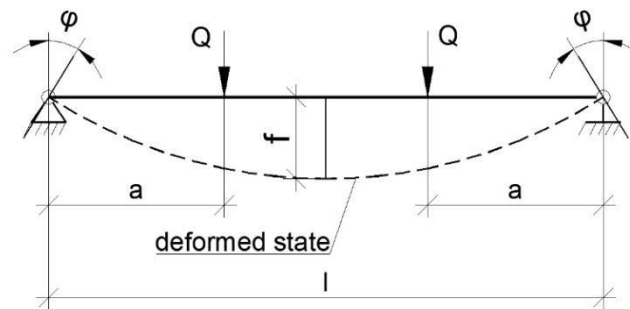


Figure 6. The scheme of deformation of the hinged beam

For the cantilever beam loaded at the end by torque (Figure 7):

- twisting angel of the cross-section at the end of the beam (in pure torsion - without considering restrained torsion):

$$\theta = \frac{Ml}{GI_t} \quad (5)$$

Sectorial moment of inertia I_w and moment of inertia in pure torsion I_t were determined with the use equations represented in [22] for closed rectangular section. The protruding parts of the flanges were neglected because of their small size in comparison with entire section (Figure 8) and because of the lack of formulas for calculating the characteristics of such a section.

Moment of inertia in pure torsion:

$$I_t = \frac{2b^2h^2g_1g_2}{bg_2+hg_1} \quad (6)$$

Sectorial moment of inertia:

$$I_w = \frac{b^2h^2}{24} \frac{(bg_2 - hg_1)^2}{(bg_2 + hg_1)^2} (bg_1 + hg_2) \quad (7)$$

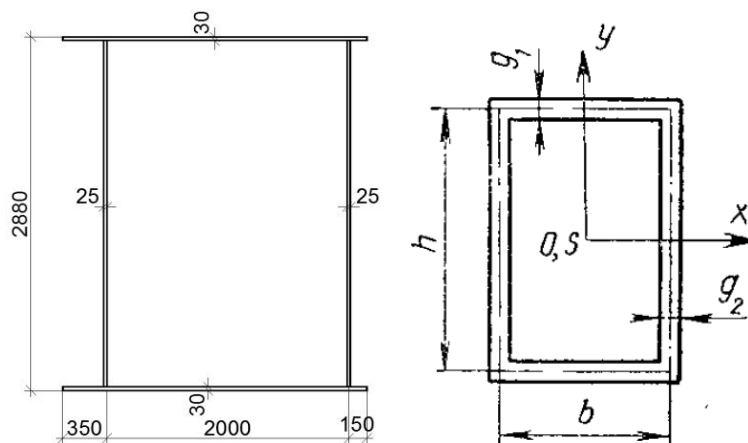


Figure 7. Cross-section of lower belt of the truss and the scheme to calculating its geometric characteristics in torsion (O - center of gravity; S - shear center)
In this case $b=2000$ mm, $h=2850$ mm; $g_1=30$ mm, $g_2=25$ mm.

Twisting angel taking into account restrained torsion is determined by the following equation [23] (Figure 8):

$$\theta(z) = \frac{M}{k^3 EI_w \operatorname{ch}(kl)} (kz \cdot \operatorname{ch}(kl) - \operatorname{sh}(kl) + \operatorname{sh}(k(l-z))), \quad (8)$$

where bending-twisting characteristic is calculating as follows:

$$k = \sqrt{\frac{GI_t}{EI_w}} \quad (9)$$

z – the coordinate of the point at which the twisting angle is determined, in this case $z=l$ – the twisting angle of the cross-section at the end of the beam is determined.

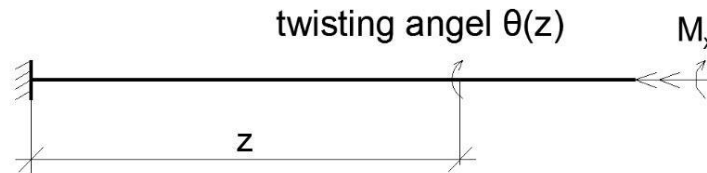


Figure 8. The scheme of deformation of the cantilever beam loaded by torque

3. Results and Discussion

The calculation of displacements and rotational angles for mentioned above boundary conditions and loads with the use of theoretical equations (formulas (1)-(8)) is represented in the Tables 1–3.

Table 1. Theoretical calculation for cantilever beam loaded at the end by concentrated force (Figure 2)

Parameter	Value
Q, kN	1000
l, m	36.5
EI_y , kN*m ²	80076419
Vertical displacement at the end of the beam f , mm (1)	202.42
Rotational angel at the end of the beam φ , rad*1000 (2)	8.32

Table 2. Theoretical calculation for hinged beam (Figure 3)

Parameter	Value
Q, kN	1000
l, m	37
a, m	12.5
EI_y , kN*m ²	80076419
Vertical displacement at the middle of the beam span f , mm (3)	22.65
Rotational angel on the support φ , rad*1000 (4)	1.95

Table 3. Theoretical calculation for cantilever beam loaded by torque (Figure 4)

Parameter	Value
M, kNm	3990
l, m	36.5
GI_t , kN*m ² (6)	28054095.94
EI_w , kN*m ⁴ (7)	2512367.22
Bending-twisting characteristic k (9)	3.34
Twisting angel in pure torsion θ , rad*1000 (5)	5.191
Twisting angel in restrained torsion θ , rad*1000 (8)	5.149

Comparison of the results of finite element analysis made with mentioned above mesh with the use of two different computing programs – Lira-SAPR 2013 and Femap 11.1.2 using the NX Nastran solver and theory (see formulas (1)-(8) and tables 1-3) is represented in the table 4.

Table 4. Comparison of the results of finite element analysis and theoretical calculation

Parameter	Theory	Lira-SAPR 2013	NX Nastran	Error	
				Lira-SAPR 2013/Theory	NX Nastran/Theory
Cantilever beam loaded at the end by concentrated force					
Vertical displacement at the end of the beam f , mm	202.42	200	199	-1.20%	-1.69%
Rotational angel at the end of the beam φ , rad*1000	8.32	8.12	8.31	-2.39%	-0.12%
Hinged beam					
Vertical displacement at the middle of the beam span f , mm	22.65	23.6	22.8	4.21%	0.67%
Rotational angel on the support φ , rad*1000	1.95	1.86	1.91	-4.68%	-2.05%
Cantilever beam loaded by torque					
Twisting angel in restrained torsion θ , rad*1000	5.149	5.567	5.337	7.51%	3.52%

Error of finite element analysis for the most of parameters does not exceed 5 % with a maximum error of not more than 8 %. That allows the use of the appointed finite element mesh of lower belt of the truss in the calculation.

The finite element mesh of truss braces made from I-profile should be based on the dimensions of the element assigned for the lower belt provided that the I-beam flange is divided into not less than 4 elements [24].

So, the following finite element mesh was assigned for the structure elements of the truss:

- 15 shell finite elements along the height of the lower belt and 14 shell finite elements along its width;
- 4 shell finite elements along the flange of the I-profile braces and 7 shell finite elements along its width.

The finite element model of the considered crane secondary truss was created with the use of program Lira-SAPR 2013 (Figure 9). Then for further analysis the created finite element model was exported into the program SCAD Office 21.1. The lattice braces were modeled with the use of beam finite elements. Shell finite elements were used to model other structure elements of the truss.

The 2-nodes beam finite elements (type 5) were used (with 6 degrees of freedom in each node). The classic scheme of beam work taking into account flat-section hypothesis was used (Euler-Bernoulli bending theory). The 4-nodes shell finite elements with 6 degrees of freedom in each node (type 44) were used. It is necessary to note that rotational angel U_z (around the normal to the surface of element) in the local coordinate system of element (type 44) is equal to zero. So there are discrepancies between the degrees of freedom of the beam and shell finite elements. But this will have a significant effect only in the case when the bending of the beam attaches to the plates will occur in the direction corresponding rotation of the plate around Z-axis. In this case, there are no such situations, because the connections of the beams to the plates is carried out at the nodes belonging to several plates lying in different planes, which corresponds to the presence in the joint of the various ribs, which are modeled by the shell finite elements.

The analysis was carried out in a geometrically linear setting because of the sufficient rigidity of the structure and the small displacements and angels of rotation.

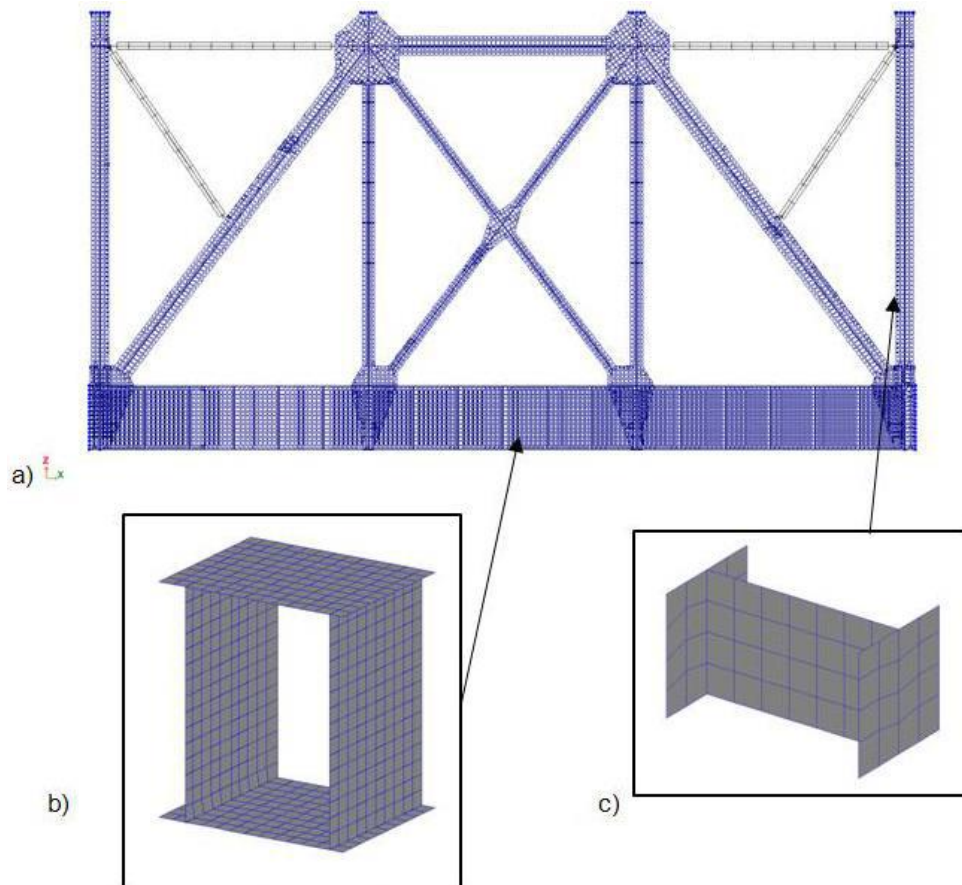


Figure 9. Finite-element model of the truss
a – general view; b – finite element mesh of lower belt of the truss;
c – finite element mesh of I-profile braces of the truss

As mentioned above, the crane secondary truss, having a sufficiently high stiffness both in its plane and out of plane, takes part in the work of the entire framework of the building, and in order to correctly take into account the forces arising in the truss rods, it is necessary to perform the calculation of the truss as the part of the full framework. But when modeling the full framework this calculation is done too long because of the large number of finite elements.

On the second step of investigation we should determine the part of the framework required for obtaining reliable results analyzing the crane secondary truss.

Beam finite element model of the full framework of the top-blown oxygen vessel plant No. 2 at NLMK in the axis 1-31/A-Y was created with the use of program SCAD Office 21.1 (Figure 10). Number of beam finite elements is 57615.

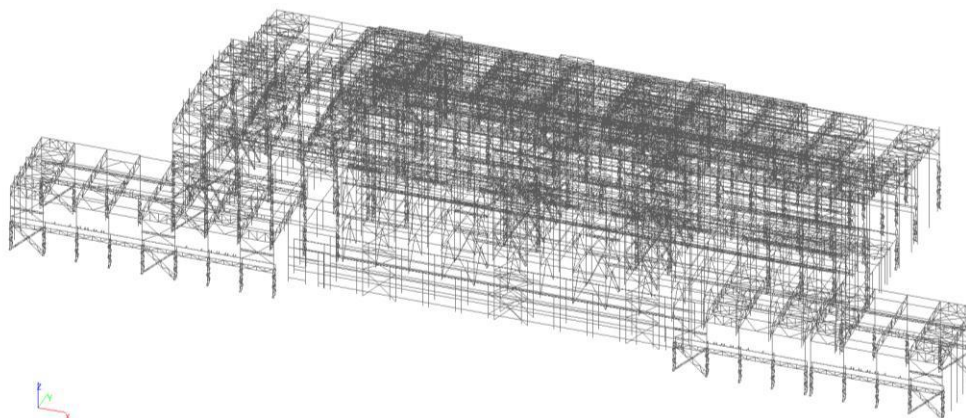
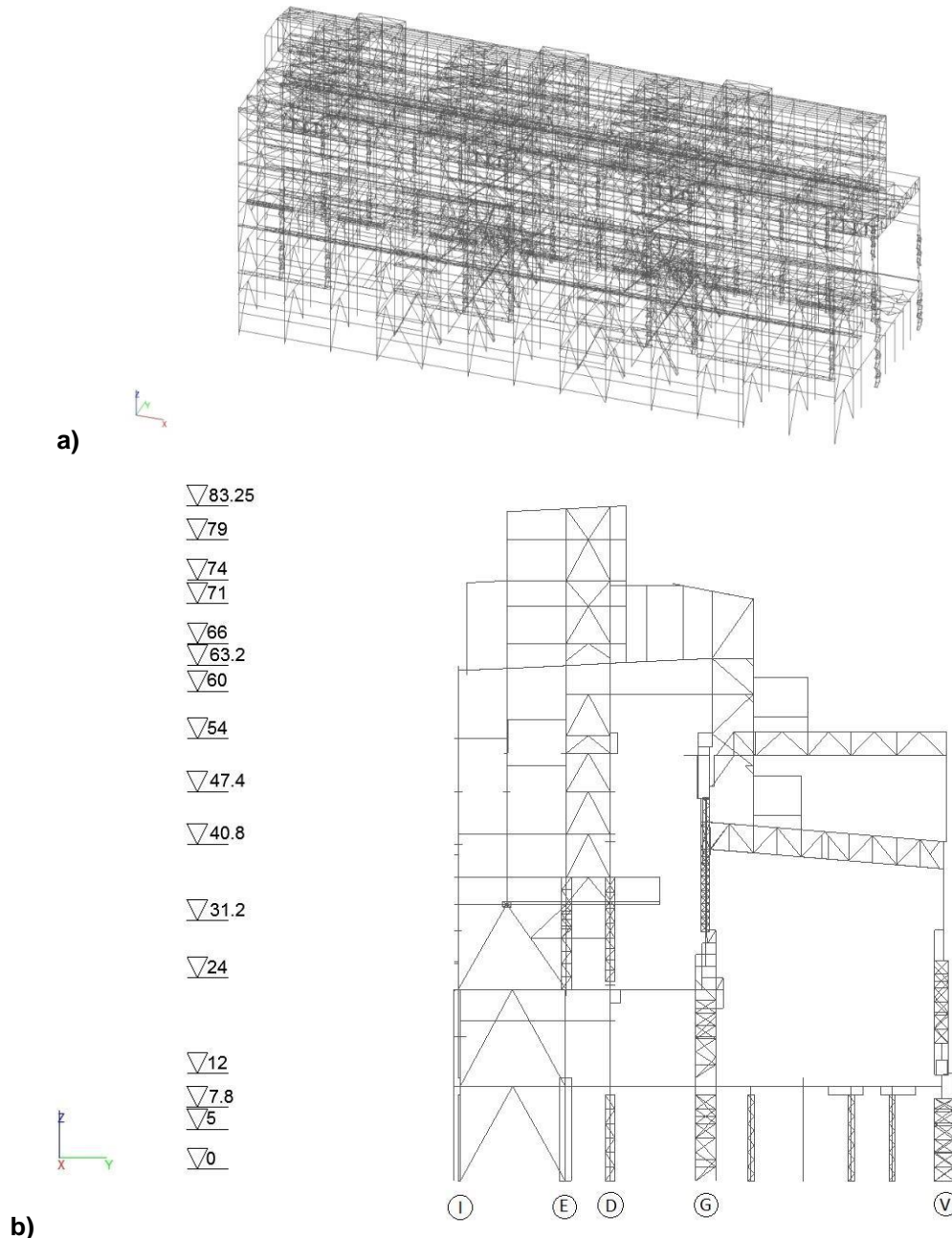


Figure 10. The finite element model of the full framework of the top-blown oxygen vessel plant No. 2 at NLMK in the axis 1-31/A-U

In the building there are 3 crane secondary trusses at axis 11-24 on the axis G. Stress-strain state of the middle truss at the axis 16-19 is analyzed in the paper (see Figure 1). The roof trusses of the span V-G and the welded beams in axis I-G which have intermediate supports on the columns along axis E and D are abutted on the crane secondary trusses.

Several variants of the design schemes of the framework part were considered.

Variant 1. All three crane secondary trusses and all structures of spans V-G and I-G are included in the model (Figure 11). Number of finite elements are 28241.



**Figure 11. The finite element model of the framework part of the top-blown oxygen vessel plant No. 2 at NLMK in the axis 11-24/V-I – variant 1
a – general view; b – cross-section**

Variant 2. All three crane secondary trusses, structures of span V-G and part of the beams in the axis D-G are included in the model (figure 12). Number of finite elements are 21036.

Variant 3. In the longitudinal direction the middle considered crane secondary truss and its adjacent braced pitches (axis 15-20) and in the transverse direction – structures of the span V-G and part of the beams in axis D-G are included in the model (figure 13). Number of finite elements are 10222.

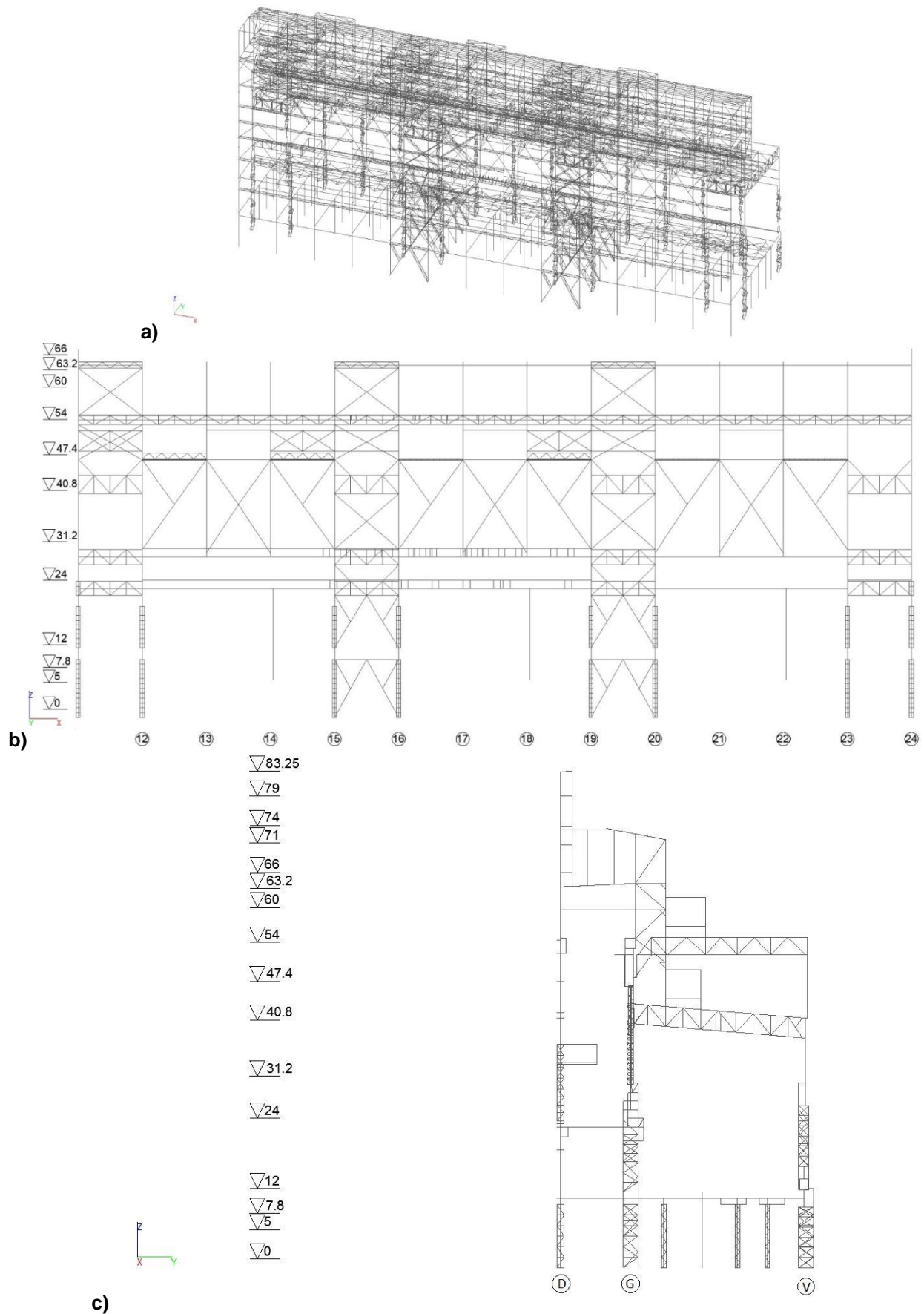


Figure 12. The finite element model of the framework part of the top-blown oxygen vessel plant No. 2 at NLMK in the axis 11-24/V-D– variant 2
a – general view; b – longitudinal section along the G-axis; c – cross-section

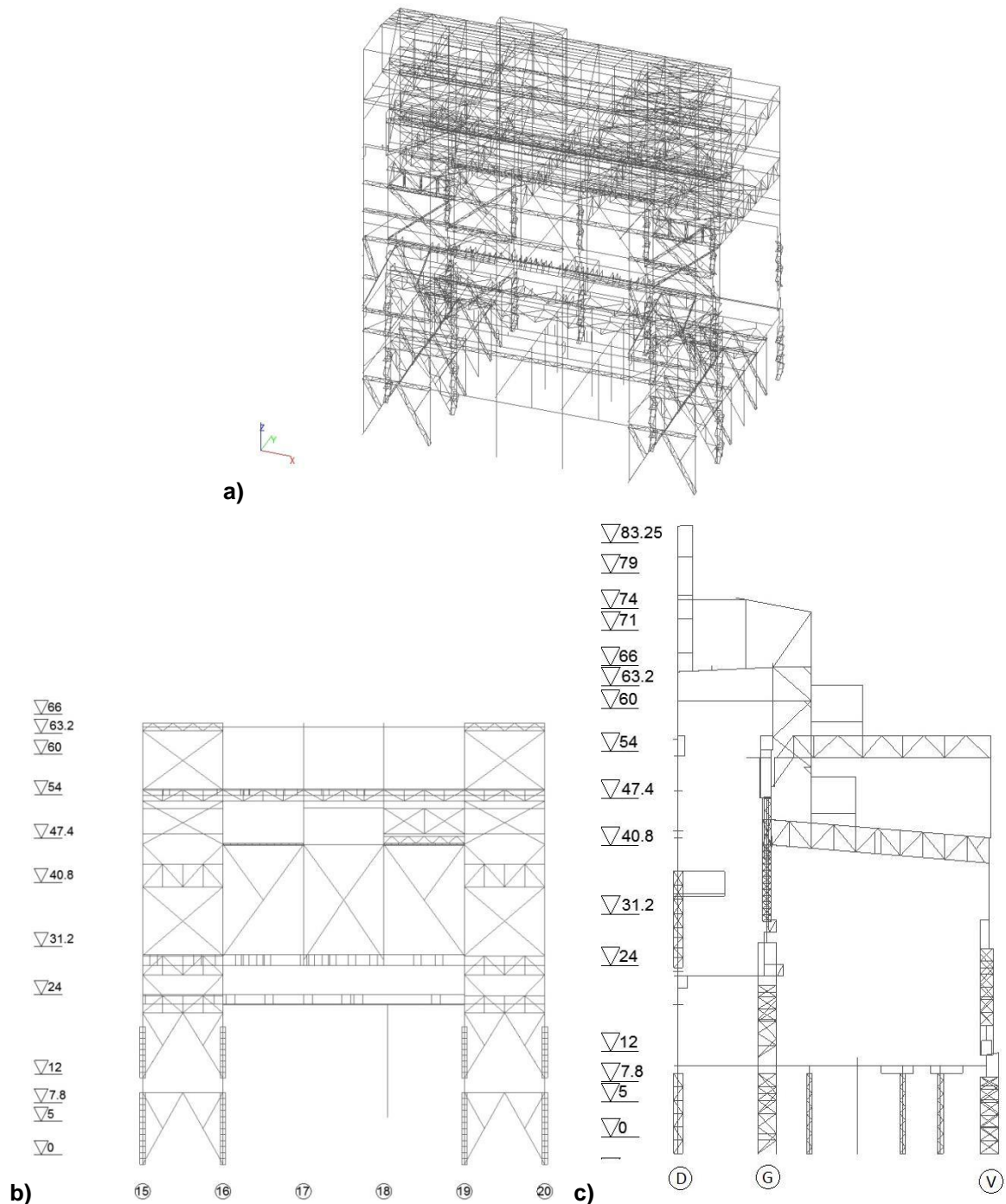
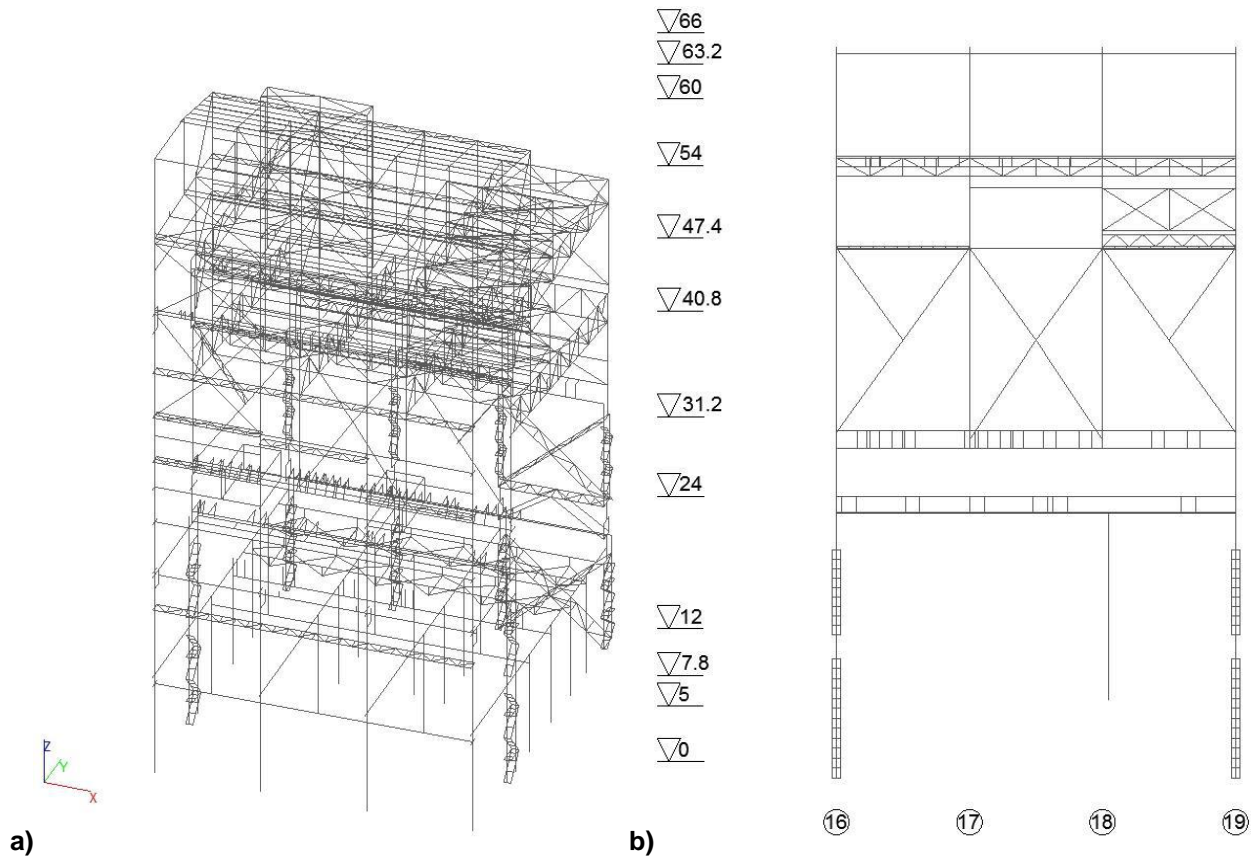


Figure 13. The finite element model of the framework part of the top-blown oxygen vessel plant No. 2 at NLMK in the axis 15-20/V-D – variant 3
a – general view; b – longitudinal section along the G-axis; c – cross-section

Variant 4. In the longitudinal direction only the middle considered crane secondary truss (axis 16-19) and in the transverse direction – structures of the span V-G and part of the beams in axis D-G (figure 14) are included in the model. Number of finite elements are 5329.



**Figure 14. The finite element model of the framework part of the top-blown oxygen vessel plant No. 2 at NLMK in the axis 16-19/V-D – variant 4
a – general view; b – longitudinal section along the G-axis**

Variant 5. In the longitudinal direction the middle considered crane secondary truss and its adjacent braced pitches (axis 15-20) and in the transverse direction – structures of the span V-G and I-G are included in the model (figure 15). Number of finite elements are 13316.

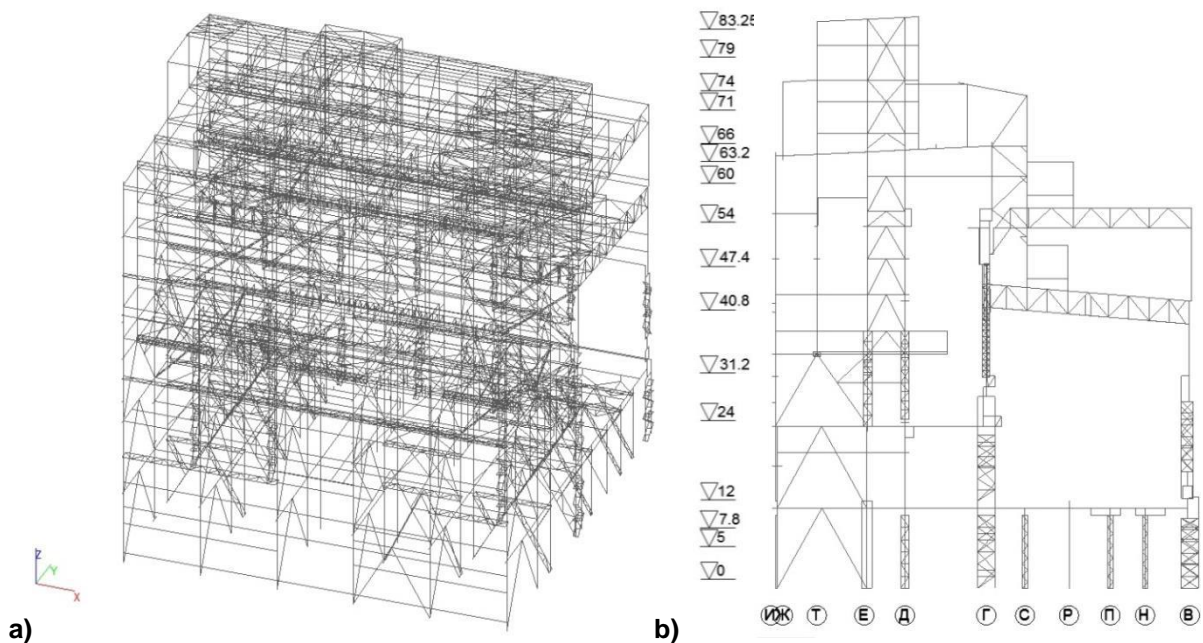


**Figure 15. The finite element model of the framework part of the top-blown oxygen vessel plant No. 2 at NLMK in the axis 15-20/V-I – variant 5
a – general view; b – cross-section**

Comparison of the results of finite element analysis of the considered variants of the schemes with the calculation of full framework is represented in the Table 2. There were analyzed forces in the support rod of the crane secondary truss (Figure 19) and displacements of the node of the intersection of central rods (Figure 20). In the table 5 there are represented results obtained from 3 variants of loading – dead load, vertical crane load and combinations of loads C1. Combination of loads C1 include loads dead load of all structures, snow load, wind load taking into account dynamic part of wind impact, equipment load and crane loads.

The column support on the base is rigid in the transverse direction and hinged in the longitudinal. The dead load of elements including crane secondary truss was appointed by means of program taking into account its specific gravity and also load reliability factor $\gamma=1.05$ (for steel structures). Dead load from walling, roof, ceiling of working platforms was appointed on elements taking into account corresponding reliability factors. The equipment load includes both dead load of equipment and its impact in working condition on structure, also taking into account snow and wind load on equipment susceptible to this influences. The load from equipment was assigned based on the data provided by supplier.

The scheme of snow load is represented on the Figure 16. The wind load is acting in considered case along the Y-axis (Figure 17). The crane load in the combination C1 is assigned in assumption that two cranes are working on the axis 16 (Figure 18). Also crane transverse loads were taking into account in combination C1.

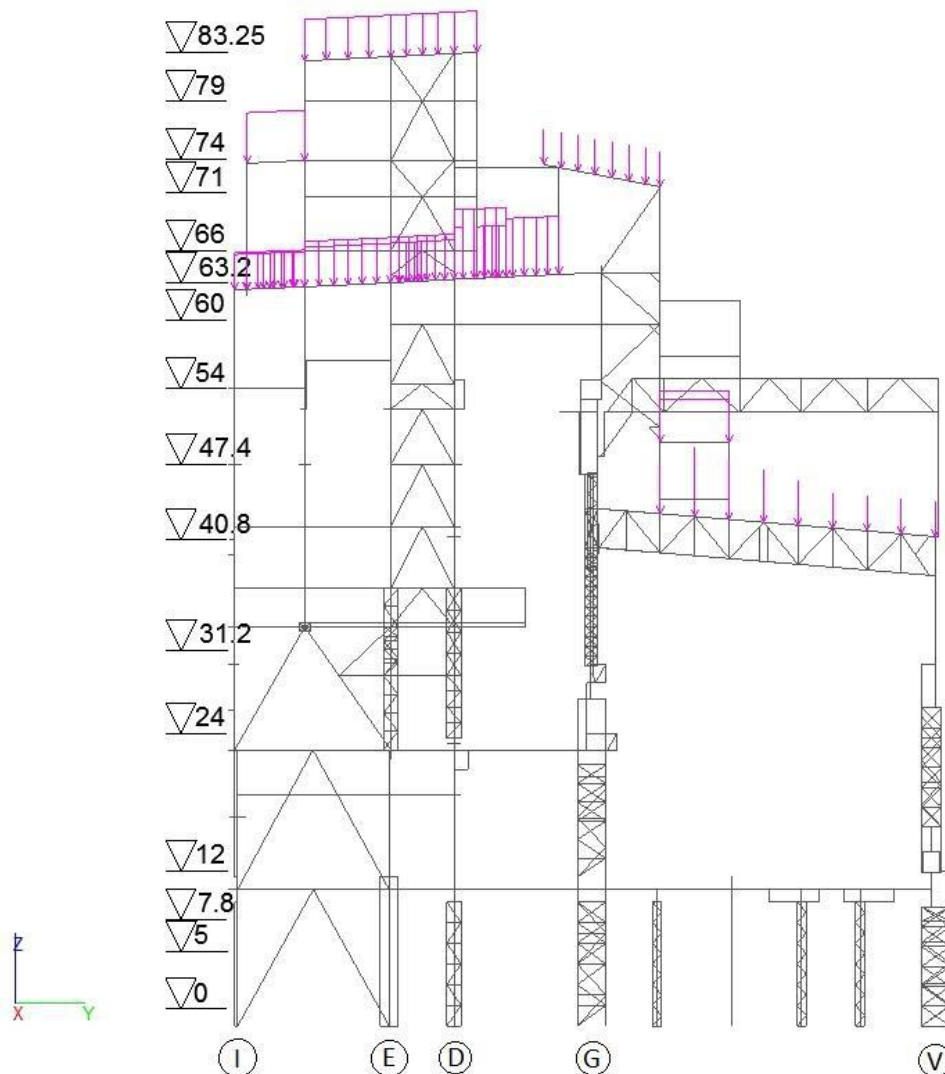
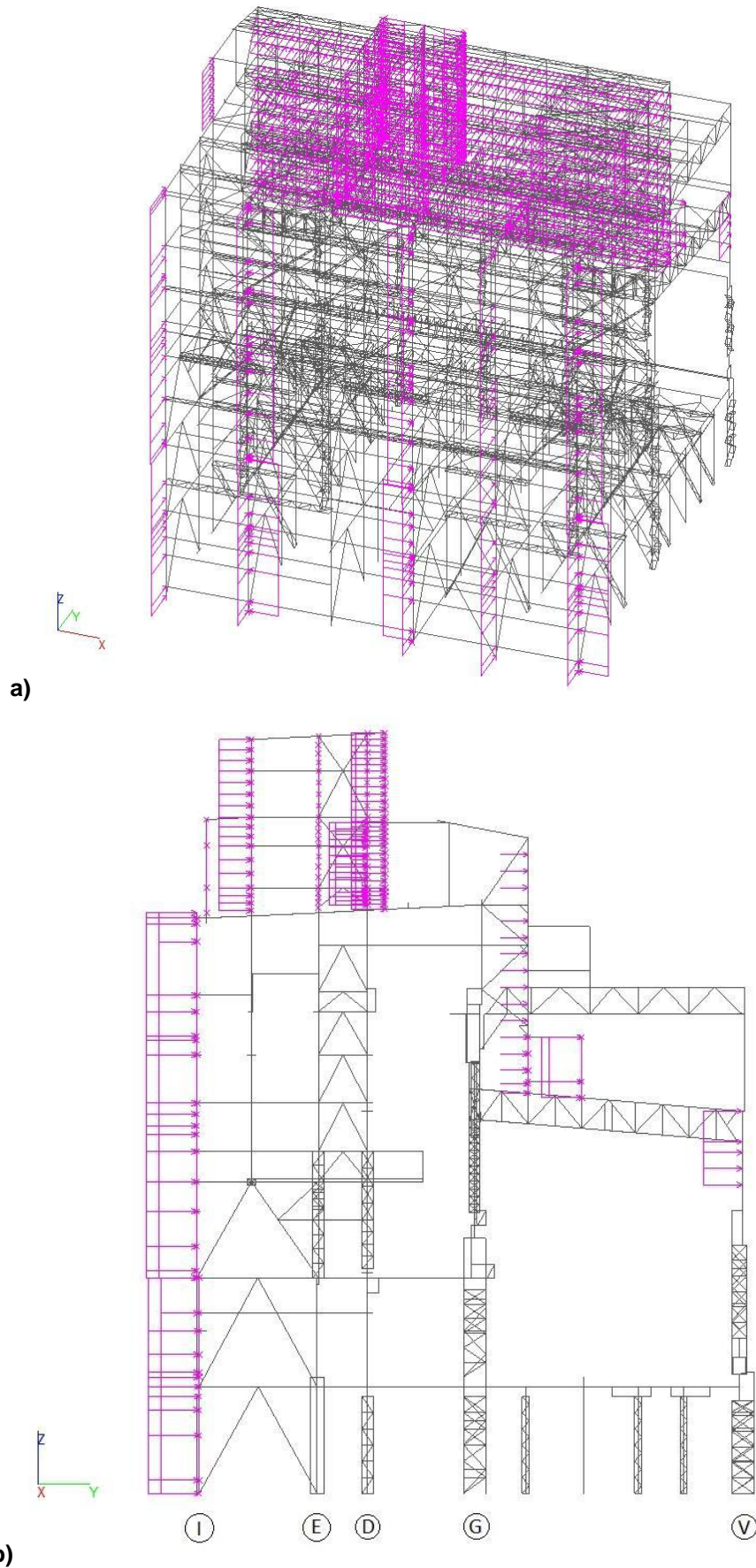


Figure 16. The scheme of snow load



**Figure 17. The scheme of wind load
a – general view; b – cross-section**

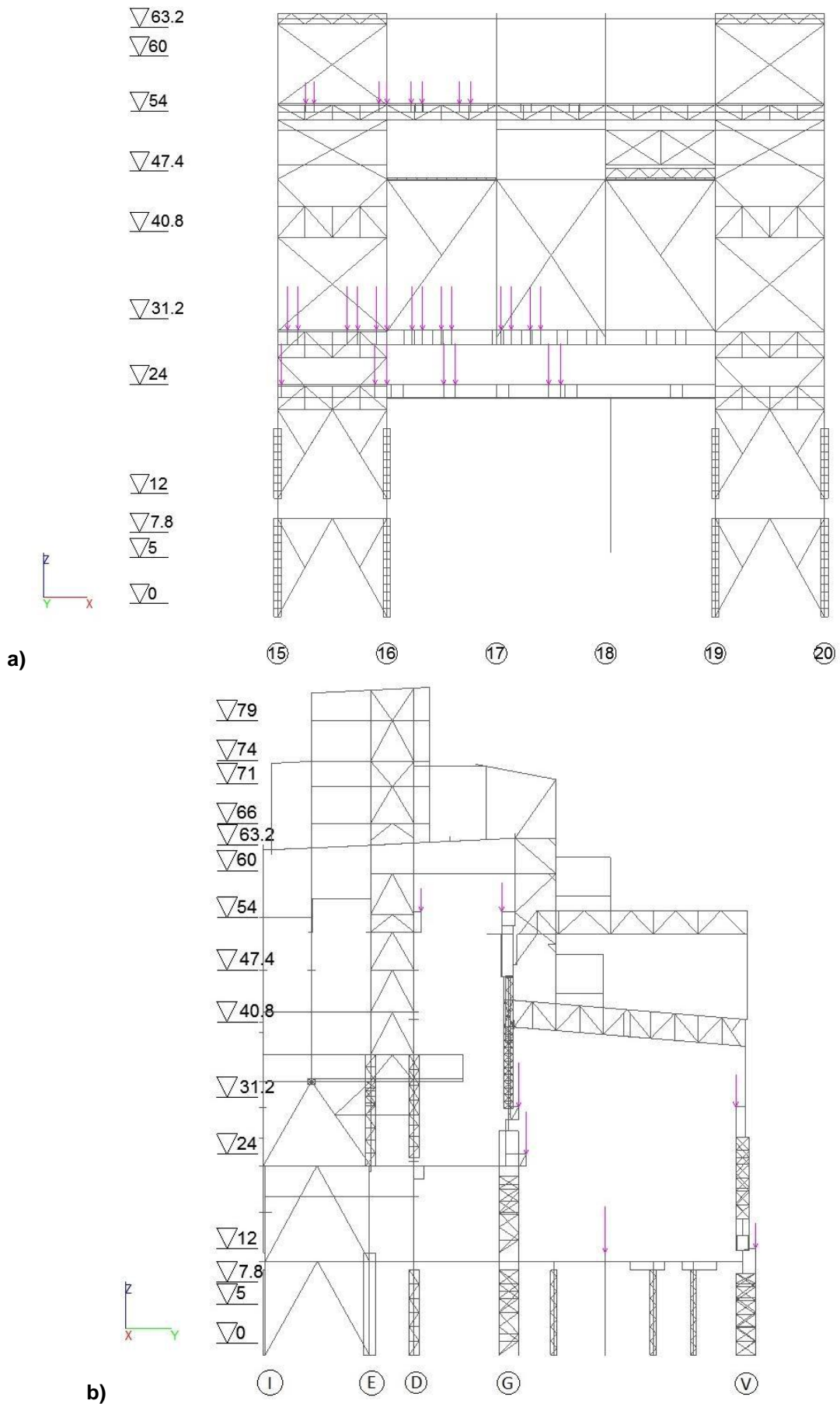


Figure 18. The scheme of vertical crane load
a – longitudinal section along axis G; b – cross-section

Table 5. Comparison of the results of finite element analysis

Variant of scheme		Full	1	2	3	4	5
Forces in the support rod from the dead load	N, t	-129	-129	-125	-126	-129	-130
	M_y, tm	215	217	196	171	232	188
	M_z, tm	52	52	52	47	-149	47
Forces in the support rod from the vertical crane load	N, t	-720	-722	-721	-715	-724	-717
	M_y, tm	1493	1515	1525	1546	1410	1538
	M_z, tm	120	113	107	87	-13	92
Forces in the support rod from the combination C1	N, t	-591	-600	-563	-556	-613	-597
	M_y, tm	1577	1647	1583	1554	1197	1593
	M_z, tm	-113	-83	-92	-91	-420	-102
Displacement of the central node from dead load	Z, mm	-6.23	-6.25	-6.29	-6.12	-7.8	-6.11
Displacement of the central node from crane load	Y, mm	17.28	17.74	21.9	31.81	47.6	20.59
	Z, mm	-27.89	-28.22	-28.27	-28.93	-40.55	-28.78
Displacement of the central node from combination C1	Y, mm	35.92	46.56	151.98	163.58	158.01	45.37
	Z, mm	-29.71	-29.69	-29.66	-29.49	-36.36	-29.76
Number of finite elements		57615	28241	21036	10222	5329	13316
Error in the comparison with full framework	Forces in the support rod from the dead load	N, t	0.0%	-3.1%	-2.3%	0.0%	0.1%
		M_y, tm	0.9%	-8.8%	-20.5%	7.9%	-12.6%
		M_z, tm	0.0%	0.0%	-9.6%	-386.5%	-9.6%
	Forces in the support rod from the vertical crane load	N, t	0.3%	0.1%	-0.7%	0.6%	-0.4%
		M_y, tm	1.5%	2.1%	3.5%	-5.6%	3.0%
		M_z, tm	-5.8%	-10.8%	-27.5%	-110.8%	-23.3%
	Forces in the support rod from the combination C1	N, t	1.5%	-4.7%	-5.9%	3.7%	1.0%
		M_y, tm	4.4%	0.4%	-1.5%	-24.1%	1.0%
		M_z, tm	-26.5%	-18.6%	-19.5%	271.7%	-9.7%
	Displacement of the central node from dead load	Z, mm	0.3%	1.0%	-1.8%	25.2%	-1.9%
	Displacement of the central node from crane load	Y, mm	2.7%	26.7%	84.1%	175.5%	19.2%
		Z, mm	1.2%	1.4%	3.7%	45.4%	3.2%
	Displacement of the central node from the combination C1	Y, mm	22.9%	323.1%	355.4%	339.9%	20.8%
		Z, mm	-0.1%	-0.2%	-0.7%	22.4%	0.2%

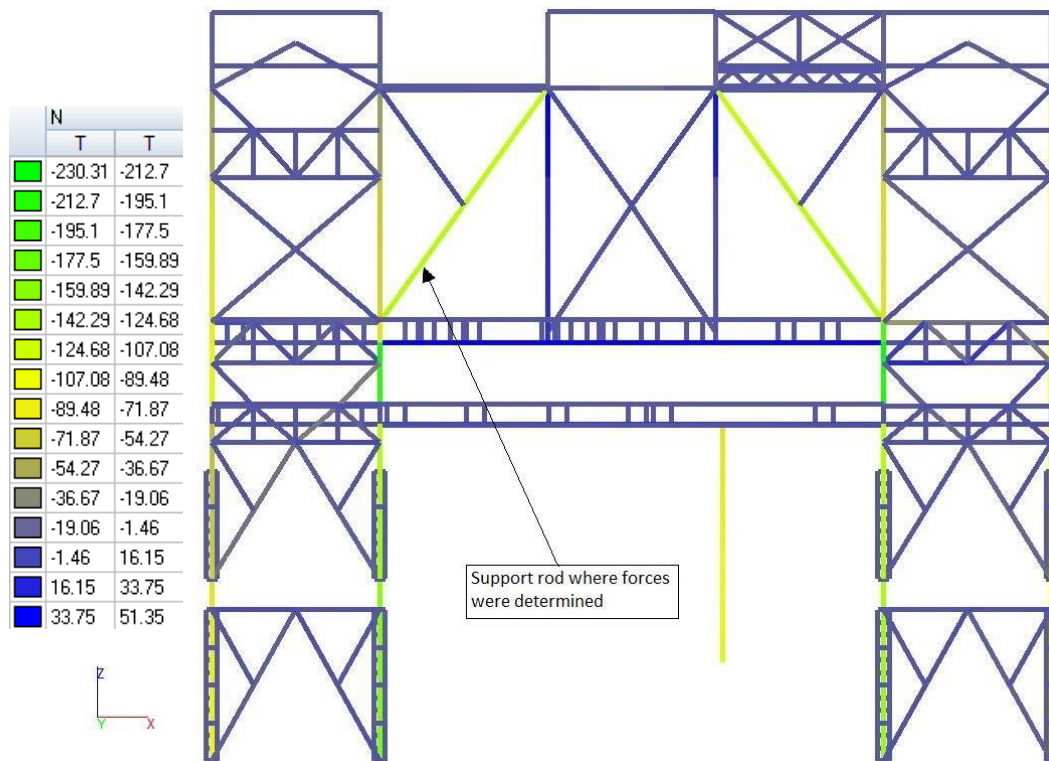


Figure 19. Axial forces diagram (tons) obtained from analyzing of variant 4 of design scheme from dead load

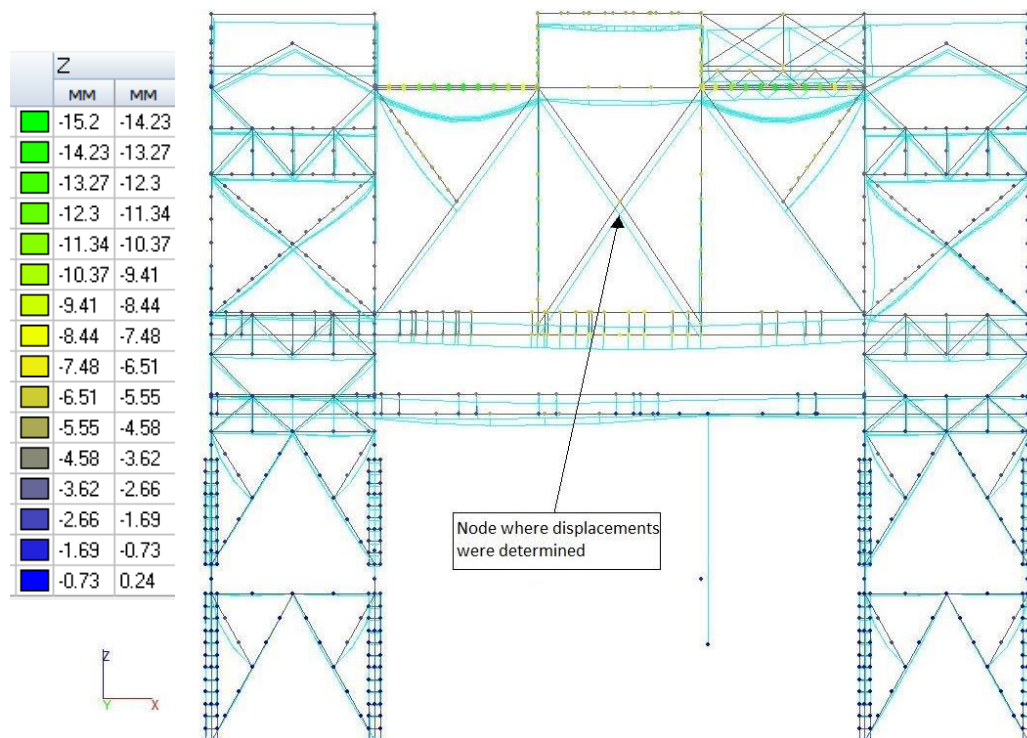


Figure 20. Vertical displacements (mm) obtained from analyzing of variant 5 of design scheme from dead load (deformed state of structure is shown by blue color)

Based on the analysis of the obtained results, the variant 5 of partial design scheme of framework was adopted as the main for analyzing crane secondary truss taking into account its spatial work in the structure of full framework.

In general these calculations allowed establishing the part of the framework that should be included in a unified calculation scheme with the truss. So, the calculation can be performed for a part of

the framework in the longitudinal direction within the considered truss and adjacent braced column pitches and in transverse direction – along span on each side.

The crane secondary truss modeled by shell finite elements in accordance with below proven mesh was embedded in the chosen design scheme (variant 5) of the part of framework. This finite element model is shown on the figure 18. Then the analysis of this model was done on the loads acting on the framework of vessel plant.

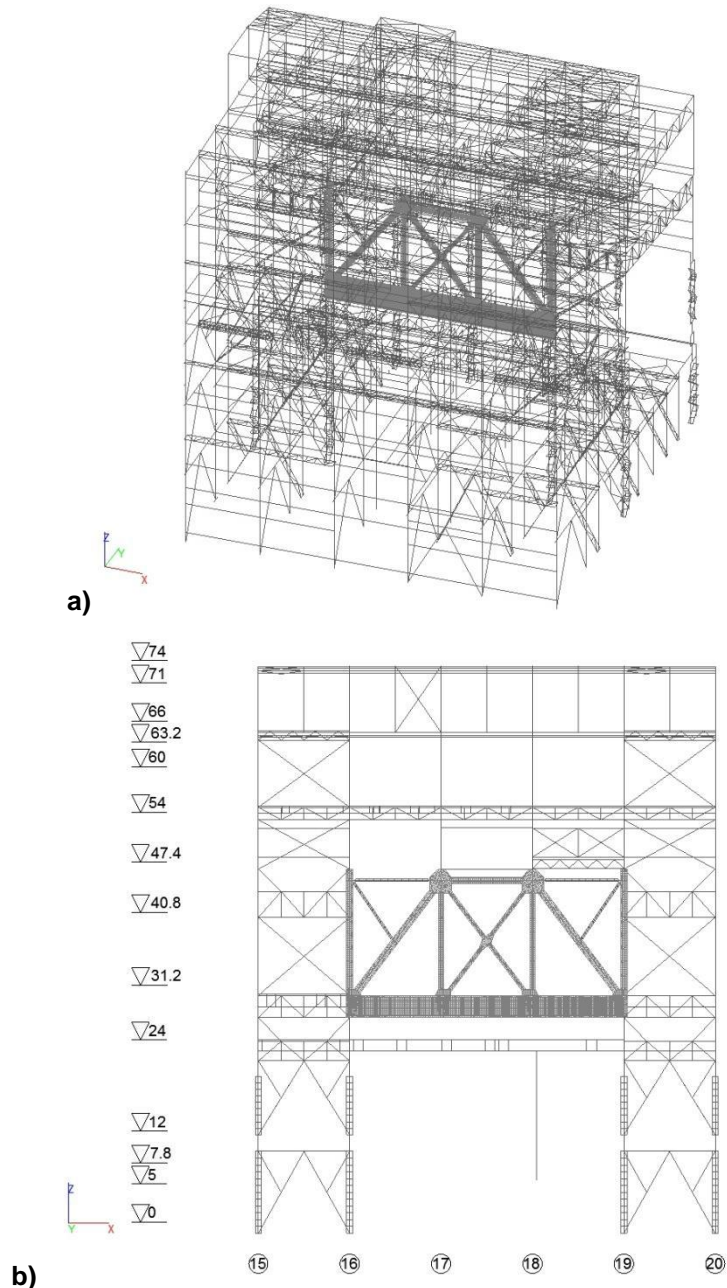


**Figure 21. Finite element model for the analysis of crane secondary truss as part of framework
a – general view; b – longitudinal section along the G-axis**

It should be noted that the medium-power laptop with an Intel Core i7 processor was used and calculation time of this chosen scheme (Figure 21) did not exceed 10 minutes. So, the calculation in this way is available to a wide range of users and does not take much time.

The results of the analysis of beam finite element model (variant 5) are compared with the results obtained with the use of shell finite elements to model crane secondary truss (Figure 18) in the Table 6.

Table 6. Comparison of the results of numerical calculation made with the use of beam and shell finite elements

Scheme		Beams	Shells	Differences
Displacement of the central node from dead load	Z, mm	-6.11	-5.79	-5.24%
Displacement of the central node from snow load	Z, mm	-2.48	-2.37	-4.44%
Displacements of the central node from crane load	Y, mm	20.59	23.85	13.67%
	Z, mm	-28.78	-25.45	-11.57%
	Ux, deg	-0.39	-0.45	13.33%
Displacements of the central node from combination C1	Y, mm	45.37	39.88	12.12%
	Z, mm	-29.76	-27.24	-8.47%

As it can be seen the difference in the obtained displacements is no more than 14 %, that allows us to conclude that the calculation scheme of the framework fragment with the finite element model of the crane secondary truss included in it gives quite reliable results.

Vertical displacements of structure are shown on the Figure 22.

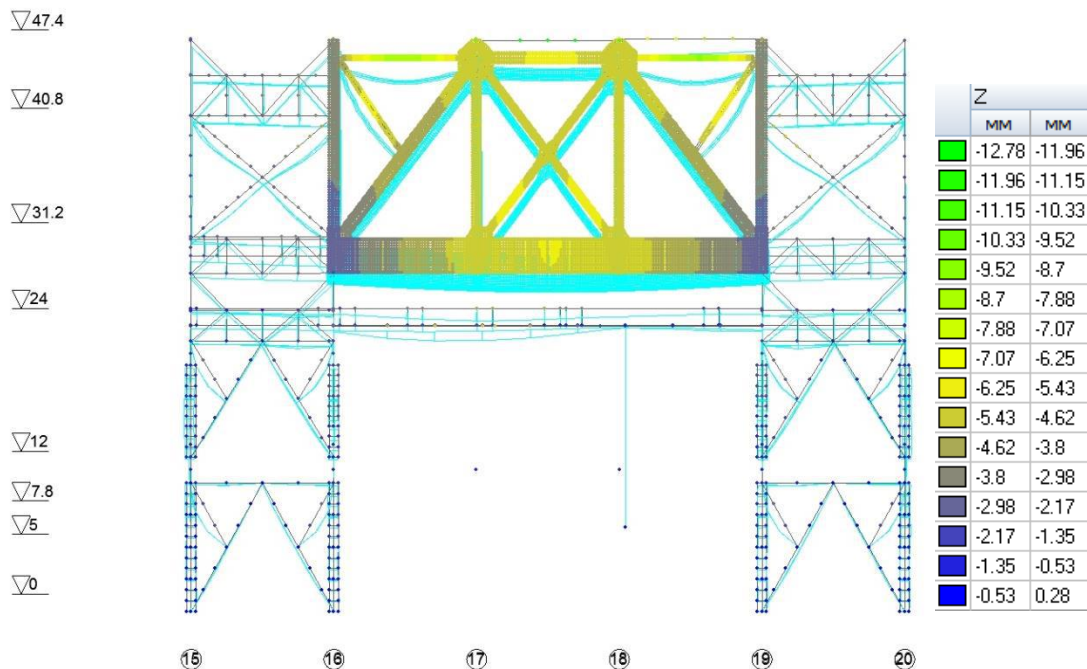


Figure 22. Vertical displacements of structure from dead load (deformed state of structure is shown by blue color)

So, we determined the finite-element model of the truss taking into account its work as the part of framework. This model will be used in further research.

The analyses of stress-strain state of the truss taking into account its current state and defects will be the next stage of the study.

The crane secondary truss is constantly exposed to the cyclic dynamic load from the cranes, which causes the development of fatigue damages in its elements. The lower belt of the truss is the most susceptible to these damages. As it was revealed in the paper [25] the particular attention should be paid to the zones of conjugation of the gussets with the upper flange of the lower belt and its walls with the upper flange at the location of diaphragms.

To analyze the state of the truss and assess the safety of its exploitation, it is necessary to perform a calculation not only for strength, but also for endurance, taking into account the defects already existing defects [18]. The endurance of solid elements (walls, flanges. etc.) is much higher than the endurance of the joint connections of these elements [17].

This is one more reason to model crane secondary truss with the use of shell finite elements, since in this way it is possible to take into account the presence of all gussets and ribs in the joints and most accurately assess their stress-strain state with the subsequent analysis of its endurance.

4. Conclusions

The following conclusions can be made based on the carried out investigations:

1. Analysis of the crane secondary truss should be done with the use of shell finite elements. It is recommended to use finite element mesh with no less than 15 elements along the height of the lower belt of the truss made from thin-walled closed box profile and no less than 4 elements along I-beam flanges. It is advisable to use quadrangular elements with the ratio of sides closed to unity. The use of triangular finite elements is not recommended.

2. Spatial work of the crane secondary truss as a part of full framework should be taken into account. To decrease number of finite elements and time of solving when compiling design scheme it is possible to allocate in the longitudinal direction of the building considered crane secondary truss with the adjacent braced column pitches and in the transverse direction – it is necessary to take into account the structures of adjacent spans.

Reference

1. Yelnov N.A., Kochetova Ye.A. Analiz primeneniya sistem tipa «podkranovo-podstroypilnye fermy» v bolsheproletnykh tsekhakh odnoetazhnykh promyshlennykh zdaniy [Analysis of the application of systems such as "crane-under-trusses" in large-span shops of single-storey industrial buildings]. *Trudy nauchnogo kongressa 14-go rossiyskogo arkhitekturno-stroitel'nogo foruma* [Proceedings of scientific congress of 14th Russian architectural and construction forum]. 2016. Pp. 143–146. (rus)
2. *Rukovodstvo po proektirovaniyu stalnykh podkranovykh konstruktsiy* [Guidelines for the design of steel crane structures]. Moscow.: TsNIIproektstalkingonstruksiya, 1976. 112 p. (rus)
3. Vlasov V.Z. *Tonkostennye uprugie sterzhni* [Thin-walled elastic rods]. Moscow: Fizmatgiz, 1959. 568 p. (rus)
4. Umanskiy A.A. *Kruchenie i izgib tonkostennykh aviakonstruktsiy* [Torsion and bending of thin-walled aircraft constructions]. Moscow: Oborongiz. 1939. 112 p. (rus)
5. Musat S.D., Epureanu B.I. Study of warping torsion of thin-walled beams with closed cross-section using macro-elements. *Communications in Numerical Methods in Engineering*. 1996. Vol. 12. Pp. 873–884.
6. Li L-Y., Easterbrook D. Free torsion of thin-walled structural members of open and closed-sections. *Applied Mathematics and Mechanics*. 2014. Vol. 35. No. 1. Pp. 25–32
7. Chiskis A., Parnes R. On torsion of closed thin-wall members with arbitrary stress-strain laws: a general criterion for cross-sections exhibiting no warping. *Journal of Applied Mechanics*. 2000. Vol. 67. Pp. 460–464.
8. Omidvari A., Hematiyan M. Approximate closed-form formulae for buckling analysis of rectangular tubes under torsion. *International Journal of Engineering*. 2015. Vol. 28. No. 8. Pp. 1226–1232.
9. Srinivasan V., Purushothaman T., Samrat Chatterjee Stress analysis of thin-walled circular and rectangular tubes subjected to torsion. *International Journal of Mechanical Engineering and Technology*. 2017. Vol. 8. No. 8. Pp. 1580–1587.
10. Doostfateme A., Hematiyan M., Arghavan S. Closed-form approximate formulas for torsional analysis of hollow tubes with straight and circular edges. *Journal of Mechanics*. 2009. Vol. 25. No. 4. Pp. 401–409.
11. Mentrasti L. Torsion of closed cross-section thin-walled beams: the influence of shearing strain. *Thin-Walled Structures*. 1987. Vol. 5. No. 4. Pp. 277–305.
12. Mentrasti L. Distortion (and torsion) of rectangular thin-walled beams. *Thin-Walled Structures*. 1990. Vol. 10. No. 3. Pp. 175–193.
13. Kujawa M. Elastic distortional buckling of thin-walled bars of closed quadratic cross-section. *Mechanics and*

Литература

1. Ельников Н.А., Кочетова Е.А. Анализ применения систем типа «подкраново-подстропильные фермы» в большепролетных цехах одноэтажных промышленных зданий // Труды научного конгресса 14-го российского архитектурно-строительного форума. 2016. С. 143–146
2. Руководство по проектированию стальных подкрановых конструкций. М.: ЦНИИпроектстальконструкция, 1976. 112 с.
3. Власов В.З. Тонкостенные упругие стержни. М: Физматгиз, 1959. 568 с.
4. Уманский А.А. Кручение и изгиб тонкостенных авиаконструкций. М.: Оборонгиз. 1939. 112 с.
5. Musat S.D., Epureanu B.I. Study of warping torsion of thin-walled beams with closed cross-section using macro-elements // Communications in Numerical Methods in Engineering. 1996. Vol. 12. Pp. 873–884.
6. Li L-Y., Easterbrook D. Free torsion of thin-walled structural members of open and closed-sections // Applied Mathematics and Mechanics. 2014. Vol. 35. № 1. Pp. 25–32
7. Chiskis A., Parnes R. On torsion of closed thin-wall members with arbitrary stress-strain laws: a general criterion for cross-sections exhibiting no warping // Journal of Applied Mechanics. 2000. Vol. 67. Pp. 460–464.
8. Omidvari A., Hematiyan M. Approximate closed-form formulae for buckling analysis of rectangular tubes under torsion // International Journal of Engineering. 2015. Vol. 28. No. 8. Pp. 1226–1232.
9. Srinivasan V., Purushothaman T., Chatterjee S. Stress analysis of thin-walled circular and rectangular tubes subjected to torsion // International Journal of Mechanical Engineering and Technology. 2017. Vol. 8. № 8. Pp. 1580–1587.
10. Doostfateme A., Hematiyan M., Arghavan S. Closed-form approximate formulas for torsional analysis of hollow tubes with straight and circular edges // Journal of Mechanics. 2009. Vol. 25. No. 4. Pp. 401–409.
11. Mentrasti L. Torsion of closed cross-section thin-walled beams: the influence of shearing strain // Thin-Walled Structures. 1987. Vol. 5. № 4. Pp. 277–305.
12. Mentrasti L. Distortion (and torsion) of rectangular thin-walled beams // Thin-Walled Structures. 1990. Vol. 10. № 3. Pp. 175–193.
13. Kujawa M. Elastic distortional buckling of thin-walled bars of closed quadratic cross-section // Mechanics and Mechanical Engineering. 2013. Vol. 17. № 2. Pp. 119–126.
14. Gonçalves R., Camotim D. Buckling behaviour of thin-walled regular polygonal tubes subjected to bending or torsion // Thin-Walled Structures. 2013. Vol. 73. Pp. 185–197.
15. Туснина А.П. Особенности взаимодействия мембраны,

Туснина О.А. Конечно-элементное моделирование и расчёт подкраново-подстропильной фермы // Инженерно-строительный журнал. 2018. № 1(77). С. 68–89.

- Mechanical Engineering*. 2013. Vol. 17. No. 2. Pp. 119–126.
14. Gonçalves R., Camotim D. Buckling behaviour of thin-walled regular polygonal tubes subjected to bending or torsion. *Thin-Walled Structures*. 2013. Vol. 73. Pp. 185–197.
 15. Tusnina A.R. Osobennosti vzaimodeystviya membrany, prikreplennoy s ekscentrisitetom k opornomu konturu iz zamknutykh tonkostennykh pryamougolnykh profilyey. [Features of interaction of a membrane attached with eccentricity to support contour from closed thin-walled rectangular sections]. *Industrial and Civil Engineering*. 2013. No. 12. Pp. 47–50. (rus)
 16. Eremin K.I., Shulga S.N. Modelirovanie razvitiya ustalostnykh povrezhdeniy v podkranovo-podstropil'nykh fermakh [Simulation of fatigue damages in secondary truss of crane]. *Proceedings of Moscow State University of Civil Engineering*. 2014. No. 2. Pp. 30–38. (rus)
 17. Eremin K.I., Shulga S.N. Napryazhenno-deformirovannoe sostoyanie uzlov podkranovo-podstropilnykh ferm [Stressed-strained state of crane-rafter trusses joints]. *Industrial and Civil Engineering*. 2012. No. 7. Pp. 52–55. (rus)
 18. Shulga S.N. Metodika otsenki zhivuchesti i opredelenie ostatchnogo resursa podkranovo-podstropilnykh ferm s treshchinopodobnymi defektami [Method for assessing survivability and determining the residual resource of cranial-substratum trusses with crack-like defects]. *Science and Safety*. 2014. No. 4(13). Pp. 2–32 (rus)
 19. Eremin K.I., Shulga S.N. Vliyaniye ekscentrisiteta na napryazhenno-deformirovannoe sostoyaniye verkhney zony stenok podkranovo-podstropilnykh ferm [Effect of eccentricity on the stress-strain state of the upper zone of the walls of the cranio-sub-spine trusses]. *Science and Safety*. 2015. No. 5(18). Pp. 49–52 (rus)
 20. Brikkel D.M. Analiz NDS podkranovo-podstropilnoy fermy (PPF) na stadii rosta ustalostnoy treshchiny [Analysis of the stress-strain state of the crane-sub-vertebral truss (PPF) at the stage of fatigue crack growth] *Materialy mezhdunarodnoy nauchno-prakticheskoy konferentsii «Nauka segodnya: zadachi i puti ikh resheniya»* [Proceeding of international scientific and practical conference "Science today: tasks and ways to solve them"]. 2017. Pp. 10–11. (rus)
 21. Shulga S.N. *Ostatochnyy resurs podkranovo-podstropilnykh ferm s nerazreznym nizhnim poyasom na stadii rosta ustalostnoy treshchiny* [Residual resource of craning-under-truss trusses with continuous underside belt at the stage of fatigue crack growth]. Doctoral Thesis 05.23.01. Moscow, 2015. 133 p. (rus)
 22. Brudka Ya., Lubinski M. *Legkie stalnye konstruksii* [Light-weight steel structures]. Moscow: Stroyizdat, 1974. 331 p. (rus)
 23. Bychkov D.V. *Stroitel'naya mekhanika strzhnevyykh tonkostennykh konstruksiy*. Moscow: Gosstroyizdat. 1962. 474 p. (rus)
 24. Tusnina A.R. *Raschet i proektirovanie konstruksiy iz tonkostennykh sterzhney otkrytogo profilya* [Analysis and design of thin-walled structures with open profile]: abstract of Doctoral Thesis 05.23.01. Moscow, 2003. 353 p. (rus)
 25. Eremin K.I., Shulga S.N. Zakonomernost povrezhdeniy podkranovo-podstropilnykh ferm na stadii ekspluatatsii. [Stressed-strained state of crane-rafter trusses joints]. *Industrial and Civil Engineering*. 2013. No. 4. Pp. 34–36. (rus)
 26. Belyayev N.M. *Soprotivleniye materialov*. [Resistance of materials] Moscow: Izdatelstvo «Nauka». 1976. 608 p. (rus)
 - прикрепленной с эксцентриситетом к опорному контуру из замкнутых тонкостенных прямоугольных профилей // *Промышленное и гражданское строительство*. 2013. № 12. С. 47–50.
 16. Еремин К.И., Шульга С.Н. Моделирование развития усталостных повреждений в подкраново-подстропильных фермах // *Вестник МГСУ*. 2014. № 2. С. 30–38.
 17. Еремин К.И., Шульга С.Н. Напряженно-деформированное состояние узлов подкраново-подстропильных ферм // *Промышленное и гражданское строительство*. 2012. № 7. С. 52–55.
 18. Шульга С.Н. Методика оценки живучести и определение остаточного ресурса подкраново-подстропильных ферм с трещиноподобными дефектами // *Наука и безопасность*. 2014. № 4(13). С. 2–32.
 19. Еремин К.И., Шульга С.Н. Влияние эксцентриситета на напряженно-деформированное состояние верхней зоны стенок подкраново-подстропильных ферм // *Наука и безопасность*. 2015. № 5(18). С. 49–52.
 20. Бриккель Д.М. Анализ НДС подкраново-подстропильной фермы (ППФ) на стадии роста усталостной трещины // *Материалы международной научно-практической конференции «Наука сегодня: задачи и пути их решения»*. 2017. С. 10–11.
 21. Шульга С.Н. Остаточный ресурс подкраново-подстропильных ферм с неразрезным нижним поясом на стадии роста усталостной трещины: дис. ... канд. техн. наук 05.23.01. Москва, 2015. 133 с.
 22. Брудка Я., Лубиньски М. *Легкие стальные конструкции*. М.: Стройиздат, 1974. 331 с.
 23. Бычков Д.В. *Строительная механика стржневых тонкостенных конструкций*. М.: Госстройиздат. 1962. 474 с.
 24. Туснина А.Р. Расчет и проектирование конструкций из тонкостенных стержней открытого профиля: автореф. дис. ... д-ра. техн. наук 05.23.01. Москва, 2003. 353 с.
 25. Еремин К.И., Шульга С.Н. Закономерность повреждений подкраново-подстропильных ферм на стадии эксплуатации // *Промышленное и гражданское строительство*. 2013. № 4. С. 34–36.
 26. Беляев Н.М. *Сопrotivление материалов*. М.: Издательство «Наука». 1976. 608 с.

Olga Tusnina,
+7(910)476-16-77; lazoltus@mail.ru

Ольга Александровна Туснина,
+7(910)476-16-77; эл. почта: lazoltus@mail.ru

© Tusnina O.A., 2018

doi: 10.18720/MCE.77.8

Strength of reinforced concrete beams of high-performance concrete and fiber reinforced concrete

Прочность железобетонных балок из высокопрочных бетонов и фибробетонов

V.I. Travush,
GORPROJECT, Moscow, Russia

D.V. Konin,

A.S. Krylov,

JSC Research Center of Construction, Moscow,
Russia

**Д-р техн. наук, профессор главный
конструктор, заместитель генерального
директора по научной работе**

В.И. Травуш,

ЗАО «ГОРПРОЕКТ», г. Москва, Россия

канд. техн. наук, заведующий сектором

Д.В. Конин,

научный сотрудник А.С. Крылов,

АО «Научно-исследовательский центр
«Строительство», г. Москва, Россия

Key words: reinforced concrete; fiber reinforced concrete; crack width; stresses; strain; standard-based calculation; crack resistance; numerical simulation; verification

Ключевые слова: железобетон; фибробетон; ширина раскрытия трещин; напряжения; относительные деформации; расчет по нормам; трещиностойкость; численное моделирование; верификация

Abstract. The strength of reinforced concrete beams made of high-performance concrete and fiber reinforced concrete was evaluated in a pure-bending test. The efficiency of using straight steel fiber in bending structures was evaluated. The fracture pattern of models was described. The results of measuring the vertical displacement and crack width are provided and compared to the rated values. The diagrams of stresses and deformation in reinforcement and concrete of models are presented, and their specific features are noted. The current methods to evaluate reinforced concrete bending structures made of high-performance concrete were evaluated for Groups 1 and 2 limit states. Results were obtained for numerical studies of high-performance concrete. The results necessary to carry out numerical studies in the sphere of high-performance concrete have been obtained.

Аннотация. Выполнена оценка прочности железобетонных балок из высокопрочных бетонов и фибробетонов при испытании на чистый изгиб. Оценена эффективность применения прямой стальной фибры в изгибаемых конструкциях. Описан характер разрушения моделей. Приведены результаты измерений вертикальных перемещений и ширины раскрытия трещин; выполнено сравнение с нормируемыми величинами. Представлены графики напряжений и деформаций в арматуре и бетоне моделей, отмечены их особенности. Дана оценка существующих методик расчета изгибаемых железобетонных конструкций из высокопрочного бетона по первой и второй группе предельных состояний. Получены результаты для проведения численных исследований работы высокопрочных бетонов.

1. Introduction

High-performance concrete that complies with the latest requirements and promotes high-rise construction has been growing increasingly popular in the construction industry. Studies of construction materials with better strength and strain features have been the focus of attention. Studies to develop high-workability and self-compacting mixes for the production of high-performance self-compacting fiber concrete, B100 or higher compression strength [1], have been recently completed. The efficiency of such material in eccentric compression structures [2] has been evaluated, the specific features of such concrete performance at the steel-concrete contact surface [3] have been assessed. The workability of the material described in [1] and its higher strength and strain features contribute to its increasing use in cast-in-place construction including floor beams. Our study is dedicated to these issues. The efficiency of the developed concrete mix in bending structures is not studied enough. This shows the actuality of the issues under consideration and of the tests conducted. In preparation for the experiment, publications on

the improvement of the theoretical foundations of reinforced concrete structures [4, 5, 12, 13, 17] and fiber-reinforced concrete [9] were studied. Special attention was paid to research in the field of contact interaction of steel and concrete [8, 10, 15, 16]. Issues of numerical modeling of reinforced concrete structures [6, 14] and cracking [7, 11] were considered.

The aim of the study is to obtain experimental data that will form a basis for numerical studies using of ANSYS models in strength calculation and in contact interaction tasks.

Objectives of the study:

- perform tests of 15 models of beams made of high-performance concrete and fiber reinforced concrete;
- to evaluate the existing methods of calculation of reinforced concrete structures at the ultimate limit state (ULS) and the service limit state (SLS) for high-performance concrete;
- to identify the characteristics of fracture, the nature of the formation and cracks propagation;
- to assess the effectiveness of the application in bending structures of 13 mm straight profile steel fiber.

Three models of high-performance concrete and twelve models of high-performance fiber concrete were tested during this research work. The models were constructed by rectangular cross-section, 200 x 150 mm, length 1.5 m. A detailed description of the models is contained in [18]. Table 1 contains the basic parameters of the models.

Table 1. Characteristics of models

Group of models	Quantity of models in a group	Material of models	Concrete compressive strength class	Fiber reinforcement factor by volume μ_{fv}	μ , % reinforcement ratio	Cross-section
B1	3	concrete	B90	-	1.9	<p>Fig. 1. Cross-section of models, Groups B1, B2, and B7</p>
B2	3	fiber reinforced concrete	B130	0.023		
B7	3	fiber reinforced concrete	B100	0.023		
B3	3	fiber reinforced concrete	B130	0.023	-	<p>Fig. 2. Cross-section of models, Groups B3 and B8</p>
B8	3	fiber reinforced concrete	B100	0.023		

2. Methods

Restrictive strain sensors were installed, as follows, to describe the relative strain pattern in the experiment: 1 piece at each reinforcement beam in the beam span middles, and 1 to 3 pieces at upper and lower edges of the concrete surface in the pure bending zone (Fig. 3). The sensor layout is shown in Figure 4.

All models were tested for pure bending (Fig. 5). Model supports were hinged. The force distribution between two points was ensured by a steel I-shaped cross arm.



Figure 3. Surface cleaning, installation of strainsensors and epoxy resin protection

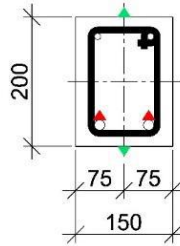


Figure 4. Layout of sensors

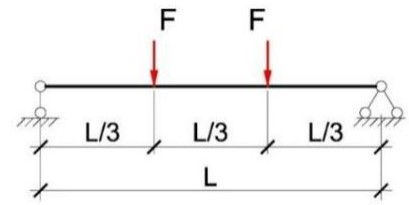


Figure 5. Model load application diagram

3. Results and Discussion

The concrete strength properties were monitored at 28 days and at the model test time; for this purpose 3 samples of 10 cm side cubes were prepared for each concrete batch. The results of cube testing according to [19] are presented in Table 2.

Table 2. Results of cube sample testing

Group of models	Cube concrete compression strength at 28 days, MPa	Cube concrete compression strength at test time, MPa
Б1	103.6	112.8
Б2	152.4	158.6
Б7	112.4	114.0
Б3	149.6	157.4
Б8	119.2	123.0

All models were tested according to provisions of standard [20]. The sequence of completed tests is described in [18].

The ultimate bending moments were calculated when preparing for testing according to [21–24]. The results of calculations and actual ultimate moments corresponding to the breaking load are shown in Table 3: Column 3 contains experimental ultimate moments, Column 4 contains theoretical values according to [21, 23], and Column 6 contains theoretical values according to [22].

A property of steel fibre concrete residual strength R_{fbt2} , R_{fbt3} has been added to the Document [22], which is being developed. No experimental data according to that property are available for the discussed material. The value of R_{fbt3} in our case was roughly obtained on the basis of the results of model tests, Groups B3 and B8, which have only dispersal reinforcement. Using the formula (6.3, 6.4) [22] we get:

$$M_{ult} = 0.5R_{fb} \cdot b \cdot x \cdot h \quad (1)$$

$$x = \frac{R_{fbt3} \cdot h}{R_{fbt3} + R_{fb}} \quad (2)$$

By plugging (2) in (1) and having the value of ultimate bending moment based on the M_{ult} experiment results, we find the R_{fbt3} value. It is noteworthy, that the R_{fbt3} value can differ from the value which is found using the method described in Appendix B [22]. The calculated R_{fbt3} values can be used in determining the beam strength, Groups B2 and B7.

Table 3. Ultimate bending moments

No.	Group of models	$M_{break, exper}$ (averaged for a group)	For models of high-performance concrete – according to [23] For models of high-performance fiber concrete – according to [21]		For models of high-performance fiber concrete – according to [22]	
			$M_{theoretical, ultimate}$	Deviation from experiment (averaged for a group)	$M_{theoretical, ultimate}$	Deviation from experiment (averaged for a group)
		kNm	kNm	%	kNm	%
1	2	3	4	5	6	7
1	B1	53.57	49.11	8.3	-	-
2	B2	63.27	62.72	0.5	56.99	9.6
3	B3	19.20	25.65	-34.1	-	-
4	B7	52.84	60.59	-14.8	50.56	4.2
5	B8	13.26	25.23	-90.4	-	-

It is apparent from Table 3 that the best convergence of theoretical calculations and experimental data was achieved for models implemented using reinforcement bars (both according to the current [21, 23] and developing standards [22]). The maximum deviation was noted in calculation according to [21] for beams with only dispersed reinforcement. The probable reason could be the use of a relatively short fiber of 13 mm, straight section, whereas the corrugated or hooked-end fiber is recommended for use in bending structures. The prestressing of fiber concrete implemented for models B7 and B8 produced no positive effect on the load-bearing capacity of those models. Therefore, the discussed fiber type (13 mm straight profile steel fiber) does not contribute significantly to the bearing capacity of bending elements. It is noteworthy that the use of ratios [22] in calculations provides for some reserve of structure bearing capacity (up to 9.6 %), whereas the ratios [21] produce results exceeding the experimental data, which is not permissible for real structures.

The pattern of crack width and distribution for each load step was registered in the experiment. The control loads to check the crack width values were found by [20]. The conditionally calculated loads were found at models by dividing the ultimate breaking loads by the safety factor (according to the terms of Russian State Standard GOST 8829-94). The nominal loads for calculating the second limit state were accepted to be conditionally equal to 0.8 of the calculated values.

As per Russian Set of Construction Rules SP 63.13330.2012 [23], the calculations for cracking that are normal to direct axis in bending structures should be made subject to:

$$M > M_{crc} \quad (3)$$

where M is the bending moment from an external load relative to the axis normal to the plane of moment action and passing through the center of gravity of the reduced cross section of a structure;

M_{crc} is the bending moment perceived by the normal section of a structure in cracking.

At this stage, the outdated (inoperative) nominal documents, the valid documents and those being developed as applicable to structures made of high-performance concrete were compared in calculation for the service limit state (SLS) (according to the crack width value). For models with reinforcement bars B1 the calculations were made according to Russian Set of Construction Rules SP 63.13330.2012 [23] using the formula (8.128):

$$a_{crc,i} = \varphi_1 \varphi_2 \varphi_3 \psi_s \frac{\sigma_s}{E_s} l_s, \quad (4)$$

where σ_s is stress in tension reinforcement with normal section with cracking;

l_s – base distance between adjacent normal cracks;

ψ_s – a coefficient to account for a non-uniform distribution of strains of tension reinforcement between cracks;

φ_1 – a coefficient to account for load time;

φ_2 – a coefficient to account for a longitudinal reinforcement profile;

φ_3 – a coefficient to account for a loading condition;

E_s – reinforcement elasticity module.

Also as per Russian Construction Norms and Rules SNiP 2.03.01-84* [24] using the formula (144):

$$a_T = \delta \varphi_l \eta \frac{\sigma_s}{E_s} 20(3,5 - 100\mu)^3 \sqrt{d} \quad (5)$$

where δ is a coefficient to account for a loading condition;

φ_l – is a coefficient to account for load time;

η – is a coefficient to account for a longitudinal reinforcement profile;

σ_s – stresses in bars of the end reinforcement row;

μ – is a coefficient to account for reinforcement section;

d – reinforcement diameter, mm;

E_s – reinforcement elasticity module.

For models with fiber concrete (B2, B7) the crack width value was found as per Russian Set of Construction Rules SP 52-104-2006* [21] using the formula (7.17*) and according [22] using the formula (6.115).

The crack width value and loads at which it could be controlled are shown in Table 4: Column 4 – crack width found by [22, 23], Column 5 – crack width found by [21, 24], Column 6 – experimental values.

Table 4. Crack width

Group of models	Concrete of models	Control load, kN	Crack width, m $\times 10^{-3}$				
			Theoretical		Experimental	Deviation from experimental data, %	
			For models of high-performance concrete - according to [23]	For models of high-performance concrete - according to [24]		For models of high-performance concrete - according to [23]	For models of high-performance concrete - according to [24]
			For models of high-performance fiber concrete - according to [22]	For models of high-performance fiber concrete - according to [21]		For models of high-performance fiber concrete - according to [22]	For models of high-performance fiber concrete - according to [21]
1	2	3	4	5	6	7	8
B1	concrete, B90	141.8	0.307	0.269	0.370	16.9	27.3
B2	fiber-concrete, B130	167.5	0.247	0.143	0.187	-32.2	23.4
B7	fiber-concrete, B100	139.9	0.259	0.120	0.198	-30.8	39.5

The values of crack width (both theoretical and actual), which are shown in Table 4, do not exceed the permissible crack width subject to reinforcement safety $a_{crc,ult} = 0.4$ mm, as envisaged by Para 8.2.6 [23] in short-term fracture opening. However, significant deviations of theoretical values from the actual crack width were revealed. The difference in values reaches 40%. The error in calculation according to actual Russian Set of Construction Rules SP 63.13330.2012 [23] is essentially lower vs that envisaged by the previous Russian Set of Construction Rules SP 2.03.01-84* [24]. For models with fiber concrete the calculations according to the document [22], which is being currently developed, provide for some reserve: up to 32 % for models B2 and up to 31 % for models B7 implemented with self-stress. The results of calculation according to [21] are lower vs the experimental data by 23 % and 40 % for Groups of models B2 and B7, respectively.

The fracture process of models in all groups was characterized by the emergence of many vertical and inclined cracks. The time of cracking was registered at the values of 20 %, 27 %, and 26 % of the breaking load for groups of models B1, B2 and B7, respectively. Therefore, the models with fiber concrete have a somewhat higher crack resistance vs the models of high-performance concrete without fiber.

The high-performance models in Group B1 collapsed due to concrete chips in the compressed area (Fig. 6a); the high-performance fiber concrete models in Group B2 collapsed due to tension reinforcement breakage (Fig. 6b); the high-performance fiber concrete models with self-stress in Group B7 broke due to concrete collapsing in the compressed area but without reinforcement rupture or concrete chips (Fig. 6c). In all cases of collapse the tension values in tension reinforcement reached the yield stress.



Figure 6a. Typical collapse in models of Group B1



Figure 6c. Typical collapse in models of Group B7



Figure 6b. Typical collapse in models of Group B2



On the basis of test results diagrams of vertical displacement for on-load models were constructed (Fig. 7), additionally, diagrams to illustrate the fracture opening width were constructed for each load step (Fig. 8).

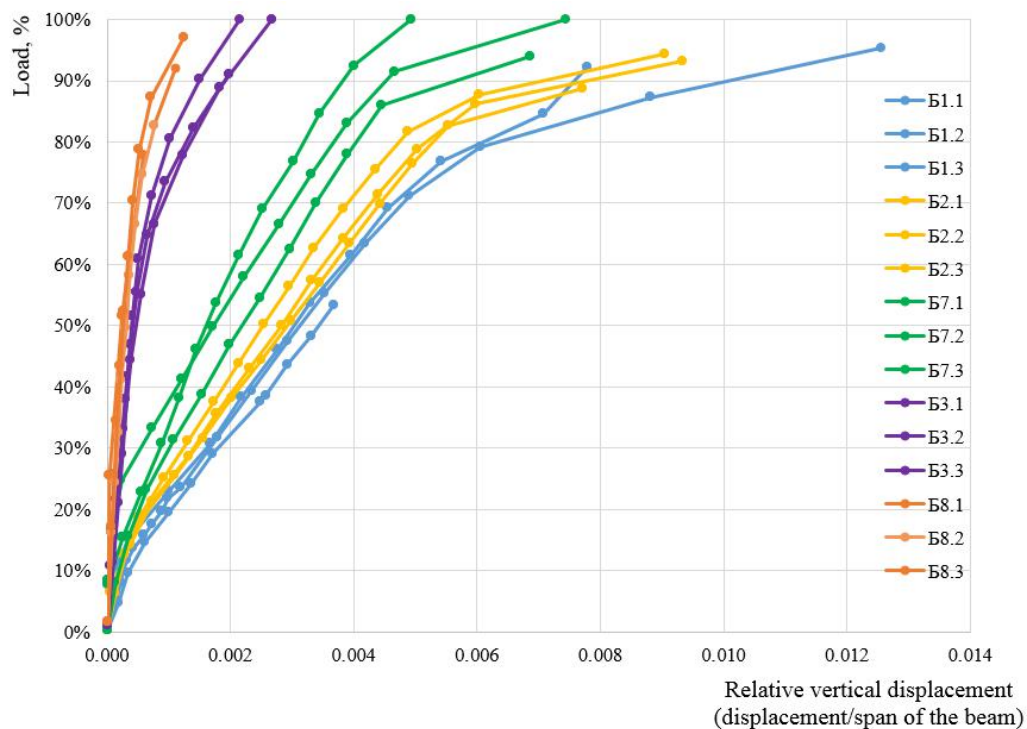


Figure 7. Vertical displacement of models B1, B2, and B7 by load steps

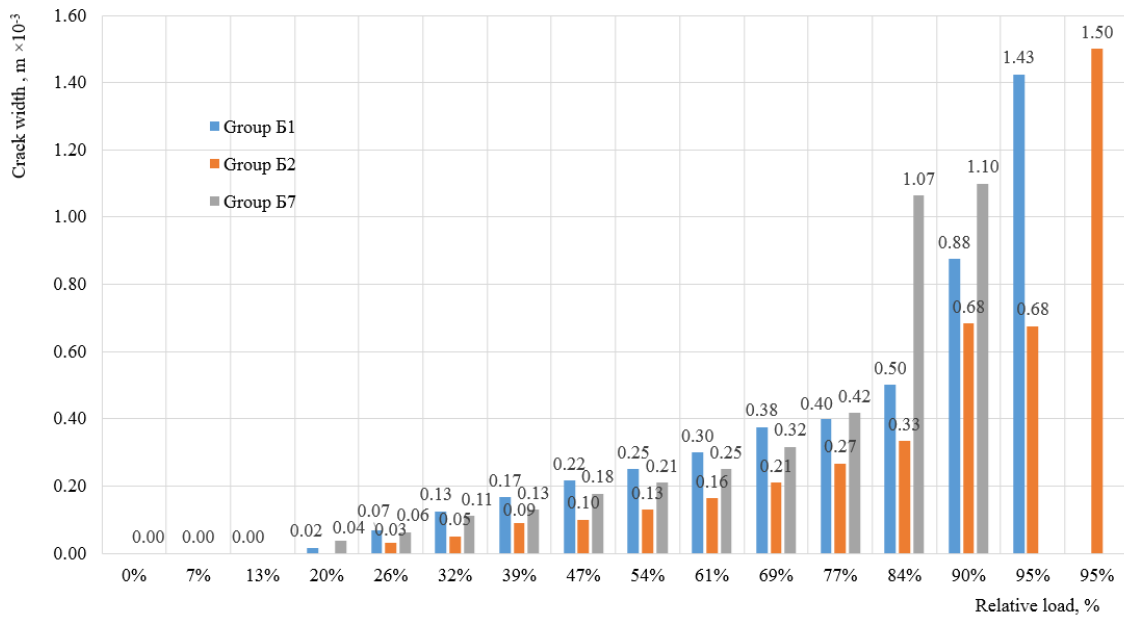


Figure 8. Fracture opening width in models B1, B2, and B7 by load steps

The maximum model displacement values at collapse time are shown in Table 5. The maximum vertical displacement values were registered for models of Group B1, i.e., 14.28 mm, which is 1/98 of the beam span value. Low vertical displacement values are typical of models with dispersed reinforcement only.

Table 5. Maximum model displacements

Group of models	Displacement, m × 10 ⁻³	Displacement in relation to beam span
B1	14.28	L/98
B2	12.48	L/112
B7	9.11	L/154
B3	3.19	L/438
B8	1.66	L/846

On the basis of interpretation of tension sensor readings diagrams for tension and deformation occurring in bar reinforcement and concrete of models were constructed; dependences are shown in Figures 9, 10.

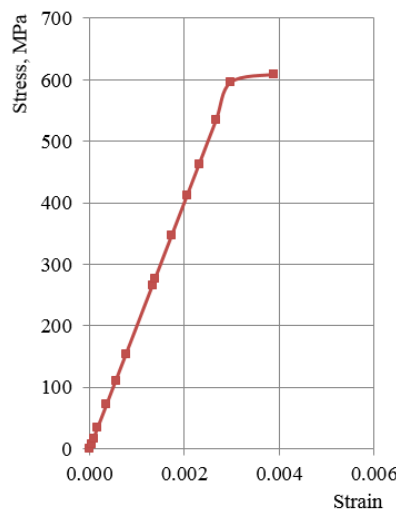


Figure 9. Dependence of tension on relative deformation for rod reinforcement, Group B1 models

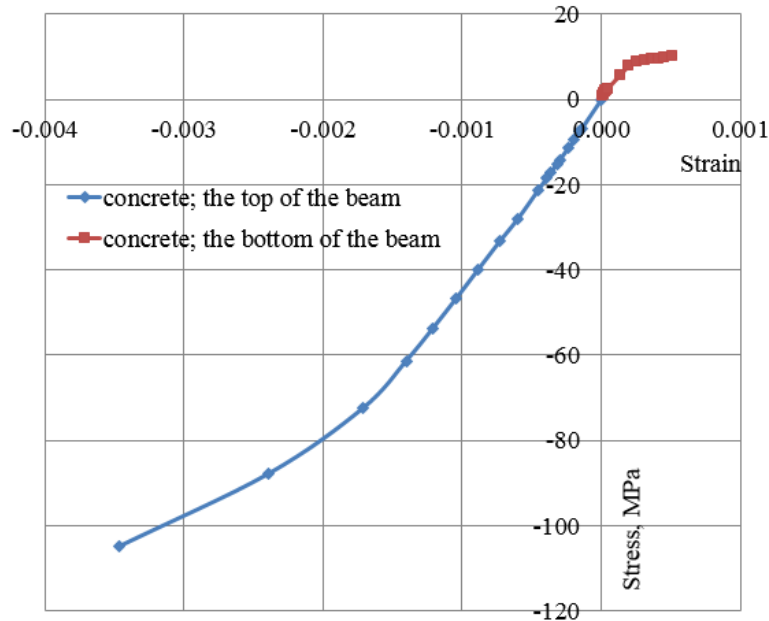


Figure 10. Dependence of tension on relative deformation for concrete, Group B1 models

Figure 9 shows distinctly the yield strength ranging from 600 to 620 MPa, which fully coincides with the results of testing the reinforcement bar samples for tension – 616 MPa. The experimentally obtained values of strains (Fig. 10) for bar reinforcement models B1, B2 and B7 somewhat exceed the values rated in [23] and presented in [25, 26]. This is explained by the uniform stressed state of concrete which is due to lateral and transverse reinforcement. The experimentally obtained limit tensile strength values (Fig. 10) exceed also the values specified in [23]. This is due to many cracks in the concrete tension area, some of which are covered by the tension sensor measuring surface.

The comparison of the obtained values of unit strains at the time of model collapses and of the values specified in [21–23, 25–26] is shown in Table 6.

Table 6. Limit unit strains of concrete models

Group of models	Experiment (averaged for a group)		Standardised according to [21, 22, 23]		Eurocode	Experimentally obtained according to [25, 26]		APOD from [21, 22, 23]	APOD from [25, 26]
	Compression	Tension	Compression	Tension		Compression	Tension	Compression	Compression
B1	0.00343	0.00216	0.00297	0.00015	0.0026	0.00254	0.00048	-15.5	-34.9
B2	0.00288	0.00331	0.00262	0.00015- for concrete matrix (0.01- 0.02 * – for concrete)	0.0026	0.00327	0.00300	-10.0	11.8
B7	0.00286	0.00232	0.00280		0.0026	0.00327	0.00300	-2.3	12.3
B3	0.00087	0.00256	0.00262		0.0026	0.00327	0.00300	66.9	73.5
B8	0.00057	0.00286	0.00280		0.0026	0.00327	0.00300	79.8	82.7
* - the value needs to be refined in testing the residual strength of fiber concrete to axial tension									

4. Conclusions

1. A series of works has been completed to study the workability of steel fiber concrete using a 13 mm straight profile steel fiber in bending structures. Nine models with reinforcement bars and 6 high-performance and fiber concrete models with dispersed reinforcement (including self-tension), B90...B130 compression breaking strength, were tested.

2. The ultimate limit state (ULS) of high-performance and fiber concrete structures with reinforcement bars is satisfactorily described by the calculation procedures presented in Construction

Rules – the difference between theoretical and experimental values does not exceed 10 %.

3. The calculation procedures for reinforced structures for the service limit state (SLS) (which is a basis for several normative documents) have been compared. The theoretical results differ from the experimental data up to 40 %.

The results of calculations of crack width according to the methods envisaged by Russian Set of Construction Rules SP XXX (draft) “Steel fibre concrete structures. The rules of design” and SP 63.13330.2012 “Concrete and reinforced concrete structures” are more consistent with the experimental data versus the calculation results according to Construction Rules SP 52-104-2006* “Steel fibre concrete structures” and SNiP 2.03.01-84* “Concrete and reinforced concrete structures”.

4. The fracture process of models in all groups was characterized by emergence of many vertical and inclined cracks. The moment of cracking was registered at the values of 20 %, 27 %, and 26 % of the breaking load for Groups of models B1, B2 and B7, respectively. Models of high-performance fiber concrete had a somewhat higher crack resistance versus the models of high-performance concrete.

The fracture pattern of reinforcement models: the high-performance models collapsed due to concrete chips in the compressed area; the high-performance fiber concrete models collapsed due to tension reinforcement breakage; the high-performance fiber concrete models with self-stress broke due to concrete collapsing in the compressed area but without reinforcement rupture or concrete chips.

The modes with dispersed reinforcement only collapsed abruptly and almost without any cracking.

5. The experimentally obtained values of strains for reinforcement models somewhat exceed the values rated in Construction Rules. This is explained by the uniform stressed state of concrete which is due to lateral and transverse reinforcement. The experimentally obtained limit tensile strength values exceed also the values specified in Construction Rules. This is due to many cracks in the concrete tension area, some of which are covered by the tension sensor measuring surface.

6. The analysis of on-load models and of fracture opening width by load steps showed no abrupt variations or difference for bar-reinforced beams. The cracks emerged and quickly opened just ahead of collapse in models with dispersed reinforcement only.

7. Summarizing the results of testing the dispersed reinforcement models (13 mm straight profile steel fiber), it can be concluded that the use of such fiber is not very effective in terms of the bearing capacity of bending elements. Other types of fiber (corrugated or hooked-end) should be used for the purpose. However, the main advantages of the used material would be wasted in such case, i.e., high workability (flow class, within the range of 70–75 cm) and a higher cohesion or non-segregation [1], which allow for classifying the material as belonging to the self-compacting category.

Having said that, the use of steel fiber concrete discussed in the study reduces the cracking width versus similar high-performance concrete structures by 1.5 – 2 times, which is necessary in some construction industry activities.

Reference

1. Kapriyelov S.S., Chilin I.A. Sverkhvysokoprochnyy samouplotnyayushchiysya fibrobeton dlya monolitnykh konstruktsiy [Ultra-high-strength self-compacting fiber concrete for monolithic constructions]. *Building materials*. 2013. No. 7. Pp. 28–30. (rus)
2. Travush V.I., Konin D.V., Rozhkova L.S., Krylov A.S., Kapriyelov S.S., Chilin I.A., Martirosyan A.S., Fimkin A.I. Eksperimentalnyye issledovaniya stalezhelezobetonnykh konstruktsiy, rabotayushchikh na vnetsentrennoye szhatiye [Experimental study of composite structures, working for eccentric compression]. *Academia. Architecture and Construction*. 2016. No. 3. Pp. 127–135. (rus)
3. Travush V.I., Kapriyelov S.S., Konin D.V., Krylov A.S., Kashaeva G.G., Chilin I.A. Opredeleniye nesushchey sposobnosti na sdvig kontaktnoy poverkhnosti «stal-beton» v stalezhelezobetonnykh konstruktsiyakh dlya betonov razlichnoy prochnosti na szhatiye i fibrobetona [Determination of the bearing capacity in shear on the contact surface "steel-concrete" of steel-concrete structures for concretes of different compressive strength and fiber reinforced concrete]. *Building and Reconstruction*. 2016. No. 4(66). Pp. 45–55. (rus)
4. Krylov S.B., Arlenin P.D. Inzhenernyy podkhod k resheniyu zadachi ob izgibe uprugopolzuchego sterzhnya [The engineering approach to solving the problem of bending of elastic-creeping rod]. *Structural Mechanics and Analysis of Constructions*. 2013. No. 2(247). Pp. 6–9. (rus)
5. Krylov S.B., Arlenin P.D. Uravneniye izgiba sterzhnya pri

Литература

1. Каприелов С.С., Чилин И.А. Сверхвысокопрочный самоуплотняющийся фибробетон для монолитных конструкций // Строительные материалы. 2013. № 7. С. 28–30.
2. Травуш В.И., Конин Д.В., Рожкова Л.С., Крылов А.С., Каприелов С.С., Чилин И.А., Мартиросян А.С., Фимкин А.И. Экспериментальные исследования сталежелезобетонных конструкций, работающих на внецентренное сжатие // Academia. Архитектура и строительство. 2016. № 3. С. 127–135.
3. Травуш В.И., Каприелов С.С., Конин Д.В., Крылов А.С., Кашеярова Г.Г., Чилин И.А. Определение несущей способности на сдвиг контактной поверхности «сталь-бетон» в сталежелезобетонных конструкциях для бетонов различной прочности на сжатие и фибробетона // Строительство и реконструкция. 2016. № 4(66). С. 45–55.
4. Крылов С.Б., Арленинов П.Д. Инженерный подход к решению задачи об изгибе упруго-ползучего стержня // Строительная механика и расчет сооружений. 2013. № 2(247). С. 6–9.
5. Крылов С.Б., Арленинов П.Д. Уравнение изгиба стержня при кусочно-линейном законе деформирования ползучего материала // Строительная механика и расчет сооружений. 2013. № 3(248). С. 9–11.
6. Lubliner, J., Oliver J., Oller S., Onate E. A. Plastic-damage

Травуш В.И., Конин Д.В., Крылов А.С. Прочность железобетонных балок из высокопрочных бетонов и фибробетонов // Инженерно-строительный журнал. 2018. № 1(77). С. 90–100.

- kusochno-lineynom zakone deformirovaniya polzuchego materiala [The equation of bending of a rod with a piecewise-linear law of deformation of the creeping material]. *Structural Mechanics and Analysis of Constructions*. 2013. No. 3(248). Pp. 9–11. (rus)
6. Lubliner J., Oliver J., Oller S., Onate E. A. Plastic-damage model for concrete. *International Journal of Solids and Structures*. 1989. Vol. 25. No. 3. Pp. 229–326.
 7. Mazars J. A description of micro- and macro-scale damage of concrete structures. *Engineering Fracture Mechanics*. 1986. Vol. 25. No. 5/6. Pp. 729–737.
 8. Willam K.J., Warnke E.D. Constitutive model for the triaxial behavior of concrete. *Proceedings, International Association for Bridge and Structural Engineering*. Zurich, 1975. Report 19. Section III. 30 p.
 9. Gribniak V., Kaklauskas G., Hung Kwan A.K., Bacinskas D., Ulbinas D. Deriving stress-strain relationships for steel fibre concrete in tension from tests of beams with ordinary reinforcement. *Engineering Structures*. 2012. Vol. 42. Pp. 387–395.
 10. Torre-Casanova A., Jason L., Davenne L., Pinelli X. Confinement effects on the steel-concrete bond strength and pull-out failure. *Engineering Fracture Mechanics*. 2013. Vol. 97. Pp. 92–104.
 11. Travush V.I., Kashevarova G.G., Martirosyan A.S., Avhacheva I.A. Experimental study of possible ways to increase cohesion strength in the “steel-concrete” contact zone under displacement conditions. *Procedia Engineering*. 2016. Vol. 153. Pp. 766–772.
 12. Shima H., Chou L.-L., Okamura H. Micro and Macro models for bond in reinforced concrete. *Journal of the Faculty of Engineering: University of Tokyo*. 1987. Vol. XXXIX. No. 2. Pp. 133–194.
 13. Smith F., Brown R. The shearing strength of concrete. *Bull. Univ. of Washington*. 2001. No. 106. 205 p.
 14. Арленинов П.Д., Крылов С.Б. Современное состояние нелинейных расчетов железобетонных конструкций // Сейсмостойкое строительство. Безопасность сооружений. 2017. № 3. С. 50–53.
 15. Schnobrich W.C., Suidan M. Finite element analysis of reinforced concrete // *ASCE Journal of the Structural Division*. 1973. October. ST10. Pp. 2109–2122.
 16. Broms B.B. Stress distribution in reinforced concrete members with tension cracks // *JACI*. 1965. Vol. 62. № 9.
 17. Goto Y. Cracks formed in concrete around deformed tension bars // *Journal of the American Concrete Institute*. 1971. Vol. 68. № 4. Pp. 244–251.
 18. Travush V.I., Konin D.V., Krylov A.S., Kapriyelov S.S., Chilin I.A. Eksperimentalnyye issledovaniya stalezhelezobetonnykh konstruksiy, rabotayushchikh na izgib [Experimental study of composite structures for bending elements]. *Building and Reconstruction*. 2017. No. 4(72). Pp. 63–71. (rus)
 19. *Russian State Standard GOST 10180-2012*. Concretes. Methods for determining the strength of control samples. Moscow. 2013. 30 p.
 20. *Russian State Standard GOST 8829-94*. Product construction of concrete and reinforced concrete prefabrication. Test methods the loading. Rules for the evaluation of strength, stiffness and crack resistance. Moscow. 1994. 27 p.
 21. *Russian Set of Rules SP 52-104-2006**. Steel fibre concrete structures. Moscow. 2010.
 22. *Russian Set of Rules SP XXX (draft)*. Steel fibre concrete structures. The rules of design. First edition.
 23. *Russian Set of Rules SP 63.13330.2012*. Concrete and reinforced concrete structures. The updated edition of SNIP 52-01-2003. Moscow. 2012.
 24. *Russian Construction Norms and Rules SNiP 2.03.01-84**. model for concrete // *International Journal of Solids and Structures*. 1989. Vol. 25. № 3. Pp. 229–326.
 7. Mazars J. A description of micro- and macro-scale damage of concrete structures // *Engineering Fracture Mechanics*. 1986. Vol. 25. № 5/6. Pp. 729–737.
 8. Willam K.J., Warnke E.D. Constitutive model for the triaxial behavior of concrete // *Proceedings, International Association for Bridge and Structural Engineering*. Zurich, 1975. Report 19. Section III. 30 p.
 9. Gribniak V., Kaklauskas G., Hung Kwan A.K., Bacinskas D., Ulbinas D. Deriving stress-strain relationships for steel fibre concrete in tension from tests of beams with ordinary reinforcement // *Engineering Structures*. 2012. Vol. 42. Pp. 387–395.
 10. Torre-Casanova A., Jason L., Davenne L., Pinelli X. Confinement effects on the steel-concrete bond strength and pull-out failure // *Engineering Fracture Mechanics*. 2013. Vol. 97. Pp. 92–104.
 11. Travush V.I., Kashevarova G.G., Martirosyan A.S., Avhacheva I.A. Experimental study of possible ways to increase cohesion strength in the “steel-concrete” contact zone under displacement conditions // *Procedia Engineering*. 2016. Vol. 153. Pp. 766–772.
 12. Shima H., Chou L.-L., Okamura H. Micro and Macro models for bond in reinforced concrete // *Journal of the Faculty of Engineering: University of Tokyo*. 1987. Vol. XXXIX. № 2. Pp. 133–194.
 13. Smith F., Brown R. The shearing strength of concrete // *Bull. Univ. of Washington*. 2001. № 106. 205 p.
 14. Арленинов П.Д., Крылов С.Б. Современное состояние нелинейных расчетов железобетонных конструкций // Сейсмостойкое строительство. Безопасность сооружений. 2017. № 3. С. 50–53.
 15. Schnobrich W.C., Suidan M. Finite element analysis of reinforced concrete // *ASCE Journal of the Structural Division*. 1973. October. ST10. Pp. 2109–2122.
 16. Broms B.B. Stress distribution in reinforced concrete members with tension cracks // *JACI*. 1965. Vol. 62. № 9.
 17. Goto Y. Cracks formed in concrete around deformed tension bars // *Journal of the American Concrete Institute*. 1971. Vol. 68. № 4. Pp. 244–251.
 18. Травуш В.И., Конин Д.В., Крылов А.С., Каприелов С.С., Чилин И.А. Экспериментальные исследования сталежелезобетонных конструкций, работающих на изгиб // *Строительство и реконструкция*. 2017. № 4(72). С. 63–71.
 19. ГОСТ 10180-2012. Бетоны. Методы определения прочности по контрольным образцам. М.: Стандартинформ, 2013. 30 с.
 20. ГОСТ 8829-94. Изделия строительные железобетонные и бетонные заводского изготовления. Методы испытаний нагружением. Правила оценки прочности, жесткости и трещиностойкости. М.: МНТКС, 1994. 27 с.
 21. СП 52-104-2006*. Сталефибробетонные конструкции. М.: Минстрой России, 2010.
 22. СП XXX (проект). Конструкции сталефибробетонные. Правила проектирования. Первая редакция.
 23. СП 63.13330.2012. Бетонные и железобетонные конструкции. Актуализированная редакция СНиП 52-01-2003. М.: Минстрой России, 2012.
 24. СНиП 2.03.01-84*. Бетонные и железобетонные конструкции. М.: Госстрой СССР, 1989.
 25. Ромкин Д.С. Влияние возраста высокопрочного бетона на его физико-механические и реологические свойства: дис.... канд. техн. наук: 05.23.01. Москва, 2007. 140 с.
 26. Мишина А.В. Влияние возраста высокопрочного сталефибробетона на его физико-механические и реологические свойства: дис.... канд. техн. наук: 05.23.01. Москва, 2013. 149 с.

Travush V.I., Konin D.V., Krylov A.S. Strength of reinforced concrete beams of high-performance concrete and fiber reinforced concrete. *Magazine of Civil Engineering*. 2018. No. 1. Pp. 90–100. doi: 10.18720/MCE.77.8.

Concrete and reinforced concrete structures. Moscow. 1989.

25. Romkin D.S. *Vliyaniye vozrasta vysokoprochnogo betona na yego fiziko-mekhanicheskiye i reologicheskiye svoystva* [The Influence of age high-strength concrete on the physical, mechanical and rheological properties]. PhD Thesis. (Engineering). Moscow. 2007. 139 p. (rus)
26. Mishina A.V. *Vliyaniye vozrasta vysokoprochnogo stalefibrobetona na yego fiziko-mekhanicheskiye i reologicheskiye svoystva* [The Influence of age high-strength fiber concrete on the physical, mechanical and rheological properties]. PhD Thesis. (Engineering). Moscow. 2013. 149 p. (rus)

Vladimir Travush,
+7(495)775-75-65; *travush@mail.ru*
Denis Konin,
+7(926)853-99-73; *konden@inbox.ru*
Alexey Krylov,
+7(919)723-05-71; *kryl07@mail.ru*

Владимир Ильич Травуш,
+7(495)775-75-65; эл. почта: *travush@mail.ru*
Денис Владимирович Конин,
+7(926)853-99-73; эл. почта: *konden@inbox.ru*
Алексей Сергеевич Крылов,
+7(919)723-05-71; эл. почта: *kryl07@mail.ru*

© Travush V.I., Konin D.V., Krylov A.S., 2018

doi: 10.18720/MCE.77.9

Strength parameters of earth dams under various dynamic effects

Прочностные параметры грунтовых плотин при различных динамических воздействиях

**M.M. Mirsaidov,
T.Z. Sultanov,**

*Tashkent Institute of Irrigation and Agricultural
Mechanization Engineers, Tashkent, Uzbekistan*

R.A. Abdikarimov,

*Tashkent Financial Institute, Tashkent,
Uzbekistan*

A.N. Ishmatov,

B.Sh. Yuldoshev,

E.S. Toshmatov,

D.P. Jurayev,

*Tashkent Institute of Irrigation and Agricultural
Mechanization Engineers, Tashkent, Uzbekistan*

**Д-р техн. наук, заведующий кафедрой
М.М. Мирсаидов,**

**д-р техн. наук, проректор по научной
работе Т.З. Султанов,**

*Ташкентский институт инженеров
ирригации и механизации сельского
хозяйства, г.Ташкент, Узбекистан*

д-р физ.-мат. наук, профессор

Р.А. Абдикаримов,

*Ташкентский финансовый институт,
г. Ташкент, Узбекистан*

канд. техн. наук, доцент А.Н. Ишматов,

старший преподаватель Б.Ш. Юлдошев,

ассистент Э.С. Тошматов,

магистрант Д.П. Жураев,

*Ташкентский институт инженеров
ирригации и механизации сельского
хозяйства, г.Ташкент, Узбекистан*

Key words: earth dam; eigenmode; strength; viscoelasticity; dissipative properties; amplitude-frequency characteristics; resonant mode

Ключевые слова: грунтовая плотина; собственная форма; прочность; вязкоупругость; диссипативные свойства; амплитудно-частотные характеристики; резонансный режим

Abstract. The paper provides the methods for evaluating the strength parameters of earth dams under forced oscillations. The methods of solving the problem are based on the expansion of sought for solution in terms of eigenmodes of elastic structure oscillations. Linear steady-state and unsteady forced oscillations of three different earth dams were studied with account of structural heterogeneity and viscoelastic properties of structure material under various dynamic effects. To describe the viscoelastic properties, the Boltzmann-Volterra hereditary theory of viscoelasticity is used. The results of investigations made it possible to reveal a number of effects that arise under forced oscillations in a dam in the pre-resonant, resonant, and post-resonant modes of oscillations.

Аннотация. В статье приводится методика для оценки прочностных параметров грунтовых плотин при вынужденных колебаниях. Методика решения задачи основана на разложении искомого решения по собственным формам колебаний упругого сооружения. Исследованы линейные установившиеся и неустойчившиеся вынужденные колебания 3 различных грунтовых плотин с учетом конструктивной неоднородности и вязкоупругих свойств материала сооружения при различных динамических воздействиях. Для описания вязкоупругих свойств использована наследственная теория вязкоупругости Больцмана-Вольтерра. Результаты исследований позволили выявить ряд эффектов, возникающих при вынужденных колебаниях в плотине в дорезонансных, резонансных и пост резонансных режимах колебаний.

1. Introduction

Dynamic behavior and assessment of stress-strain state of various earth dams under certain types of kinematic effect are considered in the paper.

Natural oscillations, steady-state and unsteady forced oscillations are mainly considered in studying the dynamics of structures. Natural oscillations in a structure are the most ordered motions of the structure in the absence of external effects.

In the study of natural oscillations, the following dynamic characteristics are determined - natural frequencies, oscillation modes and damping factors of the structure, which are the main regulatory characteristics (the passport) of the structure in question, allowing to evaluate in advance the dynamic properties of the structure as a whole.

Steady-state forced oscillations of the structure occur in the presence of external periodic effects. In this case, the initial conditions are not taken into account. The dissipative properties of the structure are manifested mainly in resonant modes. The values of the resonance amplitudes of displacements and stresses are used as a quantitative estimate of the intensity of dissipative processes

Unsteady forced oscillations of the structure occur as a result of non-periodic effects, which essentially depend on the initial configuration and the loading rate. This makes it possible to determine the maximum values of displacements, strains and stresses in any part of the dam during the entire process of time of external effects, to reveal dangerous sections of structures in terms of strength and to develop the means to reduce the stress-strain state (SSS), taking into account certain material parameters and structural features of the structure.

At the same time free oscillations of structures are considered as a particular case of unsteady forced oscillations, which is the result of initial excitations at time $t=t_0$ in the absence of external effects in subsequent moments.

Recently, a number of papers have been published that take into account the manifestation of elastic, viscoelastic linear and nonlinear as well as elastoviscoplastic and other soil properties, which, along with the above mentioned, describe dissipation in material under dynamic influences. A summary of some of them is given below.

Dynamic response of earth dams [1] is studied taking into account the nonlinear and viscoelastic properties of soil; the dependence of the magnitude of arising dynamic responses on the loading and mechanical properties of soil is established.

Dynamic behavior of earth dams, taking into account the nonlinear properties of material, is considered in [2]. Transient dynamic processes and creep effects under cyclic influences are studied. The problems are solved by the Newmark method.

In [3], using the nonlinearly rheological models, the stress state of the dam is investigated. The possibility of using this model is demonstrated by comparing the numerical results with the results of laboratory tests.

In [4] a model and a set of defining relationships for the rheological model of soft soils are proposed. The possibility of using this model is confirmed by a number of rheological consolidation experiments at different loading rates.

In [5], the properties of coarse-grained materials of a rockfill dam are investigated using the rheological models. It is shown that for strain modeling a unified description of the interaction of various factors is necessary. The obtained results of numerical simulation are compared with the available experimental data for the rockfill material.

To describe the dissipative properties of soil, the Boltzmann-Volterra hereditary viscoelasticity theory has been used recently [6–9].

The behavior of specific structures using the hereditary theory of viscoelasticity under dynamic load conditions has not been sufficiently investigated. Moreover, the overwhelming number of publications related to the dynamic problems of hereditary theory of viscoelasticity is devoted to the design of thin-walled structures: beams, plates and shells [10–17].

The scheme for solving dynamic viscoelasticity problems for thin-walled structures is fairly standard. Selecting a coordinate function that satisfies the boundary conditions, the original problem can be reduced to the problem of oscillations of a system with a finite number of degrees of freedom, i.e., to a

system of linear or nonlinear integral-differential equations with one independent time variable. As a rule, trigonometric or beam functions are used as coordinate functions. Such a choice of coordinate functions limits the class of solved problems to the simplest structural configurations - beams of constant sections, a rectangular plate, a cylindrical shell [12–14, 17].

The above authors, while admitting a number of inaccuracies in the selection of coordinate functions, try to improve the accuracy of solving the system of integral-differential equations. However, for constructions with real geometry it is impossible to select the analytic coordinate functions that satisfy the boundary conditions of the problem.

Therefore, for the structure of complex geometry, it would be useful to use as coordinate functions, the eigenmodes of oscillations, which are intrinsic ones and take into account all features of the structure under consideration.

Expansion of the solution in terms of eigenmodes of oscillations in solving specific problems for the first time was used in [18]. Then the eigenmodes of oscillations for the expansion of solution of real structures and complex viscoelastic shells under forced vibrations were used in [10, 11, 19, 23].

This review of known works shows the need to assess the stress-strain state and dynamic behavior of earth structures, taking into account the viscoelastic properties of soil, as well as the heterogeneous structural features and real geometry.

Therefore, the evaluation of the strength parameters of earth dams under various dynamic effects, taking into account the real features of the structure and the dissipative properties of the structure material, is an actual task and represents both theoretical and practical interest.

The aim of this work is to develop a methodology, an algorithm and a computer program for assessing the dynamic behavior and stress-strain state of an earth dam, taking into account the viscoelastic properties of the material and the actual geometry of the structure under various effects, as well as studying the dynamic characteristics and stress-strain state of various earth dams under some types of kinematic influences.

Considering this problem, the Boltzmann-Volterra hereditary theory of viscoelasticity [8, 21], using the Rzhnitsyn-Koltunov kernel [11, 22], is used to take into account the viscoelastic properties of soil. To formulate the problem, the principle of virtual displacements is used, and the variation problem is solved by expanding the solution in terms of the eigenmodes of vibrations of the elastic problem [10, 11, 19]. The resulting system of integral-differential equations is solved exactly for periodic effects or using quadrature formulas at nonstationary kinematic effects.

In this paper, the methods, algorithm, and results of research on strength parameters of earth dams (of various height) are presented taking into account the viscoelastic properties of soil and the heterogeneous structural features in resonant oscillation modes under various dynamic effects.

2. Methods

Consider the earth dam (Fig. 1); the volume is $V=V_1+V_2+V_3+V_4+V_5+V_6$. It is assumed that the lower part of the dam is located on rigid base Σ_u , where the kinematic effect $\vec{u}_o(\vec{x}, t)$ is applied. The hydrostatic pressure acts on the S_p part of the surface Σ_1 . The rest of the surface (Σ_2, Σ_3) is stress-free. The dam (Fig. 1) is a massive body, so mass forces \vec{f} are taken into account in the calculation. The material of different parts ($V_1, V_2, V_3, V_4, V_5, V_6$) of the dam is considered linearly elastic or linearly viscoelastic. At the boundaries of individual parts of the dam, the components of displacements and stresses are continuous.

The task is to determine the displacement and stress fields arising in the dam (Fig. 1), under the effect of mass forces \vec{f} , water pressure \vec{P}_c and kinematic influences at the base $\vec{u}_o(\vec{x}, t)$.

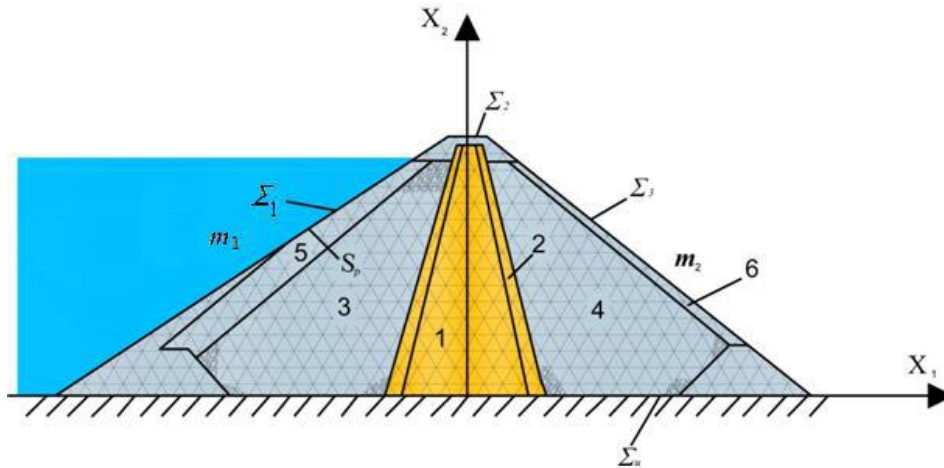


Figure 1. Model of earth dam

For the statement of the problem, the principle of virtual displacements is used, according to which the sum of the work of all active forces, including inertia ones, on the virtual displacements is zero:

$$\delta A = - \int_V \sigma_{ij} \delta \varepsilon_{ij} dV - \int_V \rho_n \ddot{u} \delta \bar{u} dV + \int_V \vec{f} \delta \bar{u} dV + \int_{S_P} \vec{P}_c \delta \bar{u} dS = 0. \quad (1)$$

Here, \vec{u} , ε_{ij} , σ_{ij} – are the displacement vector and the components of strain and stress tensors; respectively, $\delta \vec{u}$, $\delta \varepsilon_{ij}$ – are isochronous variations of displacements and strains; ρ_n – density of material of elements ($V_1, V_2, V_3, V_4, V_5, V_6$) of the system under consideration; \vec{f} – is a vector of mass forces; \vec{P}_c – is hydrostatic water pressure.

To describe the viscoelastic properties of material, the Boltzmann-Volterra linear hereditary theory is used [21]:

$$S_{ij} = G_n \left[e_{ij} - \int_0^t \Gamma(t-\tau) e_{ij}(\tau) d\tau \right], \quad (2)$$

$$\sigma = K_n \theta.$$

The following designations are accepted: S_{ij}, e_{ij} – are the components of stress and strain deviator; σ – a hydrostatic component of stress tensor; K_n, G_n – are the instantaneous bulk and shear moduli of elasticity; Γ – a relaxation kernel; $\theta = \varepsilon_{ii}$ – a volume strain. The index $n = 1, \dots, 6$ refers to respective volume $V_n, i, j = 1, 2$.

The connection between the strain tensor and the components of the displacement vector is described by the Cauchy linear relations

$$\varepsilon_{ij} = \frac{1}{2} \left(\frac{\partial u_i}{\partial x_j} + \frac{\partial u_j}{\partial x_i} \right), \quad i, j = 1, 2. \quad (3)$$

Kinematic conditions at the base are given

$$\vec{x} \in \Sigma_u : \vec{u}_0(\vec{x}, t) = \vec{\psi}(t), \quad (4)$$

and initial conditions at $t=0$:

$$\vec{x} \in V : \vec{u}(\vec{x}, 0) = \vec{\chi}_1(\vec{x});$$

$$\dot{\vec{u}}(\vec{x}, 0) = \vec{\chi}_2(\vec{x}), \quad (5)$$

where $\bar{\psi}$ – is a given function of time; $\bar{\chi}_1, \bar{\chi}_2$ – are given functions of coordinates.

An approximate solution of the problem in question is sought in the form of an expansion in terms of the eigenmodes of oscillations of the elastic problem for heterogeneous systems (Fig. 1) [10, 11, 19], i.e.:

$$\bar{u}(\bar{x}, t) = \bar{u}_0(\bar{x}, t) + \sum_{k=1}^N \bar{u}_k^*(\bar{x}) y_k(t); \quad \delta \bar{u} = \sum_{k=1}^N \bar{u}_k^*(\bar{x}) \delta y_k(t), \quad (6)$$

where $\bar{u}_0(\bar{x}, t)$ – is a known function (4), which satisfies the boundary conditions of the problem; $\bar{u}_k^*(\bar{x})$ – are the eigenmodes of oscillations of the elastic problem for heterogeneous systems; $y_k(t)$ – are the sought-for functions of time; $\delta y_k(t)$ – are arbitrary constants; N – is a number of eigenmodes retained in the expansion (6).

When using this approach, the main difficulty lies in the choice of coordinate functions $\bar{u}_k^*(\bar{x})$, which are quite simple in the case of bodies of simple shape and fastening conditions. For the bodies of complex shape, the choice of coordinate functions $\bar{u}_k^*(\bar{x})$ reducing the original system of variation equations (1) to a system of resolving equations with a finite number of degrees of freedom presents a difficult problem. Using the eigenmodes of oscillations allows one to accurately describe the real geometry and various features of bodies of complex shapes under different effects. This explains the choice of eigenmodes of oscillations as coordinate functions. Therefore, in this paper, first, taking into account all the factors, by the finite element method (FEM), the eigenmodes of oscillations of a heterogeneous dam are determined (Fig. 1) in a linear elastic statement. Further, the solution of the problem of forced oscillations of the system, taking into account the viscoelastic properties of material, is constructed in the form of an expansion in accordance with the found eigenmodes of oscillations of the elastic problem.

In the case of steady-state forced oscillations under periodic kinematic effects, taking into account the viscoelastic properties of dam material, the problem under consideration, after substitution of (6) into (1), is reduced to solving a system of linear integral-differential equations of the form

$$M_{ik} \ddot{y}_k(t) + K_{ik} y_k(t) - C_{ik} \int_{-\infty}^t \Gamma(t-\tau) y_k(\tau) d\tau = -(f_{1i} \ddot{\psi}_1(t) + f_{2i} \ddot{\psi}_2(t)), \quad (7)$$

$$i=1, 2, \dots, N; \quad k=1, 2, \dots, N.$$

The order of the system (7) is equal to the number N of eigenmodes of oscillations of elastic structure retained in the expansion (6). In studying steady-state forced oscillations, the lower bound of the integral in expression (2) is taken from minus infinity. In this case, the initial conditions are not taken into account. The system of equations (7) has an exact solution [23].

The system of integral-differential equations (7) describes the dynamic behavior of earth dams, taking into account the viscoelastic properties of soil under periodic kinematic effects. This allows one to investigate the dynamic behavior of earth dams at various external effect frequencies, including the options, when the frequency of the effect is equal to the natural frequency of the structure (resonant mode).

Under unsteady forced oscillations of the dam, the variation problem (1) after substitution (6) is reduced to solving a system of linear integral-differential equations

$$M_{ij} \ddot{y}_j(t) + K_{ij} y_j(t) - C_{ij} \int_0^t \Gamma_1(t-\tau) y_j(\tau) d\tau = F_i + Q_i f(t), \quad (8)$$

with initial conditions:

$$y_i(0) = y_{0i}, \quad \dot{y}_i(0) = \dot{y}_{0i}; \quad i, j, k, m = 1, 2, \dots, N. \quad (9)$$

Here also the order of the system of equations (8) is equal to N - the number of retained in the expansion (6) eigenmodes of oscillations of elastic dam. The coefficients $f_{1i}, f_{2i}, Q_i, F_i, M_{ij}, K_{ij}, C_{ij}$ of the system of integral-differential equations (7) and (8) are determined through eigenmodes of oscillations $\bar{u}_k^*(\bar{x})$ by integrating them over the volume of the dam in question. Here $f_{1i}, f_{2i}, F_i, f(t)$ was a total external load from mass forces, hydrostatic pressure, and kinematic effect varying in time.

The system (8), under the initial conditions (9), is solved by the method of quadrature formulas set forth in [17, 19].

To verify the reliability of the developed algorithm and the computer program, a linear integral-differential equation of the following form is solved

$$\ddot{y}(t) + \omega^2 \left[y(t) - \int_0^t \Gamma_1(t-\tau) y(\tau) d\tau \right] = f(t) \quad (10)$$

with initial conditions

$$y(0) = 1, \dot{y}(0) = -\beta \quad (11)$$

and with basic data

$$\begin{aligned} \Gamma_1(t) &= A e^{-\beta t} \cdot t^{\alpha-1}, \\ f(t) &= \left[\beta^2 + \omega^2 - \frac{A\omega^2 t^\alpha}{\alpha} \right] e^{-\beta t}, \\ A &= 0.01; \alpha = 0.25; \omega = 2\pi, \end{aligned} \quad (12)$$

both numerically by the method of quadrature formulas [17, 19], and in exact form [17]. The results of the numerical solutions obtained and their comparison with the exact solution $y = e^{-\beta t}$ are given in Table 1.

Table 1. Solutions of linear integral-differential equations (10)

Time, t, s	0.4	1.2	2.0	4.0	8.0	12.0	16.0	20.0	24.0	28.0
Solution, obtained by the authors	0.973	0.927	0.887	0.801	0.654	0.536	0.439	0.361	0.297	0.245
Exact solution	0.980	0.942	0.905	0.819	0.670	0.549	0.449	0.368	0.301	0.247

Comparison of the results (Table 1) shows that with the developed algorithm based on quadrature formulas it is possible to obtain a solution of integral-differential equations with required accuracy.

3. Results and Discussion

Dynamic behavior and stress-strain state of the Nurek (296 m high), Gissarak (138.5 m high) and Sokh (87.3 m high) earth dams [27] were studied with account of their real geometry and heterogeneous structural features.

Various mechanical properties of soil were taken into account for various sections of the dam, and Rzhantsyn's three-parameter relaxation kernels [26] were used to describe the viscoelastic properties of soil (with kernel parameters given in [8]).

To solve the above problems, first the eigenmodes of oscillations of these dams were determined with account of real features of the structures under consideration in elastic statement. The obtained natural frequencies of the Nurek dam were compared with the spectra of the oscillation frequencies of the Nurek dam [20], obtained during the earthquakes. The comparison also showed a sufficiently high accuracy of the results obtained,

3.1. Study of steady-state forced oscillations

Next, steady-state forced oscillations are studied with consideration of viscoelastic properties of soil under two-component periodic kinematic effects at the base of the structure:

$$\vec{x} \in \Sigma u : \begin{cases} u_{10}(t) = B \exp(-i\Omega t) \\ u_{20}(t) = C \exp(-i\Omega t) \end{cases}, \quad (13)$$

where B, C – are the amplitudes, and Ω – is a frequency of kinematic effect.

The result of calculation is a construction for a number of characteristic points of the dam of amplitude-frequency characteristics (AFC) of displacements (u_1, u_2) and stresses: normal – σ_{11}, σ_{22} , tangential σ_{12} , principal σ_1, σ_2 , maximal tangent τ_{max} and intensity of stresses σ_i for various frequencies “ Ω ” of kinematic action (10) in the range from 1.0 to 20.0 rad/sec. In the vicinity of the proposed viscoelastic resonance, the step for the frequency “ Ω ” is 2–3 times less. The amplitude ratio was assumed to be $B/C = 2.0$ ($B = 0.01$ m).

As an example Figure 2a shows the AFC of horizontal – u_1 and vertical – u_2 displacements of the point ($x_1 = -301$ m, $x_2 = 92.5$ m), and Figure 2b - AFC of the maximum tangential stress τ_{max} at the point ($x_1 = -204$ m, $x_2 = 104.8$ m) of the Nurek dam, with consideration of viscoelastic properties of material and without consideration of mass forces.

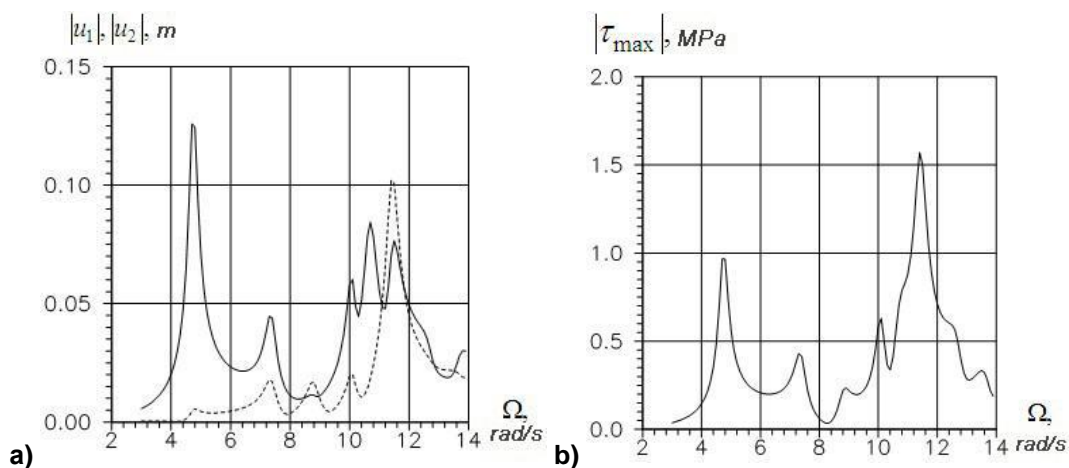


Figure 2. Amplitude-frequency characteristics of displacements $|u_1|, |u_2|$ of the point

($x_1 = -301$ m, $x_2 = 92.5$ m) and maximum tangential stresses $|\tau_{max}|$ at the point

($x_1 = -204$ m, $x_2 = 104.8$ m) of the Nurek dam, with consideration of viscoelastic properties of material: ___ horizontal displacements (u_1); --- vertical displacements (u_2).

The results obtained (Fig. 2a) indicate an excess of the amplitudes of horizontal displacements in comparison with vertical ones at the first resonant frequency. At the second resonance, on the contrary – the vertical displacements exceed the horizontal ones. This is due to the nature of the dam's eigenmodes of oscillation at the appropriate frequencies: during the first mode there occurs the shift of the central section, and during the second - the vertical strain of the dam, and so on.

Analysis of the amplitude-frequency characteristics of stresses (Fig. 2b) shows that the largest amplitudes of stresses at the points of the dam arise when the frequency of the effect Ω coincides with the first natural frequency and with the frequencies of the dense spectrum in the range between $\omega_4 \div \omega_6$ or ω_9, ω_{10} . This is explained by the interaction of eigenmodes of oscillations of a structure with close frequencies, which create a single peak with great amplitude. Therefore, for this dam it is dangerous to

operate with a frequency of $\Omega = \omega_1$ and with a frequency in the range between the frequencies ω_4 and ω_6 .

3.2. Investigation of unsteady forced oscillations

Unsteady forced oscillations were studied with account of real features and viscoelastic properties of soil of the above-mentioned dams; kinematic effect at the base of the structure Σ_u was taken as an external influence:

$$\text{horizontal } \{u_o(t)\} = \begin{cases} a \sin(pt), & 0 < t \leq t^* \\ 0, & t^* > t \end{cases}; \quad (14)$$

$$\text{vertical } \{v_o(t)\} = \begin{cases} b \sin(pt), & 0 < t \leq t^* \\ 0, & t^* > t \end{cases}. \quad (15)$$

Here: p – is a frequency; a, b – the amplitudes; t^* – effect time; t – considered time of the process. Initial conditions of the problem are homogeneous.

In calculations, the parameters of kinematic effect (14)–(15) were taken as: $a = 0.01$ m, $b = 0.01$ m; $t^* = 3$ sec. The frequency of the effect was taken: for the Gissarak dam: $p = 5.70$ rad/sec (pre-resonant mode), $p = 7.70$ rad/sec (post-resonant mode); for Sokh: $p = 16.30$ rad/sec (pre-resonant mode), $p = 22.00$ rad/sec (post-resonant mode).

At each moment of the effect the motions of various points of the dam were determined in time.

Figures 3–4 show the variation of horizontal displacements (u_1) in time of the points ($x_1 = 8.0$ m, $x_2 = 138.5$ m) of the Gissarak dam and the point ($x_1 = 5.0$ m, $x_2 = 87.0$ m) of the Sokhdam at different frequencies " p " of the two-component kinematic effect (14)–(15).

Analysis of the results shows that vertical displacements are inferior in magnitude to horizontal ones u_1 . The explanation for this is the character of the first waveform representing the shear of the cross section in the direction of x_1 axis.

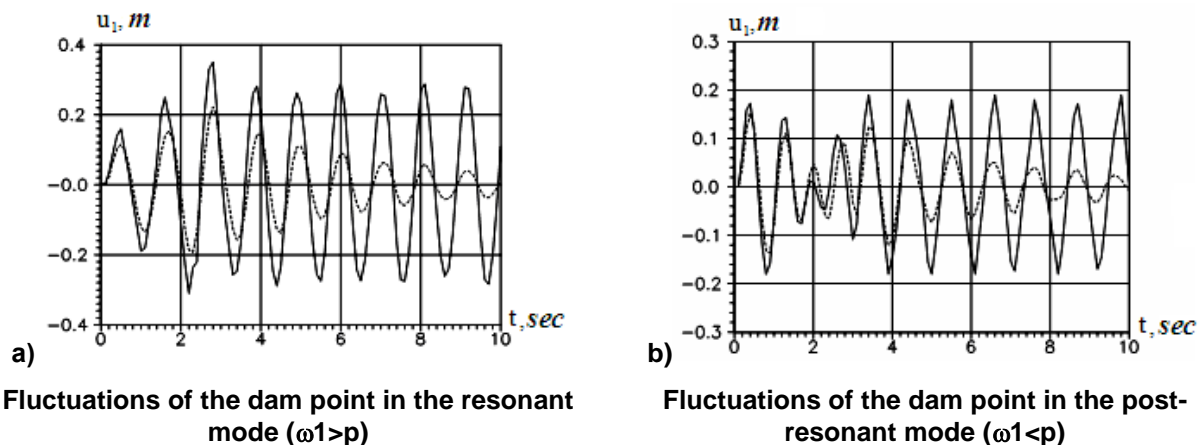
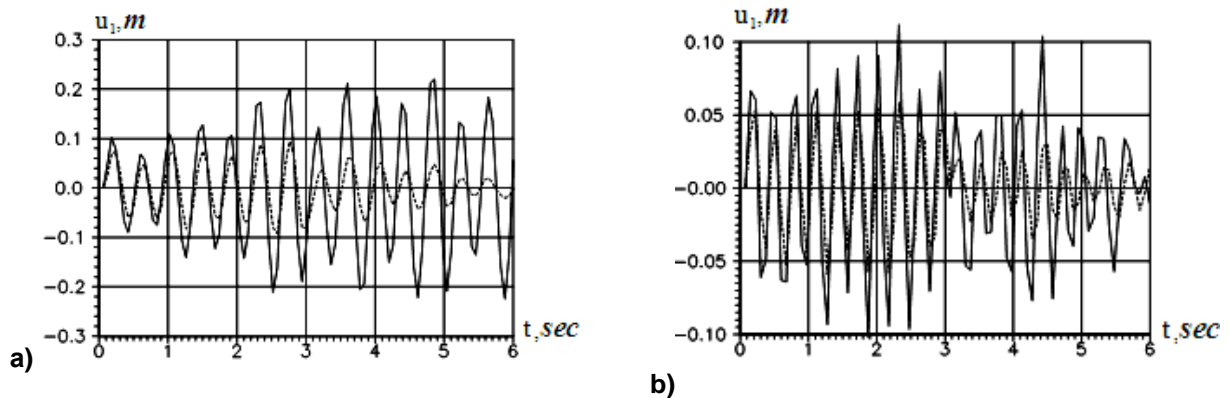


Figure 3. Change of horizontal displacements (u_1) of the point ($x_1 = 8.0$ m, $x_2 = 138.5$ m) of the Gissarak dam under two-component effect ($t^* = 3$ sec)

From the results (Figs. 3–4) it can be seen that the consideration of viscoelastic properties of soil leads to a significant attenuation of the oscillations even during the effect of the load both for structures with low-frequency spectrum (Fig. 3) and high-frequency spectrum (Fig. 4); that is explained by the use of viscoelastic model, in which the change in dissipative properties of material weakly depends on the frequency of oscillations.

Analysis of the displacements of dam points under multicomponent kinematic effects in the pre-resonant mode (at frequency $p < \omega_1$) shows that horizontal oscillations of different points of the dam occur with the greatest amplitude, almost twice exceeding the amplitude of vertical oscillations. In the post-resonant mode, the amplitudes of the oscillations of elastic structure have almost the same value for all the components of displacements.



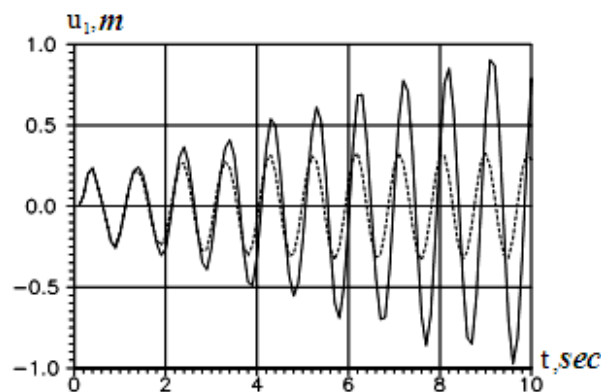
Fluctuations of the dam point in the pre-resonant mode ($\omega_1 > p$)

Fluctuations of the dam point in the post-resonant mode ($\omega_1 < p$)

Figure 4. Change of horizontal displacements (u_1) of the point ($x_1=5$ m, $x_2=87$ m) of the Sokh dam under two-component effect ($t^* = 3$ sec.)

The account of viscoelastic properties of soil strongly attenuates horizontal oscillations, both during the effect, and after it. In this case, the amplitude of horizontal viscoelastic oscillations (in the pre-resonant mode) is almost two times less than the amplitude of elastic oscillations. The damping of oscillations of other components of point displacements basically occurs after the end of the effect both in the pre-resonant and post-resonant modes. In the post-resonant mode, the amplitude of the oscillations of the point in all directions (in both elastic and viscous-elastic cases) is inferior to the amplitudes of horizontal oscillations in the pre-resonant mode. This type of oscillation is also observed for the Sokh dam, the oscillations of which are high-frequency ones.

The amplitude of oscillations of the dam point in the resonant mode in elastic soil is infinitely increasing in time (Fig. 5).



Fluctuations of the dam point in the resonant mode ($\omega_1 = p$)

Figure 5. Horizontal displacements (u_1) of the point ($x_1=8.0$ m, $x_2=138,5$ m, $x_3=330.0$ m) of the Gissarak dam under multicomponent kinematic effect ($t^* = 10.0$ сек.)

When taking into account the viscoelastic properties of soil, the amplitude of dam oscillations is limited and, with the passage of time, remains constant at the same level (Fig. 5).

4. Conclusions

The carried out researches on strength parameters evaluation of earth dams under various dynamic effects have allowed us to draw the following conclusions:

1. In solving the problem of forced oscillations of the structures of complex shapes, the use of eigenmodes of oscillations of the structures in question in elastic statement, taken as coordinate functions, makes it possible to accurately describe the real geometry and various structural features.

2. In the case of the existence of a dense spectrum of eigenfrequencies in considered structures, the oscillations in the resonant mode lead to oscillations with a larger amplitude than at the first resonance.

3. Consideration of viscoelastic properties of the dam's soil leads to a significant attenuation of the oscillations even during the effect of the load, both for the structures with low-frequency spectrum and high-frequency spectrum, although the dissipative properties of material weakly depend on the frequency of oscillations.

4. The magnitude of displacements and stresses arising at different points of the dam under forced oscillations exert a rather strong influence, not only on the amplitudes of the effect, but also on the ratio of natural frequency of the structure and the frequency of external effects.

Reference

- Xiong B.-L., Wang X.-L., Lu C.-J. Dynamic reaction analysis of tailing dams under earthquake. *Advances in Environmental Geotechnics*. 2010. No. 6. Pp. 697–701.
- Siyahi B., Arslan H. Nonlinear dynamic finite element simulation of Alibey earth dam. *Environmental Geology*. 2008. Vol. 54. No. 1. Pp. 77–85.
- Bauer E., Fu Z.Z., Liu S. Constitutive modeling of materials for rockfill dams. *6th International conference on dam engineering*. Lisbon, Portugal, 2011. Pp. 1–14.
- Ma B.-n., Xie X.-y., Liu K.-f. Rheological catastrophic model for soft clays. *Journal of Central South University*. 2012. Vol. 19. No. 8. Pp. 2316–2322.
- Bauer E., Fu Z.Z., Liu S. Influence of pressure and density on the rheological properties of rockfills. *Frontiers of Structural and Civil Engineering*. 2012. Vol. 6. No. 1. Pp. 25–34.
- Vyalov S.S. *Reologicheskiye osnovy mekhaniki gruntov* [Rheological Basis of the Mechanics of Soil]. Moscow: Vysshaya shkola, 1978. 447 p.(rus)
- Meschan S.R. *Eksperimentalnaya reologiya glinistykh gruntov* [Experimental Rheology of Clayey Soils]. Moscow: Nedra, 1985. 342 p. (rus)
- Mirsaidov M.M., Sultanov T.Z. Use of linear heredity theory of viscoelasticity for dynamic analysis of earth structures. *Soil Mechanics and Foundation Engineering*. 2013. Vol. 49. No. 6. Pp. 250–256.
- Ter-Martirosyan Z.G., Ter-Martirosyan A.Z. Rheological properties of soils under shear. *Soil Mechanics and Foundation Engineering*. 2012. № 6. Pp. 9–13.
- Mirsaidov M., Troyanovskii I.E. Forced axisymmetric oscillations of a viscoelastic cylindrical shell. *Mechanics of Composite Materials*. 1975. Vol. 11. No. 6. Pp. 953–955.
- Koltunov M.A., Mirsaidov M., Troyanovskii I.E. Transient vibrations of axisymmetric viscoelastic shells. *Mechanics of Composite Materials*. 1978. No. 2. Pp. 290–295.
- Eshmatov B.Kh., Eshmatov K., Khodzhaev D.A. Nonlinear flutter of viscoelastic rectangular plates and cylindrical panels of a composite with a concentrated masses. *Journal of Applied Mechanics and Technical Physics*. 2013. Vol. 54. No. 4. Pp. 578–587.
- Eshmatov B.Kh. Nonlinear vibrations and dynamic stability of a viscoelastic circular cylindrical shell with shear strain and inertia of rotation taken into account. *Mechanics of Solids*. 2009. Vol. 44. No. 3. Pp. 421–434.
- Eshmatov B.Kh., Khodjaev D.A. Nonlinear vibration and dynamic stability of a viscoelastic cylindrical panel with concentrated mass. *Acta Mechanica*. 2007. No. 1-4(190).

Литература

- Xiong B.-L., Wang X.-L., Lu C.-J. Dynamic reaction analysis of tailing dams under earthquake // *Advances in Environmental Geotechnics*. 2010. № 6. Pp. 697–701.
- Siyahi B., Arslan H. Nonlinear dynamic finite element simulation of Alibey earth dam // *Environmental Geology*. 2008. Vol. 54. No. 1. Pp. 77–85.
- Bauer E., Fu Z.Z., Liu S. Constitutive modeling of materials for rockfill dams // *6th International conference on dam engineering*. Lisbon, Portugal. 2011. Pp. 1–14.
- Ma B.-n., Xie X.-y., Liu K.-f. Rheological catastrophic model for soft clays // *Journal of Central South University*. 2012. Vol.19. № 8. Pp. 2316–2322.
- Bauer E., Fu Z.Z., Liu S. Influence of pressure and density on the rheological properties of rockfills // *Frontiers of Structural and Civil Engineering*. 2012. Vol.6. Issue 1. Pp.25-34.
- Вялов С.С. Реологические основы механики грунтов. Москва: Высшая школа, 1978. 447 с.
- Месчан С.Р. Экспериментальная реология глинистых грунтов. Москва: Недра, 1985. 342 с.
- Mirsaidov M.M., Sultanov T.Z. Use of linear heredity theory of viscoelasticity for dynamic analysis of earth structures // *Soil Mechanics and Foundation Engineering*. 2013. Vol. 49. № 6. Pp. 250–256.
- Ter-Martirosyan Z.G., Ter-Martirosyan A.Z. Rheological properties of soils under shear // *Soil Mechanics and Foundation Engineering*. 2012. № 6. Pp. 9–13.
- Mirsaidov M., Troyanovskii I.E. Forced axisymmetric oscillations of a viscoelastic cylindrical shell // *Mechanics of Composite Materials*. 1975. Vol. 11. № 6. Pp. 953–955.
- Koltunov M.A., Mirsaidov M., Troyanovskii I.E. Transient vibrations of axisymmetric viscoelastic shells // *Mechanics of Composite Materials*. 1978. Vol. 14. № 2. Pp. 233–238.
- Eshmatov B.Kh., Eshmatov K., Khodzhaev D.A. Nonlinear flutter of viscoelastic rectangular plates and cylindrical panels of a composite with a concentrated masses // *Journal of Applied Mechanics and Technical Physics*. 2013. Vol. 54. № 4. Pp. 578–587.
- Eshmatov B.Kh. Nonlinear vibrations and dynamic stability of a viscoelastic circular cylindrical shell with shear strain and inertia of rotation taken into account // *Mechanics of Solids*. 2009. Vol. 44. № 3. Pp. 421–434.
- Eshmatov B.Kh., Khodzhaev D.A. Nonlinear vibration and dynamic stability of a viscoelastic cylindrical panel with concentrated mass // *Acta Mechanica*. 2007. № 1-4(190). Pp. 165–183.

Mirsaidov M.M., Sultanov T.Z., Abdikarimov R.A., Ishmatov A.N., Yuldoshev B.Sh., Toshmatov E.S., Jurayev D.P. Strength parameters of earth dams under various dynamic effects. *Magazine of Civil Engineering*. 2018. No. 1. Pp. 101–111. doi: 10.18720/MCE.77.9.

- Pp. 165–183.
15. Sultanov K.S., Bakhodirov A.A. Laws of shear interaction at contact surfaces between solid bodies and soil. *Soil Mechanics and Foundation Engineering*. 2016. Vol. 53. Pp. 71–77.
 16. Kobeleva N.N. Methodical peculiarities of prognostic mathematical modelling for deformation survey of high dams. *Vestnik SSUGT*. 2017. Vol. 22(2). Pp. 55–66.
 17. Badalov F.B. *Metody resheniya integralnykh i integrodiferentsialnykh uravneniy nasledstvennoy teorii vyazkoupugosti* [Methods of Solution of Integral and Integral-Differential Equations of Hereditary Theory of Viscous-Elasticity]. Tashkent: Mekhnat, 1987. 269 p. (rus)
 18. Chelomei V.N. *Dinamicheskaya ustoychivost elementov aviatsionnykh konstruksiy* [Dynamic Stability of the Elements of Aircraft Structures]. Moscow: Aeroflot, 1939. 80 p. (rus)
 19. Ishmatov A.N., Mirsaidov M. Nonlinear vibrations of an axisymmetric body acted upon by pulse loads. *Soviet Applied Mechanics* (Prikladnaya Mekhanika). 1991. Vol. 27. No. 4. Pp. 68–74.
 20. Barysheva N.N., Seleznev G.S. Kolebaniya plotiny Nurekskoy GES pri zemletryaseni 30 iyulya 1974 g. [Dam Oscillations of the Nurek Hydropower Plant under Ground Motion. July 30, 1974]. *Seismic Stability of Dams*. No. 4. 1978. Pp. 126–134. (rus)
 21. Ilyushin A.A., Pobedrya B.E. *Osnovy matematicheskoy teorii termo-vyazkoupugosti* [Basis of Mathematical Theory of Thermal-viscous-elasticity]. Moscow. Nauka, 1970. 280 p. (rus)
 22. Rzhantsyn A.R. *Teoriya polzuchesti* [Theory of Creeping]. Moscow: Stroyizdat, 1968. 416 p. (rus)
 23. Mirsaidov M.M., Sultanov T.Z. *Theory and Methods of Strength Assessment of Earth Dams*. Lambert Academic Publishing. Germany, 2015. 341 p.
 15. Sultanov K.S., Bakhodirov A.A. Laws of shear interaction at contact surfaces between solid bodies and soil // *Soil Mechanics and Foundation Engineering*. 2016. Vol. 53. Pp. 71–77.
 16. Kobeleva N.N. Methodical peculiarities of prognostic mathematical modelling for deformation survey of high dams // *Vestnik SSUGT*. 2017. Vol. 22. № 2. Pp. 55–66.
 17. Бадалов Ф.Б. Методы решения интегральных и интегродифференциальных уравнений наследственной теории вязкоупругости. Ташкент: Мехнат, 1987. 269 с.
 18. Челомей В.Н. Динамическая устойчивости элементов авиационных конструкций. Москва: Аэрофлот, 1939. 80 с.
 19. Ishmatov A.N., Mirsaidov M. Nonlinear vibrations of an axisymmetric body acted upon by pulse loads // *Прикладная механика*. 1991. Т. 27. № 4. С. 68–74.
 20. Барышева Н.Н., Селезнев Г.С. Колебания плотины Нурекской ГЭС при землетрясении 30 июля 1974 г. // *Сейсмостойкость плотин*. 1978. № 4. С. 126–134.
 21. Ильюшин А.А., Победря Б.Е. Основы математической теории термовязкоупругости. Москва. Наука. 1970. 280 с.
 22. Ржаницин А.Р. Теория ползучести. Москва. Стройиздат. 1968. 416 с.
 23. Mirsaidov M.M., Sultanov T.Z. *Theory and Methods of Strength Assessment of Earth Dams*. Lambert Academic Publishing. Germany, 2015. 341 p.

Mirziyod Mirsaidov,
+7(987)237-09-81; theormir@mail.ru

Tohirjon Sultanov,
+7(99871)237-09-81; tz-sultanov@mail.ru

Rustamkhan Abdikarimov,
+7(99890)928-45-54; rabdikarimov@mail.ru

Alisher Ishmatov,
+7(99871)237-09-81; rabdikarimov@mail.ru

Bakhtiyor Yuldoshev,
+7(99871)237-09-81;
Bakhtiyor_Yuldoshev68@mail.ru

Elyor Toshmatov,
+7(99871)237-09-81; Elyortoshmatov@inbox.uz

Doniyor Jurayev,
+7(99871)237-09-81; tohir-zs@mail.ru

Мирзиёд Мирсаидович Мирсаидов,
+7(987)237-09-81; эл. почта: theormir@mail.ru

Тохиржон Закирович Султанов,
+7(99871)237-09-81;
эл. почта: tz-sultanov@mail.ru

Рустамхан Алимханович Абдикаримов,
+7(99890)928-45-54;
эл. почта: rabdikarimov@mail.ru

Алишер Норкобилович Ишматов,
+7(99871)237-09-81;
эл. почта: rabdikarimov@mail.ru

Бахтиёр Шодмонович Юлдошев,
+7(99871)237-09-81;
эл. почта: Bakhtiyor_Yuldoshev68@mail.ru

Элёр Сабирович Тошматов,
+7(99871)237-09-81;
эл. почта: Elyortoshmatov@inbox.uz

Дониёр Пахриддинович Жураев,
+7(99871)237-09-81; эл. почта: tohir-zs@mail.ru

© Mirsaidov M.M., Sultanov T.Z., Abdikarimov R.A., Ishmatov A.N., Yuldoshev B.Sh., Toshmatov E.S., Jurayev D.P., 2018

doi: 10.18720/MCE.77.10

Track-etched membranes back-flushing and regeneration during the natural water purification

Промывка и регенерация трековых мембран при очистке природной воды

**P.S. Barashkova,
L.M. Molodkina,**
*Peter the Great St. Petersburg Polytechnic
University, St. Petersburg, Russia*

**Студент П.С. Барашкова,
д-р физ.-мат. наук, профессор
Л.М. Молодкина,**
*Санкт-Петербургский политехнический
университет Петра Великого,
г. Санкт-Петербург, Россия*

Key words: track-etched membrane; water treatment; local water supply; flushing; regeneration; filtration; productivity; civil engineering; buildings

Ключевые слова: трековая мембрана; водоподготовка; местное водоснабжение; промывка; регенерация; фильтрация; производительность; гражданское строительство; здания и сооружения

Abstract. Membrane filtration is one of the main methods of local water treatment. Track-etched membranes allow to obtain high-quality purified water due to their high selectivity. During the filtration, the productivity of process can decrease due to the adsorption of components in the pores, pore blockages, formation of sediment layer above the membrane. To restore the productivity, the membrane should be flushed periodically or regenerated chemically.

Comparative study of the back-flushing and chemical regeneration after natural water filtration using standard 12- μm -thick track-etched membrane and new 20- μm -thick irradiated on both sides (with argon ions with the mileage less than the film thickness) was performed. The research was conducted with natural water from the pond "Zenit" (St. Petersburg) and the Volhov River (Leningrad region). The filtration was conducted in the dead-end mode. Water samples were analyzed by spectrophotometry, spectroturbidimetry and dynamic light scattering.

The size distribution of impurity particles of studied natural water, the change in their sizes during coagulation with an aqua-aurate were determined in work. The mechanisms underlying the decrease of filtration productivity were identified.

The experimental data showed that both-sided irradiated 20- μm -thick membrane has advantages over a standard 12- μm -thick membrane in natural water filtration with impurities that block the pores both in the direct filtration process and in back-flushing and regeneration. The possibility of regeneration and back-flushing of the 20- μm -thick membrane allows us to recommend it for natural water filtration.

Аннотация. Мембранная фильтрация является одним из основных методов локальной водоочистки. Трековые мембраны позволяют получать очищенную воду высокого качества благодаря их высокой селективности. Во время фильтрации производительность процесса может уменьшаться за счет адсорбции в порах, закупорки пор или формирования осадка над мембраной. Для восстановления производительности мембрану следует периодически промывать или регенерировать химическим путем.

В работе проведено сравнительное исследование процесса обратной промывки и химической регенерации трековой мембраны толщиной 12 мкм, и новой мембраны толщиной 20 мкм, облученной с обеих сторон (ионами аргона с пробегом меньше толщины пленки), после фильтрации природной воды. В экспериментах использовали природную воду из пруда «Зенит» (Санкт-Петербург) и реки Волхов (Ленинградская обл.). Фильтрацию проводили в тупиковом режиме. Образцы воды анализировали методами спектрофотометрии, спектротурбидиметрии и динамического светорассеяния.

В работе определено распределение по размерам примесных частиц используемых природных вод, изменение их размеров при коагуляции аква-ауратом. Определены механизмы, лежащие в основе снижения производительности фильтрации.

Полученные результаты показали преимущество новой, двусторонне облученной трековой мембраны толщиной 20 мкм в процессах фильтрации природной воды, содержащей примеси, способные задерживаться в порах мембран, обратной промывки и химической регенерации. Возможность промывки и регенерации позволили рекомендовать трековую мембрану толщиной 20 мкм для очистки природной воды в питьевых целях.

1. Introduction

The problem of providing the population with pure drinking water is still unresolved and in a number of countries it has reached crisis proportions [1, 2]. A particularly acute issue is the problem of providing water of appropriate quality to individual consumers living in villages, small towns, and housing estates [3–6]. Local water treatment technologies could vary greatly depending on the quality of water, the presence of accessible materials (sorbents, membranes and natural filtering materials [7, 8]), the possibility of material utilization, strength characteristics, and so on.

Microfiltration on the track-etched membrane was chosen as the primary method of water treatment because of its high-energy efficiency [9], high quality of water treatment, and due to its compactness [10–12]. Track-etched membranes are characterized by its increased flexibility, selectivity, resistance to most acids and organic solvents, alkalis and the possibility of regeneration [13–18].

During the microfiltration, the productivity of process decreases due to the following reasons:

- adsorption of components in the pores (the components are substantially smaller than the pore sizes, but they have time to be adsorbed on the walls of membrane pores);
- pore blockages (components are commensurate with pores);
- formation of sediment layer above the membrane (components larger than pores, a dynamic membrane is forming) [19].

To increase the productivity of membranes conduct:

- direct flushing at tangential mode (destroying the dynamic membrane formed on the surface of the original membrane);
- backwashing (from the reverse side of the membrane with a filtrate or pure solvent);
- regeneration with reagents (with stopping the filtration process for contact of membrane with reagents and subsequent washing the membrane off the reagent) [20–23].

Hydraulic washes are using to increase the lifetime of the membrane, but the greatest effect is achieving by using chemical washes. Correct selection of reagents, whose purpose is to transfer the deposits into a soluble form, effects on the efficiency of chemical purification. In order to choose the reagents correctly it is necessary to know the composition and structure of pollutants [24]. The most unfavorable variant of dropping the productivity of the filtration process is clogging of the pores.

The research objects are new, both-sided irradiated 20- μ m-thick track-etched membrane [25] and a standard 12- μ m-thick membrane. Productivity and efficiency of water purification process using 20- μ m-thick track-etched membrane was studied in [13].

The aim of this study is comparing the effectiveness of back-flushing and regeneration of these membranes during the filtration of natural water containing impurities, capable to be retained by the pores of membranes.

To achieve this goal, it was necessary to solve the following tasks:

1. Determine the distribution of impurity particles over size in the samples of studied water sources;
2. Carry out experiments of water samples filtering on the compared membranes in a dead-end mode; identify the mechanisms underlying the decrease of filtration productivity;
3. Compare the possibility of recovering the filtration productivity on both membranes by backwashing with distilled water and chemical regeneration;
4. Check the possibility of coagulation by aqua-aurate of colloidal impurities of studied natural waters to a size exceeding membranes pore size.

2. Methods and Materials

Experiments on backwashing and regeneration were carried out on two track-etched membranes. On the new both-sided irradiated track-etched membrane based on 20- μm -thick polyethylene terephthalate film received by irradiation of argon ions with the mileage less than the film thickness, with a pore diameter 0.22 μm , a pore density $1.5 \times 10^8 \text{ cm}^{-2}$. And on a standard 12- μm thick track-etched membrane with a pore diameter 0.205 μm , a pore density of $2.3 \times 10^8 \text{ cm}^{-2}$.

The filtration was carried out on water samples from pond "Zenit" near "Zenit Sports Games Palace" (St. Petersburg, Butlerova street, 9) and the Volhov River near the Podol village (Volhov district).

Before carrying out experiments on natural water, an experiment on the possibility of flushing the membrane by distilled water filtration was carried out. In this experiment, distilled water was first conducted in the forward direction, and then the membrane was washed, by filtering in the opposite direction.

The studies were conducted in a dead-end mode, because: it allows to determine the reason of productivity dropping and to ensure the clogging of pores with a smaller volume of sample faster than in the tangential mode. The pressure was maintained constant at 0.3 atm.

For flushing and regeneration, a dead-end model in a cell with filtration area 25.5 cm^2 and a volume 200 cm^3 was used. In the experiments of raw natural water, filtrates, and samples after flushing and regeneration, the following methods and instruments were used:

- Spectrophotometry and spectroturbidimetry methods (for determination concentrations of individual components) on KFK-3.01 photoelectrocolorimeter, SF-56 spectrophotometer;
- Dynamic light scattering - a dispersion analysis of nature water was performed on a Zetatrac laser analyser [26];

Filtration productivity G , $\text{cm}/(\text{c} \cdot \text{bar})$, was determined by the formula (1):

$$G = \frac{V}{t \cdot P \cdot S}, \quad (1)$$

where V – volume of the sample, cm^3 ; t – sampling time, s; P – pressure, bar; S – filtration area, cm^2 .

3. Results and Discussion

Experiments on determination of particle size distribution are represented in Figures 1–4.

The obtained results show that the most of suspended impurities in the water samples from Volhov River has a size from 60 to 250 μm (Fig. 2), and in the Zenit pond – from 45 to 150 μm (Fig. 4). Water samples from both water bodies contains an insignificant fraction of large particles (noticeable only in the analysis of the intensity distributions (Figs. 1 and 3).

These results show that water samples from both water bodies mostly contains suspended impurities smaller than the pore size, which could clog the membranes pores. The smallest impurities could be adsorbed in the pores of track-etched membranes.

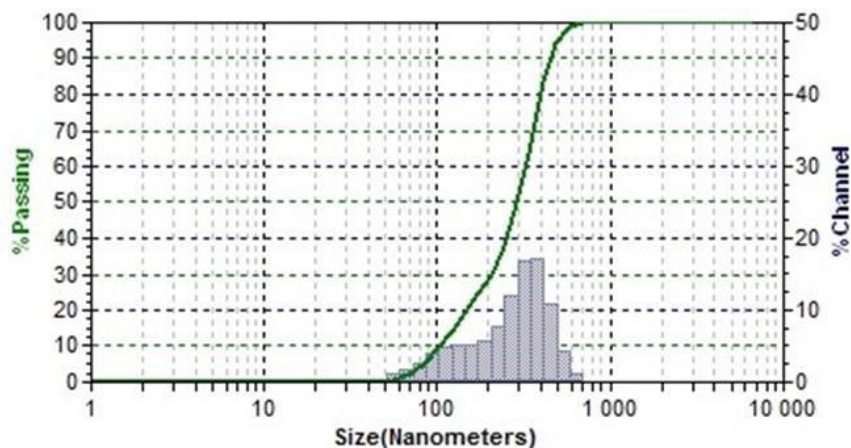


Figure 1. Intensity distributions over particle sizes for water sample from Volhov River

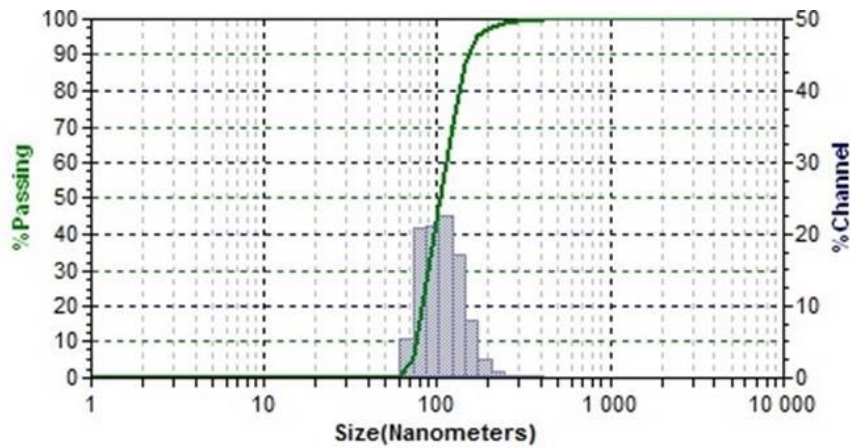


Figure 2. Number distributions over particle sizes for water sample from Volhov River

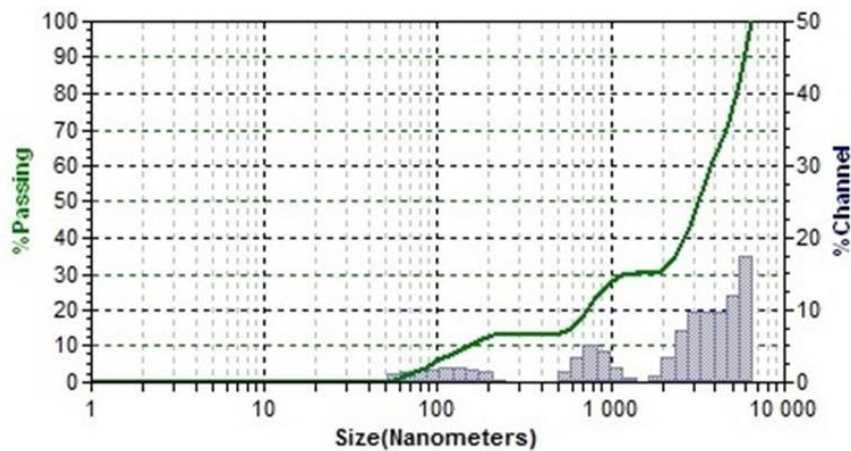


Figure 3. Intensity distributions over particle sizes for water sample from a pond "Zenit"

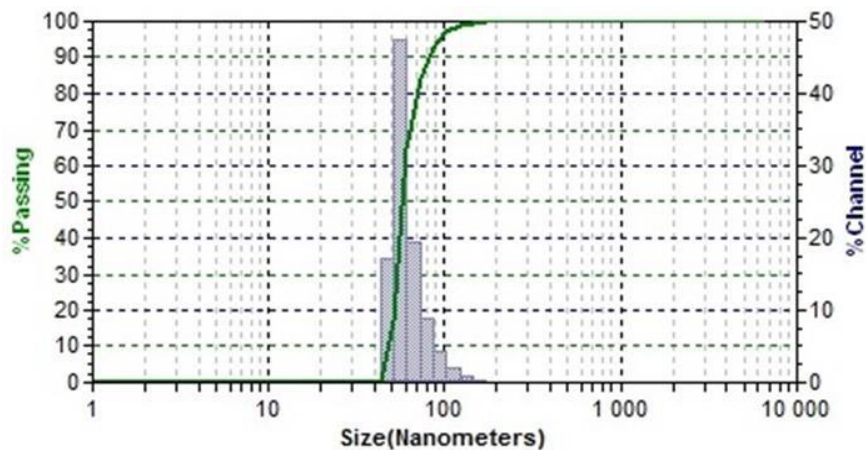


Figure 4. Number distributions over particle sizes for water sample from a pond "Zenit"

The results of filtration the water samples from both sources through the track-etched membranes are shown in Figure 5. It could be seen that the productivity of filtration falls quickly while filtering water samples with small impurity particles. After productivity dropped by 10–15 times, the membranes were flushed with distilled water in reverse direction. After filtration of water samples from the pond Zenit, the productivity has not recovered, but after filtration of water from the Volhov River – the membrane's productivity was restored to 1/3 of the initial value.

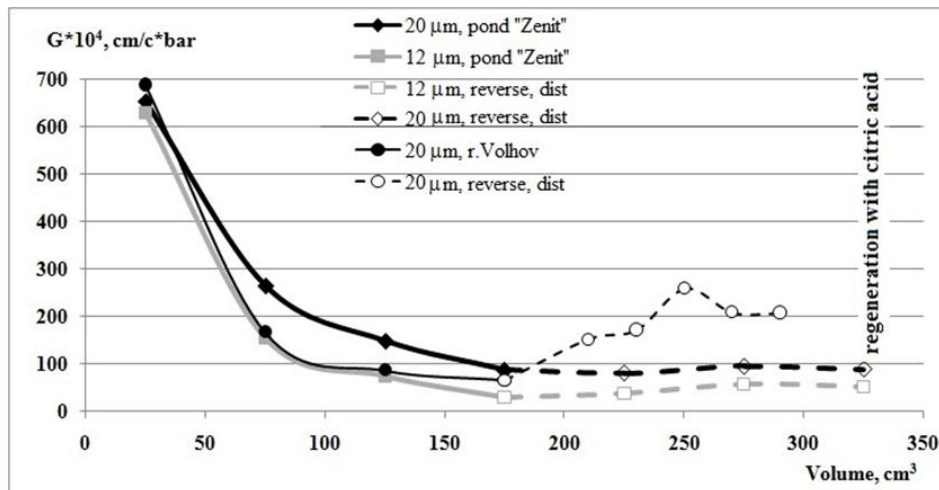


Figure 5. Dependences of the productivity of dead-end filtration water from pond "Zenit" and river Volhov through 12- μm -thick and 20- μm -thick membranes, and reverse washing of these membranes with distilled water

To explain the different results of reverse flushing (of both-sided irradiated membrane) after filtration of the water samples from the pond Zenit and r. Volhov the dependencies of the square of the reverse productivity on the time of filtration were built and analyzed (Fig. 6).

The obtained graphs (Fig. 6) were compared with the theoretical ones (Fig. 7) [19]. It was concluded that in the water samples from the Volhov River the pore blocking mechanism dominates, and for water samples from the Zenit pond adsorption in the pores dominates. These conclusions correspond to the particle size distribution in these waters and explain the greater efficiency of reverse washing for water samples from the Volhov River.

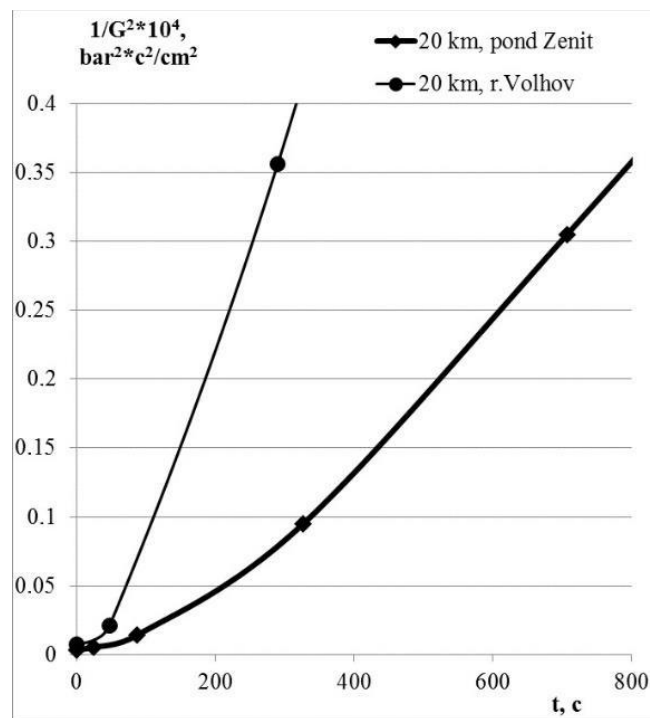


Figure 6. The initial section of the dependences of the reverse productivity on time through the both-sided irradiated membrane

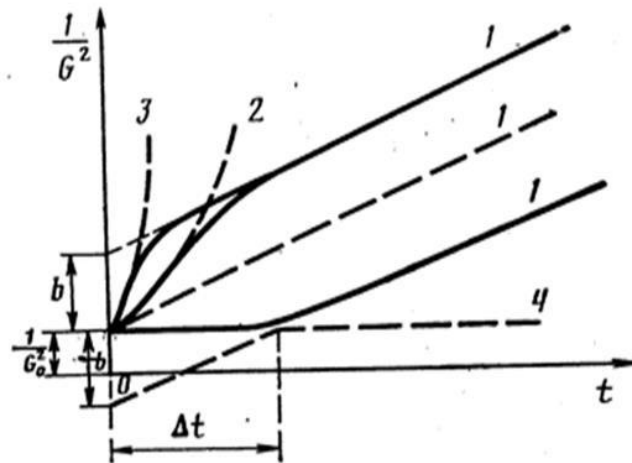


Figure 7. Dependences of the square of the reverse productivity on time, corresponding to:
1 – formation of a precipitate on the membrane surface; 2 – adsorption in pores;
3 – blockage of pores; 4 – pregel polarization [19]

For 12 and 20- μm -thick track-etched membranes after filtration of water samples from the Zenit pond and ineffective backwashing with distilled water, regeneration with citric acid was carried out (Fig. 8).

It could be seen (Fig. 8) that for a both-sided irradiated track-etched membrane, the productivity of filtration increases in 5 times during the regeneration, while for a one-side irradiated standard 12- μm -thick membrane productivity increase less than 2 times.

At the same time, when filtering the source water (from the Zenit pond) through the regenerated membranes, the productivity of the filtration process decreases quickly again.

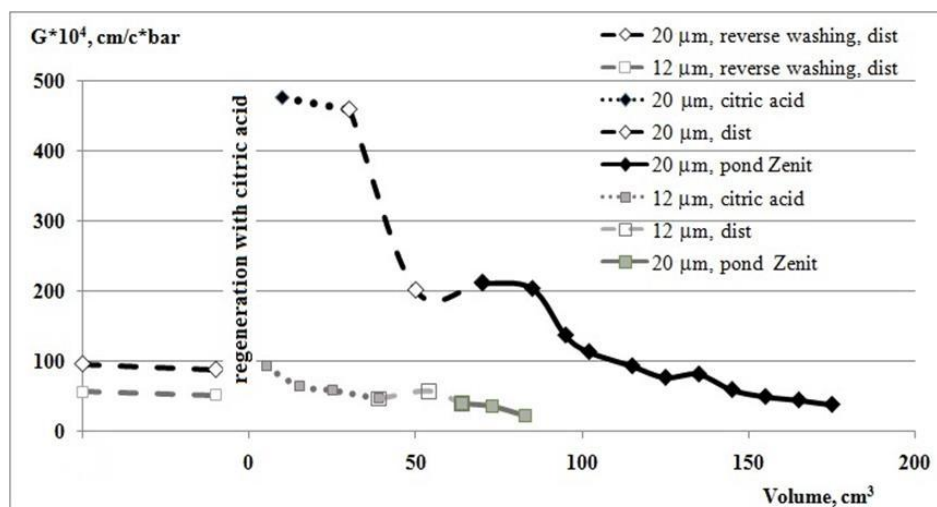


Figure 8. Change in productivity of dead-end filtration after regeneration with citric acid

Hence, for natural waters containing suspended impurities, which size is much smaller than the size of the pores of the track-etched membrane, backwashing and regeneration do not provide a constant productivity. In this case, it is possible to offer preliminary coagulation of suspended impurities [11].

It was shown for track-etched membranes [11], that when cleaning waters with high turbidity and color, an effective method for prevent a drop in filtration productivity and increasing the efficiency of backwashing is to combine the coagulation and microfiltration processes. We tested the effectiveness of preliminary coagulation of colloidal impurities for low-turbidity waters to dimensions exceeding the membrane pore size.

A modern coagulant aqua-aurate based on aluminum oxychloride was used in our experiments. The analysis of the particle size distribution (Figs. 9, 10) showed that within 5–10 minutes after the aqua-aurate addition (concentration of Al_2O_3 was 5 mg/L) a noticeable particles coagulation takes place. In subsequent studies, it is necessary to select the concentration of the coagulant and the time it takes to

enlarge the floccula to a size exceeding $0.2 \mu\text{m}$, not only in terms of "intensity distributions", but also in "number distributions". It allows to receive more efficient process of membrane filtration (of such waters).

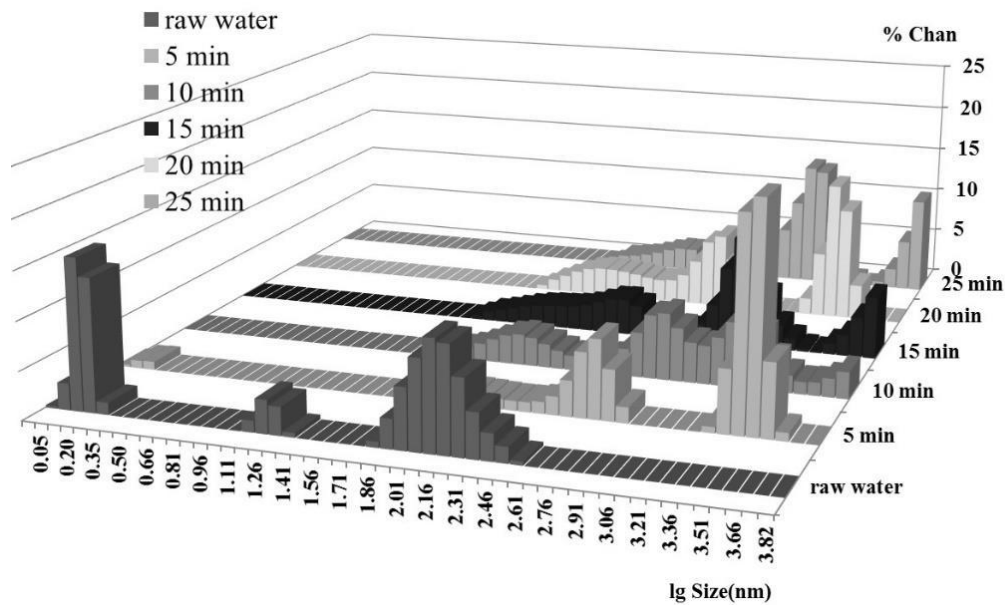


Figure 9. Intensity distributions over particle sizes for water sample from a pond "Zenit"

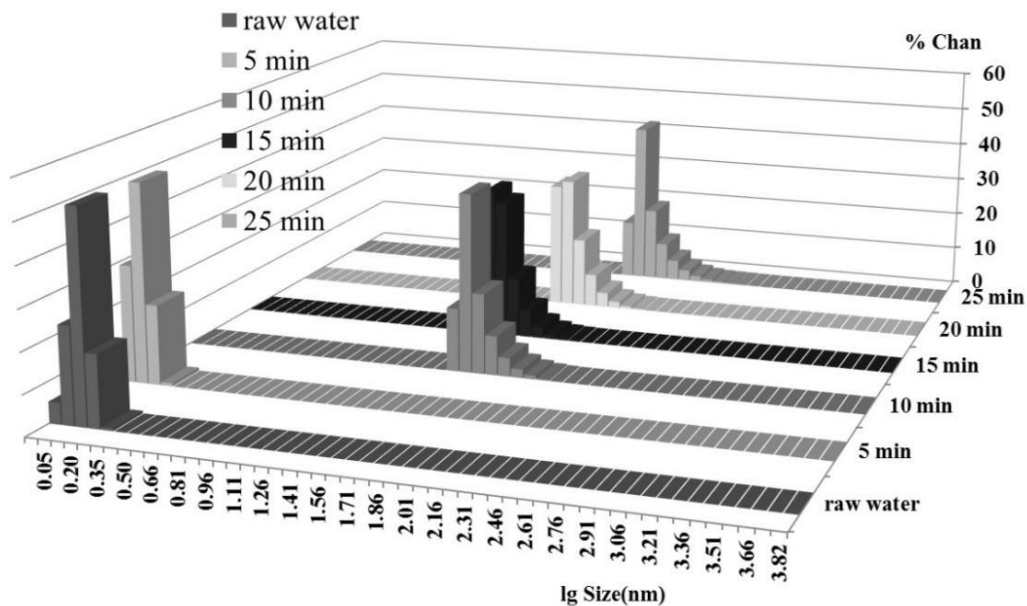


Figure 10. Number distributions over particle sizes for water sample from a pond "Zenit"

4. Conclusions

1. Both-sided irradiated 20- μm -thick membrane with a pore diameter $0.20\text{--}0.205 \mu\text{m}$ has shown advantages over a standard 12- μm -thick membrane in natural water filtration with impurities that block the pores both in the direct filtration process and in flushing and regeneration (with other equal parameters).

2. To prevent pore clogging, preliminary coagulation of impurities can be used.

3. The possibility of regeneration and flushing of the 20- μm -thick membrane allows us to recommend this membrane for natural water purification for local water supply in such objects of civil engineering as individual buildings.

Reference

1. Onishchenko G.G. Problemy kachestva pitevoy vody v Rossiyskoy Federatsii i puti ikh resheniya [Problems of drinking water quality in the Russian Federation and ways to solve them]. *Vodosnabzheniye i sanitariya*. 2010. No. 12. Pp. 5–8. (rus)
2. Shvortsov L.S., Zhmur N.S. Sovremennoye sostoyaniye i perspektivy uluchsheniya vodosnabzheniya v Rossiyskoy Federatsii [Current state and prospects for improving water supply in the Russian Federation]. *Vestnik Rossiyskoy Akademii yestestvennykh nauk*. 2010. No. 3. Pp. 35–39. (rus)
3. Lapshin A.P., Ignatyeva L.P. Sostav pitevoy vody na etapakh podgotovki i transportirovki [Composition of drinking water at the stages of preparation and transportation]. *Vodosnabzheniye i sanitarnaya tekhnika*. 2016. No. 6. Pp. 31–35. (rus)
4. Sakanskaya-Gritsay Ye.I. Problemy i perspektivy sovershenstvovaniya vodopodgotovki [Problems and prospects for improving water treatment]. *Tekhniko-Tekhnologicheskkiye problemy servisa*. 2014. No. 3(29). Pp. 88–95. (rus)
5. Kozhevnikov A.B., Petrosyan O.P. Sovremennyye sistemy vodopodgotovki stantsiy tsentralizovannogo vodosnabzheniya [Modern water treatment systems for centralized water supply stations]. *StroyPROFIL*. 2006. No. 2/1. (rus)
6. Ryabchikov B.Ye. Sovremennaya vodopodgotovka [Modern water treatment]. *Izd-vo «DeLi Plyus»*, 2013. 680 p. (rus)
7. Vatin N.I., Chechevichkin V.N., Chechevichkin A.V., Shilova Y., Yakunin L.A. Application of natural zeolites for aquatic and air medium purification. *Applied Mechanics and Materials*. 2014. Pp. 587–589, pp. 565–572.
8. Chechevichkin V.N., Vatin N.I. Specifics of surface runoff contents and treatment in large cities. *Magazine of Civil Engineering*. 2014. Vol. 50(6). Pp. 67–74. (rus)
9. Hanot H. Use of high-technology track-etched polymer membranes in a wide range of industries. *American Biotechnology Laboratory*. 2007. Vol. 25. No. 8. Pp. 24–26.
10. Geise G.M., Lee H.-S., Miller D.J., Freeman B.D., Mcgrath J.E., Paul D.R. Water purification by membranes: the role of polymer science. *Journal of Polymer Science: Part B: Polymer Physics*. 2010. Vol. 48. Pp. 1685–1718.
11. Desyatov A.V., Baranov A.Ye., Kazantseva N.N. Primeneniye rulonnykh mikrofiltratsionnykh elementov [Application of roll microfiltration elements]. *Vodoochistka*. 2012. No. 6. Pp. 24–31. (rus)
12. Desyatov A.V., Baranov A.Ye., Baranov Ye.A., Kakurkin N.P., Kazantseva N.N., Aseyev A.V. Opyt ispolzovaniya membrannykh tekhnologiy dlya oчитки i opresneniya vody [Experience in using membrane technologies for water purification and desalination]. *Khimiya*. 2008. 240 p. (rus)
13. Barashkova P.S., Molodkina L.M., Korovina M.D. Both sided irradiated track membrane in local water supply. *Magazine of Civil Engineering*. 2017. No. 3. Pp. 68–75.
14. Reutov V.F., Dmitriyev S.N. Ionno-trekovaya tekhnologiya [Ion-track technology]. *Rossiyskiy khim. Zhurnal*. 2002. Vol. 46. No. 5. Pp. 74–80. (rus)
15. Apel P. Track etching technique in membrane technology. *Radiation Measurements*. 2001. Vol. 34. No. 1–6. Pp. 559–566.
16. Makkonen-Craig S., Yashina K., Paronen M. Track-etched ultrafiltration polymer membranes produced by light ion irradiation. *Arcada Working Papers*. 2014. No.11. Pp. 1–13.
17. Siddiqui M.U., Arif A.F.M., Bashmal S. Permeability-selectivity analysis of microfiltration and ultrafiltration membranes: effect of pore size and shape distribution and membrane stretching. *Membranes*. 2016. Vol. 6. № 3. P. 40.
18. Mehta A., Zydney A.L. Permeability and selectivity analysis for ultrafiltration membranes // *J. Membranes. Sci.* 2005. Pp. 245–249.
19. Cherkasov A.N., Vlasova O.L., Tsareva S.V., Kolikov V.M., Mchedlishvili B.V. Ultrafiltration on nuclear filters // *Kolloidn. Zh.* 1990. Vol. 52. № 2. Pp. 323–328.
20. Molodkina L.M., Kolosova D.D., Leonova E.I., Kudoyarov M.F., Patrova M.Y., Vedmetkii Y.V. Track membranes in posttreatment of domestic wastewater //

Литература

1. Онищенко Г.Г. Проблемы качества питьевой воды в Российской Федерации и пути их решения // *Водоснабжение и санитария*. 2010. № 12. С. 5–8.
2. Шворцов Л.С., Жмур Н.С. Современное состояние и перспективы улучшения водоснабжения в Российской Федерации // *Вестник Российской Академии естественных наук*. 2010. № 3. С. 35–39.
3. Лапшин А.П., Игнатъева Л.П. Состав питьевой воды на этапах подготовки и транспортировки // *Водоснабжение и санитарная техника*. 2016. № 6. С. 31–35.
4. Саканская-Грицай Е.И. Проблемы и перспективы совершенствования водоподготовки // *Технико-Технологические проблемы сервиса*. 2014. № 3(29). С. 88–95.
5. Кожевников А.Б., Петросян О.П. Современные системы водоподготовки станций централизованного водоснабжения // *СтройПРОФИль*. 2006. № 2/1
6. Рябчиков Б.Е. Современная водоподготовка. Изд-во «ДеЛи Плюс», 2013. 680 с.
7. Vatin N.I., Chechevichkin V.N., Chechevichkin A.V., Shilova Y., Yakunin L.A. Application of natural zeolites for aquatic and air medium purification // *Applied Mechanics and Materials*. 2014. Pp. 587–589, pp. 565–572.
8. Чечевичкин В.Н., Ватин Н.И. Особенности состава и очистки поверхностного стока крупных городов // *Инженерно-строительный журнал*. 2014. №6(50). С. 67–74
9. Hanot H. Use of High-Technology Track-Etched Polymer Membranes in a Wide Range of Industries // *American Biotechnology Laboratory*. 2007. Vol. 25. № 8. Pp. 24–26.
10. Geise G.M., Lee H.-S., Miller D.J., Freeman B.D., Mcgrath J.E., Paul D.R. Water purification by membranes: the role of polymer science // *Journal of Polymer Science: Part B: Polymer Physics*. 2010. Vol. 48. Pp. 1685–1718.
11. Десятов А.В., Баранов А.Е., Казанцева Н.Н. Применение рулонных микрофильтрационных элементов // *Водоочистка*. 2012. № 6. С. 24–31.
12. Десятов А.В., Баранов А.Е., Баранов Е.А., Какуркин Н.П., Казанцева Н.Н., Асеев А.В. Опыт использования мембранных технологий для очистки и опреснения воды // *Химия*. 2008. 240 с.
13. Барашкова П.С., Молодкина Л.М., Коровина М.Д. Двусторонне облученные трековые мембраны в локальном водоснабжении // *Инженерно-строительный журнал*. 2017. № 3(71). С. 68–75.
14. Реутов В.Ф., Дмитриев С.Н. Ионно-трековая технология // *Российский хим. Журнал* 2002. 46. № 5. С. 74–80.
15. Apel P. Track etching technique in membrane technology // *Radiation Measurements*. 2001. Vol. 34. № 1–6. Pp. 559–566.
16. Makkonen-Craig S., Yashina K., Paronen M. Track-etched ultrafiltration polymer membranes produced by light ion irradiation // *Arcada Working Papers*. 2014. № 11. Pp. 1–13.
17. Siddiqui M.U., Arif A.F.M., Bashmal S. Permeability-selectivity analysis of microfiltration and ultrafiltration membranes: effect of pore size and shape distribution and membrane stretching // *Membranes*. 2016. Vol. 6. № 3. P. 40.
18. Mehta A., Zydney A.L. Permeability and selectivity analysis for ultrafiltration membranes // *J. Membranes. Sci.* 2005. Pp. 245–249.
19. Cherkasov A.N., Vlasova O.L., Tsareva S.V., Kolikov V.M., Mchedlishvili B.V. Ultrafiltration on nuclear filters // *Kolloidn. Zh.* 1990. Vol. 52. № 2. Pp. 323–328.
20. Molodkina L.M., Kolosova D.D., Leonova E.I., Kudoyarov M.F., Patrova M.Y., Vedmetkii Y.V. Track membranes in posttreatment of domestic wastewater //

- No. 3. P. 40.
18. Mehta A., Zydney A.L. Permeability and selectivity analysis for ultrafiltration membranes. *J. Membranes. Sci.* 2005. Pp. 245–249.
19. Cherkasov A.N., Vlasova O.L., Tsareva S.V., Kolikov V.M., Mchedlishvili B.V. Ultrafiltration on nuclear filters. *Kolloidn. Zh.* 1990. Vol. 52. No. 2. Pp. 323–328.
20. Molodkina L.M., Kolosova D.D., Leonova E.I., Kudoyarov M.F., Patrova M.Y., Vedmetkii Y.V. Track membranes in posttreatment of domestic wastewater. *Petroleum Chemistry.* 2012. Vol. 52. No. 7. Pp. 487–493.
21. Goryachiy N.V., Svitsov A.A., Mardanyan M.M., Rummyantseva G.N., Varfolomeyeva O.A. O prirode zagryazneniy membran v protsesse koncentrirrovaniya pektinovykh ekstraktov [On the nature of contamination of membranes in the concentration of pectic extracts]. *Kriticheskiye tekhnologii. Membrany.* 2002. No. 2(18). Pp. 40. (rus)
22. Klyuchnikov A.I., Potapov A.I., Polyanskiy K.K., K voprosu regeneratsii membran v protsessakh mikro- i ultrafiltratsii tekhnologicheskikh zhidkostey pishchevykh proizvodstv [To the question of membrane regeneration in the processes of micro- and ultrafiltration of technological fluids in food production]. *Vestnik Tambovskogo universiteta. Seriya Yestestvennyye i tekhnicheskiye nauki.* 2016. Vol. 21. No. 1. Tekhnika. Pp. 312–315. (rus)
23. Balandina A.G., Khangildin R.I., Ibragimov I.G., Martyasheva V.A. Razvitiye membrannykh tekhnologiy i vozmozhnost ikh primeneniya dlya ochistki stochnykh vod predpriyatiy khimii i neftekhimii [Development of membrane technologies and the possibility of their use for wastewater treatment of chemical and petrochemical enterprises]. *Elektronnyy nauchnyy zhurnal «Neftegazovoye delo».* 2015. No. 5. Pp. 336–375. (rus)
24. Prokofyeva Yu.V., Maksimova N.N., Kazantseva N.N. Pochitalkina I.A. Regeneratsiya trekovykh membran khimicheskimi metodami [Regeneration of track membranes by chemical methods]. *Uspekhi v khimii i khimicheskoy tekhnologii.* 2009. Vol. XXII. No. 10(103). Pp. 45–49. (rus)
25. Kudoyarov M.F., Kozlovskii M.A., Patrova M.Ya., Potokin I.L., Ankudinov A.V. Track membranes based on a 20- μ m-thick polyethylene terephthalate film obtained with a beam of argon ions having a range shorter than the film thickness. *Technical Physics Letters.* 2016. Vol. 42. No. 7. Pp. 704–707.
26. Zetatrac Nanotechnology Particle Charge and Size Analyzer [Online]. System requirements: AdobeAcrobatReader. URL: http://www.betatekinc.com/pdf/microtrac_zetatrac.pdf (Date of retrieval 01.10.2016)
27. Andrianova M.J., Bondarenko E.A., Krotova E.O., Chusov A.N. Comparison of chemical and optical parameters in monitoring of urban river Okhta. *EESMS 2014 - Workshop on Environmental, Energy and Structural Monitoring Systems, Proceedings.* 2014. Pp. 198–202.
- Petroleum Chemistry.2012.Vol. 52. № 7. Pp. 487–493.
21. Горячий Н.В., Свитцов А.А., Марданян М.М., Румянцева Г.Н., Варфоломеева О.А. О природе загрязнений мембран в процессе концентрирования пектиновых экстрактов // Критические технологии. Мембраны. 2002. № 2(18). С. 40.
22. Ключников А.И., Потапов А.И., Полянский К.К. К вопросу регенерации мембран в процессах микро- и ультрафильтрации технологических жидкостей пищевых производств // Вестник Тамбовского университета. Серия Естественные и технические науки. 2016. Т. 21. № 1. Техника. С. 312–315.
23. Баландина А.Г., Хангилдин Р.И., Ибрагимов И.Г., Мартяшева В.А. Развитие мембранных технологий и возможность их применения для очистки сточных вод предприятий химии и нефтехимии // Электронный научный журнал «Нефтегазовое дело». 2015. № 5. С. 336–375.
24. Прокофьева Ю.В., Максимова Н.Н., Казантсева Н.Н. Почиталкина И.А. Регенерация трековых мембран химическими методами // Успехи в химии и химической технологии. 2009. Т. XXII. № 10(103). С. 45–49.
25. Kudoyarov M.F., Kozlovskii M.A., Patrova M.Ya., Potokin I.L., Ankudinov A.V. Track membranes based on a 20- μ m-thick polyethylene terephthalate film obtained with a beam of argon ions having a range shorter than the film thickness // Technical Physics Letters. 2016. Vol. 42. No. 7. Pp. 704–707.
26. Zetatrac Nanotechnology Particle Charge and Size Analyzer [Электронный ресурс]. Систем. требования: AdobeAcrobatReader. URL: http://www.betatekinc.com/pdf/microtrac_zetatrac.pdf (дата обращения: 01.10.2016).
27. Andrianova M.J., Bondarenko E.A., Krotova E.O., Chusov A.N. Comparison of chemical and optical parameters in monitoring of urban river Okhta // EESMS 2014 - Workshop on Environmental, Energy and Structural Monitoring Systems, Proceedings. 2014. Pp. 198–202.

Polina Barashkova,
+7(921)093-23-94; barashkova.p.s@yandex.ru

Ludmila Molodkina,
+7(921)923-38-31; asminaster@gmail.com

Полина Сергеевна Барашкова,
+7(921)093-23-94;
эл. почта: barashkova.p.s@yandex.ru

Людмила Михайловна Молодкина,
+7(921)923-38-31;
эл. почта: asminaster@gmail.com

© Barashkova P.S., Molodkina L.M., 2018

doi: 10.18720/MCE.77.11

Lightweight concrete based on siliceous compositions of natural origin

Легкий бетон на основе кремнистых композиций природного происхождения

*L.V. Zakrevskaya,
A.A. Gavrilenko,
S.N. Avdeev,
I.A. Gandelsman,
A.V. Kireev,*

*Vladimir State University named after Alexander
and Nikolay Stoletovs, Vladimir, Russia*

Канд. техн. наук, профессор

Л.В. Закревская,

студент А.А. Гавриленко,

канд. техн. наук, директор С.Н. Авдеев,

канд. техн. наук, доцент И.А. Гандельсман,

канд. техн. наук, доцент А.В. Киреев,

Владимирский Государственный

Университет имени Александра

Григорьевича и Николая Григорьевича

Столетовых, г. Владимир, Россия

Key words: concrete; magnesia binder; alkali-silicate reaction

Ключевые слова: бетон; магнезиальное вяжущее; щелочно-силикатная реакция

Abstract. The focus in the release of construction materials is determined by waste recycling, saving energy costs and environmental management by means of reducing dump areas. The production of magnesia binders from dolomite waste meets all these requirements. There was made an effort to create a new material based on magnesia binder and lightweight silicate aggregate made from tripolith of Vladimir region deposit. In the course of the work, samples were synthesized and tested for strength and thermal conductivity, and also an optimal granulometric composition of the aggregate was defined. This research shows that the material is strong, cheap, alkali-silicate corrosion resisting and very promising in compare with classic Portland cement concretes.

Аннотация. Приоритет в выпуске строительных материалов определяется использованием отходов промышленности, снижением энергоемкости и решением экологических проблем за счет сокращения площадей занятых отвалами. Всем этим требованиям отвечает производство магнезиальных вяжущих из отходов доломитового производства. Была предпринята попытка создать новый материал на основе магнезиального вяжущего и легкого силикатного заполнителя, изготовленном из трепела Владимирского месторождения. В ходе работы были синтезированы образцы, которые были испытаны на прочность и теплопроводность, а также подобран оптимальный гранулометрический состав заполнителя. Исследование показывает, что материал является прочным, дешевым, стойким к щелочно-силикатной коррозии и очень перспективным по сравнению с классическими бетонами на основе портландцемента.

1. Introduction

Nowadays, the problem of high cost of housing is quite relevant for people of almost all countries in the world. At the same time, there are a lot of dolomite waste dumps in many countries including Russia. That is why magnesia concrete made from dolomite production waste was chosen as an object of this research. The works of P.P. Budnikov, M.I. Kuzmenkov, TN. Chernykh[1], A.E. Ivanov and many others[2, 3] are devoted to the issues of magnesia binders. The purpose of this work is to try to create cheap high-quality construction material from dolomite waste and reduce volumes of dolomite waste dumps.

The production of magnesia cements does not hold a prominent place in the national construction sector, which is completely unjustified by any arguments, because magnesia cements have exceptional distinct properties in strength, abrasion, and bactericidal power. Besides, their production history and applications are centuries old.

Unlike magnesia concretes, cement ones as well as Portland cement mortars are known to have a delayed hardening, nonhomogeneous composition and conglomerate structure. Therefore, traditional concretes do not meet modern standards for abrasion and crack resistance. Being formed in the process of hydration, crystalline and colloidal newgrowths dry up and thicken over time, which is followed by the cement shrinkage[4–6].

Calcium hydroxide belongs to one of the silicate mineral products (alite and belite) which interact with water. It means that as a result of hardening, an alkaline medium always appears in a cement stone. This phenomenon also has its pros and cons. As it is known, there is no iron corrosion in an alkaline medium. Therefore, concretes based on Portland cement (and its varieties) protect steel reinforcement from corrosion. This is one of the key factors for high durability of reinforced concrete.

When using magnesia binders in mortars, there forms a dense, non-porous material, having high abrasion, petrol, oil and water resistance[1, 7, 8].

Unlike other binders, magnesia binders have a very high adhesion not only to mineral, but also to organic substances. Due to a high density of the material, low alkalinity and the presence of bischofite in the magnesia cement composition, the organic fillers do not rot in them. This fact makes it possible to make a hypothesis concerning bactericidal power and mold and fungus resistance of materials based on magnesia binders.

The use of magnesium salts as grouting fluid changes the hardening mechanism [9]. High concentration of magnesium salts promotes the formation of complex salts of various composition: $MgCl_2 \cdot 5MgO \cdot 17H_2O$ (Sorel, 1867), $MgCl_2 \cdot 5MgO \cdot 8H_2O$ (Bender, 1871), $MgCl_2 \cdot 3MgO \cdot 10H_2O$ (Robinson and Wagman, 1909), $MgCl_2 \cdot 3MgO \cdot 7H_2O$ (Larman, 1911). Due to the formation of such compounds, magnesium hydroxide is removed from the solution, and new portions of magnesium oxide undergo a hydration reaction [10].

Table 1 presents the comparative analysis of Portland- and magnesia cements.

Table 1. Comparative analysis of Portland- and magnesia cements

Characteristics	Type of cement	
	Magnesia cement	Portland cement
Total composition	$3MgO \cdot MgCl_2 \cdot 11H_2O$	$12CaO \cdot 6SiO_2 \cdot 7H_2O$
Structural formula	$[Mg_4^{2+}(OH)_6^-(H_2O)_6]^{2+}Cl_2^- \cdot 2H_2O$	$Ca[Si_6O_{17}](OH)_{14}$ (hillebrandite)
Crystal structure	Roughly anisodesmic, formed by doubled chains of octahedra Mg (OH, H ₂ O) 6, connected by chlorine ions and water molecules	Quasi-coordinated, poorly anisodesmic, band, represented by alternation of xonotlitic and portlandite elements: $Ca[Si_6O_{17}](OH)_2 \cdot 6Ca(OH)_2$
Macrostructure	Felted structure	Massive structure
Density ρ , g / m ³	1.86	2.69
Fragility HV (GPa)/ K _{1c}	0.5	3.8
Thermal conductivity λ , W / (m · K)	0.5–1.6	1.3–1.8
Compressive strength, σ_p , MPa	50–120	3.5–80

Unlike Portland cement, magnesia cement does not create an alkaline medium i.e. the solubility of magnesium hydroxide is insignificant, and its basic properties are not strong. So magnesia concrete eliminates alkali-silicate reaction in concrete, which can destroy the body of the concrete and promotes the formation of cracks, especially with a large-sized aggregate [11,12,13,14,15,16]. Organic aggregates are not destroyed in a neutral medium. In addition, magnesia cement prevents the development of microorganisms that can destroy the aggregate. The application of magnesium chloride solutions, which are considered to be good fire-resistant impregnations, makes these materials fire-proof[10].

The advantages of magnesian concretes are:

- Higher adhesion to different substrates (up to 3 MPa);

- High shrink resistance. Consequently, magnesia concrete does not crack. This fact gives an advantage when arranging the surface cast: it becomes possible to create coatings on large areas without functional joints;
- Abrasive resistance and lack of dust. High-strength magnesia concretes do not raise dust throughout their entire thickness;
- Compressive strength is higher than 50 MPa. Following 3 months' operation, the magnesia concrete strength increases up to 80–120 MPa. This characteristic makes it possible to use magnesia concretes in workshops with high dynamic loads;
- Fast strength generation within a short time. At the age of 1 day the strength of concretes and mortars reaches 30–50 %, and at the age of 7 days 60–90 % of the maximum possible strength. High speed of hardening and strength generation makes it possible to use the structures a few hours after the casting;
- Oil and petrol resistance due to a dense structure with closed pores;
- Anti-electrostatic properties. The fact that magnesia concretes do not accumulate static electricity makes this material essential in premises with a large number of electrical devices (computers, motors, transformers, etc.).

Consequently, magnesia concrete is of better quality compared to the traditional Portland cement according to such characteristics as strength, abrasive resistance, good adhesion, high hardening speed, lack of shrinkage, and many other properties.

On top of that, magnesia binders are inert to different silica-containing materials. This property makes it possible to produce concretes based on a magnesia binder with a silica-containing aggregate, whereas Portland cement reacts with the aggregate silicates. This leads to an alkali-silicate interaction that destroys concrete body [10].

For the first time ever the main characteristics of alkaline-silicate reactions were described by Stanton. Hydroxide ions in a pore solution react with certain types of silica placed in an aggregate. This leads to internal stresses that can cause fracture or crack propagation [17]. Fracture can occur within a few days or only many years later. On the surface of non-prestressed concrete they normally form a small crack network and sometimes large cavity pockets. In prestressed concrete cracks tend to propagate parallel to the reinforcement. On the thin sections there can be seen cracks that can propagate through the aggregate. Silica gel is allocated from concrete and resides in cracks in the form of shells around the aggregate particles or elsewhere in the paste. High content of alkali metal oxides in cement, reactive component in the aggregate and access to water are necessary conditions for alkaline-silicate reactions in Portland cement concrete. K + and Na + ions are present in the cement in the form of sulfates and in silicate and aluminate phases. On reaction with compounds containing these ions, their anions enter the products with low solubility, for example ettringite, C-S-H or AFm-phase, and simultaneously an equivalent amount of OH-. K + and Na + ions play a negative role at this stage, because their hydroxides are soluble, which allows OH- to pass into the pore space [18].

The authors of the given article have made an effort to synthesize lightweight concrete on the basis of both traditional foam glass and lightweight aggregate made of silicon-containing natural materials, such as tripolith and diatomite.

These rocks have been called siliceous due to their high silica content, SiO₂ content in them varies from 50 up to 90 %. The second necessarily present oxide is Al₂O₃. They represent light fine-porous powders, composed of the smallest opal fragments of diatomic algae and crystalalite as well as clay minerals[19].

Table 2 represents tripolith composition of the Vladimir region.

Table 2. Chemical composition of tripolith in the Vladimir region

Chemical compounds	SiO ₂ , %	Al ₂ O ₃ , %	Fe ₂ O ₃ , %	CaO, %	MgO, %	SO ₃ , %
Quantity	73 - 89	3.8 – 15.6	0.3 – 5.3	0.5 – 2.5	0.4 – 1.9	0 -1.6

This material possesses the following physical properties:

- Porosity 50-70, (%)
- Hardness 1-3, (Mohs scale)
- Thermal conductivity 0.17-0.23, (W / (m · ° C)).

In construction and construction industry siliceous rocks are used in the form of manufactured objects (blocks, stones), crushed products (crushed stone), ground products (hydraulic additives, fillers), in the form of raw materials for the production of sintered (agloporite, sintered aggregate, lightweight bricks, wall and heat-insulating materials), foamed (expanded-clay and siliceous gravel and sand) and molten materials (glass, glaze, glass float, etc.).

In 1960s of the 20th century, on the basis of sintering processes there were launched studies on siliceous rocks with the aim to use siliceous rocks as raw materials for concrete aggregates. In the result of these studies it was established that in siliceous rocks, in the process of the aggregate production by calcination, sintering takes place more often than foaming. The obtained aggregate was used as a heat insulating material due to its microporosity. Numerous diverse studies on physical, technical and technological properties of sedimentary siliceous rocks made it possible to obtain an aggregate based on a gaize called "thermolite".

In central regions of the European Russia (including the Vladimir region) there are numerous deposits of tripolith and gaize with a productive layer from 16 up to 27 meters.

2. Methods

In the course of the given study there was synthesized a lightweight aggregate (figuratively called "diapen") based on the tripolith and diatomite of the Zheldobinsk deposit.

The production technology of "diapen" includes the following stages:

- excavated tripolith is crushed to powder
- alkaline component is added to the obtained powder
- the obtained powder is moistened and mixed to a ductile mass
- raw granules are being formed
- granules are pelletized and sintered in a rotating kiln

The obtained granules were tested for strength, thermal conductivity, water absorption. The results are presented in Table 3.

Table 3. Diapen physical and technical properties

Density, kg / m ³	Strength, MPa	Thermal conductivity, W/(m·°K)	Water absorption,% vol	Fire resistance
200-500	4-7	0.05-0.08	5-7	Non-flammable

The prime cost of tripolith excavation is not high, that's why "diapen" is almost twice cheaper than its closest competitor i.e. expanded clay and 5 times cheaper than a foam glass.

To determine the optimum grain particle size with the maximum use of the lightweight aggregate, and to achieve the maximum thermal conductivity coefficient while maintaining sufficient structural strength there was used Andreassen-Andersen formula

$$P(D) = \frac{D^q - D_{min}^q}{D_{max}^q - D_{min}^q}$$

where P(D) is the total share of the solid matter with the particles smaller than D, D is the particle size (micron), D_{max} and D_{min} are respectively the largest and smallest particle sizes (micron) in the mix, q is the distribution modulus.

Table 4 shows the grain particle size of the aggregate when selecting the optimal casting density for concrete.

Table 4. Grain particle size of the fine aggregate to achieve maximum casting density

Grain size, mm	Grain particle size of "diapen", %vol						
	C-1	C-2	C-3	C-4	C-5	C-6	C-7
5 – 2.5	65	65	65	65	65	70	70
2.5 – 1.5	5	10	10	15	20	5	10
1.5 – 1.0	10	5	10	10	5	5	10
1.0 – 0.5	20	20	15	10	10	20	10

After carrying out the tests, it was found that the composition C-1 has the optimal grain size ratio.

In this work there were synthesized lightweight concretes based on the investigated types of binders and aggregates. Compositions for lightweight concretes based on the magnesia binder and diapen are presented in Table 5.

Table 5. Compositions for lightweight concrete

Concrete grade	Components, % _{mass}			
	Semi-sintered dolomite waste	Diapen	Bishofite	Water
M-1	50	15	30	Rest
M-2	55	10	30	Rest
M-3	55	5	35	Rest
M-4	65	5	25	Rest

3. Results and Discussion

The obtained compositions were tested for mechanical and thermophysical properties. The results are given in Table 6.

Table 6. Mechanical and thermophysical properties of light concretes

Concrete grade	Characteristics		
	Strength, MPa	Thermal conductivity, W/(m·°K)	Density, kg / m ³
M-1	28	0.25	540
M-2	30	0.30	600
M-3	30	0.33	610
M-4	25	0.34	600

As it can be seen from Table 6, the composition M-1 has the optimum operational characteristics.

Tests on alkali-silicate interaction indicate that magnesia concretes do not undergo corrosion when using a silicate-containing aggregate. The results are shown in Figure 1.



Figure 1. Samples after the accelerated test on alkali-silicate interaction

Figure 2 illustrates samples of lightweight concretes based on the magnesia cement and light silicate aggregates.



Figure 2. Sample section of lightweight concrete based on the magnesia binder

The mineralogical and chemical composition of the synthesized concretes was determined by X-ray diffraction analysis on the diffractometer "D8 Advance" Bruker AXS (Germany) with the following shooting conditions: copper X-ray tube (CuK α -radiation), with a nickel filter. The voltage on the X-ray tube was 40 kW, current strength 40 mA, exposure 0.6 hours, sample diameter 10 mm.; the rotational speed of the goniometer was 4 degrees/min.; response time 1.0 sec; rate of pulses 1·10⁴ imp. / sec.

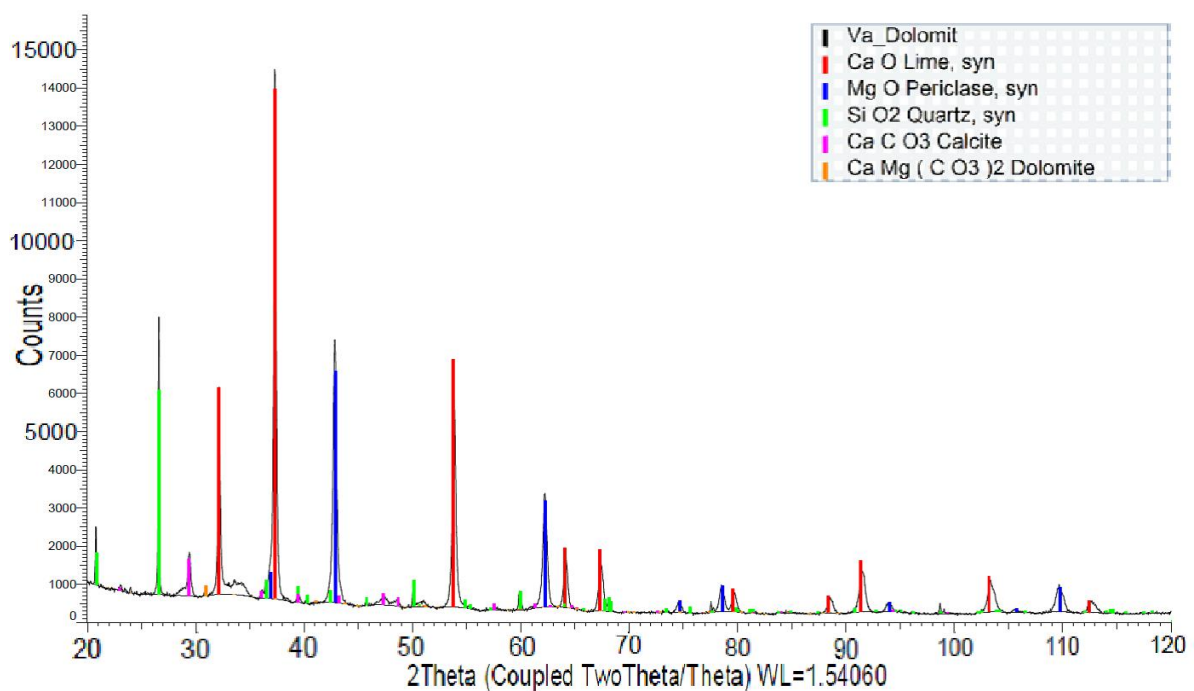


Figure 3 X-ray diffraction pattern and a pie chart of magnesia concrete phase composition

X-ray study of concrete magnesium matrix showed that the sample is periclase (magnesium oxide) MgO with a cubic structure, space group Fm-3 and a lattice size of 4.21 Å.

Figure 4 illustrates the microstructure of magnesia concrete, obtained by the scanning electron microscopy.

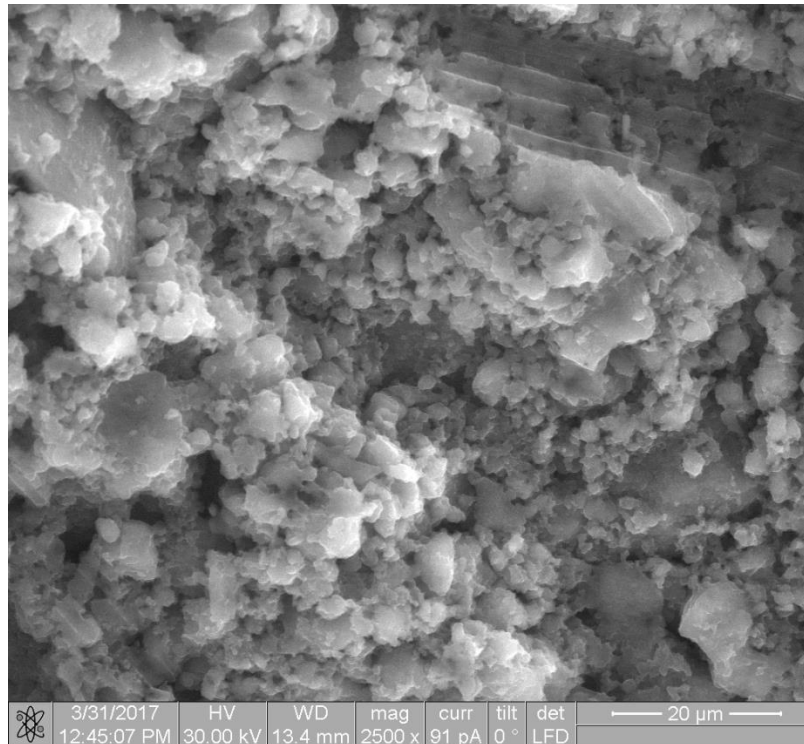


Figure 4 Micrograph of the magnesia composition with "diapen" aggregate

The results obtained during the work indicate that lightweight magnesia concrete synthesized on the basis of dolomite waste has high strength, high water resistance, high adhesion and good thermal insulation performance. The results are in full agreement with the results achieved by leading specialists in this field: M.I. Kuzmenkova, T.N. Chernykh and others.

The research allows to obtain lightweight concrete for solving the problems of "green building", which is now gaining popularity in all countries of the world [20].

4. Conclusions

1. There were developed energy-efficient construction compositions based on the integrated use of dolomite waste and domestic siliceous rocks.
2. There was calculated and selected the composition for lightweight concrete with the highest casting density in accordance with Andreassen-Andersen formula.
3. There were presented comparative characteristics for various types of concrete and made conclusions concerning reasonability of Sorel cement production from dolomite waste.
4. The studies on microstructure and phase analysis of magnesia lightweight concrete showed that the main crystalline phase is periclase.
5. There were developed basic technological parameters for obtaining a lightweight aggregate "diapen" from domestic tripolith and diatomite.
6. There was given practical and theoretical proof for the technology of the new lightweight concrete, eliminating alkali-silicate interaction.

Reference

- Chernykh T.N. Osobennosti tverdeniya magnezialnogo vyazhushchego [Features of hardening magnesia astrigent]. *Tsement i yego primeneniye*. 2006. No. 5. Pp. 58–61. (rus)
- Zvezdina Ye. V., Treskova N.V. Povysheniye vodostoykosti teploizolyatsionnykh izdeliy na osnove kausticheskogo dolomita [Increase of water resistance of heat-insulating products on the basis of caustic dolomite]. *Nauchno-prakticheskiy Internet-zhurnal «Nauka. Stroitelstvo. Obrazovaniye»*. 2011. № 1. (rus)
- Korjakins A., Shakhmenko G., Bajare D., Bumanis G. Application a dolomite waste as filler in expanded clay lightweight concrete. *10th International Conference Modern Building Materials, Structures and Techniques*. 2010. Pp. 156–161.
- Monteiro P.J.M, Metha P.K. Interaction between carbonate rock and cement paste. *Cem. Concr. Res.* 1986. Vol. 16. No. 2. Pp. 127–134.
- Chekhovskiy Yu.V., Spitsyn A.N., Kardash Yu.A., Aliyev A.D., Chalykh A.Ye. Issledovaniye kontaktnoy zony tsementnogo kamnya s krupnym zapolnitelem [Investigation of the contact zone of cement stone with a large aggregate]. *Kolloidnyy zhurnal*. 1988. No. 6. Pp. 1216–1218. (rus)
- Chernykh T., Nosov A., Kramar L. Dolomite magnesium oxychloride cement properties control method during its production. *IOP Conference Series: Materials Science and Engineering*. 2015. Vol. 71. No. 1. Article number 012045
- Chernykh T. Energy-saving magnesium oxychloride cement intensifier. *SGEM International Multidisciplinary Scientific Conference on Social Sciences and Arts*. 2015. Pp. 359–363.
- Chernykh T., Orlov A., Kramar L. Hydration features of magnesium sulfate compositions. *SGEM International Multidisciplinary Scientific Conference on Social Sciences and Arts*. 2015. Pp. 463–468.
- Sizikov A.M., Shapovalova Ye.V. *Puti povysheniya kachestva magnezialnykh betonov*. Monografiya [Ways to improve the quality of magnesia concrete. Monograph]. Omsk: SibADI, 2009. 92 p. (rus)
- Khirono S., Yamada K., Ando Y., Torii K. Problemy, svyazannyye s shchelochekremnezemnoy reaktsiyey, v Yaponii i Tailande [Problems associated with alkali-silica reaction in Japan and Thailand]. *Tsement i yego primeneniye*. 2016. No. 3. Pp. 88–94. (rus)
- Demidovich B.K. *Penosteklo* [Foam glass]. Minsk: Nauka i tekhnika. 1975. 248 p. (rus)
- Nakano K. The mechanism and features of alkali-aggregate reactions. *Concr. J.* 1986. No. 11. Pp. 17–22.
- Baranova M.N., Korenkova S.F., Chumachenko N.G. Istoriya osvoyeniya kremnistykh porod [History of development of siliceous rocks]. *Stroitelnyye materialy*. 2011. P. 72. (rus)
- Ip K., Miller A. Life cycle greenhouse gas emissions of hemp – lime wall constructions in the UK. *Resources, Conserv. Recycl.* 2012. Vol. 69. Pp. 1–9.
- Bachiorrini A., Montanaro L. Alkali-silica reaction in carbonate rocks. *Cem. and Concr., Res.* 1988. No. 5. Pp. 53–80.
- Hobbs D.V., Gutteridge W.A. Particle size of aggregate and its influence upon the expansion caused by the alkali-silica reaction. *Mag. Concr. Res.* 1979. No. 109. Pp. 20–37.
- Tosimiti L. Structural changes of concrete when alkali-aggregate reaction. *Concr.J.* 1988. No. 7. Pp. 50–60.
- Sigemasa K., Micuki K., Kunio T. Volumetric deformations of concrete at alkali-silica aggregate reaction. *Cem. and Concr.* 1981. No. 408. Pp. 8–15.
- Kawamura M. Cracking of concrete at alkali-aggregate

Литература

- Черных Т.Н. Особенности твердения магнезиального вяжущего // Цемент и его применение. 2006. № 5. С. 58–61.
- Звездина Е.В., Трескова Н.В. Повышение водостойкости теплоизоляционных изделий на основе каустического доломита // Научно-практический Интернет-журнал «Наука. Строительство. Образование». 2011. № 1.
- Korjakins A., Shakhmenko G., Bajare D., Bumanis G. Application a dolomite waste as filler in expanded clay lightweight concrete // 10th International Conference Modern Building Materials, Structures and Techniques. 2010. Pp. 156–161.
- Monteiro P.J.M, Metha P.K. Interaction between carbonate rock and cement paste // *Cem. Concr. Res.* 1986. Vol. 16. № 2. Pp. 127–134.
- Чеховский Ю.В., Спицын А.Н., Кардаш Ю.А., Алиев А.Д., Чалых А.Е. Исследование контактной зоны цементного камня с крупным заполнителем // Коллоидный журнал. 1988. № 6. С. 1216–1218.
- Chernykh T., Nosov A., Kramar L. Dolomite magnesium oxychloride cement properties control method during its production // *IOP Conference Series: Materials Science and Engineering*. 2015. Vol. 71 .№ 1. Article number 012045
- Chernykh T. Energy-saving magnesium oxychloride cement intensifier // *SGEM International Multidisciplinary Scientific Conference on Social Sciences and Arts*. 2015. Pp. 359–363.
- Chernykh T., Orlov A., Kramar L. Hydration features of magnesium sulfate compositions // *SGEM International Multidisciplinary Scientific Conference on Social Sciences and Arts*. 2015. Pp. 463–468.
- Сизиков А.М., Шаповалова Е.В. Пути повышения качества магнезиальных бетонов. Монография. Омск: СибАДИ, 2009. 92 с.
- Хироно С., Ямада К., Андо Й., Тории К. Проблемы, связанные с щелоче-кремнеземной реакцией, в Японии и Таиланде // Цемент и его применение. 2016. № 3. С. 88–94.
- Демидович Б.К. Пеностекло. Минск: Наука и техника, 1975. 248 с.
- Nakano K. The mechanism and features of alkali-aggregate reactions // *Concr. J.* 1986. № 11. Pp. 17–22.
- Баранова М.Н., Коренькова С.Ф., Чумаченко Н.Г. История освоения кремнистых пород // Строительные материалы. 2011. С. 72.
- Ip K., Miller A. Life cycle greenhouse gas emissions of hemp – lime wall constructions in the UK // *Resources, Conserv. Recycl.* 2012. Vol. 69. Pp. 1–9.
- Bachiorrini A., Montanaro L. Alkali-silica reaction in carbonate rocks // *Cem. and Concr., Res.* 1988. № 5. Pp. 53–80.
- Hobbs D.V., Gutteridge W.A. Particle size of aggregate and its influence upon the expansion caused by the alkali-silica reaction // *Mag. Concr. Res.* 1979. № 109. Pp. 20–37.
- Tosimiti L. Structural changes of concrete when alkali-aggregate reaction // *Concr.J.* 1988. № 7. Pp. 50–60.
- Sigemasa K., Micuki K., Kunio T. Volumetric deformations of concrete at alkali-silica aggregate reaction // *Cem. and Concr.* 1981. № 408. Pp. 8–15.
- Kawamura M. Cracking of concrete at alkali-aggregate reaction // *Cem. and Concr.* 1984. № 451. Pp. 7-10
- Shinzo N., Kiyoshi Y. Estimation of cracking in concrete at alkali-aggregate reaction // *J.Soc.Mater.Sci.* 1989. №431. Pp.10-17.

Zakrevskaya L.V., Gavrilenko A.A., Avdeev S.N., Gandelsman I.A., Kireev A.V. Lightweight concrete based on siliceous compositions of natural origin. *Magazine of Civil Engineering*. 2018. No. 1. Pp. 121–129. doi: 10.18720/MCE.77.11.

reaction. *Cem. and Concr.* 1984. No. 451. Pp. 7–10.

20. Shinzo N., Kiyoshi Y. Estimation of cracking in concrete at alkali-aggregate reaction. *J.Soc.Mater.Sci.* 1989. No. 431. Pp. 10–17.

Lubov Zakrevskaya,
+7(961)252-60-45; *Lftlhbxcrjt@yandex.ru*

Andrey Gavrilenko,
+7(904)250-91-36; *GavrilenkoAndrew@yandex.ru*

Sergey Avdeev,
+7(4922)47-98-70; *asf_vlgu@mail.ru*

Igor Gandelsman,
+7(910)774-68-00; *sp_vlgu@mail.ru*

Andrey Kireev,
+7(919)002-55-27; *ariant-tp@mail.ru*

Любовь Владимировна Закревская,
+7(961)252-60-45;
эл. почта: *Lftlhbxcrjt@yandex.ru*

Андрей Алексеевич Гавриленко,
+7(904)250-91-36;
эл. почта: *GavrilenkoAndrew@yandex.ru*

Сергей Николаевич Авдеев,
+7(4922)47-98-70; эл. почта: *asf_vlgu@mail.ru*

Игорь Анатольевич Гандельсман,
+7(910)774-68-00; эл. почта: *sp_vlgu@mail.ru*

Андрей Викторович Киреев,
+7(919)002-55-27; эл. почта: *ariant-tp@mail.ru*

© Zakrevskaya L.V., Gavrilenko A.A., Avdeev S.N., Gandelsman I.A., Kireev A.V., 2018

doi: 10.18720/MCE.77.12

Numerical simulation of ventilated facades under extreme climate conditions

Численное моделирование вентилируемых фасадов в экстремальных климатических условиях

*M.R. Petritchenco,
E.V. Kotov,
D.V. Nemova,
D.S. Tarasova,
V.V. Sergeev,
Peter the Great St. Petersburg Polytechnic
University, St. Petersburg, Russia*

*Д-р техн. наук, заведующий кафедрой
М. Р. Петриченко,
аспирант Е.В. Котов,
канд. техн. наук, доцент, директор
центра Д.В. Немова,
ассистент Д.С. Тарасова,
д-р техн. наук, доцент,
член-корреспондент РАН, проректор по
научной работе В.В. Сергеев,
Санкт-Петербургский политехнический
университет Петра Великого,
г. Санкт-Петербург, Россия*

Key words: ventilated facade; CFD; enclosing structure; heat-gravitational motion; average velocity; ventilated air gap; energy efficiency, civil and structural engineering, building and construction

Ключевые слова: вентилируемый фасад; численное моделирование; ограждающие конструкции; термогравитационное движение воздуха; средняя скорость; воздушный зазор; энергоэффективность

Abstract. To reduce the costs of building operation, it is necessary to provide for the use of energy-saving technologies at the stage of building design. This allows efficient use of material and energy resources, minimize costs during the design and construction of buildings and structures. One of the energy-saving technologies widely used in construction is the use of ventilated facade systems. Its application in difficult climatic conditions of many regions of Russia requires improvement and refinement of the existing methods of calculation of influence of temperature stresses in elements on strength characteristics of system, ways of the account of influence of air exchange in a backlash. The aim of the work is to determine the velocity of air flow in the gap of a ventilated facade with different width of the gap, the height of the building and climatic conditions by the method CFD (Computational Fluid Dynamics) - simulation of convective heat flux.

Аннотация. Для снижения расходов на эксплуатацию зданий необходимо предусматривать применение энергосберегающих технологий еще на стадии проектирования здания. Это позволяет рационально использовать материальные и энергетические ресурсы, минимизировать затраты на этапах проектирования и строительства зданий и сооружений. Одной из энергосберегающих технологий, широко применяемой в строительстве, является использование навесных вентилируемых фасадных систем. Её применение в сложных климатических условиях многих регионов России требует совершенствования и доработки действующих методик расчета влияния температурных напряжений в элементах на прочностные характеристики системы, способов учета влияния воздухообмена в зазоре. Целью работы является определение скорости воздушного потока в зазоре вентилируемого фасада при различной ширине зазора, высоты здания и климатических условий методом CFD (Computational Fluid Dynamics) - моделирования конвективного теплового потока.

1. Introduction

The object of study in the work are ventilated hinged system (Fig. 1), widely used to reduce heat loss and protect the walls from the adverse effects of the environment [1–5]. There are many approaches

to the study of flow in such systems [6–10]. However, studies of convective flow in ventilated facades under critical climatic conditions have not been conducted yet [11–16].

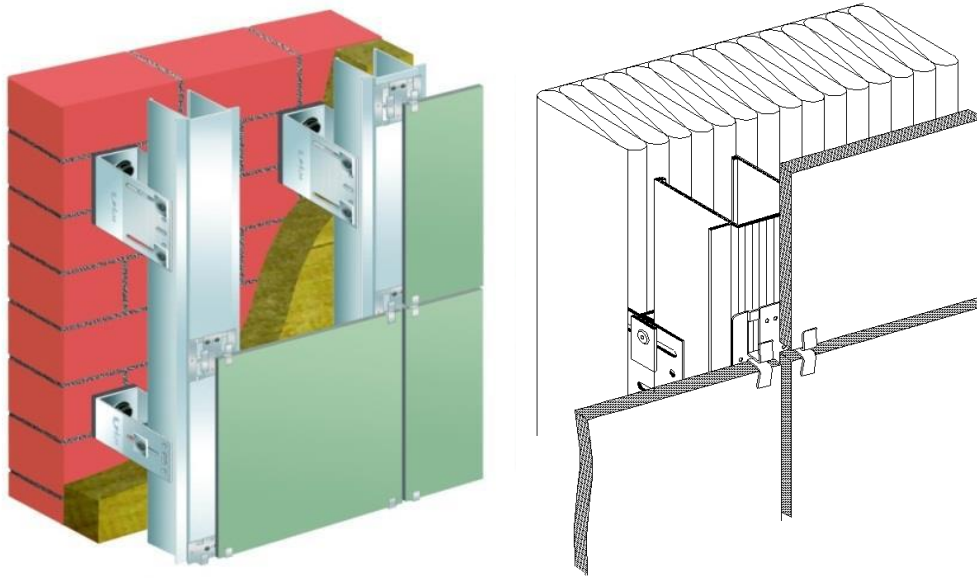


Figure 1. The design of hinged ventilated facades (axonometric perspective)

This construction technology was developed in Germany in the 1950s and has become widespread in various countries of the world, including our country, which led to the development of an international organization standardization of a number of international standards governing the methods of calculation and design of hinged facade systems.

These documents are constantly being improved, taking into account the physical properties of modern thermal insulation, building materials, especially the new construction of high-rise buildings, the reconstruction of existing buildings, the complexity of climatic conditions [17, 18].

In particular, the ISO/TC 163/SC 2 technical Committee has developed calculation methods covering the operational and thermal, hydrothermal, solar and optical characteristics of specific parts of a building, building components and components such as light-tight enclosures, Windows and facades. To a large extent, they summarize the results of studies conducted by various researchers [19].

Many of the works are related to the determination of the thickness of thermal insulation when taking into account the air exchange in the gap of the ventilated facade, the influence of metal thermal conductive inclusions by calculating the temperature fields and aimed at improving the individual bearing elements of the facade design. Thus, in [20] the program of transition systems modeling (TRNSYS) and its modification for modeling and control of air flow in buildings is used. Haase et al. [21] used TRNSYS to optimize glass facades in Hong Kong's hot and humid climate, López et al. [22] used this software to simulate the experimental module of an opaque ventilated façade. Many researchers use CFD modeling to solve similar problems [23, 24], which is an effective tool in the study and design of ventilated facades.

Thus influence of extreme climatic conditions in the operating standards and researches (sharp change of temperature of outside air from positive temperatures to negative and Vice versa at change of humidity, force of wind, falling of atmospheric pressure) on air movement in an air gap is affected poorly that significantly complicates justification of application of hinged front systems in many regions of Russia.

The aim of the work is to determine the speed of air flow in the gap of the ventilated facade with different width of the gap, the height of the building and climatic conditions. For its achievement the following tasks are solved:

- developed a CFD model of the ventilated system using the commercial package ANSYS Fluent;
- built grid;
- validation model was developed;
- comparison of simulation results with experimental data is performed.

The choice of research tool - CFD-modeling, due to the fact that it allows to provide an error of calculations within 3–5 %, comparable to the reliability of the full-scale experiment and significantly saves money and time on justification and confirmation of technical solutions.

2. Methods

Since the traditional experimental approach is expensive and does not provide complete information about the flow, it is reasonable to use the CFD approach. Computational Fluid Dynamics (CFD) uses numerical analysis and data structures to solve and analyze problems that involve fluid flows and heat fluxes. With supercomputers, better solutions can be achieved.

The calculations were carried out on a finite volume mesh, that accurately reproduces the façade geometry with variable cell size and boundary layer refinement by solving the Reynolds-Averaged formulation of the Navier-Stokes equations (RANS). A common k-epsilon turbulence closure and blended wall functions for precise boundary layer flow computations are employed, yielding the convective heat transfer at the surface boundaries.

2.1. The development of numerical methods for solving problems of heat and mass transfer

The conjugate heat transfer is considered. A model was built for different heights of the building, in which the gap between the insulation and ceramics varies from 40mm to 300mm.

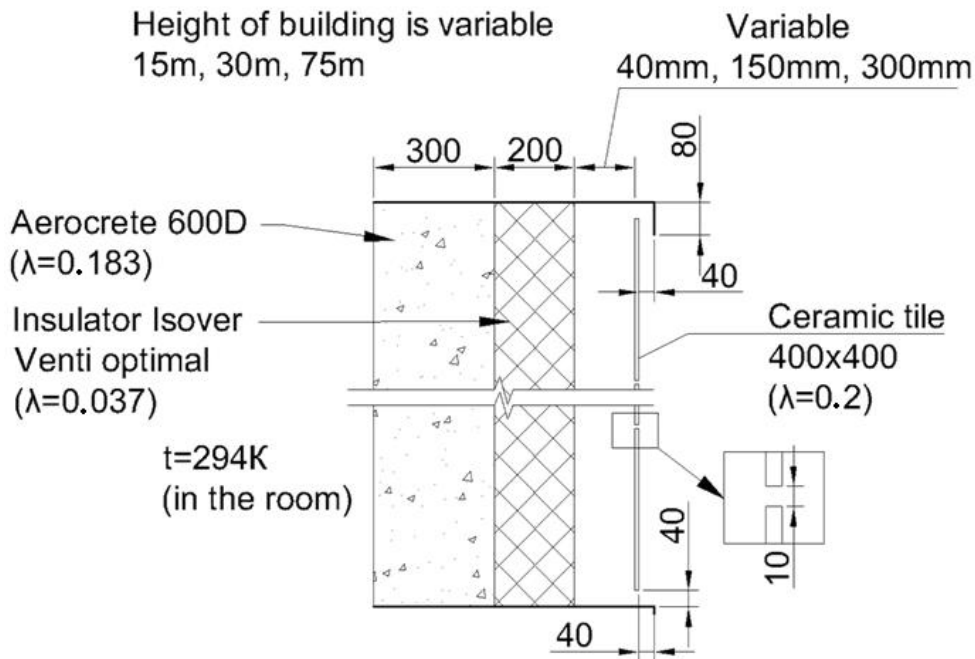


Figure 2. Design of the calculated wall

Convection and heat transfer in the presented calculation is described by the system of Navier-Stokes equations in their non-stationary formulation [25–28], taking into account the Boussinesq approximation. Decomposing the Navier-Stokes equations into the RANS equations makes it possible to simulate practical engineering flows, such as the airflow over an airplane. The assumption (known as the Reynolds decomposition) behind the RANS equations is that the time-dependent turbulent (chaotic) velocity fluctuations can be separated from the mean flow velocity. This reduces the problem to the calculation of the flow of an incompressible fluid and gas in the presence of a mass force proportional to the local temperature drop. This system of equations is as follows:

$$\begin{aligned} \nabla \cdot \mathbf{V} &= 0 \\ \frac{\partial \mathbf{V}}{\partial t} + (\mathbf{V} \nabla) \mathbf{V} &= -\frac{1}{\rho} \nabla p + \nu \Delta \mathbf{V} + \mathbf{g} \beta T \gamma \\ \frac{\partial T}{\partial t} + \mathbf{v} \nabla T &= a \Delta T \end{aligned}$$

where \mathbf{V} – fluid velocity; T – temperature; p – modified pressure; ρ – the average density; \mathbf{g} – the acceleration due to gravity; ν – the kinematic viscosity coefficient, a – the thermal diffusivity coefficient; β – the coefficient of volumetric expansion; \mathbf{y} – the unit vector directed vertically upwards.

Entering the dimensionless variables: distance – h , time – h^2/ν , speed – $g\beta\Delta T h^2/\nu$, temperature – ΔT (temperature difference), pressure – $pg\beta\Delta T h$, we get the system:

$$\nabla \cdot \mathbf{V} = 0$$

$$\frac{\partial \mathbf{V}}{\partial t} + Gr [(\mathbf{V}\nabla)\mathbf{V}_0 + (\mathbf{V}_0\nabla)\mathbf{V}] = -\nabla p + \Delta \mathbf{V} + T\mathbf{y}$$

$$\frac{\partial T}{\partial t} + Gr [\mathbf{V}\nabla T_0 + \mathbf{V}_0 \nabla T] = \frac{1}{Pr} \Delta T$$

The profiles of the velocity and temperature of the main flow are in the dimensionless variables V_0 and T_0 have the form:

$$V_0 = \frac{1}{6}(x^3 - x), T_0 = -x$$

The problem contains two dimensionless parameters that determine the similarity of convective flows – the Grashof and Prandtl number:

$$Pr = \frac{\nu}{a}, Gr = \frac{g\beta\Delta TL^3}{\nu^2}$$

In most of the literature, when examining a freely convective flow, one more criterion is used, which determines our task – the Rayleigh number, which is constructed through two other dimensionless numbers:

$$Ra = Gr \cdot Pr.$$

To solve the problem, the heat equation and the Reynolds-averaged Navier-Stokes equations (RANS), closed with the help of the k-epsilon model of turbulence, were solved. The k-epsilon model is one of the most common turbulence models, although it just doesn't perform well in cases of large adverse pressure gradients. It is a two equation model, that means, it includes two extra transport equations to represent the turbulent properties of the flow. This allows a two equation model to account for history effects like convection and diffusion of turbulent energy. The first transported variable is turbulent kinetic energy, k . The second transported variable in this case is the turbulent dissipation, epsilon. It is the variable that determines the scale of the turbulence, whereas the first variable, k , determines the energy in the turbulence.

On the boundary between two bodies, the condition of equality temperatures and flow was given.

Enhanced Wall Treatment was used to model the flow in the near-wall area. Enhanced wall treatment is a near-wall modeling method that combines a two-layer model with enhanced wall functions. If the near-wall mesh is fine enough to be able to resolve the laminar sublayer (typically $y^+=1$), then the enhanced wall treatment will be identical to the traditional two-layer zonal model (see below for details). However, the restriction that the near-wall mesh must be sufficiently fine everywhere might impose too large a computational requirement. Ideally, then, one would like to have a near-wall formulation that can be used with coarse meshes (usually referred to as wall-function meshes) as well as fine meshes (low-Reynolds-number meshes). In addition, excessive error should not be incurred for intermediate meshes that are too fine for the near-wall cell centroid to lie in the fully turbulent region, but also too coarse to properly resolve the sublayer.

The Boussinesq hypothesis was used to simulate the convection flow. The Boussinesq approximation is a way to solve nonisothermal flow, such as natural convection problems, without having to solve for the full compressible formulation of the Navier-Stokes equations.

2.2. Boundary conditions

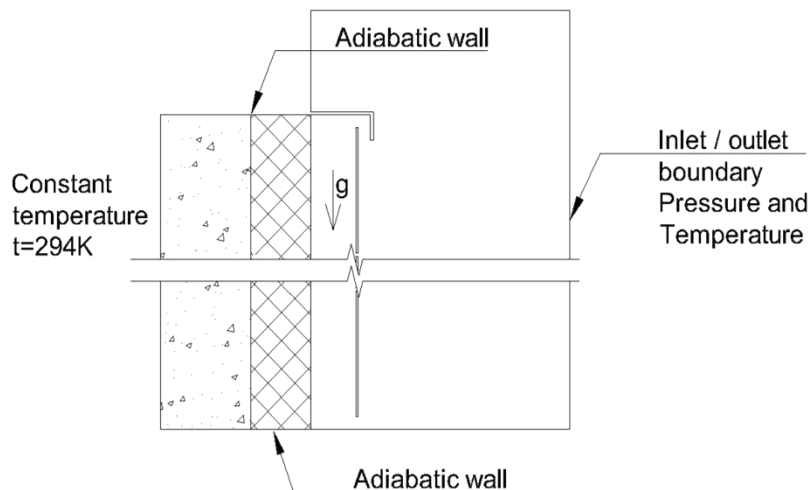


Figure 3. Research objective

The results presented below were obtained on meshes providing a mesh-independent solution.

Three temperatures were taken to calculate:

235.4 K (regions with a large temperature drop throughout the year);

289.8 K (the temperature outside the building is equal to the temperature of the external surface of the insulation);

300 K (the highest ambient temperature)

3. Results and Discussion

The highest speed of natural convection is observed in the largest gap. However, according to the norms, the speed of natural convection should not exceed 1 m/s. Therefore, it is not possible to install facades with a large gap in regions with a large average annual temperature difference.

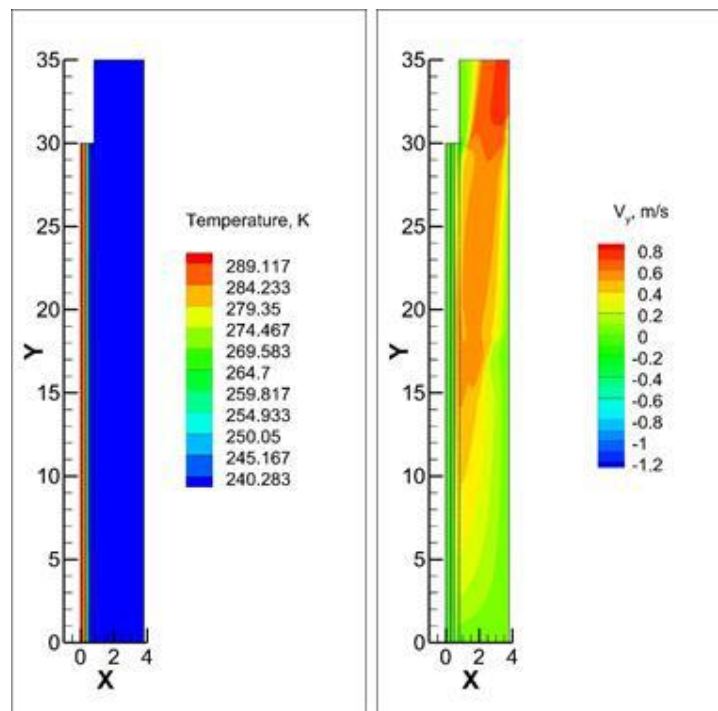


Figure 4. Isotherms, contours of velocity ($d = 300$ mm, $L = 30$ m, $T = 235.4$ K)

The diagrams show dimensionless velocity shape, temperatures and coordinates for comparing different gap values (40mm, 150mm, 300mm). The velocity is translated into a dimensionless quantity using the buoyancy velocity:

$$V_b = (g\beta\Delta TL)^{1/2}$$

Below the diagrams are just for the height that equal to 30 m. The velocity and temperature profiles are shown just in the middle of height (15 m).

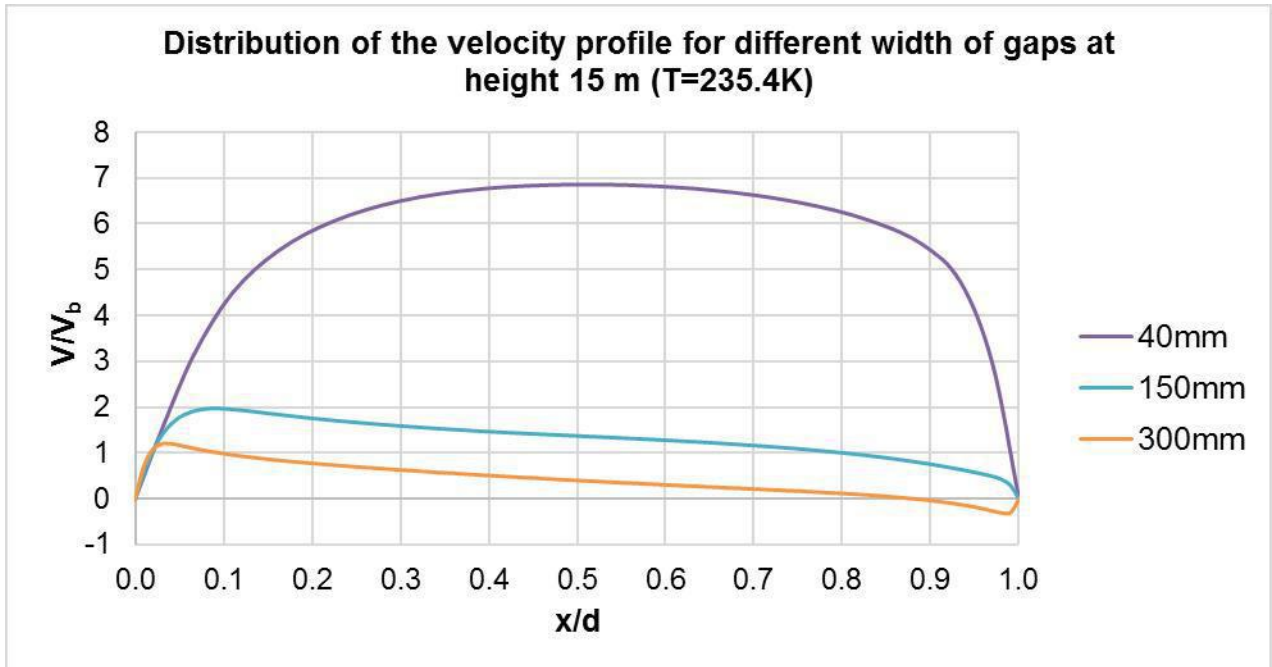


Figure 5. Distribution of the velocity profile for different width of gaps at height 15 m (T = 235.4 K)

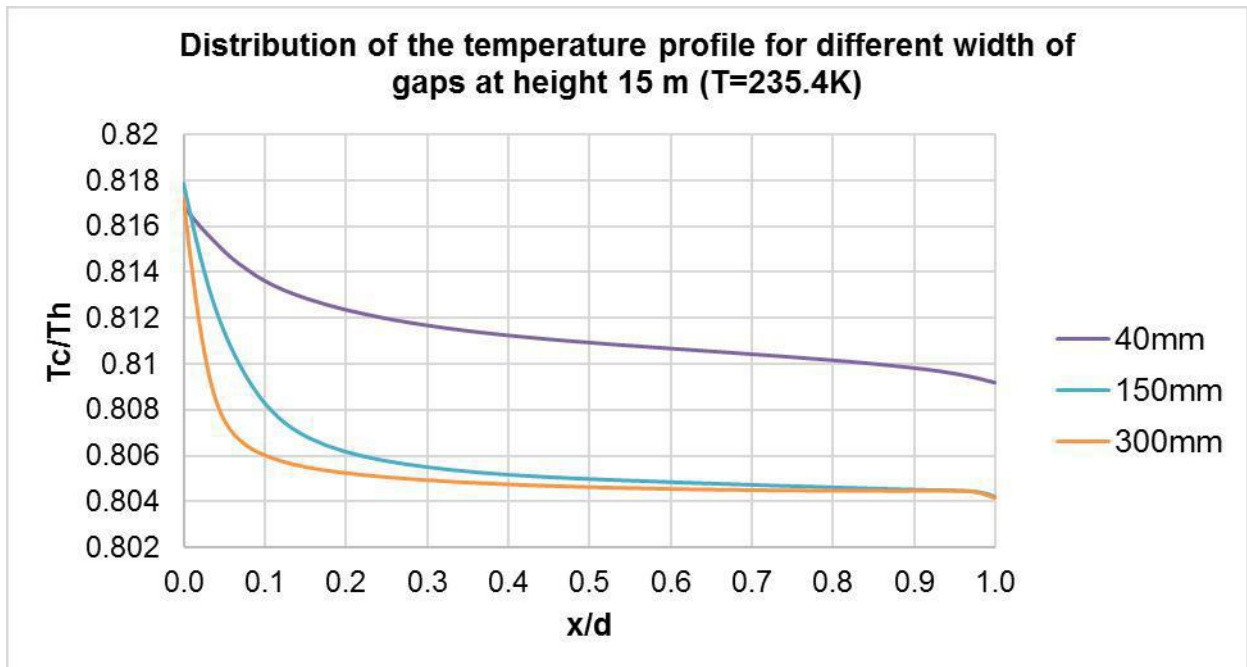


Figure 6. Distribution of the temperature profile for different width of gaps at height 15 m (T = 235.4 K)

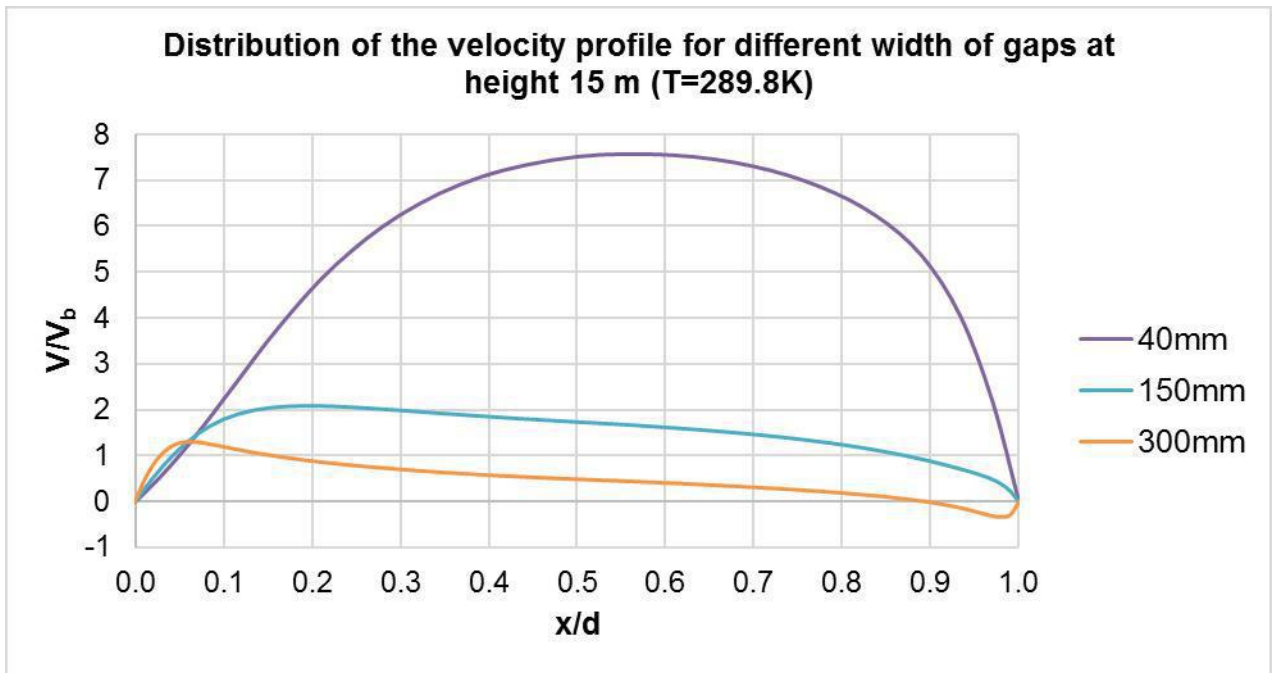


Figure 7. Distribution of the velocity profile for different width of gaps at height 15 m (T = 289.8K)

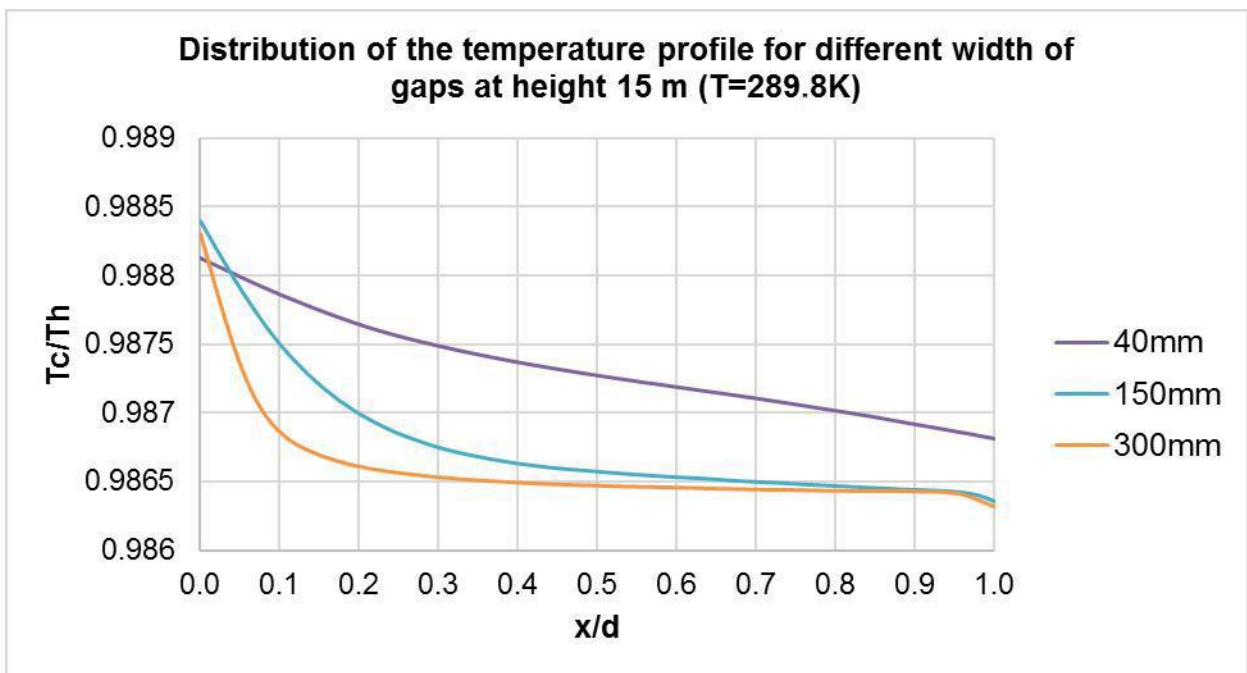


Figure 8. Distribution of the temperature profile for different width of gaps at height 15 m (T = 289.8K)

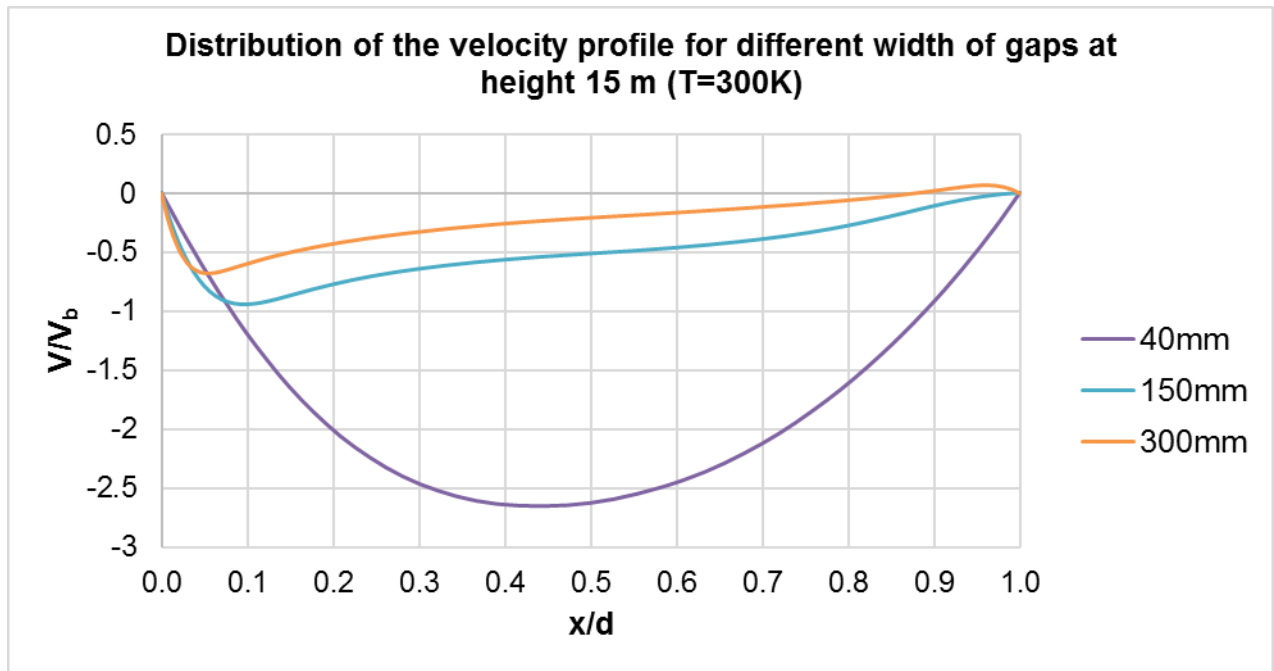


Figure 9. Distribution of the velocity profile for different width of gaps at height 15 m (T = 300 K)

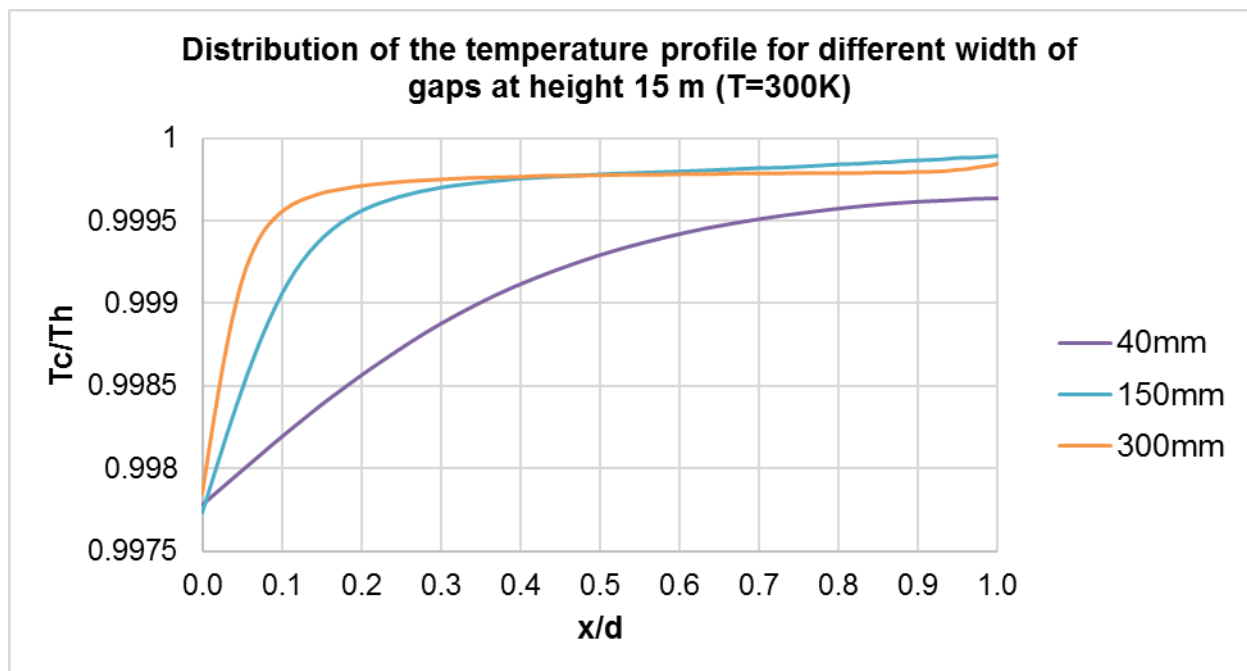


Figure 10. Distribution of the temperature profile for different width of gaps at height 15 m (T = 300 K)

Analyzing the velocity profiles in the gap, it can be said that regardless of the temperature difference for the gap of 40 mm, the highest velocity is observed. Observed a small difference between the velocity profiles for clearances 150 mm and 300 mm. the dependence for the two gaps are the same. However, the average over the cross section of the gap, the speed is less, if the clearance is wider.

The temperature profiles for the narrowest gap are more uniform because the average speed in the gap is higher. Temperature profiles for large gaps are similar and have a pronounced wall bend.

The constructed model has a number of advantages. The model takes into account the effect of gaps between tiles. The temperature on the surface of the building is determined by the solution of the conjugate heat transfer problem. The ambient temperature is set to be removed from the outer surface of

the ventilated facade, which eliminates the influence of boundary conditions. The resulting model is an improvement of the model used in the article [29].

4. Conclusions

1. The air velocity in the ventilated gap depends on the time period in the year. In winter, the speed can be equal to that required, and in summer no convection will occur. Or in the summer it works optimally, and in winter there are too high speeds which do not meet the requirements of fire resistance design and boundary layer theory. Also at high temperatures the reverse air flow can occur.

2. Facade structure can be improved by adding additional elements. Since the motion is due to the temperature difference, it is possible, as an option, to add a heating element at the bottom of the structure. Then due to temperature difference is created artificially, the difference in air densities in the lower part of the building will be realized compared to the upper one in the ventilated gap. This method is suitable when motion does not occur, or air movement is from the top to down. Thus, the air will move in the direction in which it was originally provide for by design decisions (upward). Also an additional measure can be a fan, which will mechanically promote the development of the airflow movement vertically upwards.

3. The results of this research can help for determination the necessary thickness of the gap or take additional measures to increase the efficiency of the systems.

Reference

1. Yavtushenko Y.B., Petrochenko M.V. The diffuser design of ventilated facades. *Magazine of Civil Engineering*. 2013. No. 8(43). Pp. 38–45. (rus)
2. Musorina T., Olshevskiy V., Ostrovaia A., Statsenko E. Experimental assessment of moisture transfer in the vertical ventilated channel. *MATEC Web of Conferences*. TPACEE. 2016. 02002.
3. Balocco C. A simple model to study ventilated facades energy performance. *Energy and Buildings*. 2002. Vol. 34(5). Pp. 469–475.
4. Petrichenko M.R., Petrochenko M.V., Yavtushenko Ye.B. A hydraulically optimum ventilated gap. *Magazine of Civil Engineering*. 2013. Vol. 37(2). Pp. 112–113. (rus)
5. Guillén I., Gómez-Lozano V., Fran J.M., López-Jiménez P.A. Thermal behavior analysis of different multilayer façade: Numerical model versus experimental prototype. *Energy and Buildings*. 2014. Vol. 79. Pp. 184–190.
6. Aparicio-Fernández C., Vivancos J.-L., Ferrer-Gisbert P., Royo-Pastor R. Energy performance of a ventilated façade by simulation with experimental validation. *Applied Thermal Engineering*. 2014. Vol. 66 (1-2). Pp. 563–570.
7. Petrichenko M. R., Petrochenko M. V. Hydraulics of natural convection flows in building walling with air gap. *Magazine of Civil Engineering*. 2011. No. 8(26). Pp. 51–56. (rus)
8. Nemova D.V. Integrated characteristics of thermogravitational convection in the air layer of ventilated facades. *Magazine of Civil Engineering*. 2013. No. 2(37). Pp. 25–34. (rus)
9. Iribar-Solaberrieta E., Escudero-Revilla C., Odriozola-Maritorea M., Campos-Celador A., García-Gáfaró C. Energy performance of the opaque ventilated façade. *Energy Procedia*. 2015. No. 78. Pp. 55–60.
10. Peci López F., Ruiz de Adana Santiago M. Sensitivity study of an opaque ventilated façade in the winter season in different climate zones in Spain. *Renewable Energy*. 2015. No. 75. Pp. 524–533.
11. Diarce G., Campos-Celador A., Martin K., Urresti A., García-Romero A., Sala J.M. A comparative study of the CFD modeling of a ventilated active façade including phase change materials. *Applied Energy*. 2014. No. 126. Pp. 307–317.
12. de Gracia A., Navarro L., Castell A., Cabeza L.F. Energetic

Литература

1. Явтушенко Е.Б., Петроченко М.В. Диффузорная конструкция навесного вентилируемого фасада // Инженерно-строительный журнал. 2013. № 8(43). С. 38–45.
2. Musorina T., Olshevskiy V., Ostrovaia A., Statsenko E. Experimental assessment of moisture transfer in the vertical ventilated channel // MATEC Web of Conferences. TPACEE. 2016. 02002.
3. Balocco C. A simple model to study ventilated facades energy performance // Energy and Buildings. 2002. Vol. 34(5). Pp. 469–475.
4. Петриченко М.Р., Петроченко М.В., Явтушенко Е.Б. Гидравлически оптимальная вентилируемая щель // Инженерно-строительный журнал. 2013. № 2(37). С. 35–39.
5. Guillén I., Gómez-Lozano V., Fran J.M., López-Jiménez P.A. Thermal behavior analysis of different multilayer façade: Numerical model versus experimental prototype // Energy and Buildings. 2014. Vol. 79. Pp. 184–190.
6. Aparicio-Fernández C., Vivancos J.-L., Ferrer-Gisbert P., Royo-Pastor R. Energy performance of a ventilated façade by simulation with experimental validation // Applied Thermal Engineering. 2014. Vol. 66(1-2). Pp. 563–570.
7. Петриченко М.Р., Петроченко М.В. Гидравлика свободноконвективных течений в ограждающих конструкциях с воздушным зазором // Инженерно-строительный журнал. 2011. № 8(26). С. 51–56.
8. Немова Д.В. Интегральные характеристики термогравитационной конвекции в воздушной прослойке навесных вентилируемых фасадов // Инженерно-строительный журнал. 2013. № 2(37). С. 25–34.
9. Iribar-Solaberrieta E., Escudero-Revilla C., Odriozola-Maritorea M., Campos-Celador A., García-Gáfaró C. Energy performance of the opaque ventilated façade // Energy Procedia. 2015. No. 78. Pp. 55–60.
10. Peci López F., Ruiz de Adana Santiago M. Sensitivity study of an opaque ventilated façade in the winter season in different climate zones in Spain // Renewable Energy. 2015. № 75. Pp. 524–533.
11. Diarce G., Campos-Celador A., Martin K., Urresti A.,

Петриченко М.Р., Котов Е.В., Немова Д.В., Тарасова Д.С., Сергеев В.В. Численное моделирование вентилируемых фасадов в экстремальных климатических условиях // Инженерно-строительный журнал. 2018. № 1(77). С. 130–140.

- performance of a VDSF with CPM under different weather conditions. *Materials Science and Technology Conference and Exhibition*. 2014. No. 3. Pp. 1659–1666.
13. de Gracia A., Castell A., Fernández C., Cabeza L.F. A simple model to predict the thermal performance of a ventilated facade with phase change materials. *Energy and Buildings*. 2015. Vol. 93. Pp. 137–142.
 14. de Gracia A., Navarro L., Castell A., Cabeza L.F. Energy performance of a ventilated double skin facade with PCM under different climates. *Energy and Buildings*. 2015. No. 91. Pp. 37–42.
 15. Manca O., Nardini S. Thermal design of uniformly heated inclined channels in natural convection with and without radiative effects. *Heat Transfer Engineering*. 2001. Vol. 22. No. 2. Pp. 13–28.
 16. Auletta A., Manca O. Heat and fluid flow resulting from the chimney effect in a symmetrically heated vertical channel with adiabatic extensions. *International Journal of Thermal Sciences*. 2002. Vol. 41. Pp. 1101–1111.
 17. ISO 12631:2017. Thermal performance of curtain walling — Calculation of thermal transmittance.
 18. ISO 6946:2017. Building components and building elements — Thermal resistance and thermal transmittance — Calculation methods.
 19. Bikasa D., Tsikaloudakia K., Kontoleona K.J., Giarmaa C., Tsokaa S., Tsirigotia D. Ventilated facades: requirements and specifications across Europe. *International Conference on Sustainable Synergies from Buildings to the Urban Scale, SBE16/ Procedia Environmental Sciences*. 2017. Vol. 38. Pp. 148–154.
 20. Aparicio Fernandez, C.S., Vivancos, J., Ferrer Gisbert P., Royo Pastor R. Energy performance of a ventilated façade by simulation with experimental validation. *Applied Thermal Engineering*. 2014. Vol. 66(1-2). Pp. 563–570. doi:10.1016/j.applthermaleng.
 21. Haase M., Marques da Silva F., Amato A. Simulation of ventilated façades in hot and humid climates. *Energy and Buildings*. 2009. Vol. 41(4). Pp. 361–373.
 22. López F.P., Jensen R.L., Heiselberg P., Ruiz de Adana Santiago M. Experimental analysis and model validation of an opaque ventilated façade. *Building and Environment*. 2012. Vol. 56. Pp. 265–275.
 23. Colombo E., Zwahlen M., Frey M., Loux J. Design of a glazed double-façade by means of coupled CFD and building performance simulation. *CISBAT 2017 International Conference / Energy Procedia*. 2017. Vol. 122. Pp. 355–360.
 24. Peng J., Curcija D.C., Lu L., Selkowitz S.E., Yang H., Mitchell R. Developing a method and simulation model for evaluating the overall energy performance of a ventilated semi-transparent photovoltaic double-skin façade. *Progress in photovoltaics*. 2016. Vol. 24. No. 6. Pp. 781–799.
 25. Manca O., Ricci D., Nardini S., Di Lorenzo G. Thermal and fluid dynamic behaviors of confined laminar impinging slot jets with nanofluids. *International Communications in Heat and Mass Transfer*. 2016. Vol. 70. Pp. 15–26. DOI:10.1016/j.icheatmasstransfer. 2015.11.010.
 26. Corral R., Crespo J. A hybrid unstructured/spectral method for the resolution of Navier-Stokes equations. *Proceedings of the ASME Turbo Expo*. 2009.
 27. Corral R., Crespo J. A harmonic balance method in graphics processing units for vibrating blades. *11th European Conference on Turbomachinery Fluid Dynamics and Thermodynamics*. 2015.
 28. Minea A.A. Uncertainties in modeling thermal conductivity of laminar forced convection heat transfer with water alumina nanofluids. *International Journal of Heat and Mass Transfer*. 2014. Vol. 68. Pp. 78–84.
 29. Vatin N., Gorshkov A.S., Nemova D., Gamayunova O., Tarasova D. Humidity conditions of homogeneous wall García-Romero A., Sala J.M. A comparative study of the CFD modeling of a ventilated active façade including phase change materials // *Applied Energy*. 2014. № 126. Pp. 307–317.
 12. de Gracia A., Navarro L., Castell A., Cabeza L.F. Energetic performance of a VDSF with CPM under different weather conditions // *Materials Science and Technology Conference and Exhibition*. 2014. № 3. Pp. 1659–1666.
 13. de Gracia A., Castell A., Fernández C., Cabeza L.F. A simple model to predict the thermal performance of a ventilated facade with phase change materials // *Energy and Buildings*. 2015. Vol. 93. Pp. 137–142.
 14. de Gracia A., Navarro L., Castell A., Cabeza L.F. Energy performance of a ventilated double skin facade with PCM under different climates // *Energy and Buildings*. 2015. № 91. Pp. 37–42.
 15. Manca O., Nardini S. Thermal design of uniformly heated inclined channels in natural convection with and without radiative effects // *Heat Transfer Engineering*. 2001. Vol. 22. № 2. Pp. 13–28.
 16. Auletta A., Manca O. Heat and fluid flow resulting from the chimney effect in a symmetrically heated vertical channel with adiabatic extensions // *International Journal of Thermal Sciences*. 2002. Vol. 41. Pp. 1101–1111.
 17. ISO 12631:2017. Thermal performance of curtain walling — Calculation of thermal transmittance.
 18. ISO 6946:2017. Building components and building elements — Thermal resistance and thermal transmittance — Calculation methods.
 19. Bikasa D., Tsikaloudakia K., Kontoleona K.J., Giarmaa C., Tsokaa S., Tsirigotia D. Ventilated facades: requirements and specifications across Europe // *International Conference on Sustainable Synergies from Buildings to the Urban Scale, SBE16/ Procedia Environmental Sciences*. 2017. Vol. 38. Pp. 148–154.
 20. Aparicio Fernandez C.S., Vivancos J., Ferrer Gisbert P., Royo Pastor R. Energy performance of a ventilated façade by simulation with experimental validation // *Applied Thermal Engineering*. 2014. Vol. 66(1-2). Pp. 563–570. doi:10.1016/j.applthermaleng.
 21. Haase M., Marques da Silva F., Amato A. Simulation of ventilated façades in hot and humid climates // *Energy and Buildings*. 2009. Vol. 41(4). Pp. 361–373.
 22. López F.P., Jensen R.L., Heiselberg P., Ruiz de Adana Santiago M. Experimental analysis and model validation of an opaque ventilated façade // *Building and Environment*. 2012. Vol. 56. Pp. 265–275.
 23. Colombo E., Zwahlen M., Frey M., Loux J. Design of a glazed double-façade by means of coupled CFD and building performance simulation // *CISBAT 2017 International Conference / Energy Procedia*. 2017. Vol. 122. Pp. 355–360.
 24. Peng J., Curcija D.C., Lu L., Selkowitz S.E., Yang H., Mitchell R. Developing a method and simulation model for evaluating the overall energy performance of a ventilated semi-transparent photovoltaic double-skin façade // *Progress in Photovoltaics*. 2016. Vol. 24. № 6. Pp. 781–799.
 25. Manca O., Ricci D., Nardini S., Di Lorenzo G. Thermal and fluid dynamic behaviors of confined laminar impinging slot jets with nanofluids // *International Communications in Heat and Mass Transfer*. 2016. Vol. 70. Pp. 15–26. DOI:10.1016/j.icheatmasstransfer. 2015.11.010.
 26. Corral R., Crespo J. A hybrid unstructured/spectral method for the resolution of Navier-Stokes equations // *Proceedings of the ASME Turbo Expo*. 2009.
 27. Corral R., Crespo J. A harmonic balance method in graphics processing units for vibrating blades // *11th European Conference on Turbomachinery Fluid Dynamics and Thermodynamics*. 2015.

Petritchenko M.R., Kotov E.V., Nemova D.V., Tarasova D.S., Sergeev V.V. Numerical simulation of ventilated facades under extreme climate conditions. *Magazine of Civil Engineering*. 2018. No. 1. Pp. 130–140. doi: 10.18720/MCE.77.12.

from gas-concrete blocks with finishing plaster compounds. *Applied Mechanics and Materials*. 2014. Vols. 670–671. Pp. 349–354.

28. Minea A.A. Uncertainties in modeling thermal conductivity of laminar forced convection heat transfer with water alumina nanofluids // *International Journal of Heat and Mass Transfer*. 2014. Vol. 68. Pp. 78–84.

29. Vatin N., Gorshkov A.S., Nemova D., Gamayunova O., Tarasova D. Humidity conditions of homogeneous wall from gas-concrete blocks with finishing plaster compounds // *Applied Mechanics and Materials*. 2014. Vols. 670–671. Pp. 349–354.

Mikhail Petritchko,
+7(921)330-04-29; fonpetrich@mail.ru

Михаил Романович Петриченко,
+7(921)330-04-29; эл. почта: fonpetrich@mail.ru

Evgeny Kotov,
+7(921)346-13-12; ekotov.cfd@gmail.com

Евгений Владимирович Котов,
+7(921)346-13-12;
эл. почта: ekotov.cfd@gmail.com

Darya Nemova,
+7(921)890-02-67; nemova_dv@spbstu.ru

Дарья Викторовна Немова,
+7(921)890-02-67;
эл. почта: nemova_dv@spbstu.ru

Darya Tarasova,
+7(931)256-45-94; tarasovads@gmail.com

Дарья Сергеевна Тарасова,
+7(931)256-45-94;
эл. почта: tarasovads@gmail.com

Vitaly Sergeev,
+7(921)980-54-37; sergeev_vitaly@mail.ru

Виталий Владимирович Сергеев,
+7(921)980-54-37;
эл. почта: sergeev_vitaly@mail.ru

© Petritchko M.R., Kotov E.V., Nemova D.V., Tarasova D.S., Sergeev V.V., 2018

doi: 10.18720/MCE.77.13

Hysteresis of the soil water-retention capacity: estimating the scanning branches

Гистерезис водоудерживающей способности почвы

**V.V. Terleev,
A.O. Nikonorov,
R.S. Ginevsky,
V.A. Lazarev,
I. Togo,**

*Peter the Great St. Petersburg Polytechnic
University, St. Petersburg, Russia*

**A.G. Topaj,
K.G. Moiseev,**

*Agrophysical Research Institute, St. Petersburg,
Russia*

V.A. Pavlova,
*St. Petersburg State Agrarian University,
St. Petersburg, Russia*

**K.A. Layshev,
M.V. Arkhipov,**

*Federal State Budgetary Institution "North-West
Centre of Interdisciplinary Researches of
Problems of Food Maintenance", St. Petersburg-
Pushkin, Russia*

A.Yu. Melnichuk,
*V.I. Vernadsky Crimean Federal University,
Simferopol, Russia*

I.A. Dunaieva,
*Federal State Budget Scientific Institution
"Research Institute of Agriculture of Crimea",
Simferopol, Russia*

W. Mirschel,
*Leibniz-Centre for Agricultural Landscape
Research, Müncheberg, Germany*

**Д-р с.-хоз. наук, профессор В.В. Терлеев,
аспирант А.О. Никоноров,
студент Р.С. Гиневский,
студент В.А. Лазарев,
канд. техн. наук, заведующий кафедрой
И. Того,**

*Санкт-Петербургский политехнический
университет Петра Великого,
Санкт-Петербург, Россия*

**д-р техн. наук, профессор А.Г. Топаж,
канд. с.-хоз. наук, заведующий
лабораторией К.Г. Моисеев,**

*Агрофизический научно-исследовательский
институт, Санкт-Петербург, Россия*

**канд. экон. наук, доцент В.А. Павлова,
Санкт-Петербургский Государственный
Аграрный Университет, Санкт-Петербург,
г. Пушкин, Россия**

**д-р вет. наук, профессор К.А. Лайшев,
д-р биол. наук, профессор М.В. Архипов,
ФГБНУ «Северо-Западный Центр
междисциплинарных исследований проблем»,
Санкт-Петербург, г. Пушкин, Россия**

**д-р техн. наук, заведующий кафедрой
А.Ю. Мельничук,**

*Крымский федеральный университет им.
В.И.Вернадского, г. Симферополь,
Республика Крым, Россия*

**канд. техн. наук, заведующий
лаборатории Е.А. Дунаева,**

*ФГБУН «Научно-исследовательский
институт сельского хозяйства Крыма»,
г. Симферополь, Республика Крым, Россия*

**д-р с.-хоз. наук, профессор В. Миршель,
Leibniz-Centre for Agricultural Landscape
Research, Müncheberg, Germany**

Key words: water-retention capacity; capillary pressure; hysteresis loop; scanning curves; "pump effect"

Ключевые слова: водоудерживающая способность почвы; капиллярное давление; петля гистерезиса; сканирующие ветви; эффект помпы

Abstract. Designing of underground constructions, such as irrigation and drainage systems, requires engineering surveys. Such surveys include the study of the hydrological conditions of the territory, which are determined by the hydrophysical properties of soils, such as their water-retention capacity. The formation of a hysteresis loop for the soil water-retention capacity occurs because of the variability of meteorological conditions. It is almost impossible to measure all possible scanning branches that fill the gap between the main branches of the hysteresis loop. A mathematical model of the hysteretic soil water-retention capacity is proposed. The model is based on physical concepts of the structure and

Терлеев В.В., Никоноров А.О., Гиневский Р.С., Лазарев В.А., Того И., Топаж А.Г., Моисеев К.Г., Павлова В.А., Лайшев К.А., Архипов М.В., Мельничук А.Ю., Дунаева Е.А., Миршель В. Гистерезис водоудерживающей способности почвы // Инженерно-строительный журнал. 2018. № 1(77). С. 141–148.

capillary properties of the soil pore space. Model parameters are identified by dot fitting using data on the main (boundary) hysteresis branches. Scanning branches starting with pre-calculated reversal points are evaluated. Suggested model has a quite low error to predict the scanning branches of soil water-retention capacity. The use of this model ensures reliable estimates of the hydrological conditions of the territory for underground construction. Also it gives precision irrigation rates which result in reduction of gravitational runoff of excessive moisture, preventing pollution of groundwater with agrochemicals.

Аннотация. Проектирование объектов подземного строительства, таких как ирригационные и дренажные системы, требуют проведения инженерных изысканий. Такие изыскания включают в себя изучение гидрологических условий территории, которые определяются гидрофизическими свойствами почв, например, их водоудерживающей способностью. Изменчивостью метеорологических условий обусловлено формирование петли гистерезиса водоудерживающей способности почвы. Измерение всех возможных сканирующих ветвей, заполняющих промежутки между главными ветвями петли гистерезиса, практически невозможно. Предложена математическая модель гистерезиса водоудерживающей способности почвы. Модель основана на физических представлениях о строении и капиллярных свойствах пространства почвенных пор. Параметры модели идентифицируются путем точечной аппроксимации с использованием данных о главных (граничных) ветвях гистерезиса. Оценены сканирующие ветви, начинающиеся с предварительно рассчитанных поворотных точек. Наряду с обеспечением достоверных оценок гидрологических условий территории подземного строительства, использование данной модели позволяет более точно рассчитать нормы орошения сельскохозяйственных культур. Применение прецизионных норм орошения предотвращает гравитационный сток избыточной влаги, существенно уменьшает вымывание удобрений, мелиорантов и средств защиты растений за пределы корнеобитаемого слоя почвы и, как следствие, снижает риск загрязнения грунтовых вод агрохимикатами, что имеет важное эколого-экономическое значение.

1. Introduction

To substantiate acceptance of the engineering solutions for the construction and operation of hydraulic structures (including urban underground infrastructure objects, irrigation and drainage systems of agriculture), data on the hydrological conditions of the territory are very important. These conditions are largely determined by the hydrophysical properties of the soil. Among these properties is the water-retention capacity of the soil. This property is usually described as a dependence of the volumetric soil water content θ [$\text{cm}^3 \cdot \text{cm}^{-3}$] on the capillary pressure (potential) of the soil moisture ψ [$\text{cm H}_2\text{O}$] [1–4].

Direct measurement of the $\theta(\psi)$ dependence is a rather laborious process [5]. Because of the hysteresis, the water-retention capacity of the soil is characterized by a multitude of branches of this dependence. However, usually only the main (boundary) branches of the hysteresis loop are to be measured [6]. The scanning branches that fill the hysteresis loop are measured much less frequently. Limited number of scanning branches is chosen arbitrary. Measuring the entire range of scanning branches is rather problematic. Nevertheless, during the periods of projecting and constructing activities and also under the actual conditions of operation of the irrigation and drainage systems these data can be necessary for the justification of the engineering solution. But it is not possible to predict what exact scanning branch will be required. Thus, we face the problem of estimating of the scanning branches from using the available data, for example, data on the main (boundary) branches of the hysteresis loop. The only rational way to solve this problem is the method of mathematical modeling.

Several mathematical models had been suggested before [7–14]. The authors of this paper investigated the mathematical model based on physical concepts of the structure and capillary properties of soil pores [15–19]. This model allows estimating the scanning branches of the hysteretic soil water-retention capacity. Description of the model is given in part 2 Method.

The purpose of the work is the verification of the investigated model [15–18]. Verification of this model is based on literature data on four soils: White silica sand [12], Dune sand [19], Rideau clayey loam and Rubicon sandy loam [20]. The tasks of the study are comparison the investigated model with three analogical models [12–14]. The results of the work could be applied in the various hydraulic engineering projects [21].

2. Method

Numerical methods and computational experiments are used to solve the problems posed in this study. To describe the mathematical model, an analytical method is used. The water-retention capacity of the soil is described by formula:

$$S_e = \begin{cases} \frac{1}{2} \operatorname{erfc} \left(\frac{n\sqrt{\pi}}{4} \ln \left(\frac{\psi - \psi_{ae}}{\psi_0 - \psi_{ae}} \right) \right) \approx \left(1 + \left(\frac{\psi - \psi_{ae}}{\psi_0 - \psi_{ae}} \right)^n \right)^{-1}, & \psi < \psi_{ae}; \\ 1, & \psi \geq \psi_{ae}, \end{cases} \quad (1)$$

where: $S_e = (\theta - \theta_R) / (\theta_S - \theta_R)$ – effective soil saturation with moisture; θ_S [$\text{cm}^3 \cdot \text{cm}^{-3}$] – maximum volumetric soil water content; θ_R [$\text{cm}^3 \cdot \text{cm}^{-3}$] – minimum volumetric soil water content at which the moisture has the properties of a liquid; ψ_{ae} [cm H₂O] – capillary pressure of soil moisture at air entrance (bubbling pressure); ψ_0 [cm H₂O] – capillary pressure, which corresponds to the most probable value of the random variable – the logarithm of the effective radius of the soil pore; σ – standard deviation of this random variable; $n = 4 / (\sigma\sqrt{2\pi})$; $\operatorname{erfc}(z) = 1 - \left(2/\sqrt{\pi} \right) \int_0^z \exp(-t^2) dt$ – complementary error function.

To describe the hysteretic soil water-retention capacity, formula (1) is applied with two sets of parameters: $\psi_{0,w}$ [cm H₂O], ψ_{we} [cm H₂O] and n_w (for wetting), as well $\psi_{0,d}$ [cm H₂O], ψ_{ae} [cm H₂O] and n_d (for drying). Scanning (primary, secondary, etc.) branches start from turning points. The algorithm for calculating the reversal points is proposed in the literature [13]. Formula (1) with relations for the reversal points describe the mathematical model of the hysteretic soil water-retention capacity [15-18] investigated here.

3. Results and Discussion

The model (1) parameters were identified from the measured data on the main (boundary) branches of the hysteresis. Then, using the identified parameters, the scanning branches were calculated. Based on a comparison of such calculated scanning branches with experimental data that were not used to identify the parameters, it is possible to characterize the predictive accuracy of the model with respect to the estimated hysteresis scanning branches. Using the formula (1), the following computational experiments were performed: 1) identification of the parameters of the model investigated here by dot approximation (fitting) procedure of data on the main (boundary) branches (Table 1, Table 2); 2) predictive estimation of hysteresis scanning branches.

Table 1. The parameters of the model investigated here, which have been identified from data on the main (boundary) branches of the hysteretic soil water-retention capacity by means of a dot approximation (fitting) procedure

Soils	Parameters							
	θ_R	θ_S	ψ_{ae}	ψ_{we}	$\psi_{0,d}$	$\psi_{0,w}$	n_d	n_w
White silica sand	0.0861	0.3574	-12.09	-1.797	-112.2	-41.42	3.996	2.287
Dune sand	0.0934	0.3010	-19.82	-3.594	-33.68	-19.99	3.170	3.298
Rideau clayey loam	0.2896	0.4179	-20.00	6.26	-66.96	-29.44	1.951	1.999
Rubicon sandy loam	0.1688	0.3829	-13.00	16.00	-88.42	-36.32	2.911	2.993

On Figures 1a,b–4a,b the measured data are shown by dots; the results of the dot approximation (fitting) procedure for the main (boundary) branches, as well as the results of the predictive estimation for the scanning branches of hysteresis loop (using the model investigated here) are shown by solid curves. Based on the computational experiments, a comparative analysis for an accuracy of the predictive estimating the hysteresis scanning branches was carried out. The model investigated here and three analogical models [12–14] were used.

In Table 2 and Table 3 the underlined font indicates the minimum average absolute values of the deviation of the results for the dot approximation (fitting) procedure, as well as for predictive estimating the hysteresis scanning branches, from the corresponding measured data. From Table 2 and Table 3 it is clear that the model presented in this paper most often shows the best result for dot approximating (fitting) the measured data on the main (boundary) branches, and also this model most often achieves the highest accuracy for the predictive estimates of the scanning branches of the hysteresis loop. The quite low mean absolute values of the deviation between the simulation results and the experimental data confirm that the model investigated here corresponds to physical concepts of the nature of the soil hysteretic water-retention capacity.

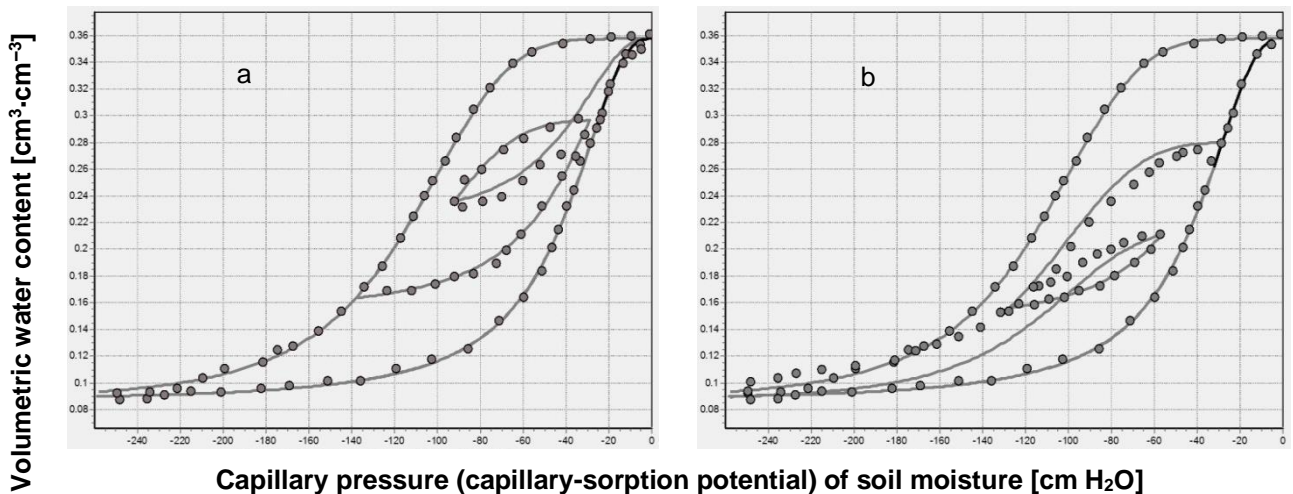


Figure 1. White silica sand. Using the investigated model for dot approximation (fitting) of measured data on the main branches and for predictive estimation of:
a) the wetting primary branch, the drying secondary branch, the wetting tertiary branch;
b) the drying primary branch, the wetting secondary branch, the drying tertiary branch

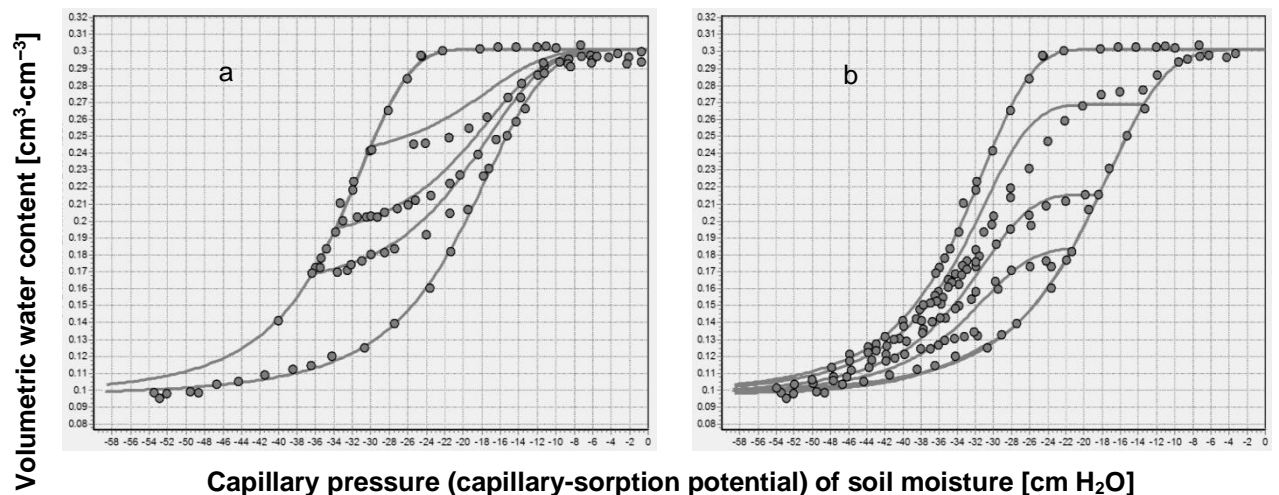


Figure 2. Dune sand. Using the investigated model for dot approximation (fitting) of measured data on the main branches and for predictive estimation of:
a) the three wetting scanning branches; b) the four drying scanning branches

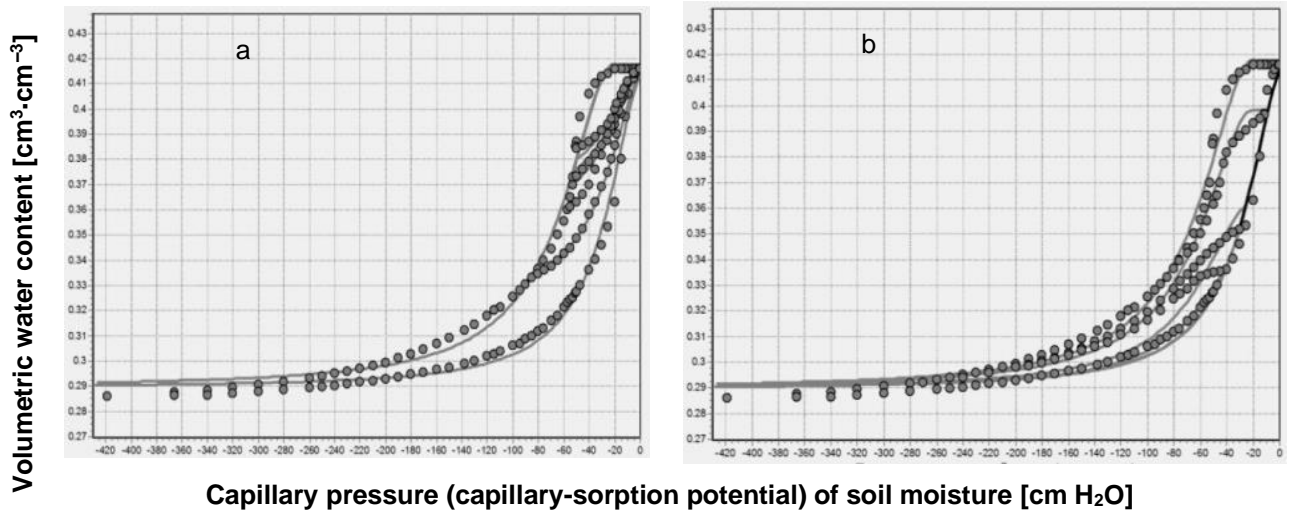


Figure 3. Rideau clayey loam. Using the investigated model for dot approximation (fitting) of measured data on the main branches and for predictive estimation of:
a) the four wetting scanning branches; b) the three drying scanning branches

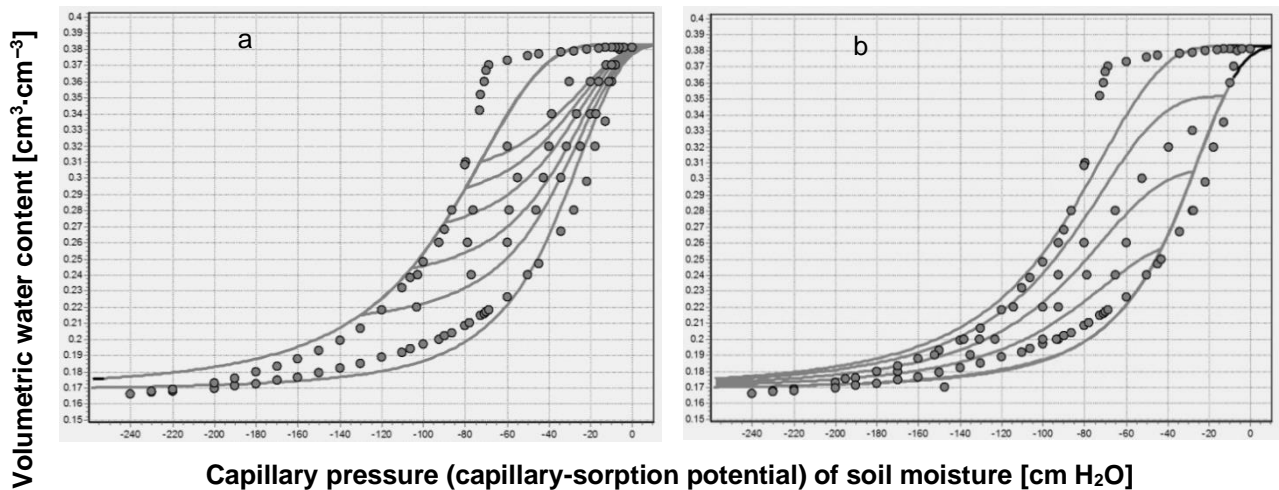


Figure 4. Rubicon sandy loam. Using the investigated model for dot approximation (fitting) of measured data on the main branches and for predictive estimation of:
a) the five wetting scanning branches; b) the four drying scanning branches

It should be noted that the investigated model, in principle, does not exclude the possibility of undesirable artificial "pump effect", as well as the intersection of the main and scanning hysteresis branches. This effect consists in the fact that with the oscillation of the capillary pressure of the moisture in a fixed range of values, the volume water content can assume values that go beyond physically acceptable frames. Such possibility is due to the formal character of the mathematical description. Indeed, for an arbitrary choice of parameter values, a "pump effect" cannot be ruled out. At the same time, if the values of the parameters are physically realistic (reliable), then the "pump effect" cannot arise. Of course, the property of physical adequacy (realistic and reliability) of parameter values is inherent only in those parameters that have a physical sense [13]. Otherwise, the absence of a "pump effect" cannot be guaranteed [14]. Models with artificially closed loops formed by the main and scanning hysteresis branches, in the opinion of the authors of this work, are physically absurd and untenable, since in this case at the reversal points the function of the soil differential moisture capacity assumes an unlimited number of values [12]. More realistic is the assumption that this function takes only two values (one for drying and one for wetting). As a rule, the formal (that have no physical interpretation) models are characterized by low accuracy of predictive estimates. Only a physically adequate model, coupled with realistic and reliable values of the interpreted parameters, excludes the appearance of undesirable artificial "pump effect", and also allows accurate prediction of the scanning hysteresis branches. The model investigated in this work refers to the type of physically adequate models [15–18]. The use of

precision irrigation rates calculated with the help of the model investigated and verified by the authors prevents the excess moisture from draining and thus minimizes the loss of irrigation water, as well as the unproductive losses of fertilizers, ameliorants and plant protection matters due to the leaching of agrochemicals beyond the root layer of the soil.

Table 2. The average absolute deviation between the measured data cited from the literature and main (boundary) branches calculated using the four models by means of a dot approximation (fitting) procedure

Soils	Models			
	Scott et al.	Kool and Parker	Huang et al.	Investigated
<i>White silica sand</i>	0.0028	0.0107	0.0030	<u>0.0019</u>
<i>Dune sand</i>	0.0027	0.0080	0.0031	<u>0.0023</u>
<i>Rideau clayey loam</i>	<u>0.0032</u>	0.0057	0.0057	<u>0.0032</u>
<i>Rubicon sandy loam</i>	<u>0.0045</u>	0.0130	0.0055	0.0098

Table 3. The average absolute deviation between the measured data cited from the literature and hysteretic scanning branches estimated using the four models

Soils	Scanning branches	Models							
		Scott et al.		Kool and Parker		Huang et al.		Investigated	
		Wetting	Drying	Wetting	Drying	Wetting	Drying	Wetting	Drying
<i>White silica sand</i>	Primary	0.0033	0.0070	0.0035	<u>0.0028</u>	0.0035	0.0066	<u>0.0024</u>	0.0087
	Secondary	0.0029	0.0035	0.0054	0.0095	0.0050	0.0031	<u>0.0014</u>	<u>0.0028</u>
	Tertiary	0.0099	0.0128	0.0130	0.0137	<u>0.0082</u>	<u>0.0042</u>	0.0130	0.0149
<i>Dune sand</i>	Primary	0.0074	0.0096	0.0096	0.0151	<u>0.0057</u>	0.0096	0.0067	<u>0.0095</u>
<i>Rideau clayey loam</i>	Primary	0.0038	<u>0.0050</u>	<u>0.0024</u>	0.0065	0.0034	0.0071	<u>0.0024</u>	0.0062
<i>Rubicon sandy loam</i>	Primary	0.0106	0.0141	0.0118	0.0175	0.0076	<u>0.0105</u>	<u>0.0052</u>	0.0108

4. Conclusions

The importance of the study is that the using the mathematical model of the hysteretic soil water-retention capacity presented here provides an opportunity to assess the soil hydrophysical characteristics that are applied in the design of hydro-technical structures, as well as in the calculation of irrigation rates. The estimates obtained in the framework of computational experiments with this model contribute to an increase in the study effectiveness of the hydrological conditions of the hydraulic structures territory when performing pre-project engineering surveys. The model investigated in the work is verified. The verification was based on literature data on four soils: *White silica sand*, *Dune sand*, *Rideau clayey loam* and *Rubicon sandy loam*. Comparisons of the investigated model were carried out with respect to three analogical models. It is shown that the model investigated in this work has the highest accuracy for estimating the scanning hysteresis branches of the studied soils. The results of the research can be applied at designing various facilities of hydraulic engineering and underground construction as well at developing a precision irrigation technology.

5. Acknowledgments

The work is supported by DAAD (PID: 91619700; A/10/01103), RFBR (No. 16-04-01473-a).

Reference

1. Brutsaert W. Probability laws for pore-size distribution. *Soil Sci.* 1966. Vol. 101. Pp. 85–92.
2. Ahuja L.R., Swartzendruber D. An improved form of soil-water diffusivity function. *Soil Sci. Soc. Am. Proc.* 1972. Vol. 36. Pp. 9–14.
3. Haverkamp R., Vauclin M., Touma J., Wierenga P.J., Vachaud G. A comparison of numerical simulation model for one-dimensional infiltration. *Soil Sci. Soc. Am. J.* 1977. Vol. 41. Pp. 285–294.
4. Shein E.V. Physically based mathematical models in soil science: history, current state, problems, and outlook (analytical review). *Eurasian Soil Sci.* 2015. Vol. 48. Pp. 712–718. DOI: 10.1134/S1064229315070091.
5. Globus A.M. *Экспериментальная гидрофизика почв* [Experimental Hydrophysics of Soils]. Leningrad: Gidrometeoizdat, 1969. 357 p. (rus)
6. Sukharev V.I. *Water-balance and Nature-protection Substantiation of Reclamative Activities in the Agricultural Landscapes of the Central Chernozem Region, the Doctor's Thesis in Agriculture* [Water balance and environmental justification of land reclamation measures in agrolandscapes of the Central Black Earth region]. Kursk: Kursk State Agricultural Academy, 2006. (rus)
7. Pedroso D.M., Williams D.J. A novel approach for modelling soil–water characteristic curves with hysteresis. *Computers and Geotechnics.* 2010. Vol. 37(3). Pp. 374–380.
8. Abbasi F., Javaux M., Vanclooster M., Feyen J. Estimating hysteresis in the soil water retention curve from monolith experiments. *Geoderma.* 2012. Vols. 189–190. Pp. 480–490.
9. Zhou A.-N. A contact angle-dependent hysteresis model for soil–water retention behavior. *Computers and Geotechnics.* 2013. Vol. 49. Pp. 36–42.
10. Hu R., Chen Y.-F., Liu H.-H., Zhou C.-B. A coupled stress–strain and hydraulic hysteresis model for unsaturated soils: Thermodynamic analysis and model evaluation. *Computers and Geotechnics.* 2015. Vol. 63. Pp. 159–170.
11. Hu R., Hong J.-M., Chen Y.-F., Zhou C.-B. Hydraulic hysteresis effects on the coupled flow–deformation processes in unsaturated soils: Numerical formulation and slope stability analysis. *Applied Mathematical Modelling.* 2018. Vol. 54. Pp. 221–245.
12. Huang H.C., Tan Y.C., Liu C.W., Chen C.H. A novel hysteresis model in unsaturated soil. *Hydrological Processes.* 2005. Vol. 19. Pp. 1653–1665.
13. Scott P.S., Farquhar G.J., Kouwen N. Hysteretic effects on net infiltration. *Proceeding of National Conference on Advances in Infiltration.* Publication 11-83, American Society of Agricultural Engineers, St. Joseph, Michigan, 1983. Pp. 163–170.
14. Kool J.B., Parker J.C. Development and evaluation of closed-form expressions for hysteretic soil hydraulic properties. *Water Resources Research.* 1987. Vol. 23(1). Pp. 105–114.
15. Terleev V.V., Topazh A.G., Mirschel W. The improved estimation for the effective supply of productive moisture considering the hysteresis of soil water-retention capacity. *Russian Meteorology and Hydrology.* 2015. Vol. 40(4). Pp. 278–285.
16. Terleev V., Nikonorov A., Togo I., Volkova Yu., Garmanov V., Shishov D., Pavlova V., Semenova N., Mirschel W. Modelling the Hysteretic Water retention capacity of soil for reclamation research as a part of underground development. *Procedia Engineering.* 2016. Vol. 165. Pp. 1776–1783.
17. Terleev V.V., Nikonorov A.O., Togo I., Volkova Yu.V.,

Литература

1. Brutsaert W. Probability laws for pore-size distribution // *Soil Sci.* 1966. Vol.101. Pp. 85–92.
2. Ahuja L.R., Swartzendruber D. An improved form of soil-water diffusivity function // *Soil Sci. Soc. Am. Proc.* 1972. Vol. 36. Pp. 9–14.
3. Haverkamp R., Vauclin M., Touma J., Wierenga P.J., Vachaud G. A comparison of numerical simulation model for one-dimensional infiltration // *Soil Sci. Soc. Am. J.* 1977. Vol. 41. Pp. 285–294.
4. Shein E.V. Physically based mathematical models in soil science: history, current state, problems, and outlook (analytical review) // *Eurasian Soil Sci.* 2015. Vol. 48. Pp. 712–718. DOI: 10.1134/S1064229315070091.
5. Глобус А.М. Экспериментальная гидрофизика почв. Л.: Гидрометеиздат, 1969. 357 с.
6. Сухарев В.И. Воднобалансовое и природоохранное обоснование мелиоративных мероприятий в агроландшафтах Центрально-Черноземного региона. Дисс. на соиск. учен. степ. д.т.н. Курск: Курская государственная сельскохозяйственная академия, 2006. 348 с.
7. Pedroso D.M., Williams D.J. A novel approach for modelling soil–water characteristic curves with hysteresis // *Computers and Geotechnics.* 2010. Vol. 37(3). Pp. 374–380.
8. Abbasi F., Javaux M., Vanclooster M., Feyen J. Estimating hysteresis in the soil water retention curve from monolith experiments // *Geoderma.* 2012. Vols. 189–190. Pp. 480–490.
9. Zhou A.-N. A contact angle-dependent hysteresis model for soil–water retention behavior // *Computers and Geotechnics.* 2013. Vol. 49. Pp. 36–42.
10. Hu R., Chen Y.-F., Liu H.-H., Zhou C.-B. A coupled stress–strain and hydraulic hysteresis model for unsaturated soils: Thermodynamic analysis and model evaluation // *Computers and Geotechnics.* 2015. Vol. 63. Pp. 159–170.
11. Hu R., Hong J.-M., Chen Y.-F., Zhou C.-B. Hydraulic hysteresis effects on the coupled flow–deformation processes in unsaturated soils: Numerical formulation and slope stability analysis // *Applied Mathematical Modelling.* 2018. Vol. 54. Pp. 221–245.
12. Huang H.C., Tan Y.C., Liu C.W., Chen C.H. A novel hysteresis model in unsaturated soil // *Hydrological Processes.* 2005. Vol. 19. Pp. 1653–1665.
13. Scott P.S., Farquhar G.J., Kouwen N. Hysteretic effects on net infiltration // *Proceeding of National Conference on Advances in Infiltration,* Publication 11-83, American Society of Agricultural Engineers, St. Joseph, Michigan, 1983. Pp. 163–170.
14. Kool J.B., Parker J.C. Development and evaluation of closed-form expressions for hysteretic soil hydraulic properties // *Water Resources Research.* 1987. Vol. 23(1). Pp. 105–114.
15. Terleev V.V., Topazh A.G., Mirschel W. The improved estimation for the effective supply of productive moisture considering the hysteresis of soil water-retention capacity // *Russian Meteorology and Hydrology.* 2015. Vol. 40(4). Pp. 278–285.
16. Terleev V., Nikonorov A., Togo I., Volkova Yu., Garmanov V., Shishov D., Pavlova V., Semenova N., Mirschel W. Modelling the Hysteretic Water retention capacity of soil for reclamation research as a part of underground development // *Procedia Engineering.* 2016. Vol. 165. Pp. 1776–1783.
17. Терлеев В.В., Никоноров А.О., Того И., Волкова Ю.В., Гиневский Р.С., Лазарев В.А., Хамзин Э.Р., Гарманов В.В., Миршель В., Акимов Л.И. Гистерезис

Терлеев В.В., Никоноров А.О., Гиневский Р.С., Лазарев В.А., Того И., Топаж А.Г., Моисеев К.Г., Павлова В.А., Лайшев К.А., Архипов М.В., Мельничук А.Ю., Дунаева Е.А., Миршель В. Гистерезис водоудерживающей способности почвы // *Инженерно-строительный журнал.* 2018. № 1(77). С. 141–148.

- Ginevsky R.S., Lazarev V.A., Khamzin E.R., Garmanov V.V., Mirschel W., Akimov L.I. Hysteretic water-retention capacity of sandy soil. *Magazine of Civil Engineering*. 2017. No. 2. Pp. 84–92.
18. Terleev V., Ginevsky R., Lazarev V., Nikonorov A., Togo I., Topaj A., Moiseev K., Abakumov E., Melnichuk A., Dunaieva I. Predicting the scanning branches of hysteretic soil water-retention capacity with use of the method of mathematical modeling. *IOP Conference Series: Earth and Environmental Science*. 2017. Vol. 90. Article#012105.
 19. Gillham R.W., Klute A., Heermann D.F. Hydraulic Properties of a Porous Medium: Measurement and Empirical Presentation. *Soil Sci. Soc. Am. J.* 1976. Vol. 40. Pp. 203–207.
 20. Mualem Y. *A catalogue of the hydraulic properties of unsaturated soils. Research Project 442*. Technion, Israel Institute of Technology, Haifa, Israel, 1976. 100 p.
 21. Makarov A., Mihailova A., Arefiev N., Pavlov S., Chashchina T., Terleev V., Badenko V. Country area territory protection from flooding; construction conditions, problem definition and solution. *Procedia Engineering*. 2015. Vol. 117. Pp. 225–231.

Vitaly Terleev,
vitaly_terleev@mail.ru

Aleksandr Nikonorov,
+7(921)385-21-80; coolhabit@yandex.ru

Roman Ginevsky,
rginevski@gmail.com

Viktor Lazarev,
lviktor.97@mail.ru

Issa Togo,
+7(921)337-37-30; issatogo@mail.ru

Alex Topaj,
alex.topaj@gmail.com

Kirill Moiseev,
kir_moiseev@mail.ru

Viktoriiia Pavlova,
vikalpav@mail.ru

Kasim Layshev,
layshev@mail.ru

Mikhail Arkhipov,
szcentr@bk.ru

Aleksandr Melnichuk,
omelnichuk61@mail.ru

Ielizaveta Dunaieva,
dunaeva_e@niishk.ru

Wilfried Mirschel,
wmirschel@zalf.de

водоудерживающей способности почвы на примере песчаных почв. 2017. № 2(70). С. 84–92.

18. Terleev V., Ginevsky R., Lazarev V., Nikonorov A., Togo I., Topaj A., Moiseev K., Abakumov E., Melnichuk A., Dunaieva I. Predicting the scanning branches of hysteretic soil water-retention capacity with use of the method of mathematical modeling // *IOP Conference Series: Earth and Environmental Science*. 2017. Vol. 90. Article#012105.
19. Gillham R.W., Klute A., Heermann D.F. Hydraulic Properties of a Porous Medium: Measurement and Empirical Presentation // *Soil Sci. Soc. Am. J.* 1976. Vol. 40. Pp. 203–207.
20. Mualem Y. A catalogue of the hydraulic properties of unsaturated soils. Research Project 442. Technion, Israel Institute of Technology, Haifa, Israel, 1976. 100 p.
21. Makarov A., Mihailova A., Arefiev N., Pavlov S., Chashchina T., Terleev V., Badenko V. Country area territory protection from flooding; construction conditions, problem definition and solution // *Procedia Engineering*. 2015. Vol. 117. Pp. 225–231.

Виталий Викторович Терлеев,
эл. почта: vitaly_terleev@mail.ru

Александр Олегович Никоноров,
+7(921)385-21-80;
эл. почта: coolhabit@yandex.ru

Роман Сергеевич Гинеvский,
эл. почта: rginevski@gmail.com

Виктор Андреевич Лазарев,
эл. почта: lviktor.97@mail.ru

Исса Того,
+7(921)337-37-30; эл. почта: issatogo@mail.ru

Александр Григорьевич Топаж,
эл. почта: alex.topaj@gmail.com

Кирилл Геннадьевич Моисеев,
эл. почта: kir_moiseev@mail.ru

Виктория Александровна Павлова,
эл. почта: vikalpav@mail.ru

Касим Анверович Лайшеев,
эл. почта: layshev@mail.ru

Михаил Вадимович Архипов,
эл. почта: szcentr@bk.ru

Александр Юрьевич Мельничук,
эл. почта: omelnichuk61@mail.ru

Елизавета Андреевна Дунаева,
эл. почта: dunaeva_e@niishk.ru

Вильфред Миршель,
эл. почта: wmirschel@zalf.de

© Terleev V.V., Nikonorov A., Ginevsky R.S., Lazarev V.A., Togo I.T., Topaj A.G., Moiseev K.G., Pavlova V.A., Layshev K.A., Arkhipov M., Melnichuk A., Dunaieva I., Mirschel W., 2018

Terleev V.V., Nikonorov A.O., Ginevsky R.S., Lazarev V.A., Togo I., Topaj A.G., Moiseev K.G., Pavlova V.A., Layshev K.A., Arkhipov M.V., Melnichuk A.Yu., Dunaieva I.A., Mirschel W. Hysteresis of the soil water-retention capacity: estimating the scanning branches. *Magazine of Civil Engineering*. 2018. No. 1. Pp. 141–148. doi: 10.18720/MCE.77.13.



ПОЛИТЕХ
Санкт-Петербургский
политехнический университет
Петра Великого

Инженерно-строительный институт
Центр дополнительных профессиональных программ

195251, г. Санкт-Петербург, Политехническая ул., 29,
тел/факс: 552-94-60, www.stroikursi.spbstu.ru,
stroikursi@mail.ru

Приглашает специалистов проектных и строительных организаций,
не имеющих базового профильного высшего образования
на курсы профессиональной переподготовки (от 500 часов)
по направлению «Строительство» по программам:

П-01 «Промышленное и гражданское строительство»

Программа включает учебные разделы:

- Основы строительного дела
- Инженерное оборудование зданий и сооружений
- Технология и контроль качества строительства
- Основы проектирования зданий и сооружений
- Автоматизация проектных работ с использованием AutoCAD
- Автоматизация сметного дела в строительстве
- Управление строительной организацией
- Управление инвестиционно-строительными проектами. Выполнение функций технического заказчика

П-02 «Экономика и управление в строительстве»

Программа включает учебные разделы:

- Основы строительного дела
- Инженерное оборудование зданий и сооружений
- Технология и контроль качества строительства
- Управление инвестиционно-строительными проектами. Выполнение функций технического заказчика и генерального подрядчика
- Управление строительной организацией
- Экономика и ценообразование в строительстве
- Управление строительной организацией
- Организация, управление и планирование в строительстве
- Автоматизация сметного дела в строительстве

П-03 «Инженерные системы зданий и сооружений»

Программа включает учебные разделы:

- Основы механики жидкости и газа
- Инженерное оборудование зданий и сооружений
- Проектирование, монтаж и эксплуатация систем вентиляции и кондиционирования
- Проектирование, монтаж и эксплуатация систем отопления и теплоснабжения
- Проектирование, монтаж и эксплуатация систем водоснабжения и водоотведения
- Автоматизация проектных работ с использованием AutoCAD
- Электроснабжение и электрооборудование объектов

П-04 «Проектирование и конструирование зданий и сооружений»

Программа включает учебные разделы:

- Основы сопротивления материалов и механики стержневых систем
- Проектирование и расчет оснований и фундаментов зданий и сооружений
- Проектирование и расчет железобетонных конструкций
- Проектирование и расчет металлических конструкций
- Проектирование зданий и сооружений с использованием AutoCAD
- Расчет строительных конструкций с использованием SCAD Office

П-05 «Контроль качества строительства»

Программа включает учебные разделы:

- Основы строительного дела
- Инженерное оборудование зданий и сооружений
- Технология и контроль качества строительства
- Проектирование и расчет железобетонных конструкций
- Проектирование и расчет металлических конструкций
- Обследование строительных конструкций зданий и сооружений
- Выполнение функций технического заказчика и генерального подрядчика

По окончании курса слушателю выдается диплом о профессиональной переподготовке
установленного образца, дающий право на ведение профессиональной деятельности

